University of Portsmouth

'Novel Nano-particulate/Polymer Treatment Systems for Masonry Enhancement and Protection'

A doctorial thesis by;

James MacMullen

Director of Studies: Dr Zhongyi Zhang

The thesis is submitted in partial fulfilment of the requirements for the award of the degree of Doctorate of philosophy of the University of Portsmouth

Advanced Polymer and Composites Research Group
School of Engineering

October 2009-2012

Declaration

Whilst registered as a candidate for the above degree, I have not been registered for any other research award. The results and conclusions embodied in this thesis are the work of the named candidate and have not been submitted for any other academic award.

James MacMullen

04/03/2013

Date

Dedicated to my parents who mean the world to me

Abstract

Fundamental issues associated with addressing the UK housing shortage problem are climate change and the lack of usable building space. Conservation of old buildings, maintaining green land and a country filled with single walled older properties mean that the UK government has to retrofit existing older building stock. This would make a significant impact on reducing the carbon footprint of each household as well as to alleviate energy supply problems.

The investigation of novel zinc oxide and titanium dioxide nanoparticulates in aqueous silane/siloxane oil-in-water (O/W) emulsions for practical exterior facade applications is presented. An initial emulsion was developed and optimised before further improvement through nanoparticulate incorporation was achieved. Nanoparticulates of zinc oxide and titanium dioxide were dispersed respectively using ultrasonication in n-isooctyltriethoxysilane before being incorporated into a base emulsion. Once formulations were optimised, applied studies and fundamental assessment of these emulsions were conducted.

The aim of the work presented was to produce a practical facade emulsion that could be used in the retrofitting of existing building stock or for heritage remedial treatments. Initial research indicated that water was the governing factor in a diverse range of facade degradation mechanisms; improving water repellence, thermal envelope efficiency while reducing biofouling was recognised as being of key interest in this field. The study gives insight into aqueous water repellent emulsions, nanoparticulate integration by commercially practical means, and assessment of the attributes exhibited by such treatments.

Rheological and morphological characterisation concluded that a gelled network structure is produced by the incorporation of the fabricated nanoparticulate colloids. The emulsions retained shear-thinning characteristics, ideal for deep treatment penetration to be achieved for porous silicate substrates. Accelerated ageing tests showed that the nanoparticulate emulsions were substantially more thermodynamically stable than the emulsion control while also being physically more stable due to surfactant-particulate stabilisation mechanisms of the polar phases.

From further investigation it was also found that hydroxyl terminated siloxane could be integrated into these emulsions, helping to improve the 'green credentials' of such systems through the replacement of conventionally used trimethoxy terminated siloxanes, that release harmful methanol upon curing, thus substitution is preferential and in line with current European policy.

Treatments improved thermal envelope efficiency of structures through the reduction of retained water in various forms including rising damp. Assessment was carried out using model houses exposed to various temperature and humidity scenarios under controlled heating. The findings showed that water was the root cause of heat loss and thus a key parameter when considering the improvement of a structures' carbon footprint. These treatments allow water vapour to permeate out of a structure passively, reducing internal humidity issues including microbiological degradation and health related problems experienced by occupants.

Investigation of bioreceptivity conducted though an 8 week algal culture streaming study concluded that treatments with <0.1wt% of the aforementioned nanoparticulates could reduce biofouling through photo-induced sanitisation. Furthermore, it was also found that while water repellence may vary at the facade interface due to the respective metal oxides photocatalytic nature, substrate interior water contact angles should remain high due to the absence of UV light. This is of key importance as it implies that simultaneous antifouling and rising damp remediation may be achieved by such treatments.

One of the major advantages of the treatments presented is that they do not effectively alter the aesthetics of the substrate, unlike photo-induced 'self-cleaning' coatings that turn the facade white. In addition, these treatments are not susceptible to problems related to the cracking or chipping of coated surfaces, allowing them to provide better protection.

From the above points it is clear that these treatments are the next paradigm in facade protection, complying with current social, ecological, political and industrial needs. This study presents the inception, development and investigation of key attributes and mechanisms of these novel treatments while showing critically that such emulsion treatments are practical with great potential to enhance the lives of UK residents.

Acknowledgements

I would like to thank Dr Zhongyi Zhang for his boundless knowledge, wisdom and support throughout my study at the University of Portsmouth. His help has led me through undergraduate, masters and PhD. Always developing and increasing my understanding of research practices, widening my fields of study and knowledge. Thank you for providing me with a strong foundation, allowing me to achieve what is required regardless of its scope.

My deepest gratitude must also be given to Dr Hom Nath Dhakal for his sustained and unrelenting enthusiasm, extensive guidance and support. Thanks must be given for his knowledge of extensive topics, general and specific practices and insightful discussions.

I would like to give Dr Jovana Radulovic special acknowledgement and thanks for her limitless contribution and help. Providing very acute knowledge and refinement which contributed immensely in publications, presentations and providing a better understanding of the field.

I wish to thank Professor Nick Bennett for his unreserved help in making the entire project a reality. Without his help and continuous support I would not have been able to continue my education after my undergraduate degree. He has helped me to gain further knowledge through masters and PhD and I am immensely grateful to be given such an opportunity.

I would also like to thank the University of Portsmouth as a whole for funding of my masters and PhD study, while providing un-mitigated support when it was counted on, and the friendliness of the people who work there.

Thanks must also go to Dr Simon Cragg and the EM Unit at the University of Portsmouth for their help with TEM, SEM, extensive knowledge and help with microbiological sample preparation. Sincere gratitude must also be given to Dr Eugen Barbu, Dr Hamde Nazar and Mrs Jill Rice for allowing me to learn and operate a rheometer; a key tool for such a project. Their help has improved my understanding of rheology, the mechanisms governing stabilisation, and helped massively with publications and understanding of the field.

I would also like to thank LPD Lab Services and MCA Services for their prompt help, good nature and all round transparency, as well as Rocara Limited for their help and generosity in procurement of various surfactants during the course of this study.

Students that need to be thanked and acknowledged for their help and contribution to this study; Durai Balasubramanian, Nicolas LeLorrain, Constandionos Herodotou, Miltiadis Totomis, Aw Yong Boon Hao, Wei Pin Tan Kevin, and Benjamin Beh Chun Srany. All of whom have worked tirelessly in their respective studies.

Finally, unyielding thanks must be given to my parents, who work tirelessly to ensure my surefooted development and happiness in very difficult times.

Dissemination

Publications

MacMullen J., Zhang Z., Rirsch E., Dhakal H.N., Bennett N. Brick and mortar treatment by cream emulsion for improved water repellence and thermal insulation. Energy and Buildings 43 (2011), pp 1560-1565.

Rirsch E., MacMullen J., Zhang Z. Evaluation of mortar samples obtained from UK houses treated for rising damp. Construction and Building Materials 25 (2011), pp 2845-2850.

Alani A., MacMullen J., Telik O., Zhang Z. Investigation into the thermal performance of recycled glass screed for construction purposes. Construction and Building Materials 29 (2012), pp 527-532.

MacMullen J., Zhang Z., Radulovic J., Herodotou C., Totomis M., Dhakal H.N., Bennett N. Titanium dioxide and zinc oxide nano-particulate enhanced oil-in-water (O/W) facade emulsions for improved masonry thermal insulation and protection. Energy and Buildings 52 (2012), pp 86-92.

MacMullen J., Zhang Z., Radulovic J., Dhakal H.N., Bennett N. An investigation of hydroxyl end-terminated polydimethylsiloxane (PDMS) in exterior oil-in-water (O/W) emulsion treatments. Construction and Building Materials 37 (2012), pp 283-290.

Zhang Z., MacMullen J., Dhakal H.N., Radulovic J., Herodotou C., Totomis M., Bennett N. Enhanced water repellence and thermal insulation of masonry by zinc oxide treatment. Energy and Buildings 54 (2012) pp 40-46.

Zhang Z., MacMullen J., Dhakal H.N., Radulovic J., Herodotou C., Totomis M., Bennett N. Biofouling resistance of titanium dioxide and zinc oxide nanoparticulate silane/siloxane exterior facade treatments. Building and Environment 59 (2013) pp 47-55.

Presentations

MacMullen J., Zhang Z., Herodotou C., Dhakal H.N., Radulovic J., Bennett N. Nano-particulate modified o/w facade emulsions for enhanced masonry water repellence. Presented January at Retrofit 2012 conference, Manchester, UK.

MacMullen J., Development and characterisation of novel nano-particulate/polymer coating systems for materials performance enhancement and protection. University of Portsmouth, School of Engineering. Research Seminar 2011.

MacMullen J., Zhang Z., Herodotou C., Dhakal H.N., Radulovic J., Bennett N. Biofouling resistance of titanium dioxide and zinc oxide nanoparticulate silane/siloxane exterior facade treatments. University of Portsmouth. Technology Faculty Research Day 2012.

Posters

MacMullen J. Investigation of polymer facade cream coating imparting enhanced water repellence and thermal insulation on building materials. University of Portsmouth Research Day 2010.

MacMullen J. Hydroxyl functionalised polydimethylsiloxane (PDMS) and its incorporation into exterior facade emulsion treatments. University of Portsmouth Technology Faculty Research Day 2011. Won second prize.

MacMullen J. Titanium dioxide and zinc oxide nanoparticulates and their role in exterior facade emulsion treatments. University of Portsmouth. Technology Faculty Research Day 2012. Won first prize.

Abbreviations & Symbols

AOT	Sodium diethylhexylsulphosuccinate
APDMS	(2-4% Aminoethylaminopropylmethylsiloxane) – dimethylsiloxane copolymer
APTES	3-aminopropyltriethoxysilane
ATP	Adenosine triphosphate
C	Carbon
Ca	Calcium
CA	Contact Angle
CMC	Critical Micelle Concentration
CO2	Carbon dioxide
C-S-H	Calcium-silicate-hydrate gel
DBS	Sodium dodecylbenzenesulphonate
Et	Ethyl (C2H5)
EU	European Union
FDA	Food and Drug Administration
H	Hydrogen
h+	Hole formed by the illumination of a semiconductor
HLB	Hydrophile-Lipophile Balance
Hv	Incident photon energy
HVAC	Heating, Ventilation and Air Conditioning
ISM	In situ Forming Microparticle
Mg	Magnesium
MTEOS	Methyltriethoxysilane
NTU	Nephelometric Turbidity Units
O	Oxygen
O/O	Oil-in-Oil
O/W	Oil-in-Water
O/W/O	Oil-in-Water-in-Oil
OH	Hydroxyl
P	Phosphorus
PDMS	Polydimethylsiloxane
PHS	Diethylphosphonatoethyl-triethoxysilane
PIT	Phase Inversion Temperature
POE (15)	Polyoxyethylen (15) stearylamine
POE (60)	Polyoxyethylene (60) stearylamine ether
PPM	Parts Per Million
RC	Reinforced Concrete
sa	Surfactant
SBS	Sick Building Syndrome
Si	Silicon
TEOS	Tetraethoxysilane
Ti	Titanium
UV	Ultraviolet (radiation)
W/O	Water-in-Oil
W/O/W	Water-in-Oil-in-Water
WCA	Water Contact Angle

Zn	Zinc
γ	Surface tension

Contents

List of Figures

List of Tables

Chapter 1: Introduction

Fundamental issues associated with addressing the housing shortage problem are climate change and the lack of usable building space. Conservation of old buildings, maintaining green land and a country filled with single walled older properties mean that the UK government has to retrofit existing older building stock. This would make a significant impact on reducing the carbon footprint of each household as well as to alleviate energy supply problems. The UK government pledged that by 2050 carbon dioxide emissions relative to the 1990 output would be cut by 60% [**1**] [**2**]. This has been superseded by a new pledge set out in the 2008 Climate Change Act which states a 34% carbon dioxide reduction by 2020 and 80% by 2050 [**3**] [**4**]. Since household heating accounted for 53% of domestic energy consumption during 2006 [**5**], it is imperative to explore practical and cost effective ways of improving thermal envelope efficiency. By doing so contribution towards meeting the government carbon dioxide pledge may be possible [**6**]. It is estimated that 75% of the dwellings existing in 2050 would have already been built implying that there is a strong need to retrofit existing structures to meet UK government targets [**7**].

Approximately 33% of total heat loss in poorly insulated buildings is thought to be from external walls; however little progress has been made on how to insulate them effectively [**8**] [**9**]; for retrofitting walls the limiting factors include space and cost. Conventional reasoning deems the use of insulation on interior or exterior wall surfaces acceptable. In reality, the cost of installation of such materials would be punitive. There would also be the imposition of reduced usable space, either internally or externally, making such efforts impractical to implement in nationwide schemes. One solution may be the application of a water based silane/siloxane treatment to make the walls water repellent and to enhance thermal envelope insulation properties. These relatively new treatments do not have the volatile organic compound problems that current solvent based treatments are associated with. It is well known that the presence of water in walls is the root cause of numerous problems such as mould growth, freeze-thaw spalling and reduced thermal insulation [**10**] [**11**] [**12**]. Keeping the wall dry is therefore crucial in combating these problems. Possible benefits include reduced maintenance costs, relieving health problems that occupants may develop, while helping to meet carbon dioxide targets [**13**] [**14**] [**15**].

Silane/siloxane emulsions have been commercially produced for several years, and may be considered relatively novel compared to solvent based alternatives; however

during this period little improvement or innovation has taken place in this field. Unlike coatings, these treatments penetrate deep into the substrate reducing problems associated with chipping of the barrier protecting the substrate. The scope of this study is to develop nanoparticulate enhanced silane/siloxane emulsions for retrofit and heritage applications. Once developed, the nanoparticulate enhanced treatments will then be characterised and evaluated through a variety of systematic and applied studies to determine whether such treatments would be practically beneficial. For the reasons given earlier, major areas of assessment include thermal insulation, water repellent characteristics, and biofouling resistance. Furthermore, a simple yet effective route for nanoparticulate incorporation is required for commercial viability and thus also a key requirement.

An area this study focuses on to achieve these aims is photo-induced sanitisation through nanoparticulate incorporation. Photo-induced sanitisation has been achieved by many commercially available coating products, photo-catalyst materials breakdown contaminants through peroxide formation by light and moisture presence at the coating surface. This reduces the contaminants adhesion to the surface, allowing contaminants to be removed more easily through rainwater run-off. It is expected that the small size of nanoparticulates may allow light to pass through the treatment reducing facade aesthetical alteration while providing photo-induced sanitisation. The treatment developed therefore should not alter the aesthetics of the building facade. Current titanium dioxide enhanced paints may reduce fouling through 'self-sanitisation', however these impose limits on the facade being coloured white due to the high concentrations of metal oxide present [**16**] [**17**]. In addition, these coatings are not effective at relieving internal humidity as they block pores and do not address problems associated with rising damp.

Silane or siloxane based emulsions for masonry treatments, and nanotechnology in colloidal systems are not new fields respectively. However, combining both and specifically with nanoparticulates that provide photo-induced sanitisation, may be considered a virgin field. Furthermore, these new treatments should be safer than solvent counterparts, reducing human, animal and environmental exposure to biocides and hazardous materials [**18**].

Chapter 2: Literature Review

2.1 Substrates

2.1.1 Overview

This study assessed treatments on what was considered three relevant substrates for UK building remediation; brick, mortar, and terracotta roofing tiles. In this section only these substrates and their constituents are mentioned in detail. A brief reference to timber is given due to its use inside UK buildings and the decay mechanisms associated with poor facade protection.

2.1.2 Bricks

Bricks are made from clay however properties may vary widely due to composition and processing. Three types of clay are available; surface clays, shales, and fire clays. These clays all have similar chemical compositions however have different physical characteristics. All of these clays are composed of alumina and silica with different amounts of metallic oxides. It is these metallic oxides that are the flux and allow sintering to occur. The sintering temperature is dependent on the lowest melting point material which in the case of clay is the metallic oxides. The flux material could be thought of as the matrix material with the alumina and silica being the reinforcement [**19**].

2.1.3 Ceramic Roofing Tiles

Berdahl [**20**] reports that biological growth such as bacteria, algae and fungi may be aided by pollutants soiling the tile substrate. Soiling by pollutants such as fly ash and soot may chemically bond with the calcite inclusions causing chemical deterioration. This soiling may increase water retention and organism adhesion to the substrate, aiding microbiological attack by increased enzyme transportation and hydraulic action. Reducing water and soiling of the tile would retard this degradation while also reducing freeze-thaw exfoliation and aesthetical hindrance [**20**]. Berdahl mentions also that wind may exert more force than conventionally considered, producing in conjunction material fatigue and crack formation over time through vibrations [**20**].

Ranogajec states that wet and freezing resistance of a ceramic roofing tile is of paramount importance with respect to the longevity of the tile. Ranogajec continues by mentioning that CaO from $CaCO_3$ decompositions in the material with the addition of pollutants and water are also a key contributor to tile failure [**21**]. Ikeda states that

frost damage from freeze-thaw exfoliation is closely related to pore size which in turn is related to the water absorption capacity of the roofing tile. Ikedas' work examined the effect of temperature on fracture toughness and fracture stress of the ceramic using a four point bend test of samples fired at different temperatures. It was found that fracture toughness and fracture stress was increased with firings up to 1100°C and attributed to pore size reduction due to the increase of glassy matrix impregnation of the particulate reinforcement. Above this temperature up to 1200°C a reduction of fracture stress was observed. It was concluded that higher temperature firings would increase frost resistance [**22**].

2.1.4 Sand

Sand is used as a fine aggregate in concrete, screeds and mortar. Sand typically has the composition shown in Table 1. Sand is considered a granular material comprising of mineral and/or rock particulates [**23**]. Exploitation of river sand has lead to other alternatives including offshore sources being used in its place; which may have elevated Cl ion content that could influence carbonation [**24**].

Table 1: Typical chemical composition of sand [25**]**

	SiO2 (%)	FeO (%)	Al2O3 (%)	CaO (%)	MgO (%)	K2O (%)	Na2O (%)
Ordinary Sand	86.55	0.98	9.74	0.96	1.09	_	_

2.1.5 Cement

Cement in general is considered a binder and is used in many different applications such as; concretes, mortars, and screeds [**26**]. Portland cement and water produces calcium-silicate-hydrate gel (C-S-H) the binder in concrete and calcium hydroxide (quicklime). The cement reaction is conventionally given with the main constituent, tricalcium silicate [**26**];

$$Ca_3SiO_5 + zH_2O \rightarrow Ca_xSi(OH)_y\ .\ Ca_xSi(OH)_y\ .nH_2O + \left(3 - \mathrm{x}\right)\mathrm{Ca(OH)_2} \qquad (1)$$

Where;

- x is the Ca/Si ratio in the gel which is typically 1.65.
- y is the number of the hydroxyl groups.

- n is the interlayer water content, which depends on different environmental factors.

2.1.6 Concrete

Concrete is the most widely used construction material in the world with exponential growth of its production. Concrete comes in two common forms, reinforced and unreinforced. Rebars are typically used to help produce more complex structures. The main constituents of concrete include sand, cement, and aggregate [**27**].

New emerging aggregates such as fly ash and reclaimed materials such as brick and glass also require consideration when designing treatments. Kou shows that glass aggregates are viable in concrete products and allow for waste mixed glass to be effectively recycled [**28**]. Fly ash has been shown to provide larger interfacial area in concretes increasing performance characteristics [**29**] [**30**]. Siddique concluded the use of up to 50% fly ash as a viable partial cement replacement in precast and reinforced cement concrete [**31**].

A major problem with reinforced concrete (RC) is the corrosion of the reinforcement [**32**]. Typically steel rebar is used to reinforce the concrete and this can corrode fast in some environments. In marine applications the RC may be corroded by chlorine induced corrosion which significantly reduces the structures service life. It is common practice to use a protective surface treatment to extend the service life for both new and existing structures [**33**].

There are three types of protective surface treatment used:

1. Surface coating: a thin or thick film is applied to the substrate.
2. Surface sealing: the pores are blocked internally.
3. Surface impregnation: the surface inside the pores is impregnated while still allowing the pores to be open [**33**].

Of the three types, the main ones used by the building industry are a silane based water repellent and sodium silicate pore blocker. Each one reacts with the hydrated cement phases and penetrates pores [**33**].

Surface preparation before treatment is important as in most cases debris will diminish the treatments ability to permeate [**33**]. UV, heat, moisture, and hygrothermal factors are also important aspects for the longevity of treatments. For

concrete UV degradation only occurs on the outer part of the substrate as UV radiation cannot penetrate concrete [**34**]. According to Vries water under a hydrophobic treatment should be allowed to evaporate freely to reduce damage from water-pressure build up or freeze-thaw exfoliation damage if the water freezes. Water-pressure build up behind a coating causes blistering, delamination at the substrate coating interface, and cracking depending on materials and conditions; impeding the coatings effectiveness to protect the substrate. Freeze-thaw exfoliation (spalling) is where trapped water freezes and can upon freezing, crack and chip the outermost substrate exposing a new surface for further spalling to occur [**34**].

Surface impregnation of un-cracked RC with silane has been proven to be a very successful method at reducing water permeation. Silane modifies the surface energy of pores, making them hydrophobic and due to their small molecular size, may penetrate deep into the substrate. However effective water repellent attributes depends on obtaining a deep penetration depth of silane greater than 5mm; reducing uptake potential through capillary action or potential to bypass the treatment to the hydrophilic portion of the substrate. RC structures impregnated before water exposure with a 2mm crack also relied on penetration depth; using a silane emulsion and gel based treatment produced a highly water repellent structure. If a crack is made after initial coating, the reinforcement has less corrosion than if uncoated, however secondary treatment was considered unavoidable in this scenario. It was also found that sodium silicate does not prevent water absorption or chloride ingress and hence cannot protect the reinforcement from corrosion [**32**] [**33**].

Hydrophobic treatment of concrete is not limited to protecting marine environments; a common problem is the use of de-icing salts on or near concrete structures which also causes chloride corrosion problems [**34**]. Vries states the structure of concrete to be composed of silicates and as both alkyl group silanes (CH_3) and silicates have a similar composition of silicon and oxygen, that they may chemically bond. Vries concludes that hydrophobic treatment of concretes reduces corrosion by chloride ions under de-icing salt conditions [**34**].

Carbonation is considered a major deterioration accelerator of steel rebar corrosion in cracked concrete (although all surfaces are affected) [**35**]. Carbon dioxide from the surrounding air especially in pollution rich air reacts with the hydration products of

the cement. This reaction causes a reduction in alkalinity and hence the concretes' ability to protect the steel reinforcement. Cracks may be formed through various means including improper curing or shrinkage when curing, or heat from hydration. When cracks are produced it allows the ingress of Chlorinates and CO_2 nearer the core which may aid in the deterioration of the concrete and reinforcement [**36**].

2.1.7 Timber

Felled trees are referred to as timber, and predominantly cut to standard sizes for building materials. Timber attributes include a high strength to weight ratio, ease of processing, abundance, relatively cheap, and a renewable resource, and other properties including aesthetics make it a prime building material [**37**]. Each tree species resist microbiological attack to a different degree, depending on their sapwood thickness, moisture content, structure and active agents which must be taken into account when testing timber decay resistance [**38**].

Weigenand wrote that the following effects may be responsible for high resistance of chemically modified wood against fungal decay [**39**]:

1. The reduction of moisture content.
2. The modification of cell wall polymers to become unrecognisable to enzymes.
3. A decreased micro-pore size in the cell wall.

Weigenand states that fungi require moisture to start colonisation and decay as well as that the moisture required must be above fibre saturation point. This is why many timber treatments are water repellents designed to keep moisture content below the timbers fibre saturation point [**39**]. The fibre saturation point is considered to be 25% to 30% for dry wood weight conventionally. Atmospheric water vapour typically ranges between 11% to 14% in dried wood, however fungal decay only starts at approximately 30% fibre saturation point. This means that the environment of the timber has the potential to affect timber decay [**40**] [**41**] [**42**].

2.2 Treatments

2.2.1 Overview

The bulk material most likely used for the coating is described below. Silicones and smaller molecules of the siloxane backbones called silane will constitute the oil phase of the product which will be complimented by a water phase for hydrolysis reaction when used.

2.2.2 Silicone

Silicone is an analogy based on ketones, and was conceived in 1901 by Kipping who first studied the newly found compounds based on the general formula R_2SiO. The term silicone is generally used to refer to polydimethylsiloxane (PDMS) although may be applied to Si – O backbone polymers (siloxanes) in general. Referring to Figure 1, methyl groups along the chain (R2) and terminations (R1) for PDMS may be substituted for many other groups e.g. phenyl, trifloropropyl, and vinyl to make very diverse siloxanes for a multitude of requirements. Hydroxyl, ethoxy and methoxy terminations may also be present and to varying degrees and configurations for networking and bonding applications. The organic – inorganic backbone of silicone attributes a multitude of properties suitable for a facade coatings including elastomeric durability though larger bond angles than hydrocarbon alternatives [**43**] [**44**] .

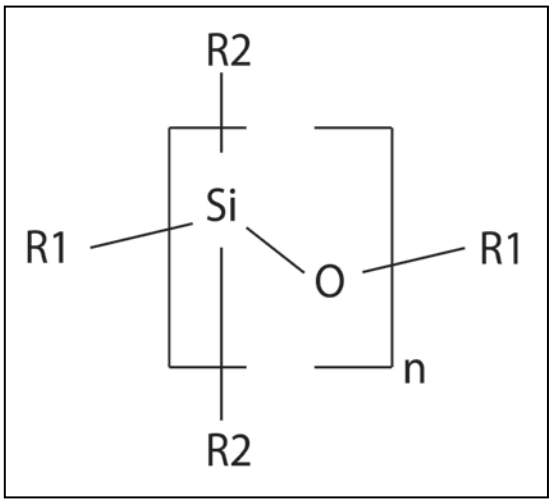

Figure 1: Siloxane chemical structure

2.2.2.1 Properties of Silicone

Since silicon is in the same period of the periodic table as carbon it is expected that similar molecular analogies could be made however this is not correct. Some molecules that do exist are analogies of the two; however these molecules react very differently with different characteristics. Bond lengths are longer for Si than C while Si – O have larger bond energy (452kJ/mole) with large bond angles allowing a highly stable and flexible polymer to be produced compared with a C – O bond alternative. In summary there are few similarities between the hydrocarbon and silicone based polymers [**43**] [**45**].

The inorganic part of the silicone chain imparts high surface energies and properties similar to silicates. Due to lack of side groups at the O sections a highly flexible polymer is possible. Due to the flexible siloxane backbone PDMS may produce a helical conformation allowing the methyl groups to form a hydrophobic surface and the oxygen backbone section a strong substrate bonding area [**43**].

Silicone organic copolymers can be created with surfactant properties, e.g. silicone glycol copolymers. Such silicone copolymers are useful for applications such as continuous ware contact lenses; requiring high moisture retention, contaminant wetting and oxygen permeability with low irritation. Such materials bio-mimetically imitate natural lipids present in the eye. Such high wetting behaviour and chemical compatibility with siloxane chemistry may be useful for emulsification in this study, while retained material after application may become part of the treatment, providing hydrophobic tendency; increasing the efficacy of the treatment to repel water [**47**] [**48**].

Polymer chains of PDMS may be cross-linked to form a three dimensional interpenetrating networks. PDMS has a high wetting characteristic allowing impregnation of most surfaces. There are many curing methods that may be implemented to facilitate curing, with this in mind, in theory a silicone formulation may be tailored to the environment that it is to serve in [**43**] [**49**].

2.2.3 Silane

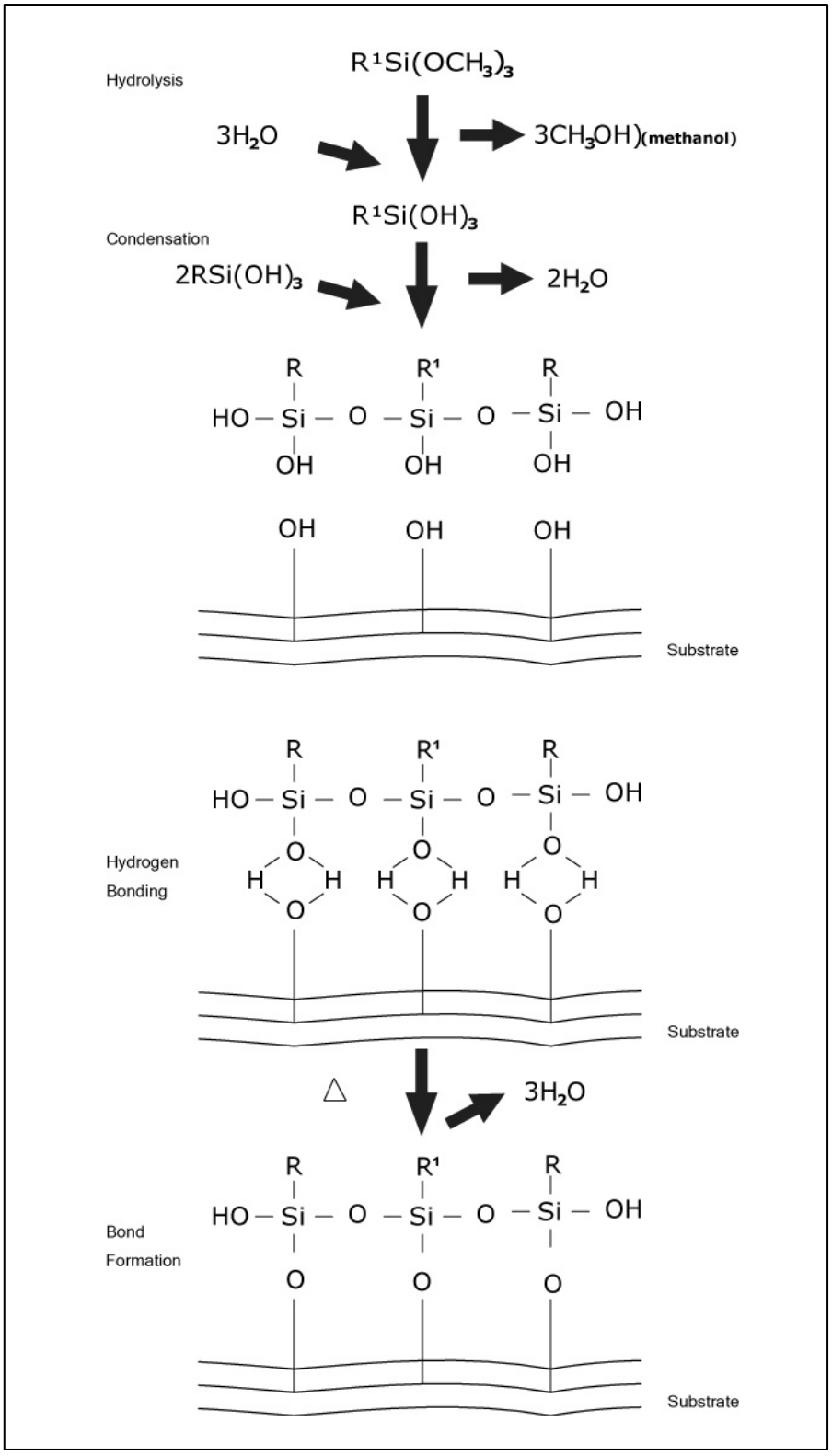

Figure 2: Diagram of alkoxysilane bonding on wood substrate [46**]**

Silanes are smaller molecules of siloxanes containing one silicon atom [**34**]. These materials are becoming more extensively used as part of hybrid products with siloxanes, being used to increase adhesion, crosslinking and hydrophobic properties in

their application [**50**]. Various functionalities are possible with silanes including terminations comprising of ethoxy, methoxy, amino, epoxy groups providing suitability in a multitude of fields including aerospace composite repair, composite sizing agents and textile hydrophobes. Alkoxysilanes first go through hydrolysis with water to form silanol, after which the silanol then goes through a condensation reaction to produce a networked phase (Figure 2) [**46**]. Reaction specific to this study is given below, 'R' denotes reaction to either silane functionality or substrate silicate active site [**51**];

[Octyltriethoxysilane] $CH_3(CH_2)7Si(OCH_2CH_3)_3$ + [Water] H_2O = [Silanol Condensate] $CH_3(CH_2)_7Si\text{-}OR_3$ + [Ethanol] CH_3CH_2OH

Silanes can migrate in coating formulations to the substrate interface which improves bonding during the curing process. Silanes, being small molecules compared to larger polymers used in treatment systems, have less inertia and thus the ability to wet the interface through greater kinetics for the same application energy. Silanes also do not need to unravel unlike siloxanes before bonding and thus requires less energy to have the potential to react under the same conditions. As these are hybrid materials which combine both organic and inorganic properties, they have the ability to react with the polymer and mineral phases. Bonds are considered to be re-hydrolysable, allowing for stress relaxing to occur at the interface and increasing adhesion and durability attributes of the coating. Silanes can also be produced with a range of functional groups allowing for a range of substrates to be treated [**50**].

Silanes and to some extent siloxanes evaporate especially when dissolved in alcohol solvents. To reduce this effect water-based systems such as micro emulsions are now produced to reduce this effect increasing the active content of the treatment available for retention after application [**34**].

2.3 Nanoparticulates

2.3.1 Overview

Nanoparticulates are <100nm in one or more dimensions and exhibit characteristics associated with their shape and composition. Properties imparted into composite materials containing such particulates may include very large increases in performance for small quantities of material [**17**] [**52**]. Performance of nanoparticles

is also typically dependent on how well they have been dispersed. The state of the art currently is more directed towards functionalising nanoparticulates for dispersion and designing new ways of viably applying and processing them, with synergistic behaviours typically achieved [**17**].

2.3.2 Titanium Dioxide

Titanium dioxide is the largest volume inorganic pigment produced in the world. It is typically used to produce white paints, papers, and used in plastic applications. Due to its high refractive index (2.76 rutile, 2.52 anatase) and uniform wavelength scattering products incorporating it appear white for relatively low concentrations, thus it is an effective colour extender [**53**]. However at smaller particle sizes such as 50nm and lower titanium dioxide allows light transmittance, and a white colour is not produced by light dispersion. A study by Bygott [**53**] shows that achieving a high degree of transparency with respect to crystallite size is offset by reduced UV absorption as well as other coating properties (shown by Figure 3). The cause for this is related to Rayleigh scattering; electromagnetic radiation at smaller particulate sizes may be scatted instead of absorbed due to wavelength and particle size characteristics. At larger particle sizes UV radiation is predominantly absorbed with less scattering occurring. In theory, to scatter UV radiation between 200nm and 400nm the optimised particle size is between 20nm to 40nm. Thus the reason why reduced particulate size could hinder photo-oxidation performance due to reduced UV absorbed for the process.

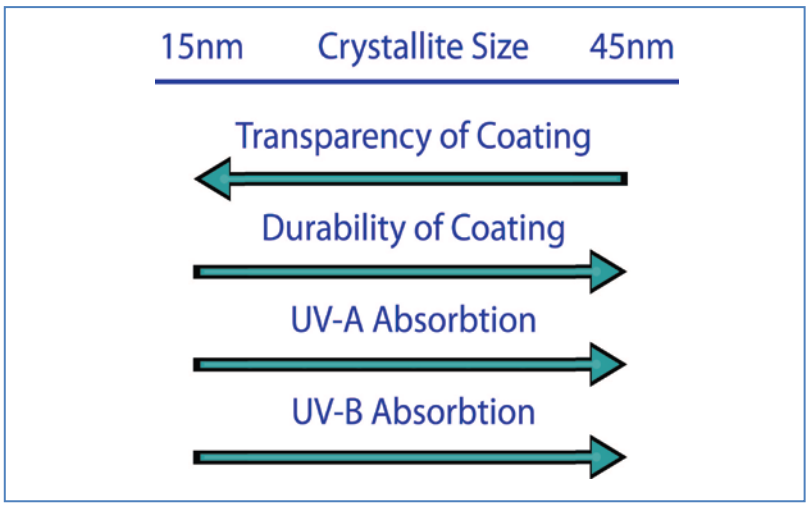

Figure 3: Summary of the effect of crystallite size on transparency and other general attributes of titanium dioxide enhanced polymers [53**]**

Titanium dioxide has photocatalytic attributes that allow the material to provide a self cleaning and self sanitising characteristic to the host material. Figure 4 shows that with the input of UV radiation, water, and oxygen hydroxyl and oxygen radicals are produced respectively. These radicals denature organic compounds by an oxidation reaction, providing self sanitising surfaces.

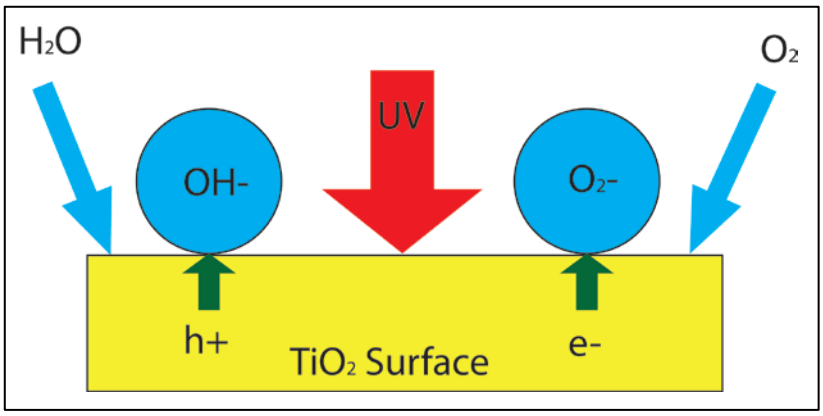

Figure 4: Photocatalytic process

The following equations show the photocatalytic reaction process:

$$TiO_2 + hv \rightarrow {e_{CB}}^- + {h_{VB}}^+ \quad (2)$$

$$H_2O + {h_{VB}}^+ \rightarrow OH^- + H^+ \quad (3)$$

$$O_2 + 2{e_{CB}}^- + 2H^+ \rightarrow H_2O_2 \quad (4)$$

Figure 5 shows the photocatalytic property of titanium dioxide and how it affects the hydrophilic nature of the surface that contains it. It is considered that the production of a unified water film allows for superhydrophilic characteristics to be obtained, which prevents adhesion to the inorganic and organic components of the surface and therefore retains a clean surface on the photocatalyst.

If the effect of the photocatalytic process for microbiological degradation is considered in conjunction with the superhydrophilicy then a coating containing such particles could breakdown pollutants and provide a transport system to remove such matter [**17**] [**52**] [**54**] [**55**].

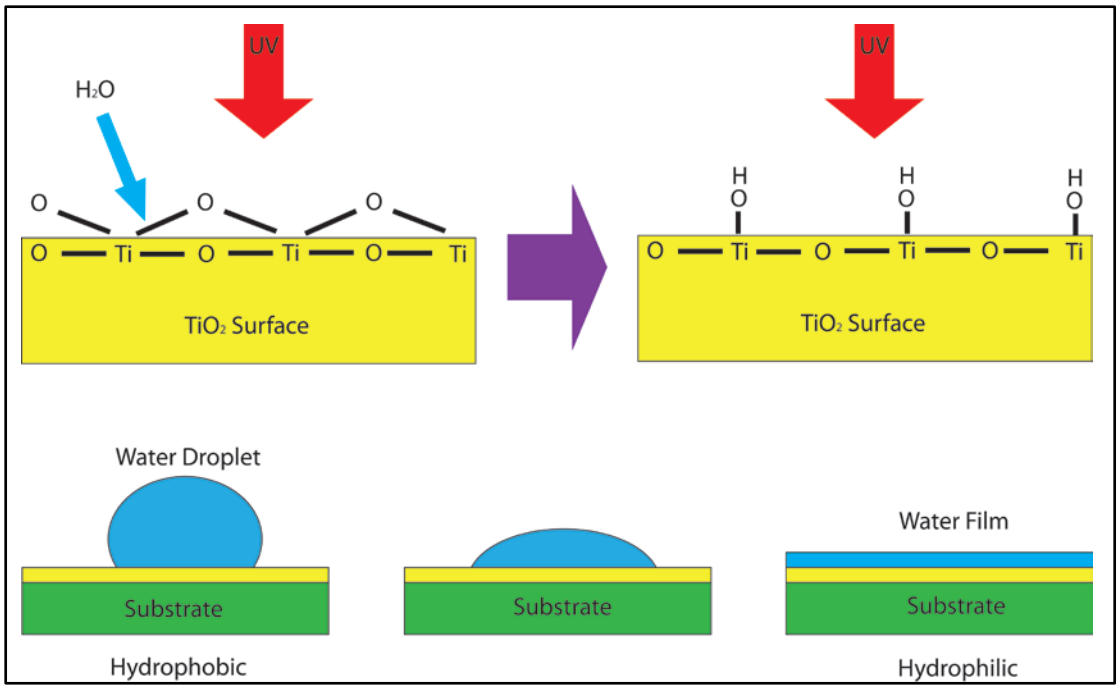

Figure 5: Photo-induced superhydrophilicity

Figure 6 (modified from [**56**]) shows the UV absorbance characteristics of anatase titanium dioxide and zinc oxide photocatalysts respectively. Solar UV radiation experienced by the Earth can be divided into three prevalent wavelengths. UV-C has a spectral range of 100-280nm, but does not reach the surface of the Earth as it is absorbed by the o-zone and other atmospheric components. UV-B has a spectral range of 280-315nm and although reaches the Earth's surface most of it is absorbed by stratospheric o-zone. UV-B alters DNA, causes sunburns, cataracts and melanoma. Conversely UV-B also is used for the production of vitamin D which helps bone development and prevention of certain types of cancer. UV-A with a spectral range of 315-380nm is less energetic while also the least absorbed of the three by the atmosphere. Recent studies have also shown that UV-A damages skin and eyes, causing wrinkles and photo-ageing [**57**] [**58**] [**59**]. Figure 6 shows that titanium dioxide has more pronounced absorbance characteristics than zinc oxide over the UV-A range and due to UV-A having the most influence at ground level, makes titanium dioxide more effective as a photo-catalyst.

In general, it may be considered that photo-induced oxidisation occurs above the band-gap energy requirement of the photo-catalyst. Since titanium dioxide has a better matching band gap compared to zinc oxide to natural radiation at the earth's surface it may be considered more appropriate for facade sanitisation [**53**].

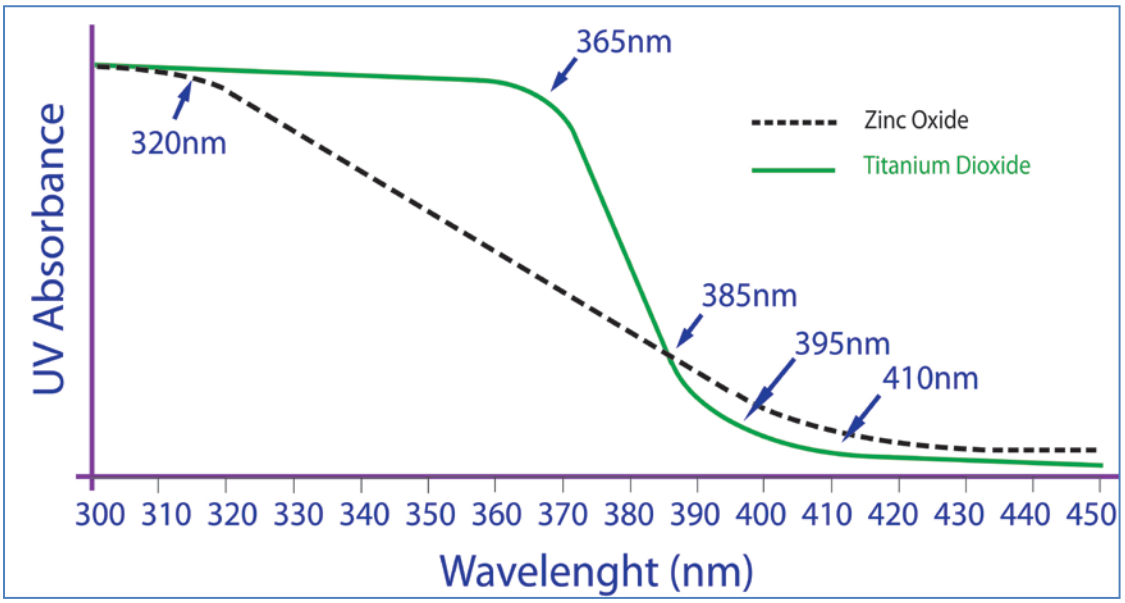

Figure 6: UV absorbance spectroscopy of anatase titanium dioxide and zinc oxide photocatalysts [56**]**

2.3.3 Zinc Oxide

Zinc oxide blocks both UV-A and UV-B radiation unlike titanium dioxide and is used in similar products due to this characteristic. UV incident energy is absorbed and then reflected as heat through crystalline excitation. Zinc oxide has this ability unlike titanium dioxide for lower wavelengths due to its wider band gap (3.37eV) [**60**] compared to titanium dioxides (rutile; 3.05eV, anatase; 3.26eV) [**61**]. Zinc oxide is also known for its fungicidal tendency [**17**].

Hegedus [**62**] states that although polymers such as polyurethanes and acrylics resist UV degredation, they do not protect the substrate from degradation. This is an important concept to grasp when dealing with the current study. Traditional organic UV absorbers may migrate out of the coating while also being susceptible to degradation due to their organic nature. These organic stabilisers may include benzophenones [**63**], hydroxyphenylbenzotriazoles [**64**], and hindered amine light stabilisers (HALS) [**65**]. As zinc oxide is inorganic and a particulate they are considered more stable and have less inclination to migrate compared to smaller organic molecular alternatives, offering increased efficacy and hence coating longevity. Hegedus also found that zinc oxide showed both chemical and humidity

resistance when tested at 4wt% to 7wt% incorporation in a polyurethane – latex hybrid coating (ZnO ~50nm) [**66**].

Ju-Nam explains that small quantities of ZnO did not induce cellular damage when tested. However damage was seen above 0.016M. Research showed that ZnO nanoparticles did not have to enter cells to cause damage to the cell membrane. Ju-Nam continues in stating that although ZnO covers a larger UV band but TiO_2 is used in its place for many applications as it has a greater photo activity. Ju-Nam also states that it is harder to find TiO_2 with highly crystalline structures in the rutile form compared to anatase [**52**].

2.4 Essential Attributes for Treatments

2.4.1 Water Repellence

In general, studies on a variety of interfaces comprised of many diverse materials have confirmed that a combination of nano-scale and micrometer-scale roughness and a low surface energy substrate allows for water contact angles greater than 150° to be achieved and are generally considered self cleaning super hydrophobic materials [**16**] [**67**]. Specifically, relating to the photo-induced oxidisation effect (Honda-Fujishima effect) achieved by materials such as titanium dioxide and zinc oxides in various studies, it is the exposure of the interface to UV irradiation or absence thereof that controls the surface energy through the (reversible) re-arrangement of the crystalline structure. In addition, ambient uptake of moisture from the surrounding environment stabilise areas of the structure which have been affected through oxygen removal during the photo-catalytic process; increasing the hydrophilic tendency at the interface. This absorption is not uniform over the crystalline interface due to the sites were oxygen is present and absent in the structure, as well as local UV influence on rearrangement of the structure. Therefore, depending on UV exposure and environmental conditions, the water contact angle of the interface may vary to a high degree [**68**] [**69**] [**70**].

There are two conventional models for water beading; the Cassie-Baxter model is a water drop modelled on top of columns, whereas the Wenzel model is of the water drop inside the gaps between the columns. These models describe hydrophobic and hydrophilic materials respectively. Assuming modelling of roughness of the surface is

being produced by square pillars, the following formulations may be used to express the contact angle (CA) [**71**]. See Figure 7 for visual representation of the model.

For the Wenzel model (homogeneous wetting) [**72**]:

$$cos\theta_r^w = r\cos\theta_e = \frac{(a+b)^2 + 4aH}{(a+b)^2} cos\theta_e \quad (5)$$

For the Cassie-Baxter model (heterogeneous wetting) [**72**];

$$cos\theta_r^c = \emptyset_s(cos\theta_e + 1) - 1 = \frac{a^2}{(a+b)^2}(cos\theta_e + 1) - 1 \quad (6)$$

Where:

θ_e & θ_r^w is the CA on smooth surface and on rough surface respectively.

θ_r^c is CA on rough surface.

$\emptyset_s$: the empty set.

a: radius of columns

b: pitch between columns

H: height of columns

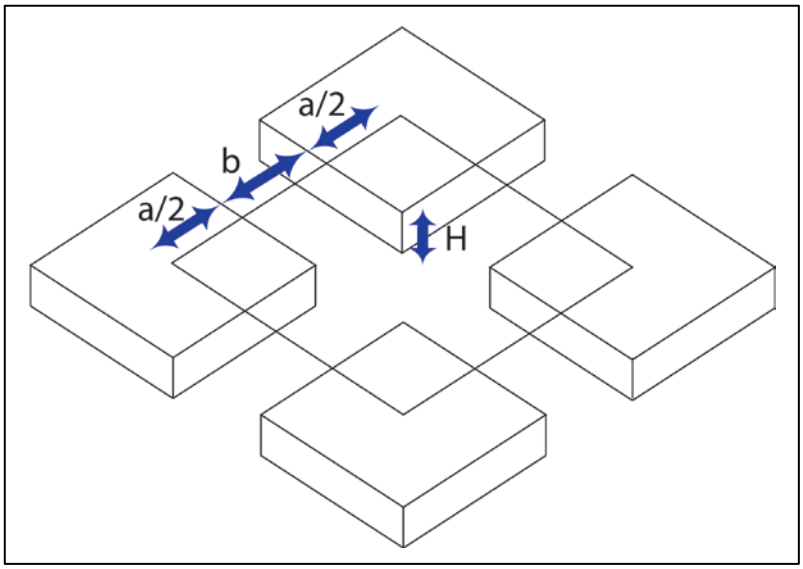

Figure 7: Theoretical diagram of surface roughness with relation to both Wenzel and Cassie-Baxter models. [Modified from; [72]]

There is a sharp transition from the Cassie-Baxter model to the Wenzel model at a pitch/size ratio of 20. This means that there is a low probability of achieving a material with a water droplet contact both on top of the columns and in the recesses

[**73**]. It should be noted also that both micro and nano scale architectures were observed on insects, showing that the two roughness levels may be used to modify the surface structure to create effective columns [**72**]. Recent superhydrophobic surface models have implied that the air between columns in the Cassie-Baxter model aids droplet suspension. Yamamoto's modelled results show that an increase in height exponentially increases contact angle potential. Depths of 15µm and greater seem to be required for superhydrophobic materials. A canal width of 6µm and below exponentially increases CA properties. Yamamoto states it is the vibration energy that is the determining factor for the slipping angle and not hysteresis (the memory of the water drop) [**74**].

2.4.2 Superhydrophilic vs. Superhydrophobic Materials

Materials that can provide a water contact angle (WCA) of greater than 150° are of interest and termed superhydrophobic. WCA's greater than 150° allows for the material to have a low sliding angle and self cleaning properties. It should be noted that both parties mention 'sticky drop', a phenomenon whereby the drop sticks to the rough surface and challenges the Cassie-Baxter model which conveys that high roughness implies low sliding planes [**75**] [**76**] [**16**].

Interest has been shown in using these materials in antifouling paints for marine applications, snow-repellent for masts and aerials, self cleaning windshields, windows and facades (to reduce soiling degradation) chemical resistant textiles for the military, and anti-fogging glasses and mirrors [**76**] [**77**]. Ma states in his paper that the lotus does not use lower surface energy groups as part of the hydrocarbon waxes secreted on the surface of the leaf such as CH_3 or fluorocarbons to produce a 160° WCA with nil sliding angles; instead it relies on epicuticular wax crystals that contain predominantly CH_2 groups to reduce the waters contact area. It is therefore the surface topography that dominates the physio-chemical influence on wetting, very low surface energy is therefore not required to produce a hydrophobic material. If a tea towel is considered, water beads are supported on peaks made by OH groups, by air. Ma describes the lotus leaf as having protruding nubs of 20 to 40µm apart, each covered with wax crystalloids. He also states that when UV irradiates ZnO surfaces, OH sites are provided, allowing a superhydrophobic material to become a superhydrophilic material, and when deprived of UV radiation returns to being a superhydrophobic [**16**].

Zhou states in general that in order to produce a surface with a contact angle (CA) greater than 150°, the surface topography must be controlled and of a hydrophobic material. Zhou continues to say that a superhydrophilic material with a CA of less than 5° may be made by providing either two or three dimensional capillaries of a hydrophilic material [**78**].

Song reports that cetyltrimethyl ammonium bromide, a cationic surfactant may be used to increase the surface roughness of a titania sol-gel films. Song continues to state that sodium dodecylbenzenesulphonate (DBS), an anionic surfactant was used to modify titanium dioxide to enable dispersion and alter the optical performance [**55**]. It is the opinion of the writer that this may decrease the photocatalytic performance of the material as it is understood that water is required for radical release from the substrate as well as UV radiation to provide a self cleaning material, however water vapour may provide the same effect.

Nimittrakoolchai states that the lotus leaf has a double scale roughness with 10µm protruding nubs. 10-30µm distance between nubs with wax crystal caps of between 0.2 to 2µm. Hu reports that 2µm precipitated calcium carbonate particles coated with fatty acid (stearic acid) produced a WCA near 150°, which shows viable passing over of column size [**79**] [**80**].

Xu created a dual roughened surface by combining SiO_2 particulates and ZnO nano rods for textile substrates. Silane (n-dodecyltrimethoxysilane) was used as the capping agent. This method is of interest as the substrate did not have to be altered. [**81**].

Wei prepared a composite column structure to mimic the nubs of the lotus leaf. The result is a material with 154° CA and 5.8° sliding angle, which is less than a lotus leaf. The paper discusses Cassie composite model and concludes that the material created has 89.5% air occupying the contact area [**82**].

The Cassie composite model:

$$\cos\theta_r = f_1 \cos\theta - f_2 \qquad (7)$$

$\cos\theta_r$: CA of composite surface

f_1 : fraction of solid surface

f_2 : fraction of air

$(f_1 + f_2 = 1)$

Lakshmi reports that a sol-gel using cheap, nontoxic superhydrophobic materials may be achieved using zinc hydroxide in a TEOS & MTEOS matrix. TEOS may be used on its own but is reportedly not scratch resistant. The composition of the sol is given and shows that a low sliding angle and high CA (up to 165°) may be fabricated. The composition was then applied to glass substrates [**83**].

Nimittrakoolchai produced SiO_2 nanoparticulates with a low surface energy semi-fluorinated silane treatment via the sol-gel process on a substrate etched before coating. The film was superhydrophobic, optically transparent with low surface energy [**79**]; it is of interest as most surfaces don't need to be etched to produce the roughness required.

2.4.3 Rising Damp

Rising damp is a key degradation route for buildings that have a compromised or missing damp proof layer. Rising damp is the process whereby water from the ground rises through a structure through capillary action. Jurin's Model may be used to assess the height rise due to capillary action, *h* [**84**];

$$h = \frac{2\gamma \cos\theta}{rpg} \qquad (8)$$

Where; γ is the surface tension, θ is the water contact angle, r is the capillary radius, ρ is the liquid density, and g is the acceleration due to gravity. However, the Jurin model does not take into account evaporation from a wall, thus the Sharp front model may give a more accurate representation of rising damp height rise. The Sharp front model may be used to calculate the height rise of the damp front and is stated as follows [**85**];

$$H = s\left[\frac{b}{2e\theta}\right]^{\frac{1}{2}} \qquad (9)$$

Where H is the height of the rising damp front, s is the sorptivity (suction of water into substrate), b is the wall thickness, e the rate of evaporation per unit area of the wetter surface, and θ is the moisture water volume fraction of the wetted region. From the Sharp front model it is clear that sealing a building with a conventional coating would thus reduce the evaporation which reduces the height rise. From this model it

may be seen that sorptivity has a large influence on height rise as does the wall's thickness, which reduces the available area for evaporation.

2.4.4 Antifouling

2.4.4.1 Overview

Fouling of a facade may be classed as two main categories; organic and inorganic fouling. Fouling may cause various problems such as 'sick building syndrome' (SBS), a problem for occupants which cause various problems to their health and wellbeing [**86**]. Usually this is due to fungi spoor release, outgassing caused by building materials containing VOCs and inadequate air supply. Thus, most of these problems may be diminished by appropriate implementation and maintenance of heating, ventilation, and air conditioning (HVAC) within the building [**87**] [**88**] [**89**]. Those treatments which allow a structure to passively balance internal humidity with the external environment would be preferable while having the added benefits of being a treatment instead of a coating [**90**].

2.4.4.2 Inorganic fouling

Inorganic fouling is from sources such as waste incineration, road pollution as well as engine pollution which may deposit on facades over their service life. Fly ash, mineral deposits and salt efflorescence are also rife. Sources for such fouling are diverse and depending on compositions, allow chemical bonding to occur. When porous materials dry out with a high enough pore salt solution content, the salts crystallise (efflorescence). If crystallisation is restricted by the morphology of the pore, damage may occur and become exacerbated by repeated cycles until the material fails. Salts encountered during this process include chlorides, sulphates, nitrates, and predominantly carbonates [**91**] [**92**].

2.4.4.3 Organic microbiological fouling

The microbiological field encompasses a large array of organisms, including; viruses, bacteria, fungi, and parasites. Of these fungi are of the most interest when considering treatments for inorganic substrates as they may be considered the most damaging through biodegradation. Fungi include lichen and may cause deterioration to masonry materials, usually with the help of bacteria acting in a symbiotic relationship [**93**] [**94**]. Fouling may also come from algae, mosses and liverworts [**95**] [**96**]. Parasites secrete enzymes and mechanically degrade substrates. This process is similar to most

fungi, which secrete enzymes and use water as the transport mechanism to bring back enzymes and nutrients [**97**]. As with fungi, moisture is favoured for insects to grow, without it these degradation processes are not feasible [**92**].

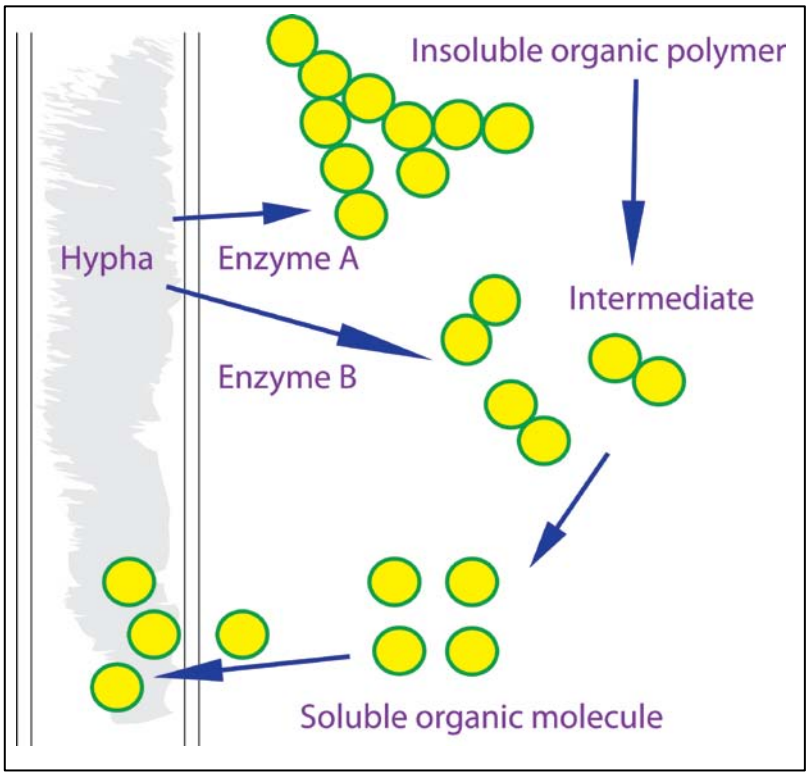

Figure 8: Fungal nutrient absorption process [97**]**

Figure 8 shows the process by which fungi expel enzymes to break down organic molecules for nutrients. It must be noted that a high moisture environment is required to enable enzyme and organic molecule transportation from and to the hyphae respectively [**97**][**98**] [**99**]. Since better knowledge of microbiology and degradation mechanisms is known, reported degradation of structures by parasites and fungal organisms has actually declined. Serpula Lacrymans, one of the main dry rot fungi (Basidiomycetes) has been found more and more rarely, implying that remediation and knowledge of how to build appropriate structures is helping situations [**100**] [**101**].

However, structures that contain dry rot spores for example are notoriously difficult to remediate. Such spores are approximately 5 to 10µm in diameter, and weigh approximately1.10^{-11}g [**100**] [**101**] allowing air or water dispersion throughout a structure. Due to xylem and phloem acting as channels in wood such as pine, boarded pits allow for cross channel movement, allowing free movement of spores and hyphae

[**92**]. It has been found however that if a structure is dry, enzymes cannot be used to breakdown and gather nutrients, thus the fungi goes into hibernation; for Serpula Lacrymans this may be as long as 10-12 years [**100**]. Of course, if there are wet periods then survival time could be significantly more.

In should be noted that lichens in conjunction with bacterial colonies degrade external facades. Commonly cracks appear due to spalling caused by water ingress, this then allows organic matter in and increases water retention. Organic matter may also retain water accelerating degradation of the substrate. Prior work has shown that these fungi and bacteria get nutrients from the substrate through this process [**102**].

In addition to these materials, mosses, hornworts and liverworts (Bryophytes) may grow in very high water content areas. Bryophytes are usually found next to streams and on the edges of wetlands, however mosses are also found in desserts and across the Arctic Circle [**96**]. Since these are not of primary concern for facade remediation and protection due to their marginal impact on facade degradation they have been omitted, for further reading [**96**].

It seems therefore reasonable that a dry structure is preferred with no cellulose or masonry hydroxyl groups available for hydrolysis and oxidation by secreted enzymes. Since water repellent emulsions may reduce the number of hydroxyl groups as well as repelling water from the substrate, this may be beneficial for reduced organic fouling [**39**] [**102**] [**103**] [**104**].

Algae like most of the organic soiling matter mentioned have a considerable resilience allowing it to survive in harsh conditions. Algae can be microscopic single cells to 30 meter brown algae called kelps [**96**]. Like other soiling matter, removal of the environmental conditions required for growth and propagation would limit its propagation on a facade, conventional paint will limit water and algal ingress and significantly reduces its retention by a facade although it does not stop growth [**105**].

2.4.5 Toxicological Responsibility

Treatments must be effective at removing contaminants but should pose minimal harm to the health and the environment. Toxicology of a treatment throughout its life cycle will have different toxicological mechanisms. Possible leaching and degradation of such treatments and its impact on different ecosystems need to be looked at.

Conversely it would be ludicrous to imagine that exposure to nanoparticulates in everyday scenarios as not occurring or having influence on health. Exposure includes nano-sized dust from fields, pollutants from combustion engines, and waste incineration [**103**]. Halloysite clays and asbestos are also naturally occurring nano-minerals that may be encountered. Due to the millimetre elongated asbestos particulates and small cross-sectional area it allows this material to pass protective systems in a human and allows it to lodge in lungs; causing possible carcinogenic influence to surrounding cells. However when incorporated into cement it may make an effective insulative panel for roofs, providing reinforcement as well as fire resistance [**104**]. Thus, the material must get to the effector site in order to produce an effect. For example, 1L of alcohol in a bottle will have little influence on a person, however, if it is consumed then it can reach effector sites.

The European biocidal products directive (98/8/EC) currently being produced will constrain biocidal products. Titanium dioxide and zinc oxide are known active semiconductor photo catalysts and have been used to breakdown organic and inorganic environmental pollutants. The European directive allows materials to be sold that contain biocides however a large amount of information is required for each biocidal product including, case studies (if any), risk assessment and life cycle analysis of such additives. The drawback with nanoparticles is that little information may be provided as well as having different mechanisms and toxicity levels than larger equivalents. If accepted that the products for sale are agreeable to the terms levied in 98/8/EC then additional annual payment to the council must be met [**105**] [**106**] [**17**].

The mechanisms that are used for toxin delivery and toxin life cycle influences are still an uncertainty. Impact of toxic materials and their mechanisms is largely theoretical and based on probable cause, which in turn may be based upon clinical trials and case studies. Thus assessing risk associated with exposure routes, complexing and retention within organisms by xenobiotics becomes exceedingly difficult. Models produced therefore share all the problems associated with theoretical models [**107**].

Generally silanes and siloxanes as well as surfactants have been extensively tested and it may be considered that toxicology levels that are socially accepted have been

met by such scrutiny. However the state of the art shows that there has been considerable conjecture on the matter with little definitive information about nanoparticulates. It therefore makes sense that these are evaluated in this section and must be evaluated within the context of the treatments they have been proposed for. This area is a new direction for these particulates, bases of assessment has to be on fields where exposure is prevalent. Thus the following has been based on dermatological and exposure route studies. Methods of cell ingress include; diffusion (passive), osmosis (passive), facilitated diffusion (active), active transport (active), particle movement across membranes [**108**] [**109**]. Figure 9 shows the levels that toxicity is presently studied at and the areas of interest when dealing with xenobiotic interaction [**107**]**.**

2.4.5.1 Immunotoxicology

Both titanium dioxide and zinc oxide are known to cause irritation to the respiratory tract. Inhalation of these particles in the form of fumes or dust is a common exposure type. Excessive exposure is known to cause obstructive lung disease. Stepwise methods to treat this include; elimination of irritants, remedy infections, steroidal medicine, artificial ventilation, and finally transplantation [**110**]. It should be noted that lung defence mechanisms such as mucus and its progression to the throat is useful for the reduced exposure by these types of particulates, after which the material is excreted. Conversely nasal hair for nanoparticulates becomes less effective at blocking particulate transport to the lungs. This evasion of the body's natural defence mechanisms is also of major concern for other methods of ingress.

A major problem with nanoparticulates regardless of the exposure mechanisms is their size. They have much larger surface areas than larger particulates per unit mass. Particle toxicity is determined by its surface reactivity and therefore these particulates should in addition to their evasive nature cause significant concern [**111**].

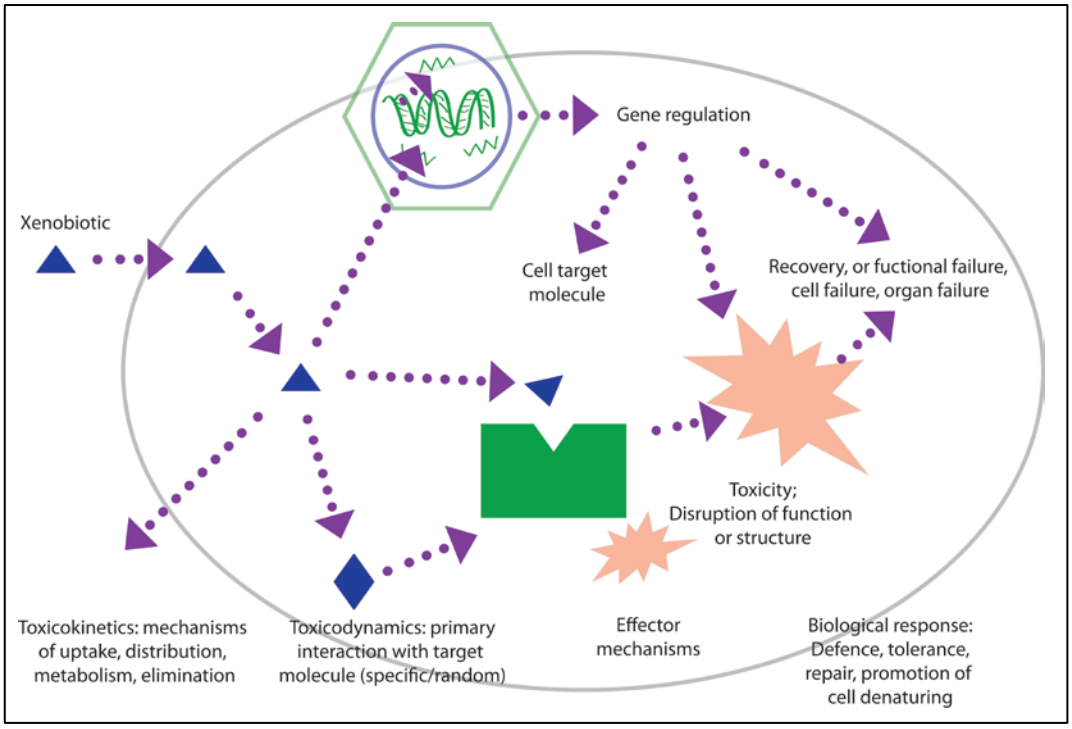

Figure 9: Levels of toxicity study [modified from [107**]]**

Dermatological ingress is also of interest. Newman et al. [**111**] conducted a review of various dermatological studies with regard to skin exposure. The purpose of the study was to assess the toxicological problems associated with particulates in sunscreens. Various studies focused on the penetration of particulates using different mammalian skin. It was found that photo-mutagenic capability of such treatments to alter DNA through the formation of reactive oxygen species with UV light was a problem if particulates could penetrate the epidermis. It was concluded from various study assessment that these particulates could not penetrate this layer and remained on the skin surface and outer layer. The smallest nanoparticulate assessed was ZnO at 20nm, and since no dispersion information as well as aggregation of particulates was given in these studies it is still unclear whether smaller particulates can be considered safe for use in sunscreen applications. In addition, to this it could be considered that nanoparticulate content and exposure to water repellent emulsions as well as the cured treatment would be significantly different.

2.4.5.2 Toxicological Regulation

Since the greatest extent of work on nanoparticulate risk on health has been carried out using dermatological studies it seems prudent to use this as the benchmark to assess regulation within the nanoparticulate community. After all, exposure to these

types of treatment would be largely due to application of material onto a facade, so skin contact would seem reasonable in this state. Exposure would also be due to breathing in the emulsion's water based vapour and day to day exposure of the cured treatment due to inhalation. However, possible exposure would occur during the manufacturing process and the disposal of these materials.

In 2006 the European Union (EU) and Australian cosmetic regulatory bodies reviewed the scientific literature and concluded; "there is evidence from isolated cell experiments that zinc oxide and titanium dioxide can induce free radical formation in the presence of light and that this may damage these cells. However, this would only be of concern in people using sunscreens if the zinc and titanium penetrated into viable skin cells. The weight of current evidence is that they remain on the skin surface and in the outer dead layer" [**111**].

In 1999 the Food and Drug Administration (FDA) made a decision to use these particles in sunscreens without new safety assessments based on previous assessments conducted on larger particles. This however was called into question by group of public interest organisations led by the International Centre for Technology Assessment in 2006. A legal partition filed against the FDA demanded amendments to its regulations with regard to nano-materials in consumer products. In 2007 the FDA implemented a new division to assess the scientific and regulatory challenges faced with the growth of nanotechnology [**111**].

On the matter of health and environment regulation of nanoparticulates in general, the EU has argued that; "precaution has already become a principle or customary rule of international law" although output may vary in both interpretation and local legislation [**112**]. In regard to new product regulation a new directive to combat unknown materials (not specific to nanoparticulates) came into force in 2007. The directive called; Registration, Evaluation, Authorisation and Restriction of Chemical substances (REACH) (EC 1907/2006 200b) [**113**] is designed to improve protection of human health and environment through earlier and better identification of intrinsic properties of chemicals. Interestingly it also calls for the substitution of more dangerous chemicals with safer variants where applicable; following the established EU 'precautionary principle'. However due to this stance, error by conservative

classification could mean products considered dangerous when actually they are usable [**114**].

2.4.6 Heat Conservation

From prior study it has been found that moisture increases the thermal conductivity of bricks and mortar. By reducing water ingression by providing a suitable barrier heat should be better conserved [**115**]. Building energy regulations also known as building energy codes emerged in the 1970's and became an essential tool for improving energy efficiency. These codes help improve HVAC within buildings and therefore help reduce sick building syndrome cases [**116**].

2.5 Emulsions

2.5.1 Overview

The definition of what an emulsion is and does vary considerably such as those listed by Becher [**117**]. In general, an emulsion is a system consisting of at least two immiscible liquids [**118**]. More specifically emulsions may be classed as the following; macroemulsions, multiple emulsions, microemulsions, liposomes, nano-emulsions, and in-situ microparticle systems [**118**]. Due to their respective nature, these emulsions may be used for various and diverse applications. There are three types of emulsions of which oil in water (O/W) is of most interest for production of a silane/siloxane emulsion. Others include water in oil emulsions (W/O), and inverse emulsions where the original emulsion is inversed to produce typically a three phase system, such as (O/W/O). This inversion is typically carried out by slowly folding in the first emulsion with surfactant into the third phase.

2.5.1.1 Macroemulsions

Macroemulsions have relatively large droplets (greater than 0.1μm) which disperse light and therefore are turbid. Due to the droplet size, these systems are not considered thermodynamically stable as micelle structures are large (with more inertia) and more susceptible to interactions having more effect; collisions lead to coalescence and phase separation [**119**]. These emulsions are used in cosmetics as either an O/W (oil-in-water) or W/O (water-in-oil) emulsion system depending on its composition and application [**118**]. Since oil is unpalatable it makes sense that milk is an O/W emulsion, whereas moisture retention for dry skin is achieved by W/O lotions [**118**].

2.5.1.2 Microemulsions

Contrary to macroemulsions, microemulsions have relatively small drops (radius in the order of <100nm) they do not scatter light and therefore are not turbid and are considered thermodynamically stable [**119**]. In order to achieve such a low surface tension to produce these microemulsions before critical micelle concentration (CMC) solubility has been reached, an additional surfactant is used [**119**].

2.5.1.3 Multiple emulsions

If a standard emulsion is emulsified into another continuous phase then this is termed a multiple emulsion. Conventional emulsions produced are either O/W/O (oil-in-water-in-oil) or W/O/W (water-in-oil-in-water), although more complex systems have been reported. This allows for all the benefits of one emulsion within the other, such as creating super-moisturisers in cosmetics or providing prolonged drug release in medicines [**118**].

2.5.1.4 Liposomes

Liposomes are vesicular lipids with a diameter ranging between 50nm to a few microns. Various membrane structures may be created including structured micelles, allowing emulsions to be used as a drug delivery system with biodegradability [**118**].

2.5.1.5 In Situ Forming Microparticle Systems

In situ forming microparticle (ISM) systems are typically a specialist drug delivery system and not found in other applications due to difficult processing and lack of requirement. The precursor as a O/O (oil-in-oil) or O/W emulsion with biocompatible and degradable stabiliser and continuous phase is injected into a patient, forming microparticles with aqueous physiological liquids in situ within muscle or skin target areas [**118**].

2.5.1.6 Nano-emulsions

The term nano-emulsions is used regarding nano sized droplets ranging between 20-200nm and unlike microemulsions are not considered thermodynamically stable. They are not in equalibium or formed spontaneously and therefore conventionally require high shear dispersion to achieve these emulsions. The literature also identifies these emulsions as miniemulsions, ultrafine emulsions, submicron emulsions but the term nano-emulsion is preferred as it helps differentiate it from microemulsions [**120**].

2.5.2 Emulsion Principles

Due to emulsions being comprised of immiscible liquids, energy is required to disperse one phase in the continuous phase. However, unless emulsified properly these phases will separate due to different surface tensions and specific gravities. Emulsifiers act as a barrier between two phases, either physically or electrostatically. Emulsifiers include surface active agents (surfactants) that can be ionic (anionic or cationic), non-ionic or zwitterionic [**119**] [**118**].

Ramsden [**121**] was the first to observe particulate stabilised emulsions, which were then evaluated extensively by Pickering [**122**]. The role of particles as emulsion stabilisers has been extensively studied ever since, with a vast number of particulate-containing foams and emulsions having been reported and characterised [**123**]. The effect of particle addition strongly depends on a number of factors; chemical nature, concentration, wettability of the particle species, as well as their size. The latter is of particular importance as decreasing particle size strongly influences the properties of the emulsion [**124**]. In addition, hydrophilic particulates stabilise o/w emulsions, while w/o emulsions are stabilised by lipophilic particulates [**125**] [**126**]. A variety of nanoparticles have been studied in numerous emulsion systems and their effect on overall stability, oil droplet size, tendency to coalesce and rheological properties have been investigated [**127**] [**128**] [**129**]. In addition to surfactants and particulates, polymer stabilisers may be used to reduce problems with differences in phase densities as well as acting as an emulsifier [**130**] [**131**].

2.5.3 Surfactants

A surfactant is a 'surface active agent' that reduces the energy required to disperse two different phases in one another. Mixing oil and water for example, results in both phases separating quickly and returning to a lower energy state. If a surfactant is added such as a non-ionic surfactant which has a hydrophilic polar region at one end and a lipophilic region at the other, joining may occur at the interface, reducing tension and allowing for a more stable solution when mixed. There is a vast range available with different compositions and properties [**44**].

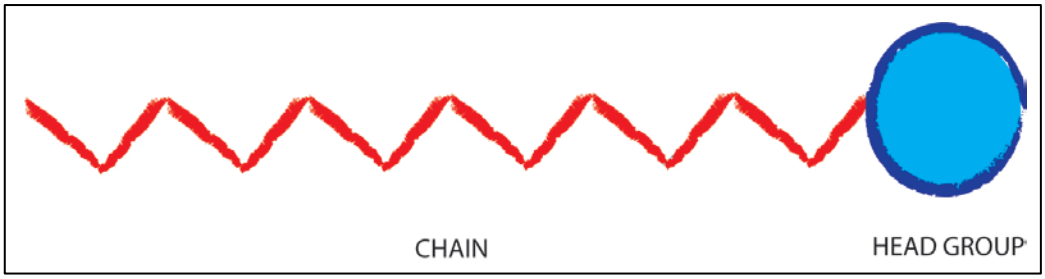

Figure 10: Most common surface active agent [132**]**

Figure 10 shows what the most abundant surfactants are composed of, a chain and head group. Typically the chain (branched or linear) is lipophilic and the head group is hydrophilic [**132**].

The two parts of the molecule interacts as follows:

- The strong interaction of the water molecules resulting from dispersion forces and hydrogen bonding act together to push the chain section out of the hydrophilic phase and hence why the chain may be considered hydrophobic.
- The ionic or polar section of the molecule is called the head group and interacts with the water through dipole to dipole or ion to dipole interactions and is therefore soluble in the hydrophilic phase.

In general, increasing the temperature of a solution increases the solubility of the solute. For surfactants there is a temperature called the Krafft point/temperature (T_k) where the solubility of the surfactant drastically increases [**132**]. In addition, for a non-ionic aqueous solution there is a defined elevated temperature that allows the solution to become cloudy, and this is called the cloud point. The cloud point is determined by the concentration of the surfactant and other variables [**119**]. When the surfactant concentration in a solution increases, so does the amount of surfactant at the interface and results in a decrease in surface tension. It may be considered that the surface tension reaches a constant at the phase interface when no more surfactant may be accommodated. This surfactant concentration – interface constant is known as the critical micelle concentration (CMC); an illustration of this typical behaviour is shown in Figure 11. CMC is defined as the concentration of surfactant in a colloidal system above which micelles spontaneously form and any additional surfactant added goes to these structures. Increased surfactant concentration may make more diverse structures based on these initial micelles, such as vesicles and laminar phases [**133**].

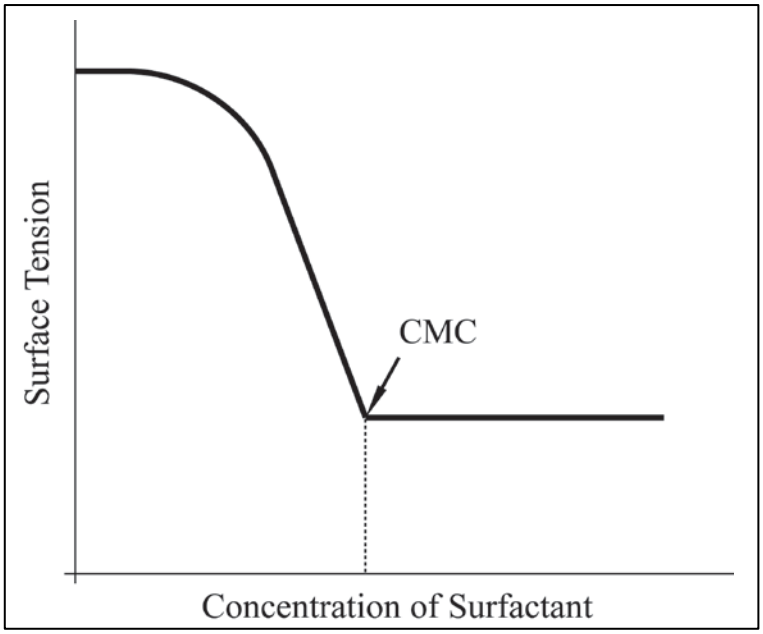

Figure 11: Illustration of critical micelle concentration

2.5.3.1 Surfactant Selection

There are four surfactant chemical types;

- Anionic (negative charge)
- Cationic (positive charge)
- Amphoteric (charge depends on pH)
- Non-ionic (no charge)

Once the chemical types have been selected, the surfactant(s) with the correct solubility must also be aptly selected for use.

Solubility required for the surfactant depends on its use;

- A highly soluble surfactant is required for detergents and other cleaning products
- A medium solubility for dispersions
- Low solubility for inverted emulsions
- A blend of solubility that enables stable O/W emulsions.

Solubility may be predicted by looking at the chemical properties and ratios.

The most common ways of selecting surfactants are very crude and involves typically prior knowledge of what worked before, trial and error, and sometimes the Hydrophile Lipophile Balance (HLB) system.

2.5.3.2 Co-surfactants

Adding a surfactant does lower the interfacial tension but usually the CMC or solubility is reached before the interfacial tension is near zero. Co-surfactants may be any type (non-ionic, ionic, zwitterionic) regardless of the primary surfactant used. Co-surfactants normally have a lipophilic or hydrophilic section that however is a different length, which helps make a micelle structure that improves the electrostatic or steric barrier between phases while helping improve the structures resilience to deformation by reducing gaps in the micelle. By adding a co-surfactant the surface tension may be reduced before saturation due to a better barrier being achieved, as shown in Figure 12 [**133**].

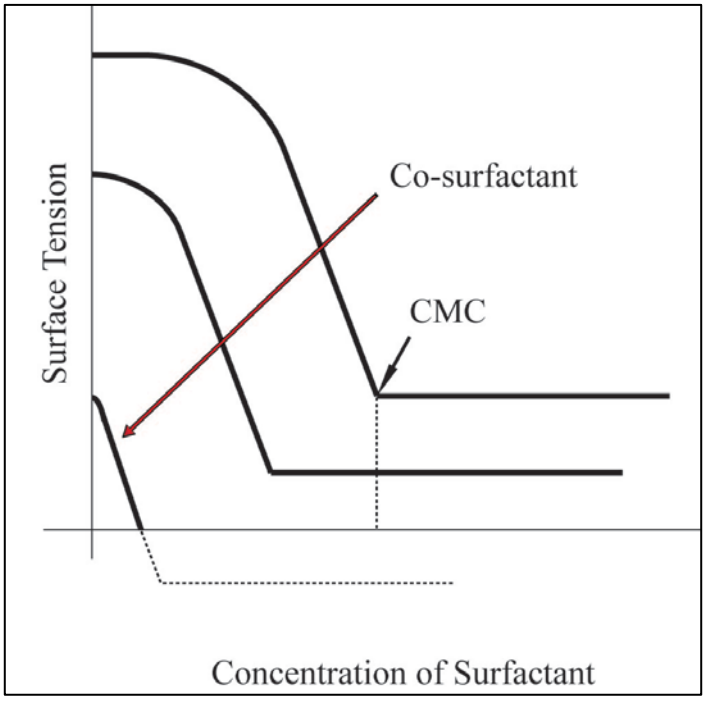

Figure 12: Illustration of co-surfactant concentration

If the surfactants produced a negative surface tension, the interface would expand to absorb the surfactants until concentration was high enough to make the surface tension positive again. Overbeek states that in some cases only one surfactant is needed (such as AOT) to produce a microemulsion, and most non-ionic surfactants near their inversion temperature [**133**]. Figure 13 illustrates two emulsion droplet types which have a co-surfactant interface.

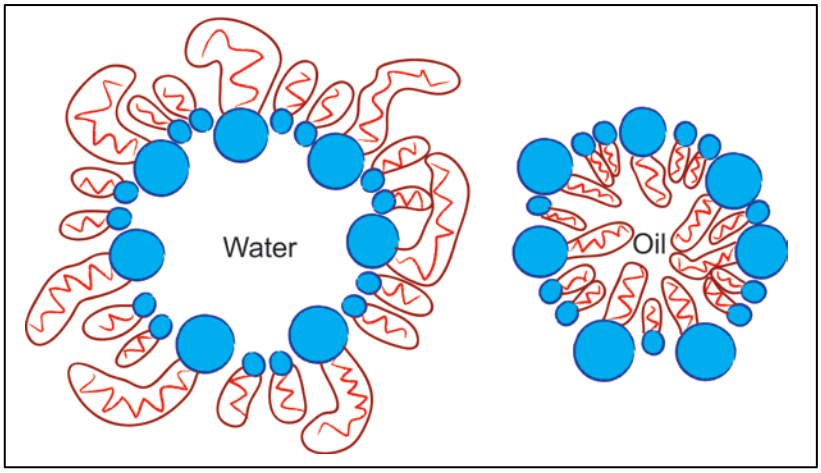

Figure 13: Illustration of W/O and O/W emulsions using co-surfactants. N.B. polar heads are more crowded in W/O

2.5.3.3 Hydrophile Lipophile Balance (HLB)

Hydrophile Lipophile Balance (HLB) is used as a guide to determine the suitability of non-ionic surfactants in particular; however general comparisons for other surfactants may be made. The surfactant in question is viewed as a ratio of hydrophile molecular weight to lipophile molecular weight (and was invented by a company bought in 1971 by ICI). The results are divided by five to help reduce the range for convenience to between 0.5 and 19.5. Comparisons between surfactants may be made by looking up the surfactant properties on a table. The HLB system was designed to help save time and money matching surfactants for requirement more easily. It is used because it provides information on the chemistry of a surfactant, which can help predict its behaviour within an emulsion, which will save time on producing the right formulations [**134**,**43**].

2.5.3.4 Micelle Formation through Surfactant Aggregation

Surfactants tend to form aggregates 'instantly' in a solution in order to form thermodynamically stable structures. These structures are called micelles and depend on the concentration of the surfactant in the solution, so too will the shape of the structure formed. Micelles start to form once a surfactant concentration has been reached, and this threshold is called the critical micelle concentration (CMC). It is therefore the micelles emulsifiers that impart the surface/interfacial tension reduction, emulsification, foaming and wetting attributes [**135**].

The aggregation of the surfactants may produce a micelle or a reverse micelle, the difference being due to the solubility of the surfactant within the system. With the increase in surfactant(s) concentration then the shape changes from a sphere to an elongated tube. This is reflected in the increase in the solutions viscosity due to the change in shape. If increasing the concentration in certain solutions 'sheets' are formed with aligned polar and non-polar groups, allowing pockets for each phase to form and typically transparent [**119**].

2.6 Emulsion Processing & Manufacture

Approximately four emulsifying techniques may be classified [**118**];

1. Internal phase addition to the external phase while providing a shear mechanism.
2. Phase inversion method, *see Figure 14*; external phase is added to the internal phase. Once the inversion point has been reached addition of more of the external phase inverts the system, i.e. W/O inverts to an O/W emulsion. The advantage of this method is that small droplets are produced with little mechanical shearing or heat energy introduced when processing.

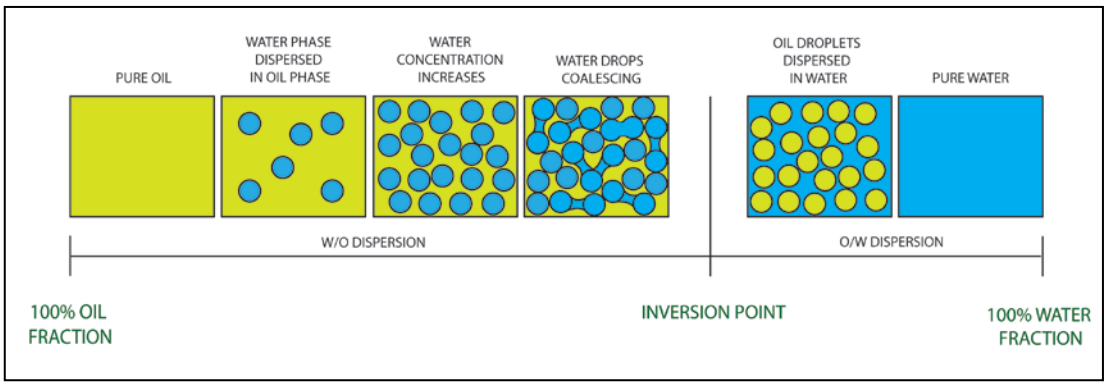

Figure 14: Schematic of phase inversion process

3. Heating both phases and then mixing. This method is typically used in cream/cosmetic preparation due to some materials such as waxes requiring melting before homogenising. Both phases must be heated to the same temperature before mixing. It is recommended that once mixing has started it should be continued until the emulsion cools to ambient temperature to reduce potential for emulsion separation.

4. Alternative addition of each phase to surfactant in small measures. This method typically is used in the food industry.

Trituration, homogenisation, agitation and heat are all methods of providing energy to create an emulsion [**136**] [**137**] [**138**].

2.7 Nanoparticulate Colloids

Extensive work has been conducted on nanoparticulate incorporation in the dispersed phase of colloids. As with larger particles used in the paint or printing industry such as titanium dioxide stabilisation is attributed to either steric or electrostatic stabilisation, through polymer incorporation or surfactant usage [**139**]. One of the most successful surfactants used for titanium dioxide dispersion is sodium acrylate as it can be efficiently absorbed by the particulates interface and work through electrostatic repulsion [**139**]. Titanium dioxide particulates have a physical size and a hydrodynamic size due to a double electron charge layer. This difference in size is due to a potential called zeta potential. For this reason wetting of titanium dioxide and simular metal oxide particulates in water is difficult leading to aggregation of particulates, as sedimentation due to the Stoke-Einstein effect [**140**] [**141**]. Therefore to aid dispersion and thus aid stabilisation, better wetting through steric and/or electrostatic repulsion is required. The reason for nanoparticulate dispersion in these systems is often attributed to the notion of increased efficacy of the treatment; however for polar based solvents such as the silane/siloxane presented in this study stabilisation is difficult [**142**]. While it is possible to produce a highly stabilised emulsion comprised of conventional co-surfactant systems, the quantity of surfactant required is detrimental to the surface modification needed [**124**] [**135**]. To solve this problem, architectural paints, agricultural biocides and cosmetics all typically use branched non-ionic surfactants to reduce the concentration required for stabilisation [**135**]. These types of surfactants conventionally have branched polar head groups which bond with local continuous phase molecules to reduce micelle hydrodynamic interactions [**142**]. However, in the specific case of silane/siloxane emulsions previous studies have shown that either solely particulate-stabilised or surfactant-stabilised emulsions are not stable for long; even at high concentrations they typically separate within two days [**135**]. The amphiphilic nature of the oil phase allows for a degree of aqueous solubility, making segregation of phases difficult and thus causing

irreversible micelle rupture and coalescence. However, it has been reported that stabilisation of these types of emulsions by various surfactant and particulate co-emulsifier systems was achievable by using silica or metal oxide particulates and a polyoxyethylene based surfactant [**135**], [**143**], [**144**].

Ramsden [**121**] was the first to observe and report particulate stabilised emulsions, which were then evaluated extensively by Pickering [**122**]. The role of particles as emulsion stabilisers has been extensively studied for a century with a vast number of particulate containing emulsions reported and characterised [**123**]. Interest wavered from conventional particulates until the fairly recent introduction of nanoparticulates and their use as stabilisers, which showed great potential. Nanoparticulates can improve micelle shape compliance, provide greater surface area for networking and are less influenced by sedimentation [**124**].

Prior studies highlighted the following general rules which apply to particulate-surfactant stabilised emulsions: i) particles have to be wettable by both phases to be effective stabilisers; ii) similar is held true for surfactants; iii) particle-particle interactions are of importance with flocculated dispersions improving stability [**126**] [**143**]. It has been found in earlier studies that hydrophilic particulates stabilise o/w emulsions, while w/o emulsions are stabilised by lipophilic particulates [**126**], [**125**]. The lipophilic-hydrophilic tendency of such particles is of particular interest and has been studied extensively. Recent fabrication of Janus particulates is a prime example of tailoring particulates to suit stabilisation requirements, including both phase preference and flocculation characteristics [**145**]. For conventional particulate-surfactant systems Midmore [**135**] claims that surfactants promote flocculation of particulates, alter wettability, allowing oil/water interfacial adsorption, while reducing the interfacial tension. These key points work synergistically to stabilise amphiphilic oil based emulsions.

Nanoparticulates in the continuous phase have been studied in numerous emulsion systems and their effect on overall stability, oil droplet size, tendency to coalesce and rheological properties have been investigated [**127**], [**128**], [**129**]. Surfactants used in such emulsions may often severely affect the route of nanoparticulate incorporation and, consequently, the overall stability [**146**] [**147**]. If the amount of surfactant in a system is below critical micelle concentration (CMC), it has been found that

particulates first stabilise the micelles by filling gaps, after which micelles are aggregated with excess monomeric or oligomeric particulates achieving greater stability. If there is too little surfactant absorbed on the outer layer of aggregated particulates bridging may not be achieved, which in turn reduces flocculation. In addition to this, smaller surfactant molecules produce larger micelles and bridging is also hindered due to smaller surface area available for interaction between micelles, which reduces stability. On the other hand, if the surfactant concentration is too high, surfactant may cover particulates achieving an isotropic surface tension, causing irreversible particle-micelle separation and thus destabilising the emulsion [**135**]. The major drawback in the silane/siloxane water repellent field is that most studies are conducted with carefully selected materials in laboratory conditions, producing findings that may not be applicable in practice [**124**].

2.8 Summary

Based on the information gathered, to date much work has been carried out in the fields of silane/siloxane based exterior wall facade coatings, emulsions, and nano-particulate additives. The majority of the studies found were related to various fields not directly relevant to the present study. Little work has been carried out with respect to combining all three fields. Key points found include;

1. Water is considered the root cause of facade degradation. Reducing water content in a facade relieves; rising damp problems, sick building syndrome, and fouling problems.
2. Extensive work has been conducted on the use of nanoparticulates in photo-induced sanitisation of facades through coatings, but not through treatments that are designed to maintain the aesthetics of the substrate.
3. Surfactant-nanoparticulate stabilisation of amphiphilic macroemulsions have been achieved to a limited extent and further exploration of this field is required for a variety of commercial applications.
4. Silane/siloxane based emulsion information on fabrication and its characterisation is sparse and requires further study and exposure.
5. Toxicological research seems to show that zinc oxide and titanium dioxide nanoparticulates are safe for dermatological contact and unlikely to cause

problems when incorporated into a silane/siloxane emulsion system or after treatment curing.

Chapter 3: Experimental

3.1 Experimental Overview

The following experimental process was used during this study to develop nanoparticulate emulsions and to characterise them. Figure 15 shows a schematic representation of the development of nanoparticulate processing and incorporation while specific details are given in later sections. A general description of the processes used during this study to create and optimise nanoparticulate emulsions is given below;

A. **Pilot Study**

   a. Assessment of various surfactant co-surfactant systems at various concentrations and surfactant ratios with regard to stability.
   b. Assessment of various phase ratios with regard to stability and mechanisms.
   c. Emulsions were applied to various substrates and assessed through thermal conductivity, surface energy, sorptivity, to assess general characteristics of the prepared treatments and the mechanisms governing final performance.

B. **Base Emulsion Formulation and Optimisation**

   a. A surfactant system is developed requiring less than 0.5wt% for emulsion stabilisation, and assessed similar to that of the pilot study emulsion.
   b. Processing was then optimised though systematic evaluation of surfactant ratio and concentration, phase volume ratio, and siloxane incorporation. Mixing time and speed was assessed through turbidity, stability based upon both physical and thermal stress testing, and optical microscopy.

C. **Nanoparticulate Dispersion and Characterisation**

   a. Nanoparticulates where dispersed using an ultrasonic probe mixer and times assessed through transmission electron microscopy. Due to the nature of the equipment output of the probe was fixed.
   b. Nanoparticulate morphological characteristics were assessed through nitrogen isothermal analysis.

D. **Nanoparticulate Emulsion Characterisation**

a. Mixing times assessed of nanoparticulate incorporation into the base emulsion.
b. Siloxane optimisation was then also assessed at various concentrations and molecular weights.
c. Rheological characterisation of emulsions with and without siloxane and nanoparticulates were assessed respectively to assess stabilisation mechanisms and emulsion rheological properties.

E. **Applied Characterisation of Thermal Insulation, Water Repellence, Pore Modification and Biofouling**

a. Applied assessment of produced emulsions based around facade degradation mechanisms and thermal insulation was implemented.

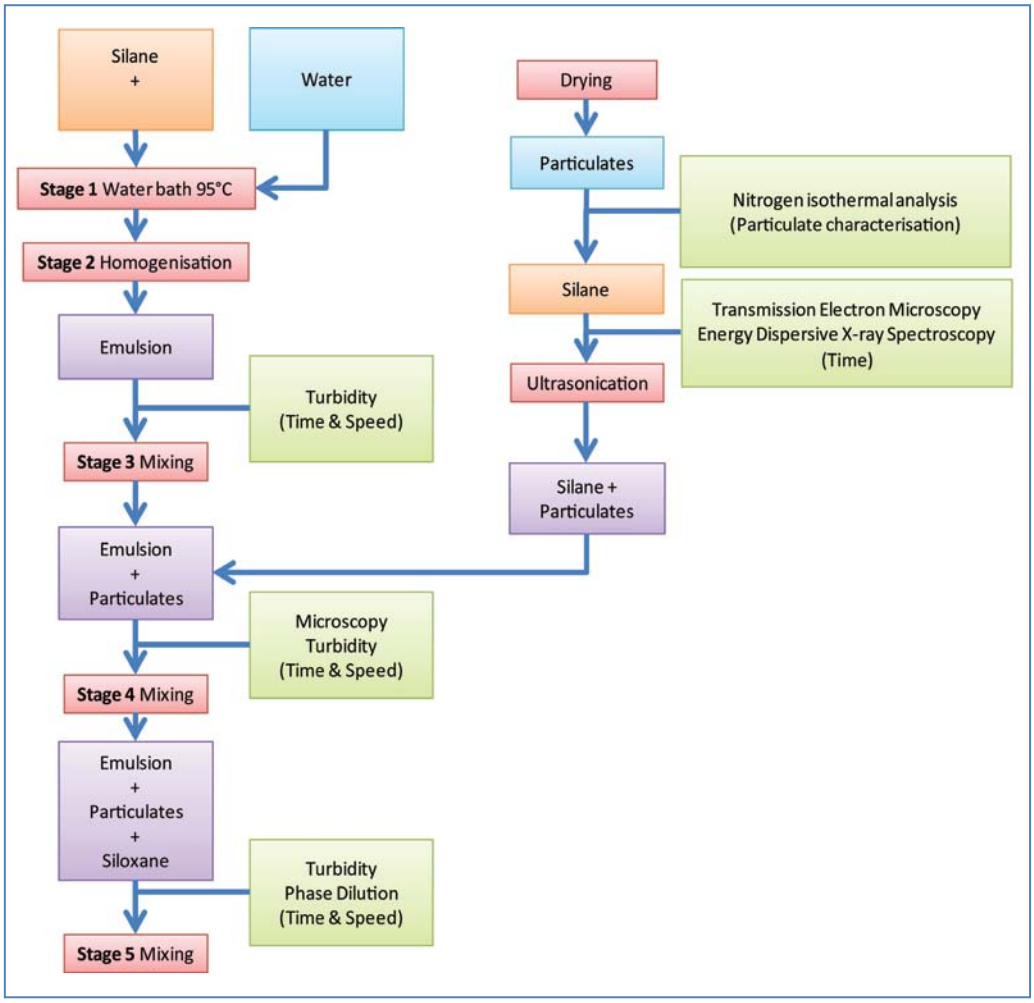

Figure 15: Nanoparticulate and emulsion optimisation testing scheme

3.2 Materials

3.2.1 Water

Water used throughout this study was distilled water, assessed as containing 0 parts per million contaminants. The majority of the water was sourced from ReAgent Ltd.

3.2.2 Surfactants

polyoxyethylen stearylamine (15) (POE 15) was purchased from ABCR Gmbh & Co. KG.

Polyoxyethylen stearylamine (60) (POE 60) was purchased from Jiangsu Haian Petrochemical Plant.

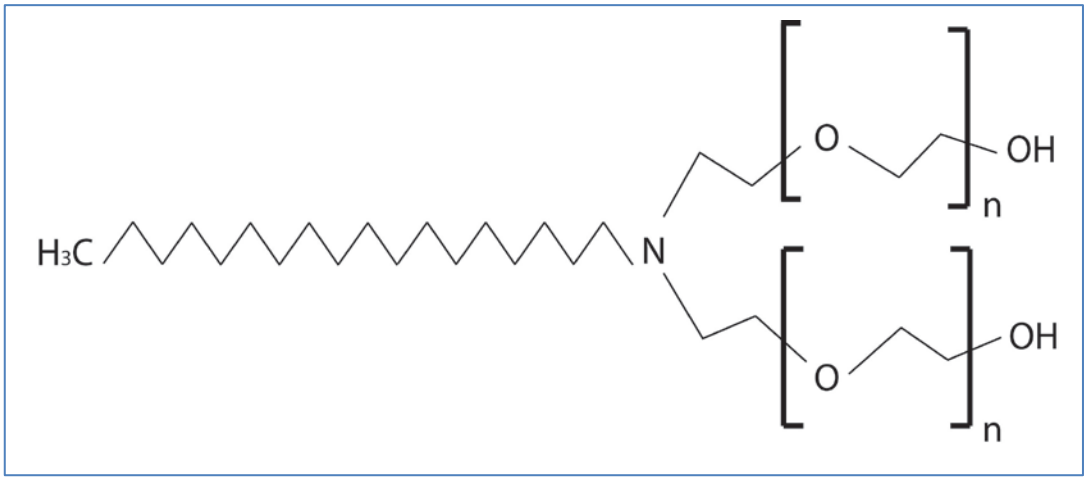

Figure 16: Polyoxyethylen stearylamine where n is 15 or 60 for POE (15) or POE (60) respectively

Aradet N237(90) was received from Rocara Limited.

Description; C12 - C13 alcohol + 7 ethoxylate.

Formula; CH3.(CH2)n.(O.CH2.CH2)p.OH. Where n = 11-12, p = 7.

Aradet N233 was received from Rocara Limited.

Description; C12 - C13 alcohol + 3 ethoxylate.

Formula; CH3.(CH2)n.(O.CH2.CH2)p.OH. Where n = 11-12, p = 3

Aradet BAC 50 (Alkyl Dimethyl Benzyl Ammonium Chloride) was received from Rocara Limited.

Description; C10-C16 alkyl dimethyl 50wt%, and benzyl ammonium chloride (predominantly C12 - C14) 50wt%.

3.2.3 Silane

n-isooctyltriethoxysilane 95% (ITES) was purchased from ABCR Gmbh & Co. KG.

3.2.4 Siloxanes

Hydroxyl end terminated polydimethylsiloxane (PDMS) 3500cSt, 50000cSt, and 90-120000cSt, with molecular weights 43500Da, 110000Da, and 139000Da respectively, were purchased from ABCR Gmbh & Co. KG.

3.2.5 Fumed Silica

Hydrophilic fumed silica from Cab-O-Sil; Sigma, Particle size 0.012µm. surface area 200m2/gram.

3.2.6 Nanoparticulates

15nm Titanium dioxide (anatase) 99% was purchased from Nanostructured & Amorphous Materials, Inc., Texas.Certificate of Analysis states via inductively coupled plasma the following impurities Table 2. Further analysis of particulates morphology, size distribution, and aggregation was carried out using nitrogen isothermal analysis, energy dispersive x-ray spectroscopy and transmission electron microscopy. Results are given in Chapter 5: Nanoparticulate Optimisation and Influence on Colloidal Dynamics.

Table 2: Titanium dioxide specified contaminants

Components	Contents (%)
Fe	0.004
Na	0.01
Mg	0.006
Cl	0.01

20nm zinc oxide 99.5% was purchased from Nanostructured & Amorphous Materials, Inc., Texas. Certificate of Analysis states the following impurities given in Table 3.

Table 3: Zinc oxide specified contaminants

Components	Contents (≤PPM)
Cu	3
Cd	8
Mn	5
Pb	9
As	5

3.2.7 Bricks

Frogged Regency London bricks manufactured by Hanson were used throughout the study. The specification supplied for the bricks is given in Table 4 and stated as being manufactured to BS EN 771-1 [**148**].

Table 4: Specified brick specification

Brick Type	Category II, HD, clay Masonry Unit
Standard work size (mm)	215 x 102.5 x 65
Dimensional tolerances	Tolerance category: T2, Range Category: R1
Compressive strength (N/mm3)	≥ 25
Water absorption (%)	≤ 23
Durability	F1
Active soluble salts content	S2
Dry weight per brick (Kg)	1.95

3.2.8 Sand

Standard yellow builder's sand was used throughout the project.

3.2.9 Cement

Lafarge Ordinary Portland cement (OPC) was used throughout the study. Cement was stated to have been made to BS EN 197-1. In addition the cement was stated as having no accelerators or admixtures.

3.2.10 Terracotta Roofing Tiles

Plain terracotta roofing tiles were purchased from a nationwide supplier. The dimensions are as follows; 170 x 270 x 12mm.

3.2.11 Terracotta Roofing Tiles – Cut Samples

In addition to larger tile samples, smaller sections were cut to 48 x 97 x 12mm were also used.

3.3 Finalised Emulsion Definitions

3.3.1 Base Emulsion

In this thesis, 'base emulsion' refers to an emulsion that does not contain siloxane or nanoparticulates. In some sections however, it may refer to an emulsion containing siloxane however this would be clearly stated.

3.3.2 Siloxane Emulsion

'Siloxane emulsion' refers to a 'base emulsion' that has had siloxane incorporated into it.

3.3.3 Nanoparticulate Dispersion/Colloid

'Nanoparticulate dispersion' or 'nanoparticulate colloid' refers to a solution comprising of a 10wt% of respective nanoparticulates and the rest of n-isooctyltriethoxysilane. Such suspensions are made through ultrasonication using a horn probe. The ultrasonic probe was set up to produce a 20kHz frequency at 70% output, with a mean power output of 240W. Duration of ultrasonic processing was 1 hour. Temperature after processing was 90°C.

3.3.4 Nanoparticulate Emulsion

Defined in this project as an emulsion that includes a 'nanoparticulate colloid'.

3.3.5 Sample Descriptions

Full emulsion descriptions are given where required in each respective chapter of this study. However, to allow quick comparisons of the final formulations to be made, the following abbreviations have been applied and descriptions given in Appendix E: Table 46;

- Tile control (TC) and/or brick control (BC) refers to the substrate without treatment.
- Emulsion control (EC) refers to the base emulsion with siloxane.
- Emulsion zinc oxide (EZ) refers to an EC emulsion with zinc oxide nanoparticulates.
- Emulsion titanium dioxide (ET) refers to an emulsion with titanium dioxide nanoparticulates.

3.4 Phase Dilution

To help establish the type of emulsion, a phase dilution test was carried out for all emulsions. A drop of each emulsion is placed in distilled water and n-isooctyltriethoxysilane respectively. A solvent should dissolve miscible phases; 'like dissolves like.' An emulsion may be either oil in water (O/W), water in oil (W/O) or an emulsion in an emulsion (typically either O/W/O or W/O/W). If the continuous phase of an emulsion is for example oil, the placing of a drop of the emulsion to be

tested in oil will show a film of the emulsion being produced radiating from the drop. If the emulsion drop was placed in water there should not be any film or drop breakup due to the continuous phase having hydrophobic tendency in a hydrophilic environment. This makes this method a highly effective method to assess the continuous phase.

Apparatus:

6x Petri dishes
Emulsion Control (EC)
Emulsion Titanium dioxide (ET)
Emulsion Zinc (EZ)
n-isooctyltriethoxysilane
Distilled water
Labels
Digital camera

Method:

Emulsion preparation; n-isooctyltriethoxysilane and surfactant were put into a container with distilled water placed into another container. Both were heated at 95℃ in a water bath until the surfactant dissolved. All of the water was added quickly to the oil mixture.The oil container was removed from the water bath and homogenised for 30s. Assess a base emulsion with various quantities of titanium dioxide and zinc oxide colloidal dispersion medium respectively to assess the effect such medium has on the continuous phase conductivity. 10wt% nanoparticulate colloidal dispersions in n-isooctyltriethoxysilane produced through ultrasonication for 1hr, was prepared and incorporated at the relevant concentrations into the base emulsion using the homogeniser for 30s (post emulsion preparation).

1. Place Petri dishes on table.
2. Half fill six Petri dishes, three with n-isooctyltriethoxysilane, and three with distilled water; do not cross contaminate.
3. Put roughly 10ml of each emulsion to be tested in each solvent and label each Petri dish.
4. Take photos and record results.

5. Analyse results.

3.5 Electrical Conductivity

Apparatus:

Distilled Water 0PPM
n-isooctyltriethoxysilane 95%
polyoxyethylen stearylamine (15)
polyoxyethylen stearylamine (60)
10wt% titanium dioxide colloidal dispersion.
10wt% zinc oxide colloidal dispersion.
Myron L Company; calibration solution KCL-700 (700µS at 25°C)
Myron L Company; Ultrapen PT1electrical conductivity meter with automatic temperature correction (range 1-9999µS, resolution 0.1µS between 1.0µS to 99.9µS and 1µS between 100-9999µS, accuracy ±1% of reading)
Homogeniser

Method:

Calibrate electrical conductivity meter using calibration solution.

(i) Assess the electrical conductivity of component materials used in the emulsion as is.

(ii) Assess the electrical conductivity of simple two phase systems containing water and n-isooctyltriethoxysilane and the phases made after 30s homogenising at 35,000rpm.

(iii) Assess a base emulsion at various dilutions by distilled water. These emulsions were prepared by the following method;

> ITES and surfactant were put into a container with distilled water placed into another container. Both were heated at 95°C in a water bath until the surfactant dissolved.
>
> All of the water was added quickly to the oil mixture.
>
> The oil container was removed from the water bath and homogenised for 30s.

(iv) Assess a base emulsion with various quantities of titanium dioxide and zinc oxide colloidal dispersion medium respectively to assess the effect such medium has on the continuous phase conductivity. 10wt% nanoparticulate colloidal dispersions in n-isooctyltriethoxysilane produced through ultrasonication for 1hr, was prepared and incorporated at the relevant concentrations into the base emulsion (made as stated in (4)) using the homogeniser for 30s (post emulsion preparation).

All testing was repeated in triplicate.

3.6 Turbidity

Turbidity was measured using a TU-2016; Lutron. Calibration was achieved before testing using NTU 0 and 100 standard solutions. Accuracy of meter; ±0.01NTU. Range; 0.00 to 50.00NTU, 50 to 1000NTU. Test vials were washed three times with distilled water and air dried before use. Once loaded with emulsion, vials were wiped with a cleaning cloth before placed in instrument. Testing was conducted three times and results averaged.

3.7 Rheology

Yield stress, zero-rate viscosity and index ratios were evaluated using a cone and plate rheometer (AR 2000; TA Instruments). A stainless steel cone used in conjunction with a Pelter plate maintained at 20±0.1℃. The cone angle was 1°59'56" with a truncation and truncation gap of 58μm. Thermal expansion and inertia of the geometry was assessed and calibrated using the AR 2000 software before testing commenced. Rotational mapping of the optical encoder was carried out to ensure variations in bearing geometry were taken into account before each test. In addition, the gap between the cone and plate was zeroed before each testing procedure to help produce consistent results after the geometry had been cleaned. A two minute conditioning stage was implemented before continuous viscosity was assessed based upon a 0.01 to 1000 (1/s) shear rate testing scheme. To assess the data retrieved the following models were applied to the viscosity profiles. The Herschel-Bulkley model was used for the yield stress, and the Cross model to assess the ratio index and zero-rate viscosity.

Herschel-Bulkley Model [**149**]*:*

$$\sigma = \sigma_y + \eta * \dot{\gamma}^n \quad (10)$$

Where;

$\sigma = Shear\ Stress\ (Pa)$

$\sigma_y = Yield\ Stress\ (Pa)$

$\eta = Viscosity\ (Pa.s)$

$\dot{\gamma} = Shear\ Rate\ (^1/_s)$

Cross Model [**150**]*:*

$$\eta = \eta_\infty + \frac{\eta_0 - \eta_\infty}{1 + C\dot{\gamma}^m} \quad (11)$$

Where;

$\eta = Viscosity\ (Pa.s)$

$\eta_0 = Zero\ Shear\ Viscosity\ (Pa.s)$

$\eta_\infty = Infinate\ Shear\ Viscosity\ (Pa.s)$

$\dot{\gamma} = Shear\ Rate\ (^1/_s)$

$C = Cross\ Time\ Constant\ or\ Consistancy\ (s)$

Rheological Techniques used & Ranges

(1) Zero shear viscosity 'flow curve' may be used with the following ranges;

Viscosity Pa.s; 1 to X

Shear rate (1/s); 1.000E-5 to 100.0

Or **Viscosity profiling** 'flow curve' if more apt e.g. less time intrusive.

Viscosity Pa.s; 1 to X

Shear rate (1/s); 0.1000 to 100.0

Logarithmic data logging

Power-law or cross model may yield;

- Consistency
- Power Law Index (n)
- Standard Error (Under 20% is ok)

(2) Oscillation Stress Sweep to gather stiffness and yield stress (gel strength) values.

Complex modulus $|G^*|$ (y-axis) vs. Oscillation stress (Pa)

Frequency: 1Hz

Start Stress (Pa); 0.001 to 100

Logarithmic data collection

3.8 Physical Stressing by Centrifuge

To assess the physical stability of the treatments, 15ml graduated centrifuge vials were filled with the respective emulsion and placed in a centrifuge (Mistral 2000; MSE Ltd) with an arm radius of 0.1m, at 3750rpm for 5 hours. This was to simulate 1 year of physical ageing according to the method given by Becher [**117**]. After each hour, results were taken on the visible separation observed, and the centrifuge then started again until the end of the five hours. The results were then converted into a percentage to reduce error from differences in material contained in each vial for evaluation.

3.9 Thermal Stressing by Environmental Chamber

In order to assess the emulsion stability, thermal stress testing was also required since the emulsions were thermodynamically unstable [**118**]. The experiment was comprised of putting each emulsion into a 15ml graduated centrifuge vial and placing it with the others into an expanded polystyrene rack. These were then stored over 24 hours in an environmental chamber (LTCL 350; TAS Ltd) programmed to run at different temperatures over the duration. The rack was used to reduce influence of thermal difference from the chamber floor as well as to keep a space for air to flow freely around the specimens. After 24 hours, the emulsions were taken out and visually assessed for phase separation. The temperature ranged from -20°C, 25°C, to 45°C over 8 hour discrete periods respectively to reflect extreme European weather. Ramps between temperature differences were conducted at 2°C per minute.

3.10 Scanning Electron Microscopy (SEM) & Energy-Dispersive X-ray Spectroscopy (EDAX)

Aim (1): to assess the mechanisms that moss uses to destroy terracotta roofing tiles.

Aim (2): to assess the final six treatments produced when applied to brick substrates using Energy-dispersive X-ray spectroscopy (EDX).

Apparatus:

1 x Electron scanning microscope with compatible digitiser; JEOL JSM-6060LV

Method for Mosses (1):

1. Place moss body with terracotta root fragments attached into Petri dish.
2. Cut each moss body into four sections using the razor and use tweezers to place each into different specimen vials and label each.
3. Pour into specimen vials under fume cabinet glutoraldehyde/sodium cacodylate until covering each sample and seal containers with caps.
4. Put specimen vials into agitator and allow samples to rotate for 2 hours.
5. Rinse each sample twice in buffer solution before the next stage.
6. For the second fixation, use osmium tetroxide to cover the samples, seal with caps and replace in agitator for 2 hours.
7. Use distilled water to rinse for 15 minutes and repeat three times.
8. For dehydration; rinse each sample in 30wt%, 50wt%, 70wt%, 90wt%, and finally absolute ethanol solutions respectively for 30 minutes each.
9. Leave each sample in Absolute acetone for 30 minutes and then critical point dried with carbon dioxide for 1 hour.
10. Once samples have been dried, use carbon cement and the aluminium stubs and mount.
11. Place samples into gold-palladium plasma coater and coat for 30 minutes.
12. Samples are ready for SEM and EDX testing.

Method for Bricks (2):

1. Pot brick samples on specimen mount using carbon black tack.
2. Gold palladium coat in plasma coater for 30 minutes.
3. Put Specimens in SEM

4. Create vacuum in SEM chamber.
5. Photographs taken by a compatible digitiser.
6. EDX carried out on selected sites and elements assessed.

3.11 Transmission Electron Microscopy (TEM)

Transmission electron microscopy (TEM) was used to find the optimum ultrasonic probe dispersion for nanoparticles in an oil phase solution.

Apparatus:

30x 15ml Centrifuge Vials

Centrifuge vial holder

n-isooctyltriethoxysilane 95% in ethanol

3ml pipettes

TiO2 nanoparticle 15nm 99%

ZnO Nanoparticle 20nm 99.5%

Transmission electron microscope JEOL JEM-1400

Transmission electron microscope chemical vapour deposition (CVD) graphite on copper 2000 series substrate grids.

Scanning electron microscope (SEM)

Method:

1. Nanoparticles were measured and weighed using the analytical balances and paper props with mask and gloves being worn; nanoparticles were placed in their respective vials (premarked).
2. The ultrasonic probe was set up to produce 20kHz frequency at 70% output.
3. A 1wt% solution of each nanoparticulate type in n-isooctyltriethoxysilane (75ml total) was produced and placed into the mixing receptacle during the start of each test.
4. The respective test was carried out with the probe suspended in the solution and sealed by rubber using weights to create a seal around the mid probe shaft.
5. The mixing was carried out for 0, 0.5, 1, 1.5hrs respectively for each variation respectively.
6. After each mixing the ultrasonic probe was allowed to cool for 45 minutes due

to heat potentially melting the plastic pipettes used.

7. Each final composition was placed within respective prelabled centrifuge vials with duplicates used to contain all the material.
8. Each sample was mixed with 20wt% distilled water and placed onto the TEM graphite CVD copper grids and left to air cure, and then placed briefly in an oven at 60° to ensure complete drying before insertion into the TEM respectively.
9. Results were analysed and assessed, with crystallinity and particle size assessed.

Additional SEM:

10. This was then followed by scanning electron microscopy (SEM) of the samples.
11. Vial solutions were dried at low heat in crucibles and stuck to aluminium mounts with carbon tack, plasma coated with gold palladium and assessed using SEM with energy dispersive x-ray spectroscopy (EDAX) material confirmation.

Table 5: TEM sample definitions

Sample Id.	Mixing Time (hrs)	Nanoparticulate	Content of dispersion tested before dilution (wt%)
A2	0.0	Zinc Oxide	0.1
B2	0.5		
C2	1.0		
D2	1.5		
A3	0.0	Titanium Dioxide	0.1
B3	0.5		
C3	1.0		
D3	1.5		

3.12 Mercury Intrusion Porosimetry (MIP)

Porosity of the mortars was determined through mercury intrusion porosimetry (MIP) using an AutoPore IV 9500; Micromeritics. The method measured pore size by impregnating the mortar with mercury. Washburn in 1921 derived an equation that states that the pressure required to force a non-wetting liquid into a capillary of circular cross-section is inversely proportional to the diameter of the capillary and directly proportional to the surface tension of the liquid and the solid surface contact angle [**151**]. Mercury is predominantly used therefore due to its non-wetting

behaviour to most solid material interfaces [**151**]. Increased internal pressure had to be applied to cause the mercury to penetrate into the decreasing pore size of the samples. The total volume of mercury was therefore equal to the pore volume.

3.13 Optical Microscopy

Optical Microscopy was conducted using a (DM2500M; Leica Microscopes UK). 50v/v% solutions were produced by diluting each respective emulsion with distilled water. These emulsions were then fixed using a water based fixative to microscope slides and pictures of each emulsion were taken through digital camera. These images were then transformed into 256-grayscale images and a threshold of 130-256 was used to produce droplet size data.

3.14 Nitrogen Absorption/Desorption Isotherms; BET Analysis

The textural characteristic of each nanoparticulate was determined by nitrogen absorption-desorption isothermal testing and Multipoint Brunauer Emmett Teller (BET) analysis using a Micromeritics TriStar II 3020 surface area and porosity analyser. Samples were degassed under vacuum over night before testing commenced. Bath temperature during testing was -196.15°C and sample mass for each nanoparticulate was ~0.3g. The nitrogen cross-sectional area value used for calculations was 0.1620nm^2. The BET equation used to assess the surface area is as follows;

$$\frac{P/P_0}{a(1-P/P_0)} = \frac{1}{a_m C} + \frac{C-1}{a_m C}\left(\frac{P}{P_0}\right) \qquad (12)$$

Where; *C* is constant and related to free monolayer energy absorption. *P* is vapour pressure, P_0 is the saturation vapour pressure at the set temperature, the vapour amount absorbed is *a*, and a_m is the monolayer capacity at the surface [**152**].

3.15 Water Absorption

The water absorption test was carried out following BS EN 771-1:2003. The water absorption percentage was calculated by Equation (13) [**148**];

$$W_m = \frac{m_w - m_d}{m_d}\, x\, 100\% \qquad (13)$$

Where; W_m is the water absorption (%), m_w is the wet mass (g), and m_d is the dry mass (g).

3.16 Sorptivity

To assess water absorption over time and a samples water repellent attribute in a practical manner that may be used to make a quantitative assessment between samples, sorptivity must be calculated. Mortar samples were weighed after post curing and then submerged in a water tank over 24hrs with periodic weighing occurring during this period. Excess water was dabbed off before readings were taken. Three mortar results were averaged to produce the final water absorption results. After the results were collected the sorptivity was then calculated using the following formula [**153**];

$$i(t) = St^{1/2} \qquad (14)$$

Where; *i(t)* is the cumulative volume of liquid absorbed at time *t*, and *S* is the Sorptivity.

3.17 Thermal Conductivity

Thermal conductivity was measured by the hot wire method. A wire of a known dimension passed a known current across it and the resistance is monitored as a function of temperature which is measured by a thermocouple. The thermal conductivity is then calculated using the gradient of the graph produced from these two variables. A quick thermal conductivity meter (QTM-500 from Kyoto Electronics Manufacturing Company Ltd) was used to measure the thermal conductivity of samples in 'as received' and wet scenarios. For the wet scenario, samples were placed in water for 24 hours before being tested. Treated and untreated samples were tested for each scenario.

3.18 Treatment Depth

The treatment depth was assessed by breaking each sample in half using a chisel. One cross-section was quickly dipped into water and then compared with the other cross-section. The presence of water darkened the area where the treatment was absent and

therefore showed how far the treatment penetrated. Treatment depth was assessed using a ruler with an accuracy of ±0.5mm; five results were used to calculate the average treatment depth.

3.19 Goniometry

3.19.1 Water Contact Angle (WCA) and Surface Free Energy (Sfe)

Water contact angle and surface energy of both bricks and mortar were tested using a goniometer (CAM101, KSV Ltd) with testing based upon the method stated in BS EN 828: 1998 [**154**]. Calibration of the equipment was conducted using a precision 4mm diameter ball bearing. The water contact angles of samples were assessed using distilled water as the probe liquid. The probe was dispensed rapidly by syringe and displaced due to the reciprocal action of the dispenser mechanism onto the substrate. Measurements were taken by a digital camera and subsequently analysed. Surface energy was assessed by repeating the process with glycerol as the other probe liquid. This was then followed by both sets of results being used to calculate the surface energy of each substrate. Both sets of results were then used to calculate the surface energy of each substrate using the OWRK Fowkes equation as it takes into account both polar and dispersive energies as described below [**155**];

$$\gamma_{SL} = \gamma_S + \gamma_L - 2\sqrt{\gamma_S^d \gamma_L^d} - 2\sqrt{\gamma_S^p \gamma_L^p} \qquad (15)$$

Where; γ_{SL} is the solid/liquid interfacial tension, γ_S is the solid interfacial tension and γ_L is the liquid interfacial tension. Dispersed or polar surface energy constituents are denoted by *d* and *p* respectively.

3.19.2 Surface Tension – Pendent Drop

Calibration of a CAM101; KSV Ltd was conducted using a precision 4mm diameter ball bearing. The software was setup to conduct the pendent drop experiment. 'Heavy' and 'light' phases were predetermined values given in Table 6. Each liquid was dispensed from the syringe tip and visually recorded using the camera. Each test was conducted 5 times with 5 frames recorded for each. The base line was set to the syringe tip and the Young/Laplace equation was used to model the drop produced [**156**]. These values were then averaged from the results. Anomalous results may have

to be removed before this in each calculation that was carried out. Good standard deviation values were given by the supplier as being around 0.01 to 0.05.

Table 6: Predefined phase definitions

Characteristic	Distilled Water	Ethanol	n-isooctyltriethoxysilane	Air
Density (g/cm^3)	0.9986	0.7937	0.88	0.0013
γ (mN/m)	72.80	22.40		
γd (mN/m)	21.80	18.80		
γ+ (mN/m)	25.50	0.02		
γ- (mN/m)	25.50	68.00		

3.19.3 Surface Tension – Wilhemy Plate

Nine concentrations of each surfactant as well as a 1:1wt mixture solution was prepared by initially diluting a 10wt% concentration. Initial solutions were prepared by weighing 10g of each surfactant into volumetric flasks. Water was then added to make up to a volume of 100ml. These solutions were then used to prepare the test solutions. Test solutions were premixed and stored in cleaned bottles.

The surface tension of each solution was measured using a Wilhemy plate in a Dataphysics DCAT 21 tensiometer. Prior testing, glassware was cleaned using laboratory detergent and rinsed in water. This was followed by several rinsing stages in deionised water and dried prior to use. The Wilhemy plate was washed in 3 separate beakers containing deionised water. The plate was then heated until red hot by blowtorch to remove any residual contaminants and allowed to cool before use.

The test liquid during each test was poured into a clean beaker and mounted into the tensiometer and the test started. Mass before, during, and after testing was measured. These were used to calculate the surface tension in addition to the dimensions of the plate. Inflection points were calculated and the critical micelle concentration (CMC) point was determined.

3.20 Photospectrometry

Three spectrophotometer (Spectromatch Gloss Meter; Sheen Instruments Ltd) readings were taken and averaged for the brick samples. To assess visual alteration in a quantitative manner, spectrophotometry was conducted and evaluated using the

CIElab D65/10° method. The total colour difference ΔE* of the examined surfaces were determined by [**157**];

$$\Delta E^* = \sqrt{\Delta L^{*2} \Delta a^{*2} \Delta b^{*2}} \quad (16)$$

Where L^* is the lightness (0 to 100, black to white respectively), a^* is the red-green component (positive for red, negative for green) and b^* is the yellow-blue component (positive for yellow, negative for blue). Chromatic variations ΔC^* were calculated to assess colour purity, and the change in hue ΔH^* was also determined by the respective equations [**157**];

$$\Delta C^* = \sqrt{(a_1^*)^2 + (b_1^*)^2} - \sqrt{(a^*)^2 + (b^*)^2} \quad (17)$$

$$\Delta H^* = \sqrt{(\Delta E^*)^2 - (\Delta L^*)^2 - (\Delta C^*)^2} \quad (18)$$

Where a^*_1 and b^*_1 are a* and b* values for the treated tile and control samples, respectively.

3.21 Model House – Thermal Envelope Efficiency

The main objective of this study was to develop an understanding of the effectiveness of a nanoparticulate based silane/siloxane emulsion treatment in achieving household heating energy savings. A prior investigation on pore alteration concluded that nano-particulate incorporation of either titanium dioxide or zinc oxide (<0.1wt%) was found to provide beneficial characteristics of interest and hence provided the motivation behind this study. Due to limited supply of remote probes and relay equipment the zinc oxide emulsion was used to treat one of two model houses and tested in parallel to assess energy efficiency of heating both structures in both wet and dry scenarios. In addition to the model houses, the assessment of the component materials of the structures was tested to assess their respective influence on thermal insulation properties.

3.21.1.1 Material Preparation

The emulsion contained <0.1wt% 20nm zinc oxide nano-particulates which helped improve various attributes such as water repellence and emulsion stability. Oil phase volume fraction was 0.8 for optimised emulsion stability and siloxane content was

<5wt% for better treatment penetration of the substrate. Frogged Regency London bricks were tested along with mortar samples cast 10mm thick using glazed tiles to create flat samples. Mortar was left for 48 hours at ambient conditions to allow consolidation to occur before treatments were applied. The treatment amount used for each sample in this study was calculated based upon a 200g/m^2 coverage. Emulsions were weighed on each respective sample and then applied by a pre-wetted brush to reduce variation.

3.21.1.2 Model house rig setup

Two model houses were constructed using two courses of four bricks for experimental assessment of energy consumption. One model was treated while the other acted as a control. The setup of the rig is shown in Figure 17.

Figure 17: Internal and external view of test rig

The lid and base of each model house was made from high density Styrofoam for insulation, so other variables such as floor and roof thermal leakage could be minimised. In addition to the standard mortar, a specially formulated base mortar was used to aid adhesion of the bricks to the foam base. The main mortar used will be referred to in this paper as 'mortar' for simplicity. The mortar used for building the model houses were similar to that used in modern building practices, and is shown in Table 7.

A schematic of one of the two test rigs used is shown in Figure 18. Three remote data loggers (Ibuttons; Maxim) were used to monitor the temperature and humidity inside the model houses and environmental conditions externally. They acted as a primary data source and helped to validate results. Probes were attached to the inside wall surface of each model house half way from the top, while the third was positioned

approximately 30cm from the rig. Each probe was retained using a tack adhesive, which allowed easy removal for data acquisition and reprogramming.

Table 7: Mortar compositions

	Base Mortar Composition		Main Mortar Composition	
Materials	Mass (g)	Percentage Total (%)	Mass (g)	Percentage Total (%)
Ordinary Portland Cement	540.0	19.6	1420.0	17.3
Latex	60.0	2.2	0.0	0.0
Soft Sand	1800.0	65.2	5780	70.5
Water	359.0	13.0	1000	12.2
Total	2759.0	100.0	8200	100.0

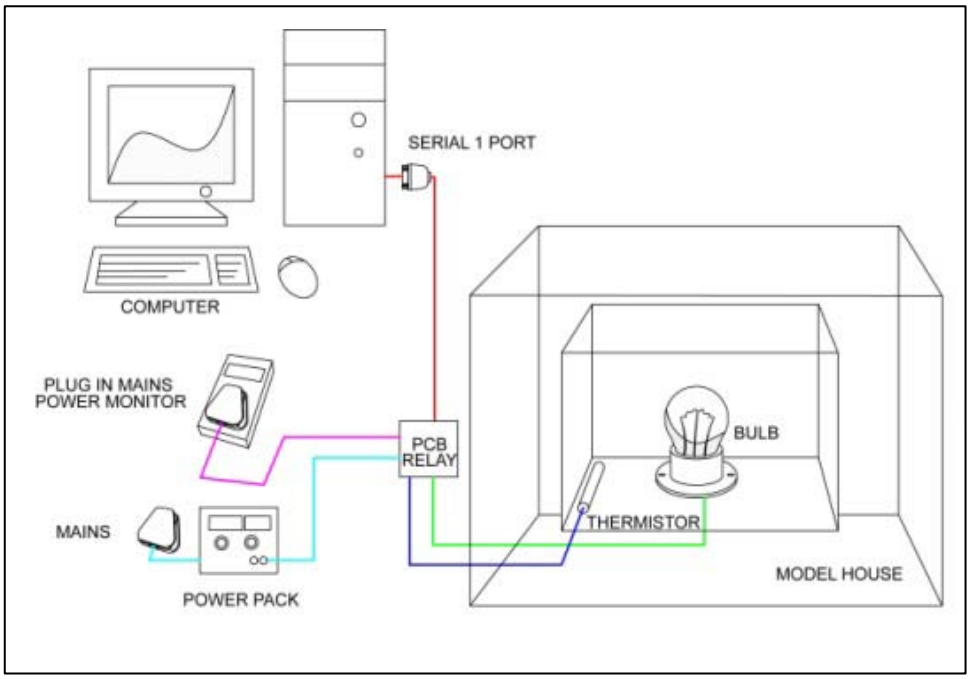

Figure 18: Schematic of one of two energy consumption test rigs used simultaneously

A printed circuit board (PCB) containing a relay for a 40 W light bulb was used to heat the internal environment of each model house. The thermistor (accuracy ±0.1°C) secured in each model provided data to the programme. When values deviated from a pre-set temperature it prompted the relay to turn the bulb on or off. The bulb was powered by mains electricity which was interrupted by the PCB relay. A power meter was used to monitor the energy consumption and electrical source characteristics of the bulb (accuracy; ±0.1W, ±1V, ±0.01A). Both PCB relays and bulbs were powered from separate sources, giving a better representation of the energy used by the system. The bulb was positioned in the middle of the model house, ensuring that uniform heating took place. The thermistor turned the bulb on and off intermittently but also

was used to log temperature data to help establish the time duration when the bulb was on.

One of the model houses was treated with 200g/m² of emulsion. A brush was used to apply the emulsion with the mass of the treatment weighed by scientific scales (accuracy ±0.01g). In order to achieve a uniform treatment for each side of the model house, the brush was pre-wetted each time with emulsion to reduce discrepancies occurring from brush absorption. This procedure was repeated for each side, with an average of 13.7g of treatment used per side. Both treated and untreated model houses were then left for two weeks to ensure curing prior to testing.

The model houses were produced and situated in a relatively insulated room to ensure temperature and air flow abnormalities were diminished. Internal temperatures were set at 25°C, 30°C and 35°C for 'dry' and 'wet' scenarios and external temperatures monitored. Testing for each regime was conducted for two weeks. For the wet conditions a brush was used to apply 32.5g of distilled water to each side of the models to simulate post-rain conditions before testing. Results were only taken when the inputs were constant for all data loggers. Two hour durations were retrieved and assessed from these periods.

3.21.1.3 Modelling of energy dissipation rates

From the thermal conductivity results a simple model was created to establish the real world implications of using such treatments. A wide range of temperature scenarios were used to assess the energy saving potential of each emulsion. The model used thermal conductivity to calculate the energy output of a wall section comprised of standard terracotta bricks considered to have 23wt% porosity. The model was based upon 10kW heat source emitting energy upon a 10m^2 by 10.3cm thick single isotropic section. A temperature range of 10°C to 25°C produced results considered apt for a real world scenario. Both thermal conductance (C) and thermal transmittance (U) were expressed by the following equations [**158**] [**159**];

$$C = Q/A(T_{s1} - T_{s2})\ (\mathrm{W/m^2K}) \qquad (19)$$

$$U = Q/A(T_{s1} - T_{s2})\ (\mathrm{W/m^2K}) \qquad (20)$$

Where Q is the heat flux through the measured area and may be considered as the total energy used to heat the system (W). A is the area cross section being monitored

(m^2). T_{s1} is the average test surface temperature from 'internal' conditions (°C). T_{s2} is the average test surface temperature for 'external conditions' (°C). T_{A1} is the air temperature for 'internal conditions' (°C). T_{A2} is the air temperature for 'external conditions' (°C).

Surface coefficients (R_1) and (R_2) for both 'internal' and 'external' interfaces can be used to find the thermal conductivity (k). Equation (19) & (20) therefore derived Equation (21) & (22);

$$R_1 = Q/A(T_{A1}\text{-}Ts_1) \text{ (W/m}^2\text{K)} \quad (21)$$

$$R_2 = Q/A(T_{S2}\text{-}T_{A2}) \text{ (W/m}^2\text{K)} \quad (22)$$

Hence the heat transfer going from the 'internal' wall to/from the 'external' wall may be expressed as;

$$k = Ql/A(T_{S1}\text{-}Ts_2) \text{ (W/m}^2\text{K)} \quad (23)$$

The thickness of the sample wall is expressed by l (m). The overall systematic model used has been well established in prior work, and is described below [**160**] [**161**];

$$Q = (T_i\text{-}T_e)(V+\Sigma AU) \quad (24)$$

Where Q is the total heat required to heat the room. T_i is the room index temperature, which may be considered the driving mechanism to achieve a steady state heat loss until the system reaches an equilibrium ambient/base temperature (T_e). This mechanism in this model may only be facilitated by either ventilation (V) or conduction loss (ΣAU).

For this particular model it is assumed that there is no ventilation, since it is only the energy efficiency that is of interest to the study. It is therefore assumed that the 'internal' heating is homogenous and constant for simplicity. The time taken for the energy input by the heat source was calculated through simple rearrangement of power, thermal conductivity, and specific heat equations. Specific heat values were taken from existing work [**162**]. The heat flow was then used to find the lag time between the 'internal' and 'external' parts of the system and hence possible annual consumption.

3.22 Photocatalytic Potential

Aim: to evaluate the self cleaning properties of treatments through the assessment of contaminant breakdown during UV exposure via WCA modification

Background:

Testing is based upon BS ISO 27448:2009 [**163**].

Apparatus:

1 x Black-light fluorescent lamp peak wavelength 351nm and blue glass (Eterna Lighting, Model; D126 (T8) 18W max)
Stand for light.
Distilled water; Reagent (0ppm contaminants)
~50ml Oleic acid assay 70.0wt% (60.0wt% min required)
Test samples
3ml pipette
Non-woven cloth
Radiometer 2.0±0.1 mW/cm^2 (QLab; CR10 used)
Water contact angle (WCA) machine (KSVLtd; CAM 101 used).
Scientific scales accuracy ±0.01g

Method:

1. Calibrate lamp to emit 2.0mW/cm^2 onto samples.
2. Test the WCA of samples before and after oleic acid treatment.
3. Treat samples with oleic acid with a coverage of 20mg ± 2.0mg achieved by rubbing with a non-woven cloth oleic acid into the substrate while weighing continually.
4. Place samples under lamp and take readings over time.
5. When WCA readings after three successive readings fluctuate below 3°, stop experiment.
6. Calculate the final WCA by averaging the final three results.

3.23 Biofouling Study

3.23.1 Overview

In order to ascertain the performance of the nanoparticulate treatments, a culture streaming study was conducted. The principle of the culture streaming test is as follows; water containing algal culture was pumped onto mortar samples hung on a rack inclined 45° inside a tank. The culture that was not retained by the mortar would then run off back into the tank base and then be recycled.

3.23.2 Mortar Preparation

The mortar samples used for the culture streaming study are defined in Table 8.

Table 8: Emulsion descriptions

Abbreviation	Treatment Description	Nano-particulate incorporation (wt%)
TC	Mortar control (no treatment)	N/A
EC	Control emulsion (no nanoparticles)	N/A
EZ	Zinc oxide emulsion	<0.1
ET	Titanium dioxide emulsion	<0.1

Testing was carried out on mortar slabs (17cm x 27cm x 2cm). Due to easier mould removal and better surface finish a 3:1 sand-to-cement mortar was selected over a 4:1 mortar. Water/cement weight ratio was relatively high, 0.6, as a study conducted by Giannantonio et al. [**164**] showed that higher ratios produce more porous substrates, making them potentially more susceptible to biofouling. The mortar was put in wooden preforms using a float and left for three days to cure. The samples were then removed and left to dry for a week. Each sample was treated using a pre-wetted brush with 40g of emulsion and allowed to cure for another week. Additionally, plastic rods were attached to the top rear of each culture streaming test sample using epoxy resin so that these could be mounted inside the rig; samples were left for 24 hours before installation.

3.23.3 Culture Streaming Setup

Water containing algal culture was pumped onto mortar samples placed on a rack (inclined at a 45° angle) inside a tank. The culture that was not retained by the mortar was collected in the tank's base and then recycled. Prior studies were used as the basis for the test design [**165**,**166**,**167**,**168**,**169**]. The system consisted of a 179 x 60 x 70cm acrylic tank containing a double pitched acrylic rack. A 45° pitch was used to allow

the culture the most contact time on the mortar. Internal parts of the tank were joined by polycarbonate glue first and then sealed using marine sealant containing no biocides. Two 36W 150cm fluorescent lights were bolted to the tank sides at a point where light would be equidistant from the surface of the samples to be tested. Above these, two 36W 120cm UV-B lights were added to represent UV influence on fouling and the treatments to be tested. The top of the tank was not hermetically sealed, however it was covered by aluminium foil to help focus light sources on the samples and culture. Two 300W aquarium heaters were placed in opposing corners of the tank and set to 25°C. Two magnetic stirrers were placed approximately 45cm in from each end of the tank. These stirrers were used to help reduce settling and consolidation of algal matter. 6cm plastic coated magnets were set to rotate to form a vortex in the 125L of culture used during the study. In order to place stirrers under the tank, a wooden stand was constructed. Figure 19 to 21 show rig setup and mortar sample placement.

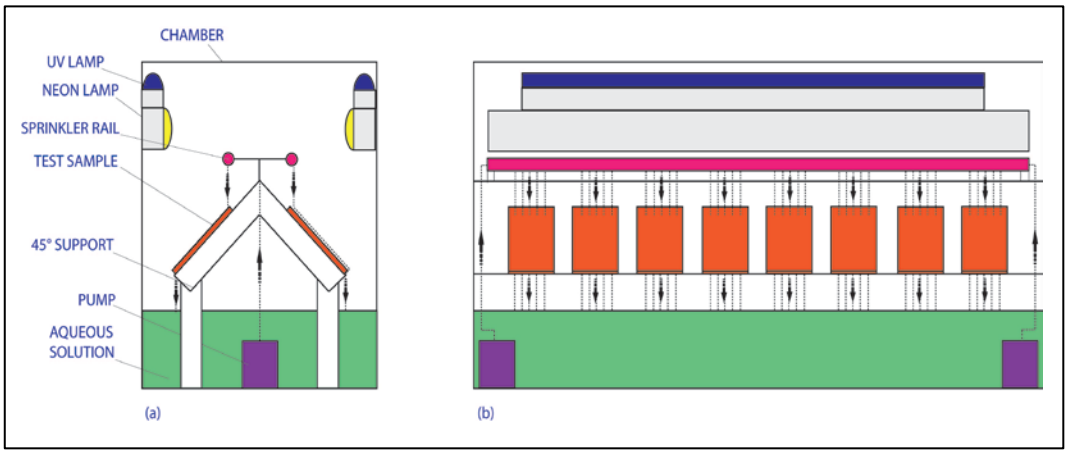

Figure 19: Simplified schematic representation of antifouling rig setup (a) side view, (b) front view

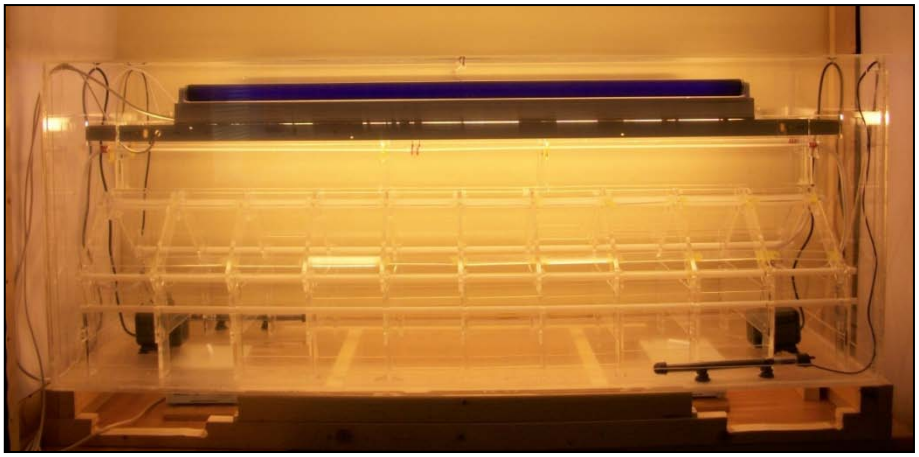

Figure 20: Front view of culture stream chamber

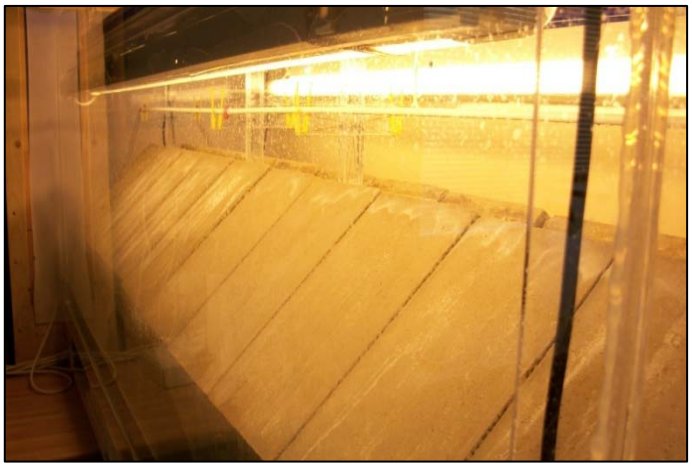

Figure 21: Mortar samples during testing

5 mortar samples of each type were hung on the rack. Above the samples an 8mm diameter plastic rail containing 1.5mm holes every 20mm was mounted on plastic supports attached to the rack. The distance from the rails to the sample surface was approximately 15cm and designed to allow water to fall approximately 2-3cm from the top of the sample. The tank contained two 1400L/h 24W water pumps. Each pump was attached to both rails at either end using T-connectors. At one end two remote probes of a data logger (TR-74Ui; T&D Corporation) were mounted onto one of the rail stands. The remote data logger measured light illumination, UV irradiance, temperature and humidity during testing. This was setup to record data every 10 minutes over the eight week testing duration. Water was sprayed for 90 minutes every 12 hours for the duration of testing. The lights for this period were turned on at the start of the first streaming cycle and turned off at the finish of the second. The rig was set up in a large wooden frame that was covered with black-out cloth to reduce

external influence. Every week periodic scans were conducted using an Epson 1250 Photosmart scanner. These images were then used to assess changes in colonisation kinetics of each sample. Scanned images were transformed into 8-bit greyscale images containing a range of 0 to 256 possible intensities; dark to light respectively. A histogram of each image was then calculated using imaging software (IRIS; Christian Buil) which helped identify any change in colour during the study. Changes in colour would alter the produced histograms, allowing a percentage difference to be calculated during testing. Different imaging software (ImageJ; Wayne Rasband) was used to assess surface growth coverage due to its ability to calculate area as a percentage. After assessing the samples and standard practice in the literature, it was thought prudent that a similar threshold value to the one stated by De Muynck et al. (2009) should be used [**168**]. Thus, growth area was assessed by simplifying each greyscale image using a 138 threshold value and then calculating the difference in pixels as a percentage.

3.24 Algal Source & Propagation

The culture used for streaming comprised of algae collected locally from 'Canoe Lake' in Portsmouth, UK. The initial concentration of contaminant collected locally before testing was 0.52wt% (dry weight). Scanning electron microscopy (SEM) was used to visually identify the types of algae used; sample preparation is given in section 3.10. Results from this testing indicated that blue-green algae along with green algae was present with common forms identified as Volvox, Chlorella, Aphanothece and Pleurococcus surrounded by various primary bacteria and protozoa (Figure 22) [**170**]. Collected algae were used in the culture streaming study to help provide a realistic representation of possible biofouling.

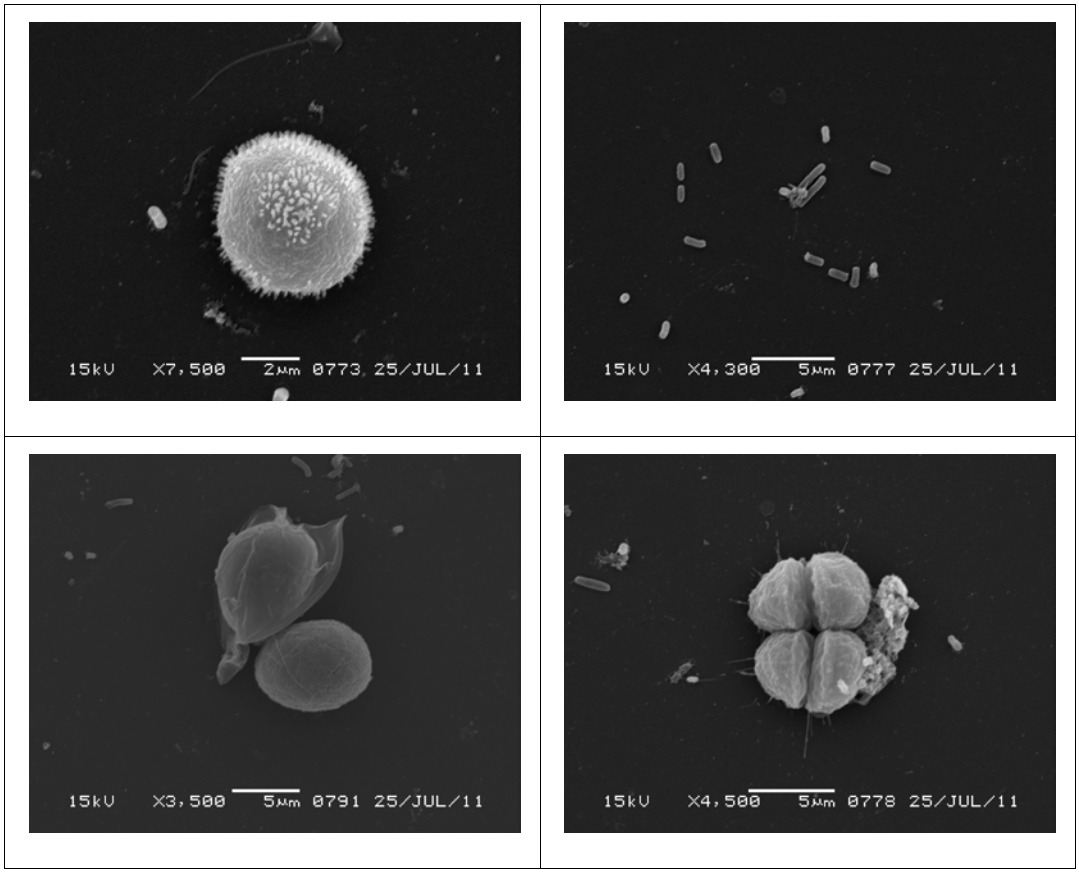

Figure 22: Clockwise from top left; Volvox (green algae), Aphanothece (blue-green algae), Chlorella (green algae), and Pleurococcus (green algae)

Bold basal modified freshwater medium (BBM) as a 50x concentrate solution, was purchased from Sigma Aldrich Co LLC. BBM was used during dilution of cultures to 0.05vol%. The initial algae solution retrieved for this study was approximately 2L. Dilution of culture by half the volume with distilled water occurred every 5 days during growing to help increase culture volume and sustain growth rates. Algae were grown in a photo-bioreactor with a 60L capacity as shown in Figure 23.

Figure 23: Photo-bioreactor during use

During this growing process culture was placed in 2L plastic bottles with an air diffuser in each and stood next to two 30W fluorescent lights in the photo-bioreactor. Remote probes (TR-74Ui; T&D Corporation) were placed at the same distance the bottles were from the light sources (4cm) and the following average data was produced for a 5 day cycle: Illumination; 10840.8Lx, UV irradiance; 0.0250mW/cm^2, temperature; 32.9°C, and relative humidity; 20.7%RH. The air diffusers were used to help produce uniform growth and reduce settling which may have denatured concealed algae. Two 3.5W air pumps provided 180L/h each to the system equating to approximately 12L/h air supply per bottle. Bottles were capped with aluminium foil to reduce contamination during this period. Once 60L of culture had been grown by this process it was added to the culture streaming tank and diluted with distilled water and 500ml of BBM concentrate to make up the 125L total volume used for testing. During testing 100ml of BBM 50x concentrate was added each week to the tank culture to help maintain growth rates.

Chapter 4: Emulsion Formulation and Optimisation

4.1 Pilot Study – Volume Fraction

The aim of the pilot study was to find the optimum oil to water phase ratio through gravitational stress testing. A co-surfactant system using two alcohol ethoxylate non-ionic surfactants was used to help determine this. N237(90), N233, and BAC 50 (Alkyl Dimethyl Benzyl Ammonium Chloride) were referred to as surfactant A, B, and C. Surfactant C was used to assess if cationic surfactant would make any difference and was incorporated with surfactant B. Sample descriptions used during testing are given in Appendix A. For the first volume fraction study 2wt% of surfactant components (at varying ratios) was used to assess stability at different phase ratios. For the second volume fraction study 2wt% and 4wt% of surfactant components (at varying ratios) were used to assess stability at different phase ratios.

Testing initially examined volume fractions of two similar silane materials to assess any difference between similar molecules (n-isooctyltriethoxysilane 95%, and n-octyltriethoxysilane 97%; ABCR). Testing was then conducted with one of these silanes and compared to a longer polymer chained siloxane with hydroxyl terminations (PDMS 3500cSt; ABCR). Emulsions were produced by homogenising oil and surfactant together at 35,000rpm for 1 minute. This was followed by 2 minutes of homogenisation at 35,000rpm where the water was added at 7ml/min. Finally the emulsion was mixed for a further 2 minutes at 35,000rpm. Samples were then centrifuged at 3000rpm in a centrifuge with an arm radius of 0.1m for 1 hour.

Figure 24 shows that there is an increase in stability of both silane emulsions tested up to roughly a 80:20wt% ratio of oil to water respectively (a phase dilution test showed an O/W system produced during the pilot study). This shows that these emulsions seem to follow the power law ratio and described practices [**119**]. Since both silanes are similar in chemical structure and have similar characteristics it was thought that a different oil phase should be tested to assess this further. In addition, surfactant concentration and type were also used to validate that it was solely a physical mechanism causing destabilisation to these emulsions. The ionic surfactant tested against non-ionic surfactants provided no overall difference in outcome of the physical stress test as did the different silane used. In addition, concentration of surfactant had no bearing, showing that there was enough surfactant to adequately stabilise these emulsions and that electrostatic or steric stabilisation produced by the

various systems tested also did not alter the destabilisation characteristics produced, thus differences in density and droplet size should be the determining influence on stability of the emulsions produced as described by Stokes law [**117**].

Figure 25 shows that there is an increase in stability of both silanes tested up to ca. 80:20 weight ratio of oil to water respectively. It should be noted that due to the small volume of the test the n-isooctyltriethoxysilane anomalous result may be due to systematic measurement error(testing was conducted in triplicate). Both sets of results seem to show that the oil phase characteristics does not affect 80:20 ratio stability optimisation, however, the PDMS seems to be slightly more stable at higher ratios. This may be due to the density of the PDMS tested being 0.98g/cc compared with the silanes 0.9g/cc, and the increased energy required to move larger molecules. Polymer entanglement may also reduce movement of phases, reducing separation exhibited. The cause for the destabilisation above 80wt% oil in both silane and siloxane tests is attributed to film drainage in the continuous phase. A lack of excess water in between droplets allows film drainage under stress, which is followed by coalescence due to micelle-micelle interference and rupture. Results show that creaming may be reduced by using an oil phase with similar density characteristics as the water phase, while retaining adequate water in the continuous phase to reduce coalescence potential. Figure 26 shows the similar phase attributes are achievable at larger concentrations of surfactant, thus showing that surfactant concentration was not the determining factor in testing at 2wt% surfactant concentrations with regard to phase separation. This helps verify that the observed destabilisation was due to the phase ratio characteristics of prepared emulsions. This means that in to prepare a stable emulsion of the tested phases, an 80:20 weight ratio of oil to water would be the most suitable regardless of surfactant concentration.

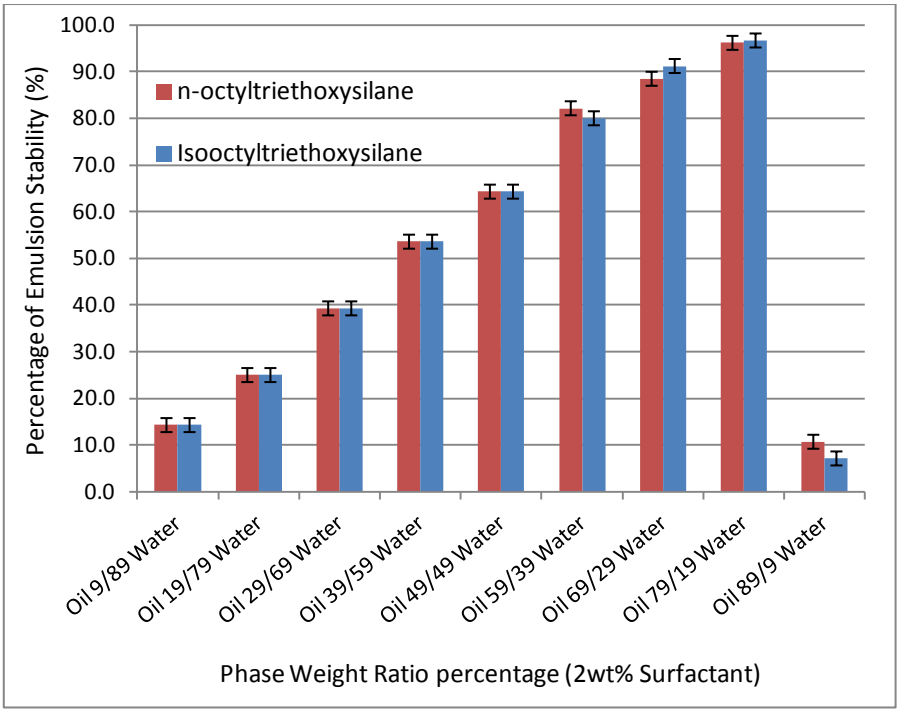

Figure 24: Phase ratio stability results

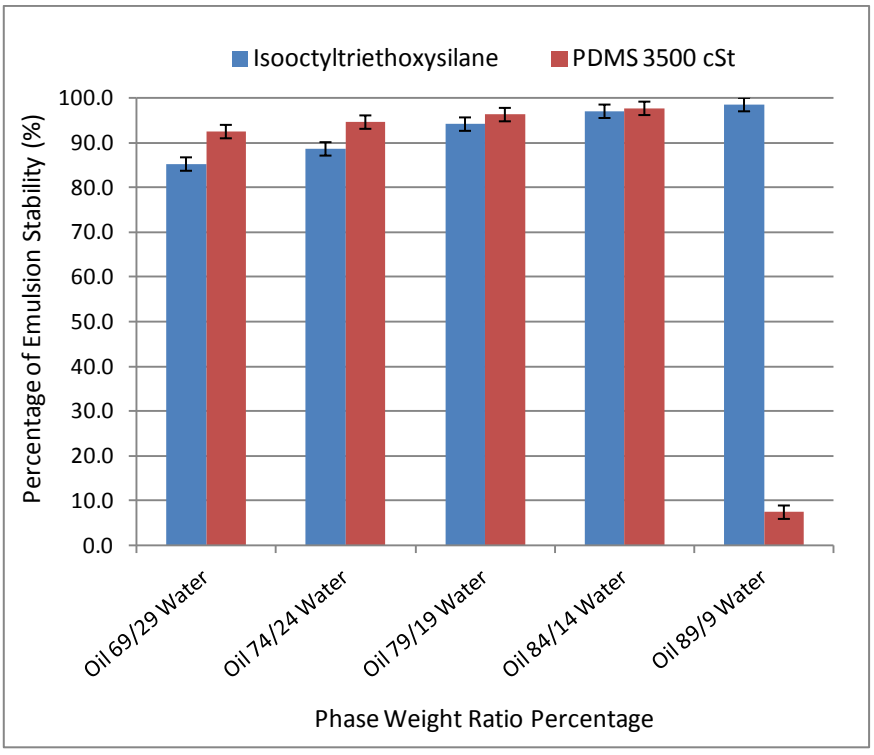

Figure 25: Phase ratio stability results at 2wt% surfactant concentration

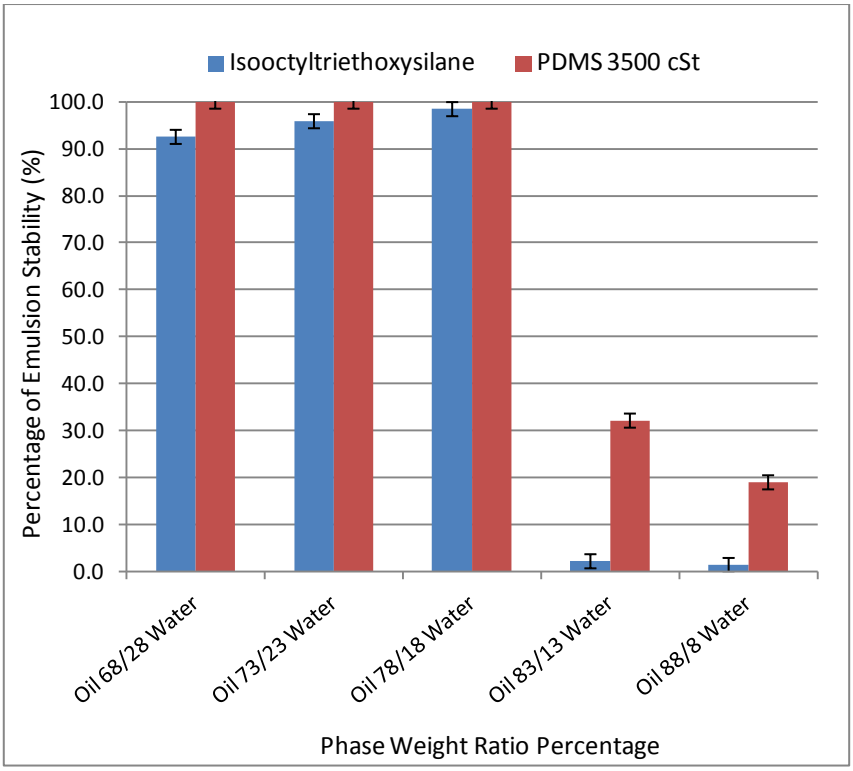

Figure 26: Phase ratio stability results at 4wt% surfactant concentration

4.2 Optimisation of Surfactant

4.2.1 Surface Tension – Pendent Drop

Elongation/shape of the droplet during the pendent drop method is due to two determining influences gravity and surface tension. Therefore if the drop shape can be determined, so can the surface tension value [**160**]. 5 samples were assessed for each test and averaged.

The aim of this study was to assess the surface tensions of major emulsion phase constituents using the pendent drop method. From this an assessment of the difference between surface tensions of these phases could be made. In addition to distilled water and n-isooctyltriethoxysilane, ethanol was tested to assess its impact on the oil phase which contained ca. 5wt%.

Results are shown in Tables 9 to 11. From these it was found that the distilled water used has a relatively high surface tension compared to the silane and ethanol. It stands to reason since it has a higher availability of OH groups at the interface for hydrogen bonding; helping to retain the droplets structure.

Silane had a lower surface tension to the ethanol since ethanol has a greater proportion of OH groups per unit volume and thus has a higher surface tension. Since silane has a hydrocarbon tail, this reduces surface tension due to diminished polar activity. Both ethanol and silane therefore have similar surface tensions. This means that both should be miscible in each other.

A reading from a mercury thermometer showed testing was carried out at 25±1°C. Figure 27 shows an example of fitting by the Young-Laplace model during testing. Phase values used during testing are stated in Appendix B.

Table 9: Distilled water surface tension results

Test Number	Mean Surface Tension (mN/m)	Standard Deviation of Surface Tension (mN/m)	Mean Droplet Volume (microL)	Standard Deviation of Droplet Volume (microL)
1	71.52	0.25	11.06	0.01
2	70.11	0.07	11.98	0.01
3	70.92	0.30	11.49	0.02
4	70.85	0.19	11.84	0.01
5	71.27	0.13	12.52	0.02
Average	70.93	0.19	11.78	0.01

Table 10: Ethanol surface tension results

Test Number	Mean Surface Tension (mN/m)	Standard Deviation of Surface Tension (mN/m)	Mean Droplet Volume (microL)	Standard Deviation of Droplet Volume (microL)
1	23.76	1.05	4.85	0.09
2	24.16	0.94	4.99	0.05
3	25.68	-	4.98	-
4	24.28	1.82	5.03	0.09
5	22.19	1.83	5.01	0.05
Average	24.02	1.41	4.97	0.07

Table 11: n-Isooctyltriethoxysilane surface tension results

Test Number	Mean Surface Tension (mN/m)	Standard Deviation of Surface Tension (mN/m)	Mean Droplet Volume (microL)	Standard Deviation of Droplet Volume (microL)
1	23.59	0.05	4.50	0.00
2	23.13	0.01	4.47	0.00
3	23.65	0.10	4.52	0.00
4	23.73	-	4.43	-
5	24.36	-	4.45	-
Average	23.69	0.05	4.48	0.00

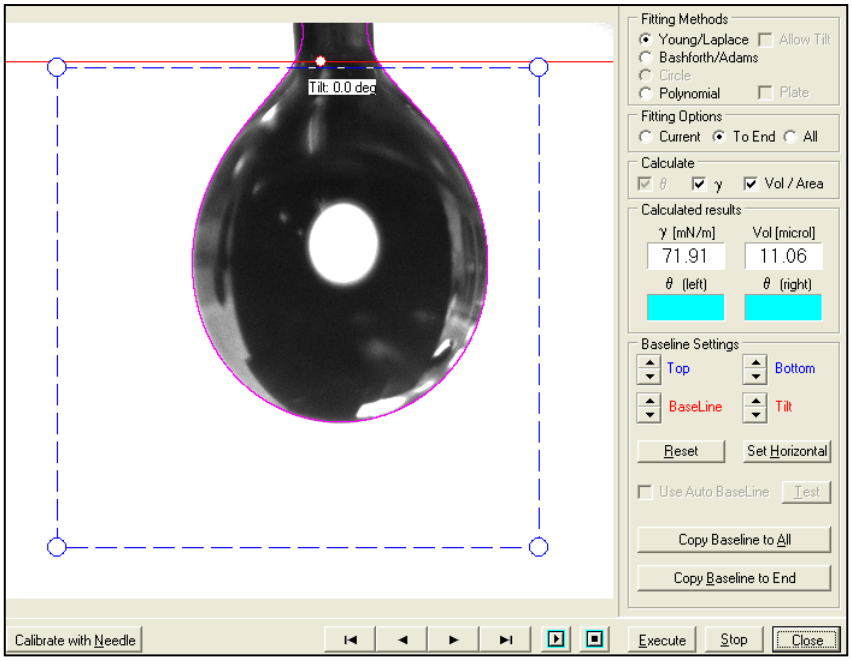

Figure 27: Pendent drop; Young/Laplace fitting of distilled water

4.2.2 Surface Tension – Wilhemy Plate

In order to assess the extent surfactants used during the study reduced interfacial tension as well as the minimum required for micelle formation, tensiometry was conducted using the Wilhemy plate method. Different surfactant ratios and concentrations were assessed in deionised water to assess micelle formation points and impact on surface tension. From the pendent drop experiment the average surface energy for distilled water and n-isooctyltriethoxysilane was 70.93mN/m and 23.69mN/m. From this study POE (15) had a reduced surface tension of ~41mN/m and POE (60) ~50mN/m. In addition to this the 1:1wt% mixture of POE (15/60) had a reduced surface tension ~42mN/m. So the surfactants reduced the surface tension of water (~71mN/m) but not enough to meet the n-isooctyltriethoxysilane surface tension, one of the major constituents in the studied emulsions. Thus, either constant input of energy and/or an additional stabiliser is required by the system. Alternatively a different surfactant system may minimise this difference.

It was estimated that the CMC points were 0.0064g/ml, 0.00036g/ml, and N/A g/ml for the POE (15), POE (60) and POE (15/60) respectively. POE (15/60) needed more points in a different range to accurately assess the CMC point. When comparing surface tension and concentration of all three samples as shown in Figure 28 it is clear

that POE (60) is not reducing surface tension as well as the POE (15). However rheological benefits as well as reducing temperature sensitivity of the emulsion may be of importance. In addition, POE (60) does not seem to modify the POE (15/60) as much as the POE (15). Thus, from adding small quantities of POE (60) beneficial thermodynamic stability and rheological modification may theoretically be achieved with little compromise of surface tension. This therefore helps to characterise and formulate the emulsion system.

Table 12: POE 15 CMC results

Sample no	Vol H20 (mL)	Vol Det (mL)	Total Volume (mL)	Wt of Detergent assuming 10% Conc (g)	Concentration (g/ml)
1	30.00	0.05	30.05	0.005	0.00017
2	30.00	0.15	30.15	0.015	0.00050
3	30.00	0.45	30.45	0.045	0.00148
4	30.00	1.50	31.50	0.150	0.00477
5	30.00	3.50	33.50	0.344	0.01028
6	30.00	7.00	37.00	0.690	0.01865
7	30.00	13.00	43.00	1.286	0.02991
8	30.00	19.00	49.00	1.877	0.03831
9	30.00	21.00	51.00	2.085	0.04089

Table 13: POE 60 CMC results

Sample no	Vol H20 (mL)	Vol Det (mL)	Total Volume (mL)	Wt of Detergent assuming 10% Conc (g)	Concentration (g/ml)
1	30.00	0.05	30.05	0.005	0.00018
2	30.00	0.15	30.15	0.015	0.00051
3	30.00	0.45	30.45	0.041	0.00134
4	30.00	1.50	31.50	0.148	0.00471
5	30.00	3.50	33.50	0.345	0.01029
6	30.00	7.00	37.00	0.691	0.01866
7	30.00	13.00	43.00	1.283	0.02984
8	30.00	19.00	49.00	1.869	0.03814
9	30.00	21.10	51.10	2.114	0.04137

Table 14: POE (15/60) CMC results

Sample no	Vol H20 (mL)	Vol Det (mL)	Total Volume (mL)	Wt of Detergent assuming 10% Conc (g)	Concentration (g/ml)
1	30.00	0.05	30.05	0.005	0.00017
2	30.00	0.15	30.15	0.015	0.00049
3	30.00	0.45	30.45	0.043	0.00142
4	30.00	1.50	31.50	0.150	0.00475
5	30.00	3.50	33.50	0.345	0.01030
6	30.00	7.00	37.00	0.689	0.01862
7	30.00	13.00	43.00	1.277	0.02970
8	30.00	19.00	49.00	1.899	0.03875

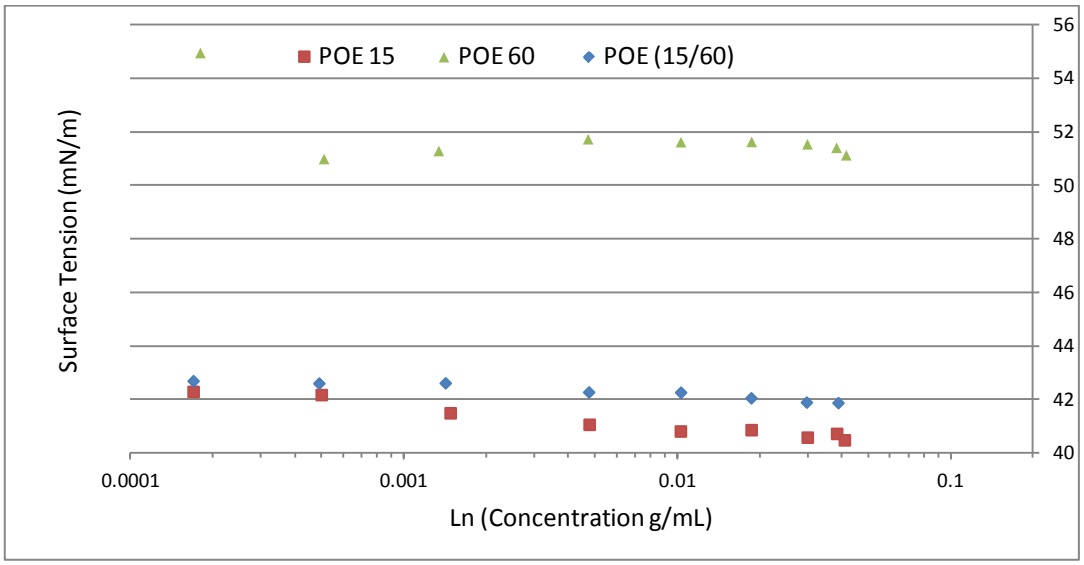

Figure 28: Comparison of surfactant surface tension vs concentration

4.2.3 Rheology of POE (60) in Emulsion

To help identify the CMC point and to assess what impact POE (60) had on rheological alteration to the emulsion, rheological study was conducted using a cone and plate rheometer configuration. Sample definitions are given in Appendix C; Table 42.

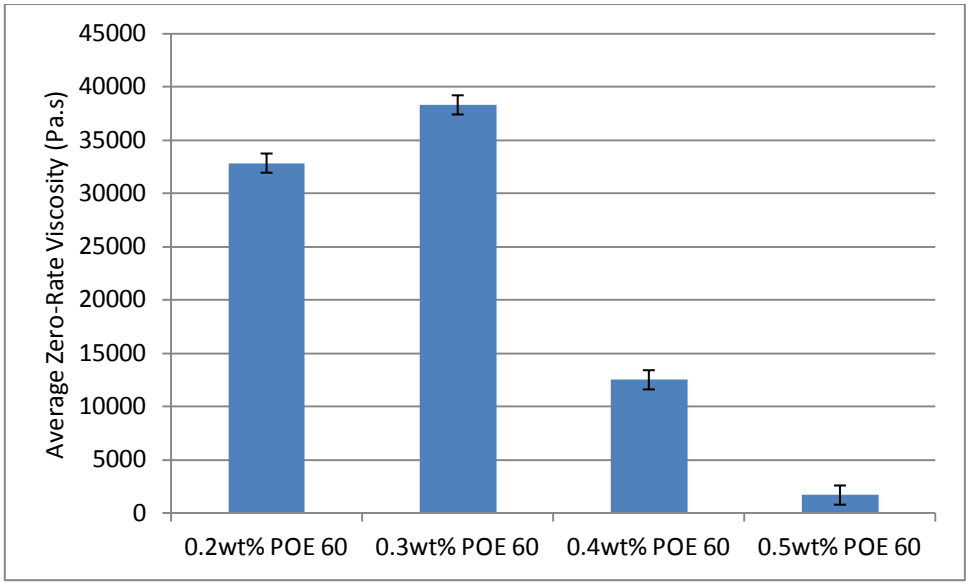

Figure 29: Average zero-rate viscosity of emulsions with different POE (60) concentrations

Zero-rate viscosity results derived from the Cross model are shown in Figure 29. It shows that around 0.3wt%, the emulsions have the highest viscosity at rest. Below this point viscosity is increased as micelles are being partially formed, and the extent is dependent on concentration. This continues until the micelle forms in the polydispersed system providing the greatest shear resistance. Above this concentration, surfactant aggregates around the siloxane present (7.5wt%) reducing solubility and networking; minimising viscosity by increasing drainage potential. From these results it shows that less surfactant in silane/siloxane emulsions is desired and supports work carried out by other parties on polymer complexation [**171**] [**172**]. Further work in this field would be required to characterise this process in more detail however results do verify the requirement for low and precise concentrations of surfactant in the emulsion formulations. Formulations were not tested above 0.5wt% as emulsions become a semi-solid gel at 0.6wt% and above that broke up under shear; thus unsuitable for the desired application. The reason for this gellation due to low concentrations is attributed to the branched nature and extensive size of the surfactants polar groups. In addition, after application it also had detrimental surface energy characteristics for water repellent treatments, thus limiting the surfactants concentration to 0.5wt% and below.

4.3 Optimisation of Emulsification Process

4.3.1 Overview

In order to produce the emulsions presented in this thesis without other additives, emulsions were prepared through the following method;

1) Oil and surfactant were placed in one container, and water in another container.
2) Both containers were heated in a water bath at 90°C until the surfactant melted.
3) Once the surfactant was melted and without agitation, water was added quickly and again without agitation.
4) A high shear homogeniser was used at 35,000rpm at the phase interface to create a high concentration area of emulsion. This then was quickly expanded using the homogeniser to prepare an initial emulsion.
5) To control stability and uniformity, the emulsion was then quickly mixed for two minutes at 11,000rpm. This produced a 'base emulsion' to which siloxane and nanoparticulates were then mixed at varying degrees depending on the scenario tested.

The reason for this study was to optimise stability and rheology of the emulsion system at the later stages of processing. Droplet size, distribution and processing will affect the final emulsions shelf life and application behaviour and thus optimisation and characterisation of such is of interest during emulsion formulation. To achieve the characterisation for these stages, turbidity, droplet morphology, and physical stability was assessed according to the method stated in Appendix D: Emulsification Optimisation. Results are also show in this section with regard to mixing times and mixing speeds. This section deals with sub-sections (4) and (5) and the impact of altering mixing times. It should be noted that the temperature mentioned in section (2) and the water addition rate was studied in an earlier pilot study which highlighted this method as a suitable procedure to make these particular emulsions. It should also be noted that the process optimised here relates to the production of 100ml of emulsion at one time using specific equipment. Furthermore, that scaling up of such process or using different equipment would strongly affect the final emulsion. Finally, any variation with regard to materials incorporated will also affect the optimisation of

processing, and for this reason only highlighted points have been included within this study.

4.3.2 Colloidal Nanoparticulate Incorporation into Base Emulsion Optimisation

The aim of this study was to evaluate the mixing time required to incorporate 10wt% titanium dioxide and 10wt% colloidal dispersions into the base emulsion. For results *see Appendix D Section A.*

4.3.3 Siloxane Mixing Time

The aim of this study was to evaluate the effect of mixing on the studied emulsions with respect to the stability and homogeneity of the emulsion. To minimise the possibility or extent that destabilisation was due to siloxane influence on the base emulsion at mixing times <0.1wt% hydrophilic fumed silica was incorporated into the base emulsion. Hydrophilic fumed silica was used as the majority of the particle will be present in the continuous phase and thus alter stability though streric mechanisms. From earlier studies it was found that small quantities of fumed silica were effective at stabilising the base emulsion. Thus to reduce variables from the exclusion of nanoparticulates in the emulsion this was used in their place. *For results see Appendix D Section B.*

4.4 Siloxane Incorporation and Optimisation in Base Emulsion

4.4.1 Overview

During the study, a siloxane with hydroxyl end terminations was used. The study shows that hydroxyl terminated siloxanes may take over from more conventional methanol producing siloxanes in the emulsions studied, creating a more environmentally and user friendly system. Sample descriptions are given in Appendix D Section C.

4.4.2 OH Terminated Polydimethylsiloxane

Three different viscosity hydroxyl terminated siloxanes were evaluated in the following tests to assess its suitability in silane/siloxane aqueous emulsions. Conventionally, amino-functionalised siloxanes are used in emulsion systems due to

their efficacy at bonding. During curing however, the majority of amino-functional siloxanes produce a methanol by-product, which is considered toxic. However, similar hydroxyl functionalised alternatives produce water as the by-product [**171**]. Both silane and siloxanes having ethoxy and hydroxyl functional groups respectively and therefore may form three dimensional interpenetrating networks through hydrogen bonding to masonry and wood [**43**] [**44**]. Thus, there is substantial interest in hydroxyl functionalised siloxane emulsions as a safer, more eco-friendly alternative.

4.4.2.1 Physical Stressing

Stability of an emulsion is critical for its performance and shelf-life. Emulsion instability may lead to premature curing as silane and siloxane components react with the water phase to cure, and therefore reduce the active content of material that could be used effectively for facade protection. Macro-emulsions are influenced by gravitational stressing, and hence emulsions were tested to assess physical ageing [**117**].

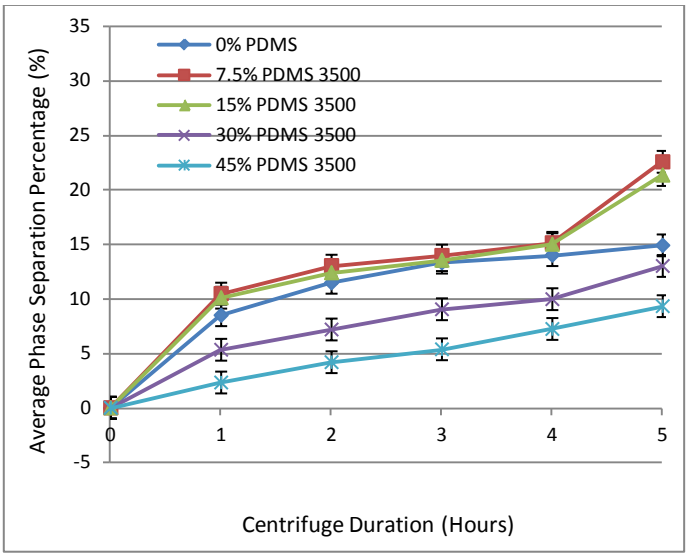

Figure 30: Mean physical stress results for 3,500cSt siloxane

Figure 30 to Figure 32 show a general increase in destabilisation with time for higher PDMS concentrations and viscosities respectively. The 3,500cSt PDMS emulsions showed less separation than the longer chained siloxane emulsions for the same concentrations. It is suggested that when siloxane is incorporated into the base emulsion, it forms a 'second' oil phase. Since the surfactant, which is present in very small quantities (<0.5wt%.) is already adsorbed on silane droplets, it does not play a

significant role in the stabilisation of the newly formed siloxane phase. Instead, the highly flexible PDMS chains expose their OH endings to the water phase and effectively cover the drop with polar groups, similar to a micelle. Unfavourable interactions are hindered as the hydrophobic part of the chain is hidden inside the droplet, which lowers the total energy of the system. Effectiveness of this specific spatial orientation is reduced for longer chain lengths due to a lower quantity of terminations present: 3,500cSt PDMS; 0.08wt% OH, 50,000cSt PDMS; 0.03wt% OH, 90-120,000cSt PDMS; 0.02wt% OH. In addition, longer-chained PDMS tends to form larger oil droplets than shorter-chained alternatives. At higher concentrations PDMS cannot be contained in droplets and the excess siloxane enters the continuous phase, altering the emulsions' rheological characteristics, and hence its stability.

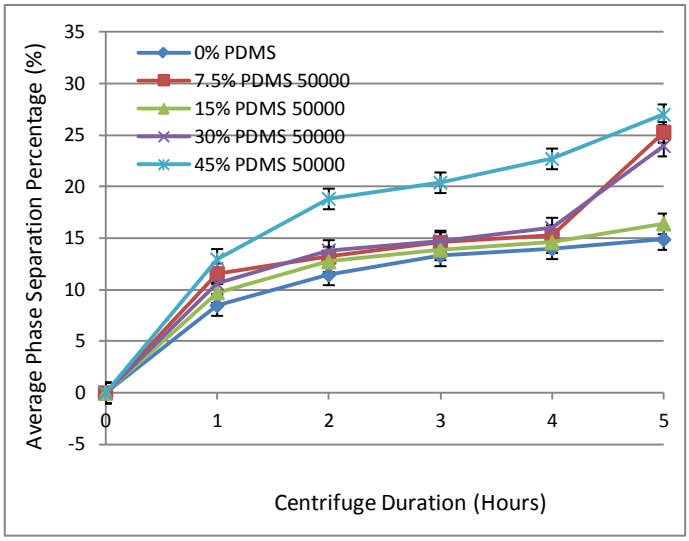

Figure 31: Mean physical stress results for 50,000cSt siloxane

Droplet size is known to be one of the major factors affecting the stability of emulsions, with higher stability expected for smaller droplets [**172**]. Smaller droplets are more stable in the emulsion attributed to favourable interactions between the water and the polar surface layer of the PDMS droplets, as well as having reduced slipping potential. Hence the reason higher concentrations of short 3,500cSt PDMS chains exhibited an increase in emulsion stability. Conversely, longer-chained PDMS emulsions exhibited reduced stability with time and increasing concentration, due to larger droplets and less favourable interaction potential. Figure 31 and Figure 32 show longer siloxane chains are less stable due to less OH terminations and larger droplet sizes, and thus are more prone to coalescence and separation. Therefore, for longer

chains, separation between phases occurs sooner and to a greater extent, providing a more pronounced trend at higher concentrations.

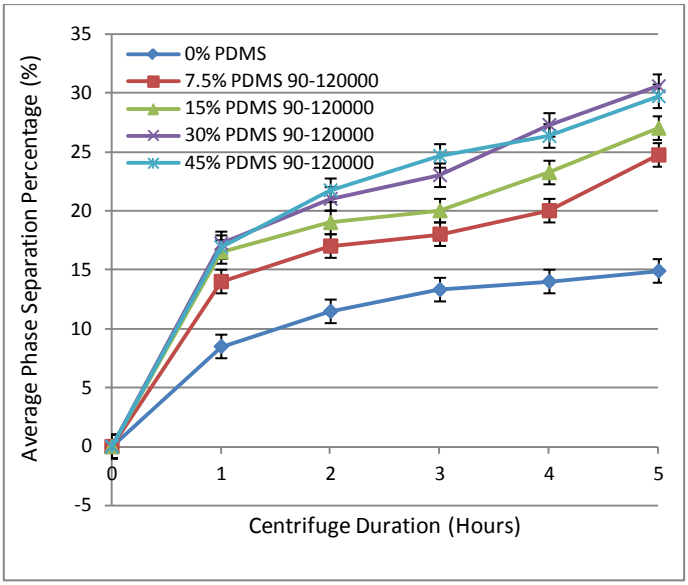

Figure 32: Mean physical stress results for 90-120,000cSt siloxane

Complexation of polymer-surfactant systems is known to alter the stability and rheological characteristics of colloidal systems. Above critical aggregate concentration (CAC), surfactant is thought to effectively stabilise primary oil droplets, with the addition of polymer at sufficient concentrations allowing complexation to commence. Polymer functional groups may fill gaps in micelles, reducing interfacial tension from exposed hydrophobic regions that are still accessible. Figure 33 shows that the absorbed layer thickness (δ) of polymer at the micelle interface with siloxane increases until a 'critical' concentration is reached. After exceeding this, the excess polymer is suspended in the continuous phase. At greater concentrations, this 'third' phase of siloxane becomes the continuous phase [**119**] [**173**]. Figure 33 suggests that δ surface area exposed for inter-micelle interaction can change with polymer content. Greater possible interaction between micelles, through long range forces and hydroxyl bonding of the surfactant head groups, may be achieved until a maximum surface area threshold is reached. Polymer aggregates may form networks with micelles in the continuous phase until free siloxane micelles become segregated. It has been reported that below a critical concentration, emulsion rheological characteristics are attributed to the microscopic properties of the system. Above this concentration, rheological characteristics are attributed to both the morphology of droplets and dispersed phase networking [**174**]. These findings confirm that the concentration of siloxane is crucial,

the faster separation observed for higher viscosity siloxane emulsions, highlight the necessity for optimisation [**131**].

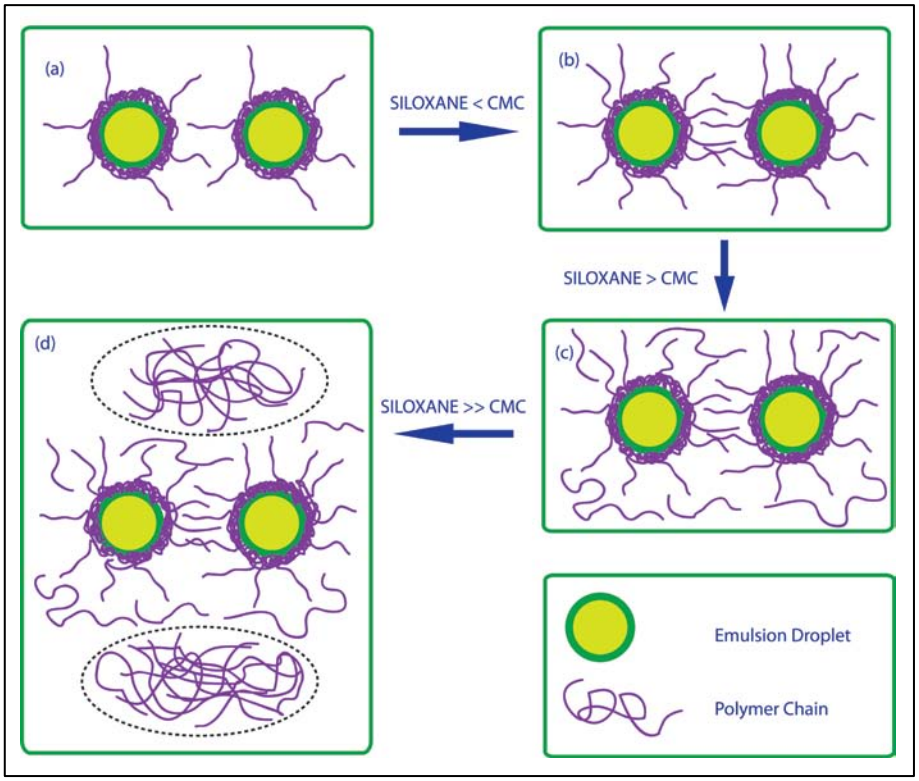

Figure 33: Schematic representation of polymer/surfactant complexing in O/W emulsion; (a) polymer aggregation on emulsion drops, (b) increased aggregation by siloxane, (c) critical micelle concentration (CMC) surpassed, free siloxane in continuous phase (d) coalescence of siloxane producing a discrete third phase

4.4.2.2 Thermal Stressing

Thermal stressing is attributed to the environmental conditions in which the emulsion will be stored and transported. Emulsions must be able to withstand more diverse conditions than conventionally expected in order to provide assurance that they will be effective at the point of use. The testing scenario therefore attempted to replicate reported extreme European weather conditions to assess stability effectively.

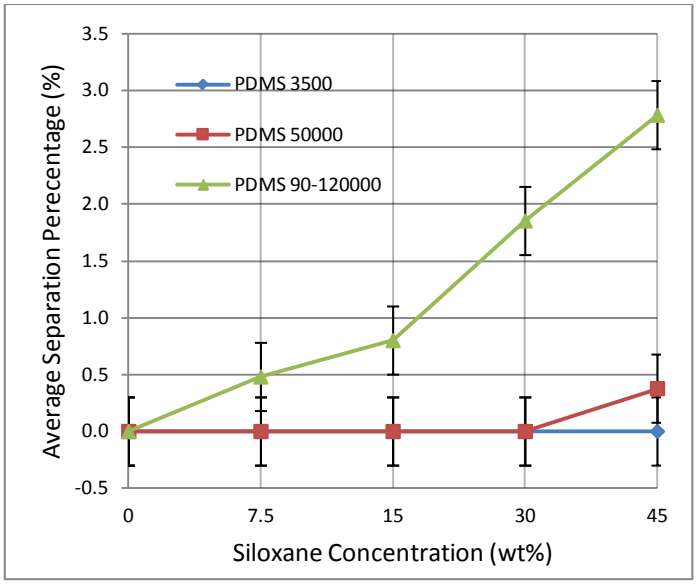

Figure 34: Mean thermal stress results

Figure 34 shows the average phase separation produced after a thermal stress cycle. Observed instabilities are in accordance with the theory stated prior. Longer continuous chains are less soluble, and consequently have different rates of expansion than shorter PDMS chains. Since the siloxanes tested have different characteristics, they exhibited dissimilar thermal mobility and the rates of stressing varied for different PDMS viscosities. Lower viscosity siloxanes with shorter chains can adapt faster to thermal stresses compared with those of higher viscosity. In addition, longer-chained siloxane forms a less networked structure, thus the emulsion becomes more susceptible to temperature changes, and hence less stable.

4.4.2.3 Rheology

Rheological scrutiny of such emulsions can provide an insight into the morphology of an emulsion and the extent of networking occurring in a quantitative manner. Viscosity, yield stress and ratio index numbers were all assessed to help determine how siloxane affected emulsion characteristics.

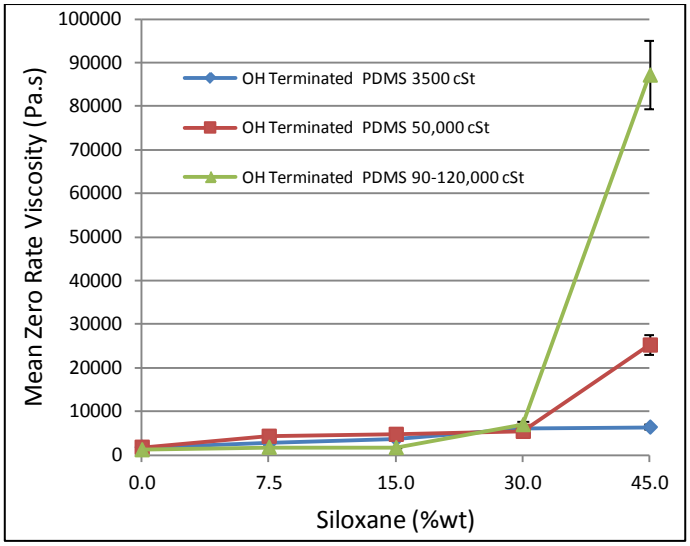

Figure 35: Mean zero rate viscosity

Figure 35 shows the viscosity increases with concentration, implying that the excess siloxane at higher concentrations moves into the continuous phase either in a partial or discrete manner. The viscosity of 3500cSt PDMS emulsions negligibly increased even for very high siloxane concentrations, showing good stability of PDMS droplets. Conversely, longer-chained PDMS emulsions showed a substantial increase in viscosity above 30wt%, indicating the inclusion of siloxane in the continuous phase. The siloxane present would act to reduce mobility of smaller molecules through association and hence increase emulsion viscosity substantially.

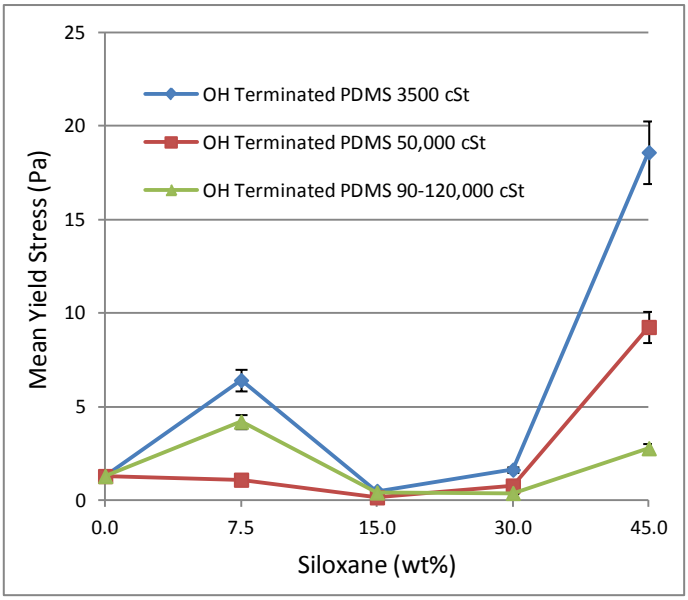

Figure 36: Mean yield stress

Figure 36 shows that yield stress increases sharply above 15wt% concentration, which is in good agreement with the literature. Highest yield stress values were measured for 3500cSt PDMS emulsions. The least viscous siloxane formed smaller micro droplets, which essentially increased the viscosity of the emulsion and thus made it less deformable [**172**]. Due to their size and inter-chain entanglements longer PDMS chains arranged in larger aggregates, which at higher concentrations group into discrete regions creating a third phase, decreasing the stability of the emulsion and provided a lower resistance to deformation. Measurements confirmed the general trend, but also revealed an unexpected behaviour for the emulsions with low siloxane content. At 7.5wt% of siloxane, the yield stress suddenly increased, only to drop again for further increase in concentration. This phenomenon was attributed to steric interaction between micelle polymer aggregates. Since the increase in siloxane content may restrict inter-micelle long range interaction through increasing interfacial density, this explains the effect of yield stress diminishing. The micelle at 15wt% showed that the interface had less interaction potential due to more uniformity from micelle saturation, and discrete free siloxane may in addition help increase micelle segregation and slipping potential. As the chain length increased in this region (50,000cSt), long-range interactions were diminished and a negligible increase in yield stress was observed. Longer chained siloxane showed steric behaviour on silane micelles and network formation. This suggested that discrete networking between PDMS domains had little strengthening effect for longer chains at low concentrations, and diminished considerably with further increase in concentration. This was attributed to increased micelle segregation occurring.

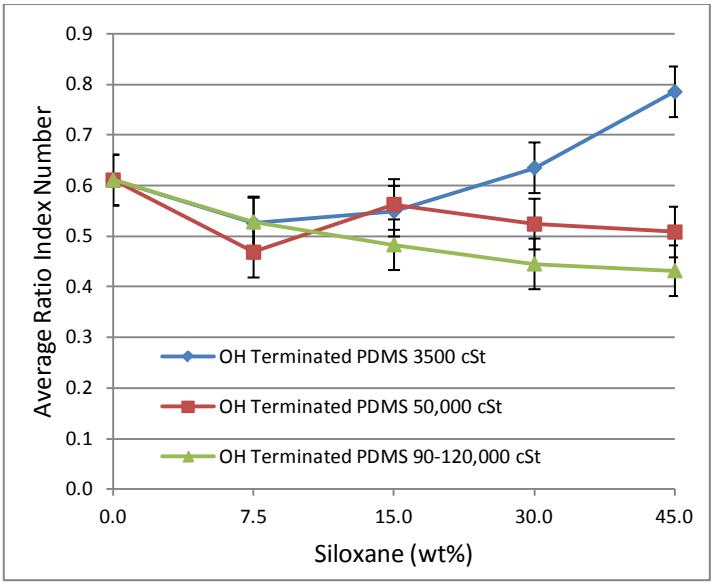

Figure 37: Mean ratio index

Figure 37 shows the mean ratio index number of each emulsion. The index is used to quickly assess if the rheology is Newtonian (1), shear thinning (<1), or dilatant (>1) in nature [**175**]. It may be clearly seen that as the values are all less than one, all emulsions produced had shear-thinning properties. The higher viscosity siloxanes at higher concentrations were more inclined to produce a shear-thinning emulsion, which seems reasonable as they could provide less discrete third phases compared with the lower viscosity siloxanes. Conversely, the 3500cSt siloxane emulsions seemed to tend toward Newtonian behaviour at higher concentrations, which may be explained by the high concentration of surface OH groups effectively reducing slipping potential, providing a more uniform phase interactive emulsion.

4.4.2.4 Water Contact Angle

The beading behaviour of a facade treatment is of key interest for water repellents. If water stays on the surface of masonry over time, it gets absorbed through capillary action into the substrate, significantly reducing thermal efficiency.

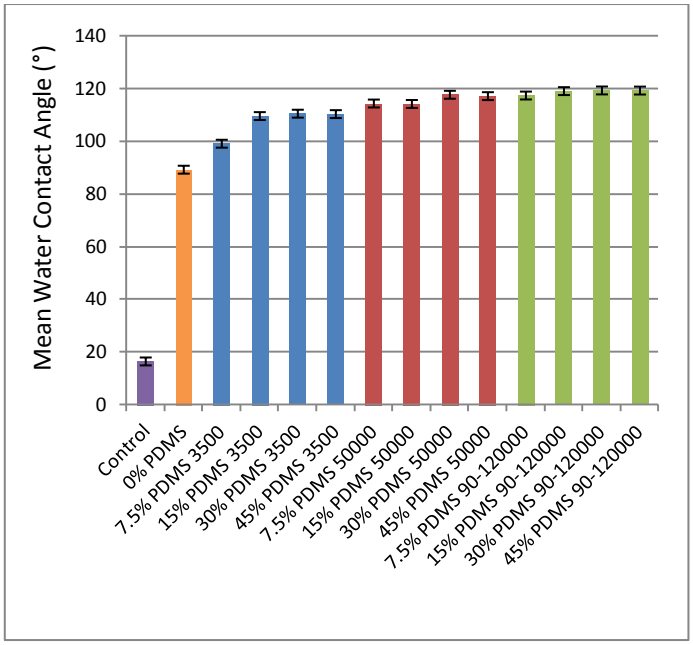

Figure 38: Mean water contact angle results

Figure 38 shows that the addition of siloxane increases the hydrophobic tendency of the treated substrate, and increased proportionally with chain length. An increase in hydrophobicity was also observed for higher PDMS concentrations. It is suggested that less hydroxyl terminations present decreased the number of polar regions throughout the treated substrate. Therefore the proportion of hydrophobic domains increased with longer chain length and concentration, and hence the water is repelled from the surface more effectively. It seems clear that it is the chemical nature of the siloxane itself that is the limiting factor when improving the substrate's hydrophobic tendency and not interfacial roughness, due to diminishing WCA improvements for increased chain length.

4.4.2.5 Treatment Depth

Treatment depth is of great interest in assessing the effectiveness of a treatment's performance against rising damp and water absorption. A treatment that penetrates deep into a substrate is also less susceptible to degradation and allows longer protection than a coating or a film.

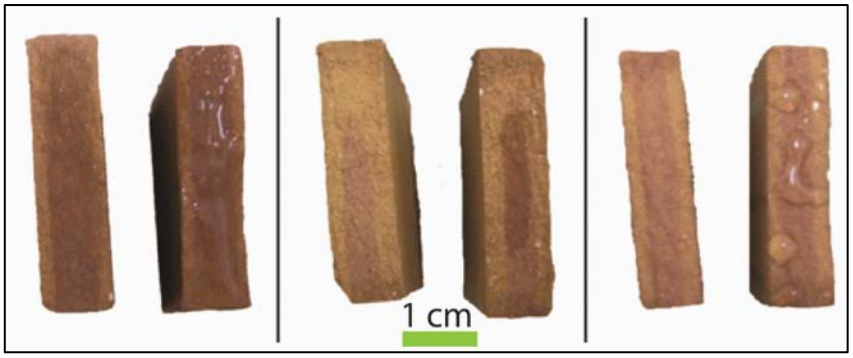

Figure 39: Treatment depth test examples; (left) no treatment (middle) semi-penetrated treatment (right) total penetrated treatment

Figure 39 shows various treatment depth test examples compared to the control cross-section (shown to the left of each). The tile with no treatment shows hydrophilic water filming tendency after submersion. The semi-penetrated treatment tile shows a dark patch in the centre compared with the control, showing the effective depth of the treatment. Finally the tile with total treatment penetration shows water beading on the surface across its entire cross-section. These attributes therefore made it relatively straight forward to assess the effective treatment depth.

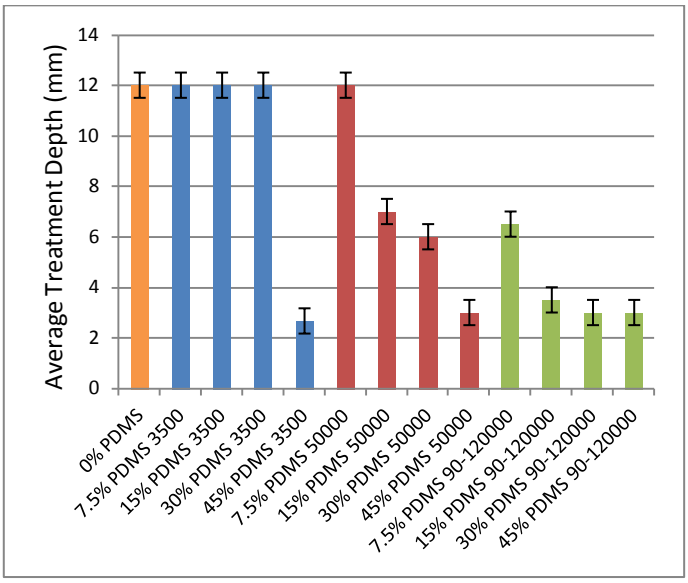

Figure 40: Mean treatment depth results

Figure 40 shows that a significant treatment depth can be achieved with a single application, however it is dependent upon siloxane chain length and concentration. For higher viscosity siloxanes penetration depth was reduced, while increasing PDMS concentration was also found to have a similar effect. The ceramic tiles had an average thickness of 12mm, therefore some results in Figure 40 exhibit total

penetration. These results need to be considered with discretion, as the porosity of substrates will not be the same; a brick may have a porosity of 23wt% compared to a 7wt% terracotta tile. It also assumes that the substrate is homogenous and does not have any glassy vitrified regions or different pore diameters that could invalidate such a test. The force of application may vary, as well as the viscosity of the emulsion depending on its history. However, setting aside these points, the experimental results revealed that treatment depth is compromised by the type and concentration of the siloxane used.

4.4.2.6 Spectrophotometry

Aesthetical alteration of a substrate is detrimental to large scale remediation, heritage, and retrofit projects, since many properties require aesthetical preservation. To assess alteration in a quantitative manner the CIElab D65/10° method was used.

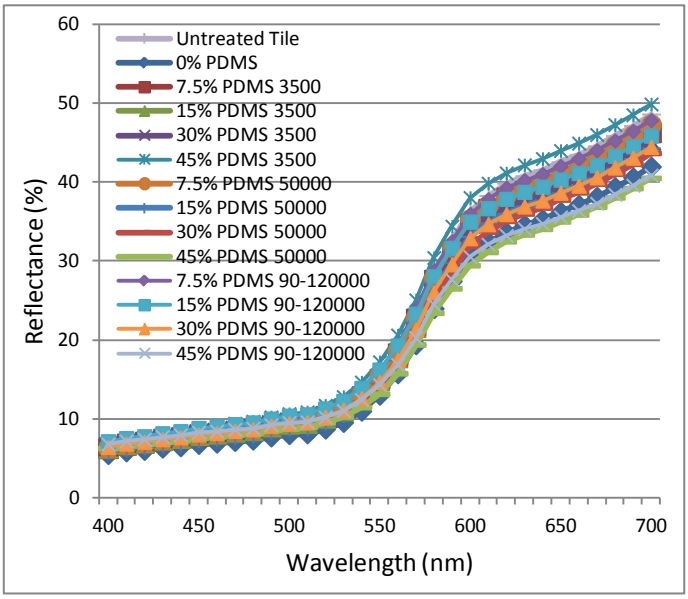

Figure 41: Mean colour spectrum

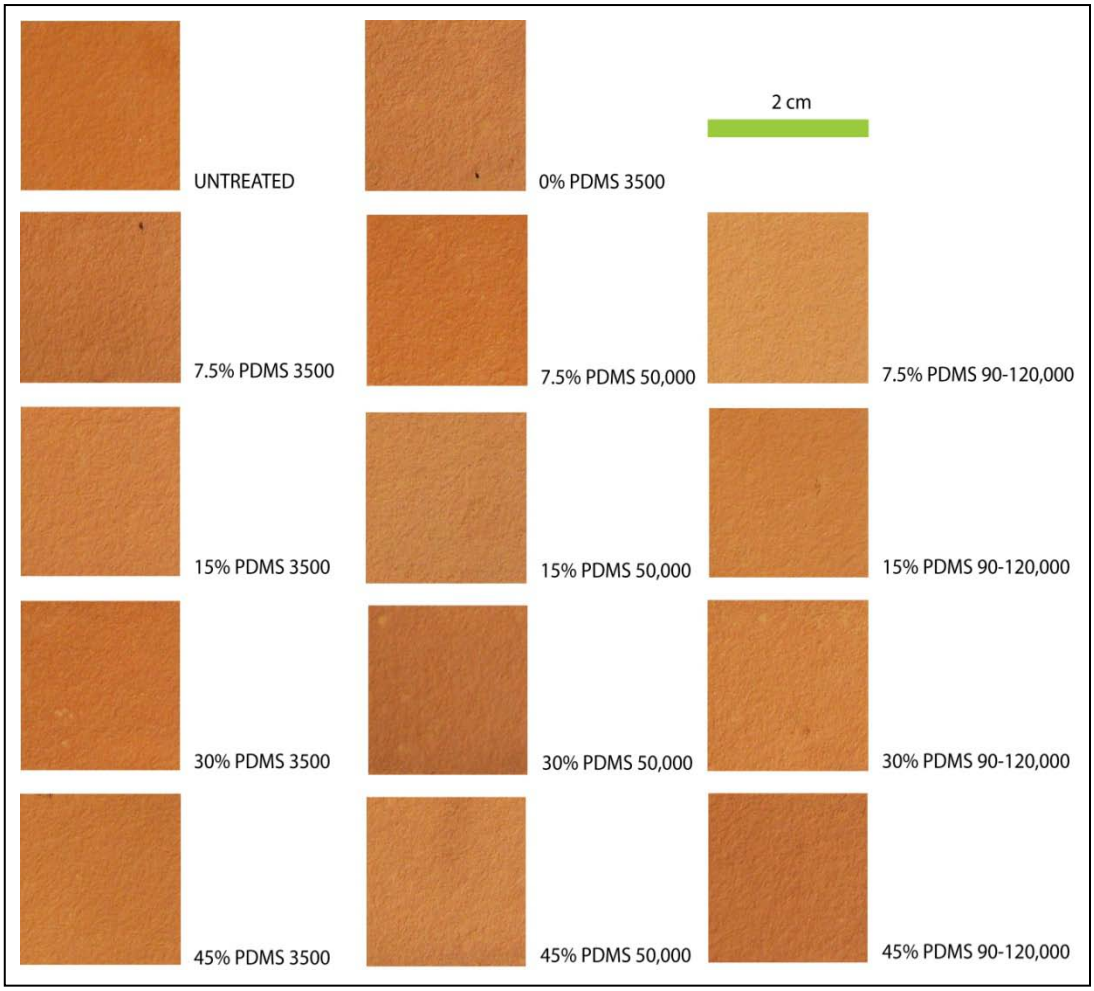

Figure 42: Visual examples of tested samples

Figure 41 shows that the colour of the control matches the colour of the treatments tested with only slight variation. Figure 42 shows that treated samples were similar in colour and gloss to untreated samples, verifying the photospectroscopy results. Table 15 shows that there is a small hue variation (ΔH*%) associated with the build-up of siloxane at the interface for higher concentrations and longer siloxane chains, but this may be considered negligible.

Table 15: CIElab D65/10° mean colour results

	L*	a*	b*	ΔE*	ΔC*	ΔH*	ΔH*(%)
Untreated Tile	51.06	25.00	30.98	64.75	0.00	0.00	0.00
0% PDMS	48.62	24.90	28.88	61.79	2.07	1.73	0.69
7.5% PDMS 3,500cSt	51.49	25.21	30.31	64.85	0.66	0.39	0.15
15% PDMS 3,500cSt	50.80	24.38	29.11	63.42	1.86	1.88	0.74
30% PDMS 3,500cSt	50.86	24.43	28.78	63.34	2.18	2.12	0.80
45% PDMS 3,500cSt	53.55	25.03	30.92	66.71	0.07	0.03	0.01
7.5% PDMS 50,000cSt	51.68	25.11	30.03	64.83	0.94	0.68	0.27
15% PDMS 50,000cSt	50.37	24.82	29.44	63.41	1.52	1.33	0.52
30% PDMS 50,000cSt	49.98	23.91	27.33	61.78	3.62	3.68	1.41
45% PDMS 50,000cSt	48.94	23.91	26.23	60.17	4.71	5.13	1.85
7.5% PDMS 90-120,000cSt	52.44	23.17	29.82	65.13	1.16	1.21	0.42
15% PDMS 90-120,000cSt	52.36	24.54	28.11	63.94	2.86	3.22	1.24
30% PDMS 90-120,000cSt	50.36	23.78	27.53	62.13	3.42	3.59	1.31
45% PDMS 90-120,000cSt	49.57	22.71	25.90	60.37	5.05	5.73	2.08

The average gloss value for the untreated control was 1.4Ill/Obs, with all samples averaging gloss values being between 1.2 to 1.6Ill/Obs. This indicates that the gloss of the treatments when cured is similar to that of the natural aesthetics of the substrate before treatment. Thus, a major benefit may be achieved by using these emulsions for remediation of heritage buildings or buildings requiring aesthetical conservation without effectively compromising the original appearance.

4.5 Morphological Characterisation

4.5.1 Droplet Size and Distribution

To assess the size and distribution of droplets in emulsions containing metal oxide nanoparticulates against a control, optical microscopy was conducted for samples mixed at different durations using a 175W mixer with a blade head after incorporation of dispersions (made through 1 hour ultrasonication of particulates in 90wt% n-isooctyltriethoxysilane). To assess this effectively each emulsion was diluted by 50 %v/v with distilled water. Emulsion descriptions used during the study are shown in Appendix E, Table 45.

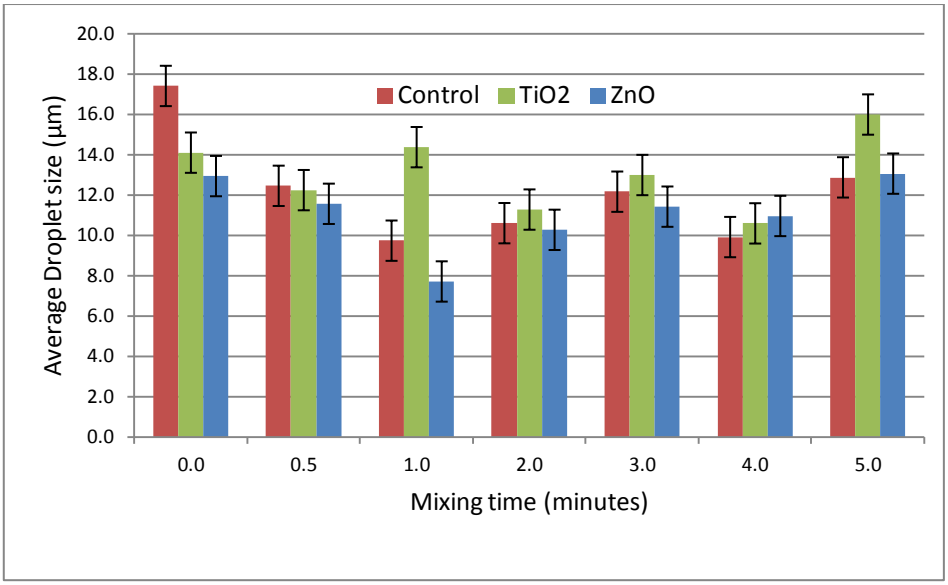

Figure 43: Average emulsion droplet size results

Figure 43 shows that droplet size is reduced on average (testing was repeated for each sample) during mixing until ca. 1 minute however after this time mixing is counterproductive as the formed micelles coalesce and the emulsion destabilises. Results seem to show that the control emulsion and emulsions containing the metal oxide nanoparticulates behave in the same manner at <0.1wt% concentration. Regardless of the emulsion or duration of mixing, Table 45 (Appendix D) shows that emulsions are polydispersed and thus should be relatively stable. Figure 44 shows an example of an emulsion during study after applying a 256 bit greyscale filter. The threshold filter was then applied and droplet characteristics then calculated from this.

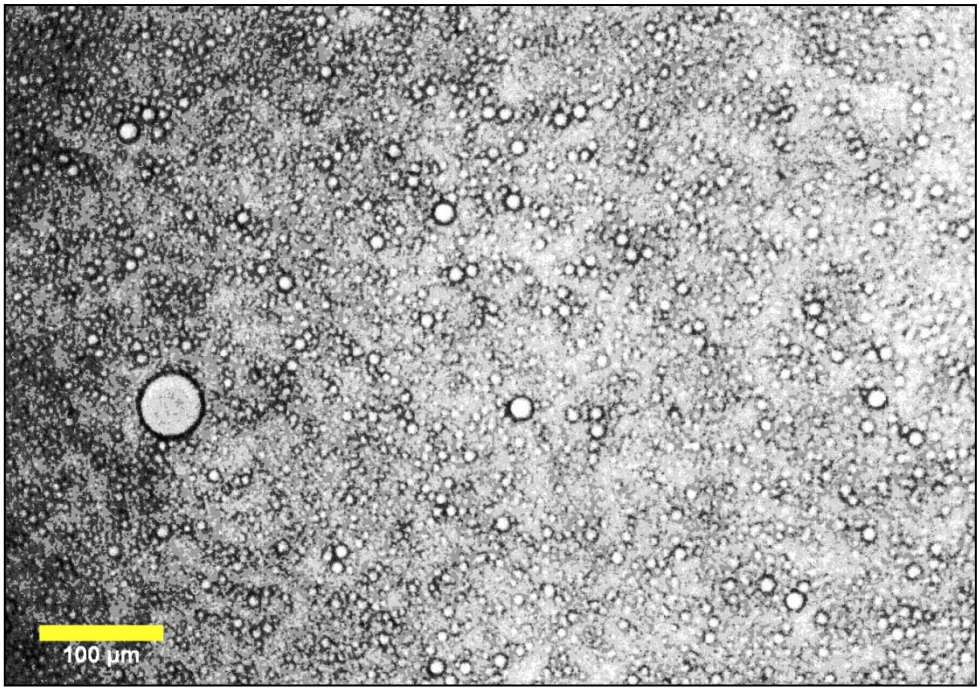

Figure 44: Example of emulsion during optical assessment

4.5.2 Phase Dilution

To comprehend whether an emulsion is oil in water or water in oil by visual means a phase dilution test may be conducted. A solvent should dissolve miscible continuous phases; 'like dissolves like.' An emulsion may be either oil in water (O/W), water in oil (W/O) or an emulsion in an emulsion (typically either O/W/O or W/O/W). If the continuous phase of an emulsion is for example hydrophobic, the placing of a drop of the emulsion to be tested in oil will show a film of the emulsion being produced radiating from the drop. If the emulsion drop was placed in water there should not be any film or drop breakup due to the continuous phase having hydrophobic tendency in a hydrophilic environment. Emulsion descriptions are given in Appendix E, Table 46.

Figure 45 and Table 16 shows that all emulsions exhibit oil in water (O/W) characteristics since water dissolves each emulsion and shown by the film produced. However, in a complex/tertiary system this test would not provide accurate insight into the true phase characteristics; this method gives only a simplistic understanding of the exposed continuous phase. However, looking at the microscopy results, no droplets within droplets were observed thus the emulsions produced are not tertiary in nature. In addition, the majority of observable phase present is dispersed which would imply that the emulsion is O/W as the majority of the material present in these

formulations is silane. To further assess the continuous phase characteristics electrical conductivity testing was conducted.

Table 16: Phase solubility results

	n-isooctyltriethoxysilane Solvent	Distilled Water Solvent
EC	No Film Forms	Film Forms
EZ	No Film Forms	Film Forms
ET	No Film Forms	Film Forms

Figure 45: Dilution of samples in n-isooctyltriethoxysilane *(left)* and water *(right)*; *(top)* control, *(middle)* TiO_2, and *(bottom)* ZnO emulsions

4.5.3 Electrical Conductivity

Microscopy results show that no complex/tertiary emulsions have been produced and that the major volume of liquid is in the dispersed phase pointing toward an O/W emulsion. Phase dilution seems to imply that emulsions again are O/W, however to help complement this and to help understand the type of emulsions produced, electrical conductivity was measured.

Water should be more conductive than silane due to its polar nature [**177**]. Figure 46 shows that water is more conductive than neat silane in simple two phase systems. In addition, results show the majority of the silane is unaltered after mixing in distilled

water, this was confirmed visually by similar separated volume fractions after mixing (due to its density). Testing of the top phase showed distinctly little electrical conductivity which is associated with neat silane. The increased electrical conductivity of the lower phase with increase in silane present in the system shows that there is a better potential for silane hydrolysis to occur with the water phase upon mixing to produce silanol. Due to this reaction, it is suspected that small quantities of silanol is present in the water phase as it is more miscible and that it is these silanol groups that help increase the electrical conductivity of the water phase overall due to the relative size and type of the molecules and their possible structuring within the solution. As activation energy is required for hydrolysis, processing conditions as well as environmental conditions will be important variables during this process. In addition, there needs to be water in specific hydrolysis sites to achieve these reactions during this mixing process thus a possible stoichiometric effect could explain the silanol yield increasing with silane content as the large molecules of silane could be retaining more heat energy within the system for this process.

At lower silane concentrations hydrolysis potentual is reduced through a reduced probability of ion collisions at active sites over the mixing period; the presents of the shear energy of the homogeniser and the presents of water and silane together would have been reduced. Collision time therefore may be a critical factor in emulsion preparation and stabilisation.

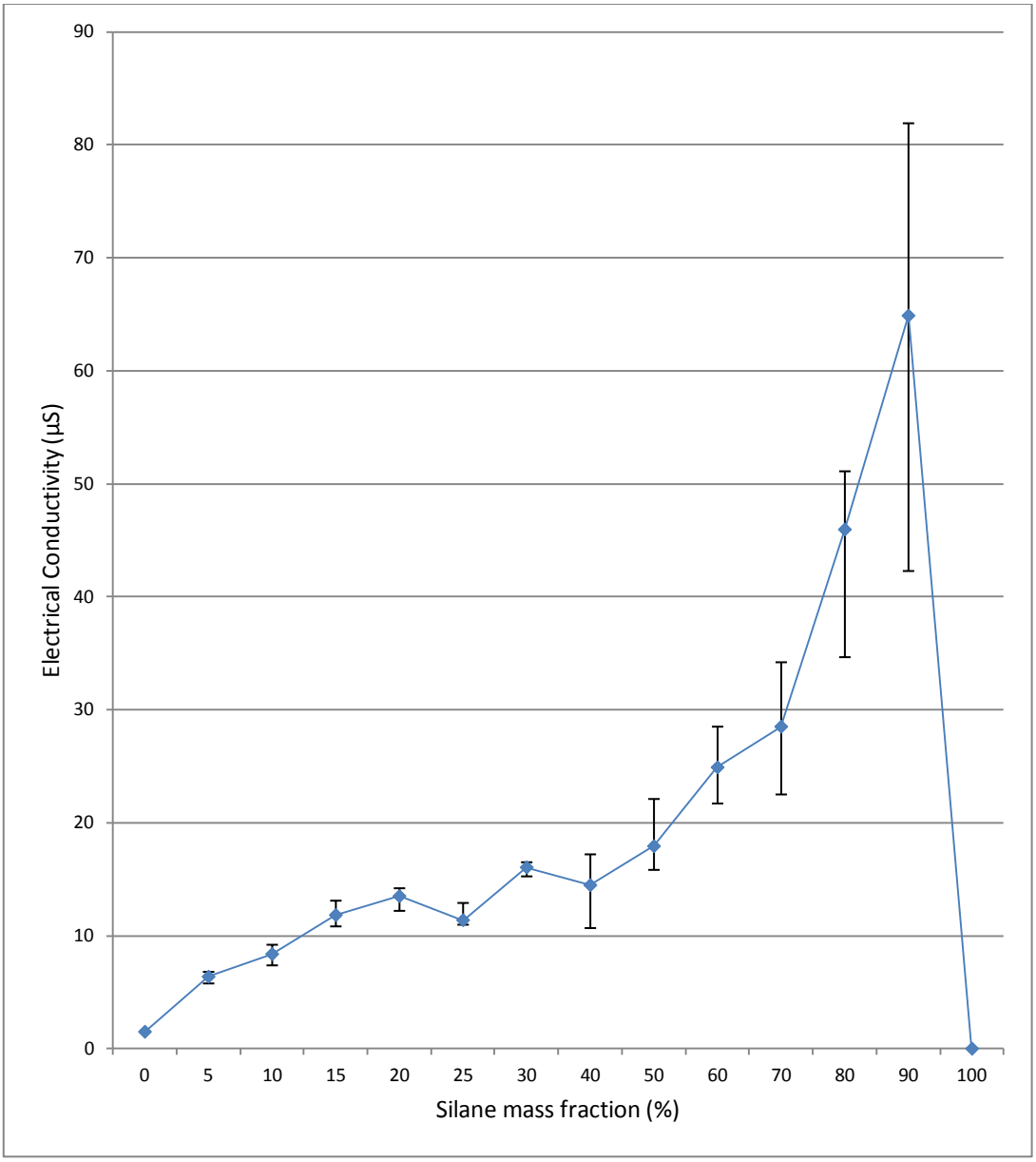

Figure 46: Electrical conductivity results of silane and water (without surfactant) at different dilutions after 30s mixing at 35,000rpm; top phase was 0µS, results are from turbid bottom phase where applicable.

Figure 47 shows what the electrical conductivity of a typical control emulsion would be under different silane concentrations through dilution with water. Again even though a co-surfactant system has been used it appears that the continuous phase is relatively conductive compared to pure silane and pure water respectively, implying that silanol is present which is affecting conductivity. This combined with the phase dilution test (showing water as a solvent to these emulsions compared to silane) and microscopy (showing large volumes as the dispersed phase implying neat silane) these emulsions may be considered in simple terms as O/W and not W/O, however

further testing is needed to fully comprehend the extent of silanol content and influence on the system.

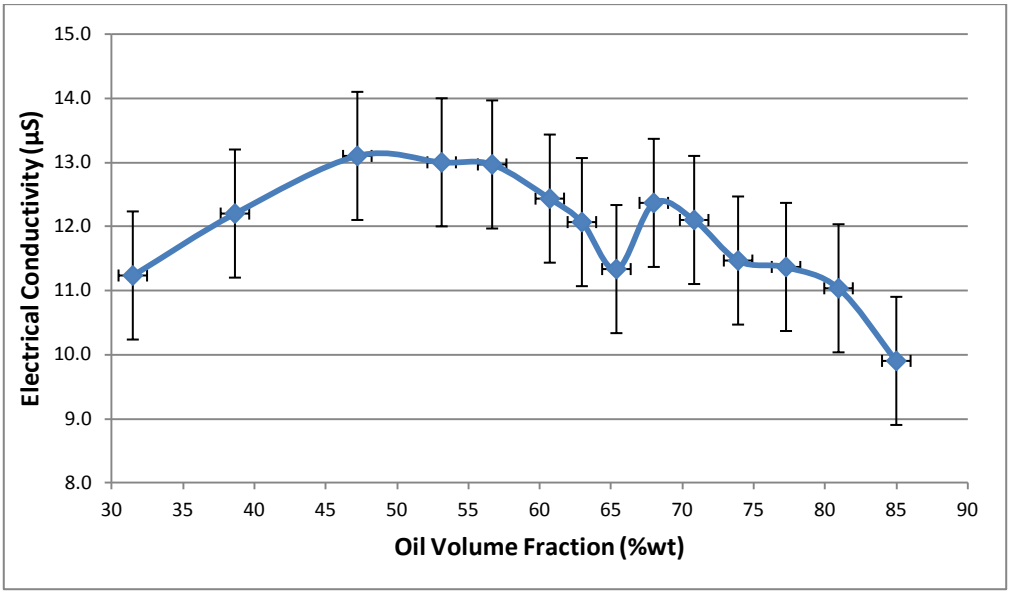

Figure 47: Electrical conductivity results for base emulsion at different dilutions with 0.2wt% POE surfactant

Table 17 shows that it is unlikely that the surfactant used in this study has a significant influence on emulsion electrical conductivity. Figure 48 shows that for emulsions containing nanoparticulate colloidal dispersions conductivity increased with content, this could either be due to silanol present from the silane medium or it may be due to the nanoparticulates. Since Table 17 shows that the medium itself is a poor conductor due to the silane being the continuous phase. This knowledge combined with the results shown in Figure 48 and from previous tests showing that most of the silane is not reacted to form silanol under the presented conditions; the majority of the colloidal silane must be absorbed by the emulsion itself. Rheological evidence shown in a later section (4.4.2.3) that a 'gelled network structure' is formed with viscosity increasing significantly with nanoparticulate colloidal dispersion. It therefore may be the nanoparticulates and/or silanol influencing the morphology of the emulsions produced. Further work is recommended to help understand this system in depth.

Table 17: Electrical conductivity results for emulsion components

	Average Electrical Conductivity (µS)	Maximum Electrical Conductivity (µS)	Minimum Electrical Conductivity Min Value (µS)
Titanium Dioxide 10 wt% ITES Colloid	0.0	0.0	0.0
Zinc Oxide 10 wt% ITES Colloid	0.0	0.0	0.0
POE (15)	0.0	0.0	0.0

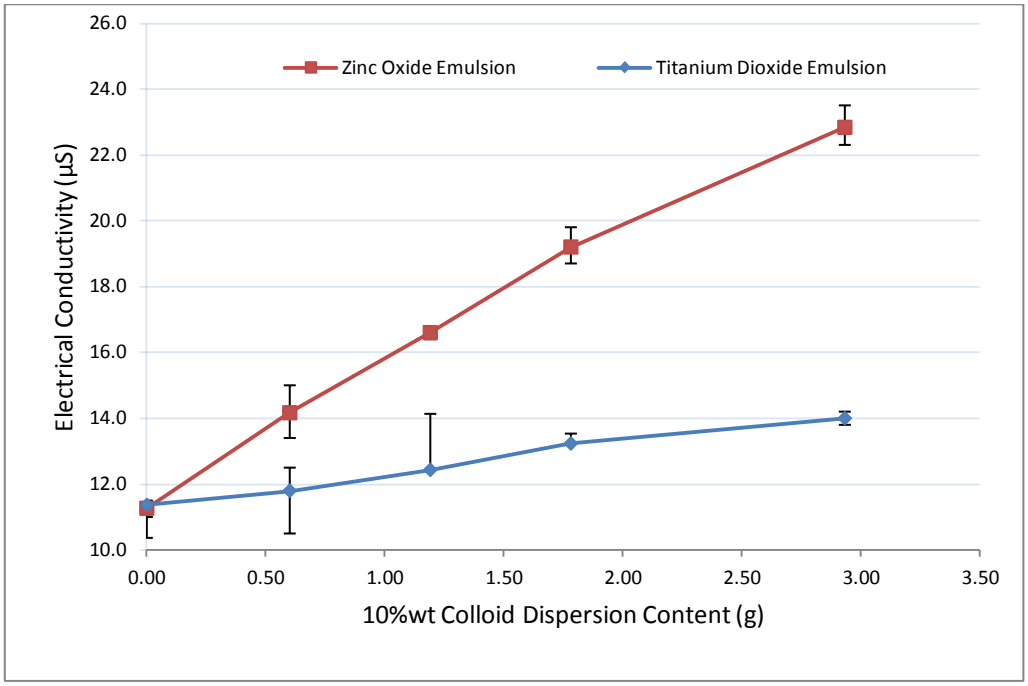

Figure 48: Electrical conductivity results of emulsions containing various quantities of nanoparticulate colloids

4.6 Summary

4.6.1 Volume Fraction

Both silanes tested exhibited phase stability results optimised at 80:20wt% phase ratio. Cationic surfactant did not seem to alter these results, showing head charge of the surfactant did not alter this. Addition of PDMS to the emulsion did not seem to stabilise the emulsion but may have fitted the 80:20 weight ratio if it had achieved a better solubility with the other phases. It would seem from this study that other systems could be optimised based on this principle, this was confirmed through the pilot study, were various co-surfactant systems were tested and based on readily available surfactants (ionic, non-ionic and mixed). However due to them specifically requiring relatively high concentrations for stabilisation (ca. 1wt%), these results are not shown in this study. They were found to be detrimental to reduced surface energy characteristics required for water repellent attributes although robust and highly

stable.

4.6.2 Pendent Drop

- Ethanol and silane had similar surface tensions allowing them the potential to be miscible with one another.
- Distilled water had a higher surface tension than the ethanol or ITES.
- Reducing the surface tension through use of a surfactant would help retain emulsion stability.

4.6.3 Wilhemy Plate

- POE (15) was more effective at reducing surface tension compared to POE (60) across a range of concentrations.
- POE (60) reached CMC at a lower concentration than POE (15).
- Combining POE (15) and POE (60) increased surface tension slightly more than neat POE (15); however it might be valid that an improved stability to the emulsion may be achieved from its addition.

4.6.4 Rheology of POE (60) in Emulsion

Zero-rate viscosity results showed that small quantities of POE (60) did increase viscosity up to ca. 0.3wt% significantly. Beyond this, it was considered that complexation between siloxane and excess surfactant reduced solubility and networking of the system, reducing its stability.

4.6.5 Siloxane Incorporation and Optimisation in Base Emulsion

Rheological characteristics showed at lower concentrations of PDMS droplet morphology controlled the drainage of the continuous phase and hence the emulsions overall viscosity and stability. At higher concentrations, emulsions were governed by a third phase comprising of un-aggregated siloxane that acted to segregate micelles and govern emulsion stability by modifying the continuous phase viscosity. The cross over point was considered to be where siloxane-micelle aggregation potential became essentially zero. The stability of emulsions was governed by the drop size and discrete third phase networking, again depending on the concentration and the chain-length. Water-repelling properties characterised by WCA were improved by viscosity and concentration. This improvement was considered due to the reduced quantity of

hydroxyl groups available for polar interaction. A general treatment depth trend was observed, showing a reduction in penetration with the increase in emulsion siloxane concentration and chain-length. Finally, hydroxyl terminated siloxanes are a promising solution for exterior facade treatments due to their lack of methanol by-products, making them essentially greener and safer during application than amino-functional siloxanes. Treatments evaluated during this study provided water repellent characteristics and penetrated the substrate without effectively altering the visual aesthetics. This makes these O/W silane/siloxane emulsions suitable for large scale retrofit schemes.

4.6.6 Droplet Size and Distribution, Phase Dilution and Electrical Conductivity

All emulsions are polydispersed and therefore help increase stability. In addition, all emulsions follow traits resembling O/W characteristics with regard to general morphology, solvent susceptibility and electrical conductivity. It is considered that the produced emulsions are O/W although it is highly likely that silanol is present in the aqueous continuous phase. Emulsions are not tertiary in nature as found by the optical microscopy. Due to the magnitude of evaluation required, the emulsions produced in this study for simplicity will be referred to as O/W with further work required to investigate the phase characteristics more in depth at a later point.

Chapter 5: Nanoparticulate Optimisation and Influence on Colloidal Dynamics

5.1 Nanoparticulate Dispersion Optimisation

In order to assess the time required to ultrasonically mix nanoparticulates in ITES, TEM was conducted. ITES was used instead of water due to being considered that it would be partially absorbed at the interface of the titanium dioxide allowing better absorption at the interface of micelles; using Janus particulate principles as discussed in the literature review. It was considered in addition that since ITES has the ability to be soluble in water to a certain degree it would also help stabilisation while aiding the reduction of aggregates through steric interaction. Finally, due to ITES being used in these emulsions it would mean that it would provide a higher active yield for emulsions as it would condensate into the 3D interpenetrating networks of the silane condensates. This should aid better integration of nanoparticulates into the treatment interface and increase the treatments longevity and reduced leaching. The reason that ultrasonic mixing was used instead of mechanical stirring was that prior research showed it as an effective means to disperse nanoparticulates by providing high shear forces through the expansion and then collapse of voids during processing [**17**] [**53**] [**181**].

Figure 49 shows that ultrasonic mixing does not seem to reduce the size of the nanoparticulates but can breakdown aggregates formed in the powdered state. The results seem to show that ultrasonic mixing for ca. 1 hour may be the most practically useful mixing time due to problems associated with equipment cooling and thus the reason for its use within this study. Further work may show with improved rig design and setup that further aggregation reduction may be possible although solvent breakdown at higher temperatures may constrain dispersion times. Figure 50 shows the ultrasonic mixer during use; Figure 51 shows a schematic of the rig setup.

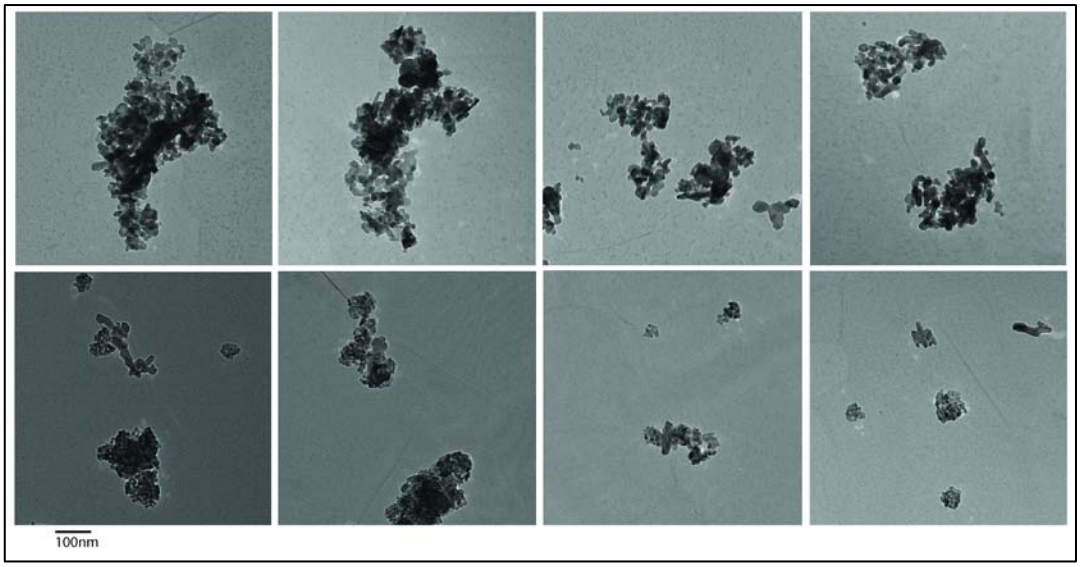

Figure 49: ***(From left to right)*** **TEM results (80kV) for 10wt% ITES** ***(Top)*** **Zinc oxide** ***(Bottom)*** **Titanium dioxide colloidal mixing; 0hr, 0.5hr, 1hr, 1.5hr**

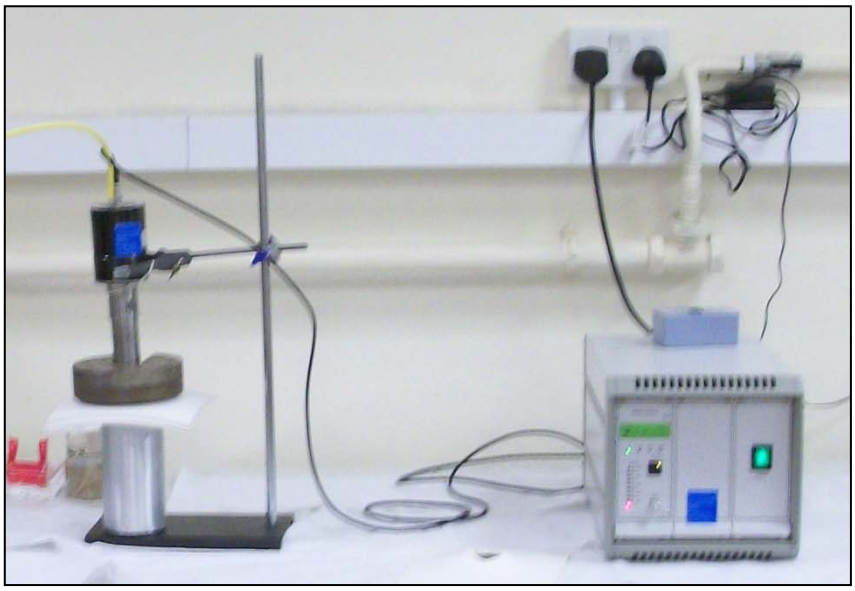

Figure 50: Ultrasonic mixer during use

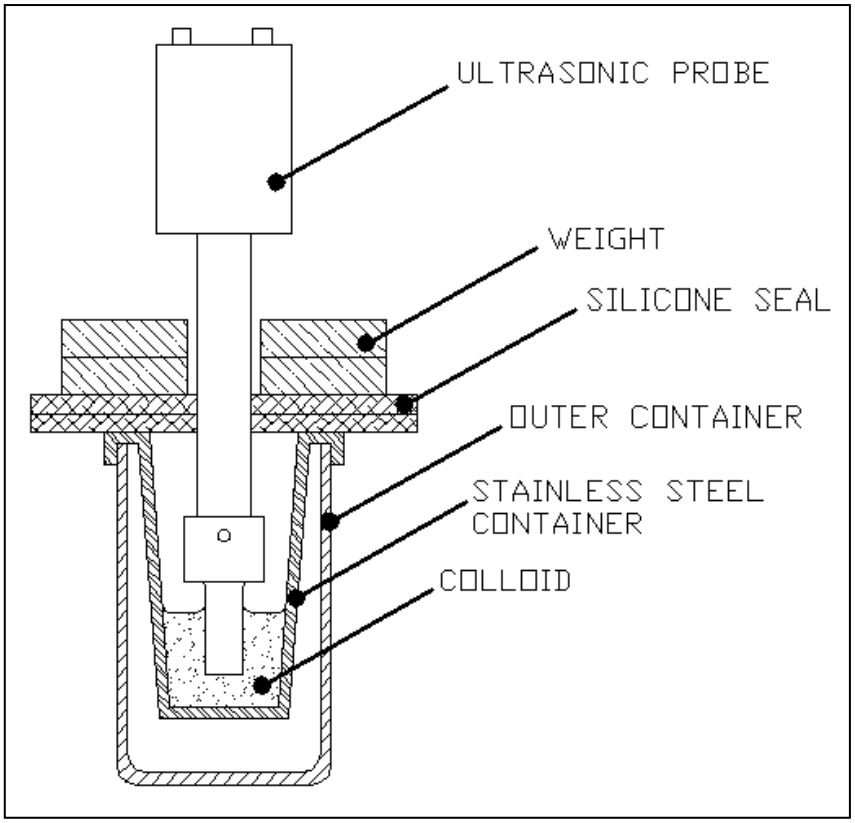

Figure 51: Ultrasonic mixer rig schematic

5.2 Nanoparticulate Influence on Colloidal Dynamics

5.2.1 Overview

In order to assess the stabilisation mechanisms imparted by nano titanium dioxide and zinc oxide dispersions in the silane/siloxane emulsions, aggregation mechanisms of these particulates have to be characterised. This study assessed aggregation through various means such as transmission electron microscopy (TEM), nitrogen absorption-desorption isothermal analysis including multipoint Brunauer Emmett Teller (BET) analysis. From this in conjunction with thermal and physical stressing and rheological assessment colloidal dynamics were evaluated. Dispersion testing showed these emulsions were O/W in nature. Emulsion descriptions are given in Appendix F; Table 47.

Results showed that excess dispersive medium did increase slip potential of emulsions however a significant stabilisation was achieved regardless. It was also found that aggregation affected stabilisation of emulsions significantly as did the particulate size

and morphology. From this study it was concluded that incorporation of such particulates in these emulsions by the method used was beneficial.

5.2.2 Physical and Thermodynamic Stressing

Stability of an emulsion is an essential feature for its performance and shelf-life. Low emulsion stability may lead to premature curing, reducing its effectiveness. Long-term stability of prepared emulsions and the effect of gravitational stresses were simulated by centrifugation, and the results are presented in Figure 52. All emulsions were tested in triplicate. Thermal effects on emulsion stability were investigated by replicating extreme European temperatures in order to evaluate properties of emulsions during storage and transport (Figure 53).

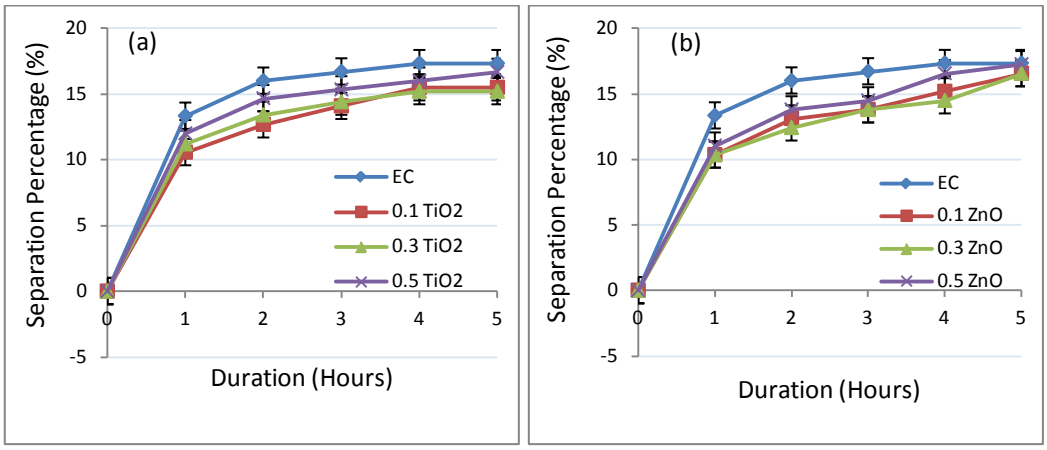

Figure 52: Degree of separation due to physical stressing for (a) titanium dioxide; and (b) zinc oxide emulsions.

Results presented in Figure 52 indicate a lower degree of separation for emulsions containing nanoparticulates compared to that of the control. Due to the small volumes used during testing, distinct variation between sample results could not be fully ascertained. However, results confirm emulsions containing nanoparticulates are more stable than the control. It should be noted that during testing no sedimentation of particulate material was observed. Additionally, all nanoparticle emulsions were found to be significantly more resistant to thermal stressing than the control emulsion. Figure 53 shows more pronounced separation of zinc oxide emulsions, and the degree of instability was found to be proportional to nanoparticle concentration. Samples were cycled through a ramp down and up in temperature before being returned to ambient before each assessment as described in the experimental section. After each cycle the separation of the emulsions were assessed. Due to the extremes of

temperatures used and duration of each ramp segment, results show that nanoparticulates greatly improve the thermodynamic stability. All titanium dioxide emulsions exhibited virtually no separation over a significant number of cycles, irrespective of nanoparticulate concentration. Experimental results confirm improved stability of emulsions due to nanoparticulate addition. Indisputably, the enhanced stability is a consequence of specific interactions between the metallic nano-oxides with different emulsion entities, which will be discussed in more detail below. Testing again was conducted in triplicate and results were practically congruent, with a percentage error of 1.5% on average.

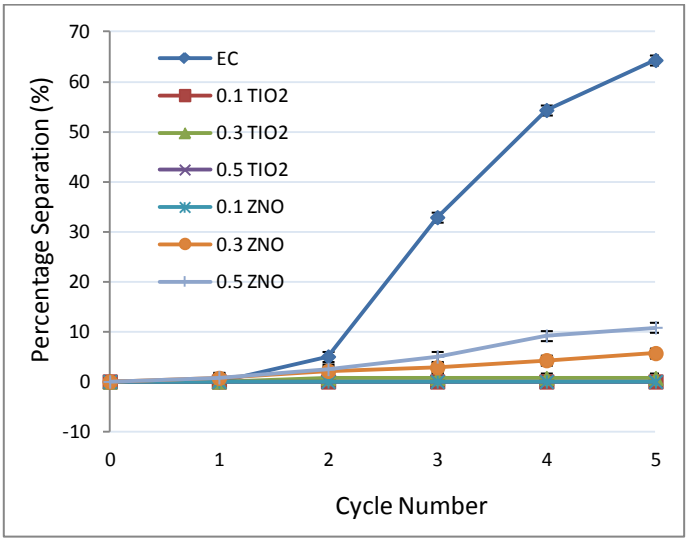

Figure 53: Thermal stress phase separation over multiple cycles

5.2.3 Aggregate Shape and Size

Two generally accepted routes for emulsion stability through particulate incorporation are steric stabilisation due to close packed aggregates, or alternatively, the formation of bridges between emulsion droplets discretely populated by particulates [**125**]. The former requires particulates to be smaller than the droplet in order to stabilise it effectively. However, in the light of relatively low concentrations of the surfactant and nanoparticles and high oil content, the latter is a more probable mechanism. Given the hydrophilic nature of the metallic oxides used, once mixed into an O/W emulsion it is expected that particles preferentially adsorb at the micelle interface to fill the 'gaps'. At higher concentrations excess nanoparticles stay in the continuous phase, yet flocculate around these micelles. The size and nature of the particles determine the efficacy of interactions between compatible groups on the micelle

interface. Both types of nanoparticulates have extensive hydroxyl groups, which allow for hydrogen bonding with surfactant polar head groups adsorbed at the oil droplet interface and bridging between discrete oil regions. However, since the emulsion contains a relatively small optimised amount of surfactant (pilot study and CMC testing), the favourable hydrophilic interaction between the micelles and the continuous phase is additionally altered by PDMS chain organisation and complexation. Hydroxyl terminated PDMS chains expose their polar endings to the water phase, while keeping the hydrophobic part of the chain efficiently folded and hidden inside the siloxane droplet above micelle aggregation concentrations [**173**]. This in turn increases the number of potential sites for favourable hydrogen bonding with the nanoparticles, which is thought to increase the stability of the oil droplets and consequently, the overall emulsion stability. As the nanoparticles interact with the hydrophilic groups on the surface of the oil droplet, they strengthen the micelle interface and make it less deformable; hence the higher resistance to physical and thermal stressing.

Figure 54 shows a simplified stabilisation networking mechanism (modified from [**124**]). Stabilisation is discussed below but it is considered in general that hydrogen bonding occurs between the surfactant polar regions increasing its efficacy and providing separation of the oil and water phases; water molecules essentially make the polar region bigger and causes a gelled network structure to be produced [**135**]. Since nanoparticulates have polar regions they also aid in this network and due to large surface areas, substantially enhance stability. This effect would not be possible with standard non-ionic surfactants, due to relatively small polar regions, nor molecules which do not achieve hydrogen bonding. Water as a liquid essentially has a bound structure similar to ice and unbound clustered structure at the same time due to hydrogen bonding. The proportion of each remains constant over time in a constant environment but the molecules that are bound or unbound change. This means that emulsions stabilised by this method must be created without contaminants or changes to pH as these networks would become destabilised [**179**].

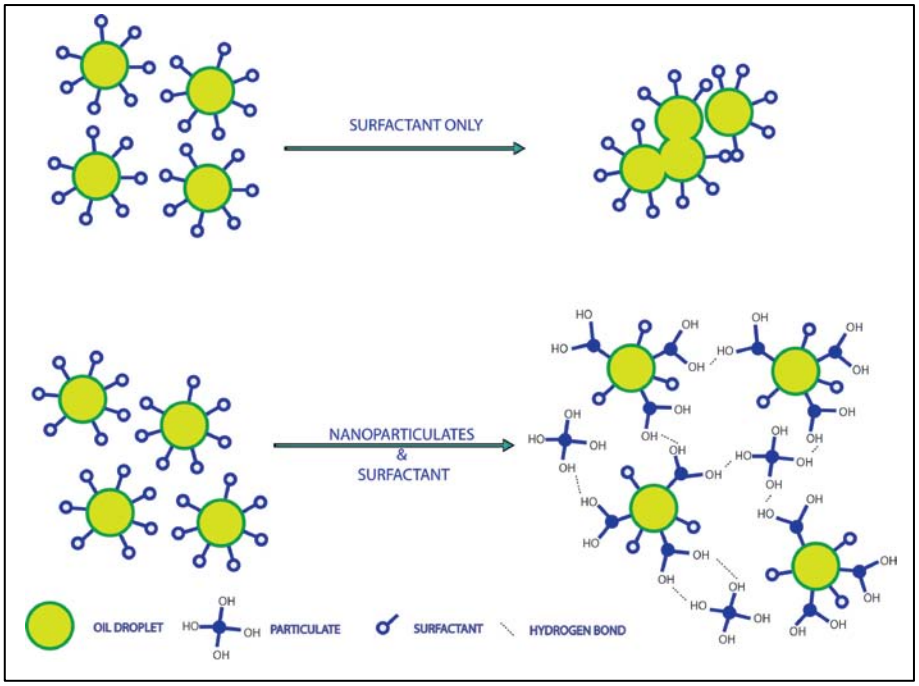

Figure 54: Schematic representation of stabilisation mechanism

Incorporated zinc and titanium oxide nanoparticles have a mean size of 20nm and 15nm, respectively. In purely theoretical scenario, without any aggregation between nanoparticles in the emulsion, titanium dioxide is expected to be more effective. The surface area, *SA*, of a single spherical particle with a radius *r* may be calculated as $SA = 4\pi r^2$ [**17**], giving 1257nm^2 and 707nm^2, respectively; almost 44% difference in interaction potential. However, aggregation between nanoparticles occurs spontaneously to a certain extent before they are added to the emulsion, which affects their properties, and also their role as surface stabilisers.

In order to gain a deeper understanding of the effect of nanoparticle aggregation on the stability and other emulsion properties, TEM analysis was conducted to establish the size and shape of the particulates in the emulsion after processing. Figure 55 shows zinc oxide aggregated into more elongated, loosely-packed asymmetrical particles compared to the titanium dioxide, which formed spherical agglomerates. Although the emulsions were produced by following the same procedure, and despite the similar size of both nanoparticles added, zinc oxide aggregated to a larger extent. The mean geometrical dimension of zinc and titanium dioxide aggregates was estimated to 120nm and 40nm, respectively. Assuming simple spherical aggregates in both cases the aggregate surface area is found as 45239nm^2 and 5027nm^2. Despite these being very rough and imprecise estimates, the general tendency is clear:

titanium dioxide is expected to be vastly superior to zinc oxide as an emulsion stabilizer due to its smaller aggregate size.

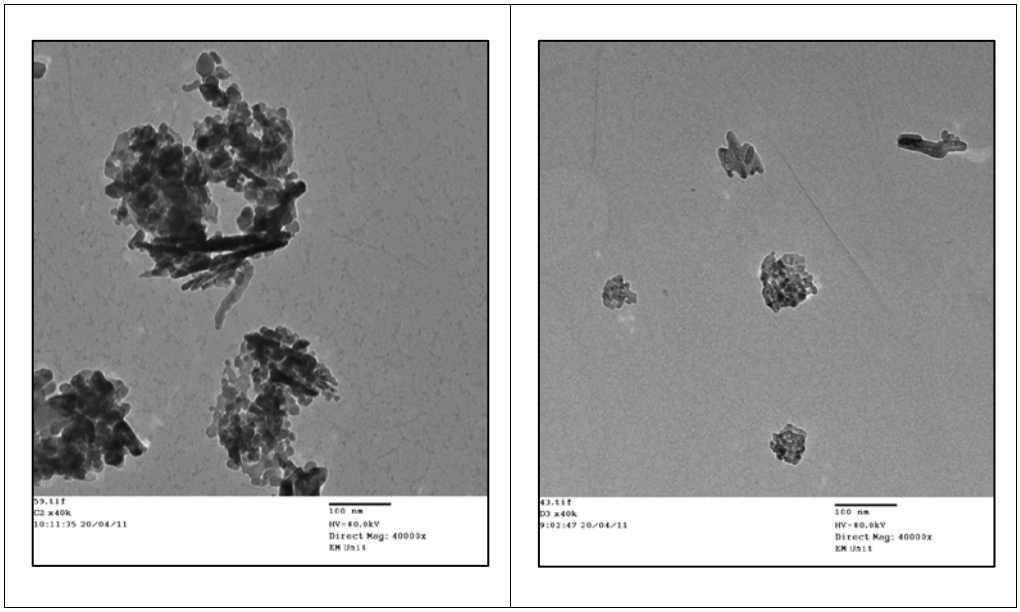

Figure 55: (Left) TEM of zinc oxide at 40,000x magnification (Right) TEM of titanium dioxide at 40,000x magnification

Smaller particle and aggregate size allows a higher degree of interaction at the interface and better overall incorporation into the emulsion, which is confirmed by the experimental results. The shape of the particle is the critical but often overlooked parameter for emulsion properties. Particulates with a smaller aspect ratio would be more suited, assuming that there were no chemical differences which may alter micelle stabilisation. A spherical titanium dioxide has a more favourable packing factor compared to the hemi-spherical zinc oxide. Zinc oxide aggregates formed more elongated irregular structures, which are believed to have attributed to the somewhat reduced thermodynamic stability of zinc oxide emulsions compared to more regular and compact agglomerates of the titanium dioxide. Formation of fractal nanoparticle structures has been discussed in the literature [**176**] and references therein; the specific size and geometrical shape of fractal aggregates reveals the physical mechanisms of aggregation and allows for characterisation of efficiency of packing and chemical potential of the aggregate. Relatively large, irregular shape of zinc oxide fractal aggregates has unbalanced distribution of prospective networking sites on its surface and therefore, their potential for interfacial absorption and bridging is significantly diminished. On the other hand, smaller, compactly-packed pseudo-spherical titanium dioxide aggregates have higher density of networking sites per unit

surface area and achieve more prominent bonding with other emulsion entities due to more pronounced surface areas for bridging by surfactant, and consequently stabilises the interface through monomeric and oligomeric flocculation. Smaller aggregates are more effective at creating a steric barrier between the phases due to larger potential surface areas present and a better packing factor; reducing possible coalescence due to physical and thermodynamic stresses.

Table 18: Nitrogen isotherm results

	Titanium Dioxide	Zinc Oxide
BET Surface Area (m^2/g)	97.2665	40.3934
Single point adsorption total pore volume of pores less than 170nm diameter at $P/P_0 = 0.99$ (cm^3/g)	0.276476	0.184645
Adsorption average pore width (4V/A by BET) (nm)	11.36986	18.28465
BJH Adsorption average pore diameter (4V/A) (nm)	8.9009	13.8436

More prominent aggregation of zinc oxide and dissimilar morphology has additionally been confirmed by nitrogen isothermal analysis. Calculated multipoint BET surface areas for the particulates provided in Table 18 show a considerable difference, which implies that titanium dioxide nano-aggregates has higher interaction potential. This confirms fewer prospective networking sites on zinc nanoparticulates compared to titanium ones per unit mass are due to a larger degree of agglomeration of the former. Figure 56 reveals additional information about the particulate morphology. The Barrett Joyner Halenda (BJH) absorption results show titanium dioxide has significantly larger pore areas; however, the average pore width was found to be smaller for titanium dioxide. On the other hand, zinc nano-oxide with a ~36% bigger pore geometrical factor has a considerably smaller pore area; hence less absorption sites on its surface. This is additionally confirmed by absorption-desorption isotherms presented in Figure 57. The results show that titanium dioxide retains more nitrogen over a wider range of relative pressures. The larger porosity of titanium dioxide has been thoroughly studied in the literature [**184**]. A pore with a small throat diameter relative to its cavity size will retain more molecules on desorption of the vapour and therefore a larger hysteresis will be present at the relative pressure. The zinc oxide absorbs less nitrogen in total however unlike the two stage hysteresis produced by the titanium dioxide in the mid pressure range, it has a sharp increase/decrease when

nearing the saturation pressure. Conversely, it is clear that titanium dioxide absorbs more nitrogen at all pressures, yet again confirming larger bonding potential of less aggregated particles.

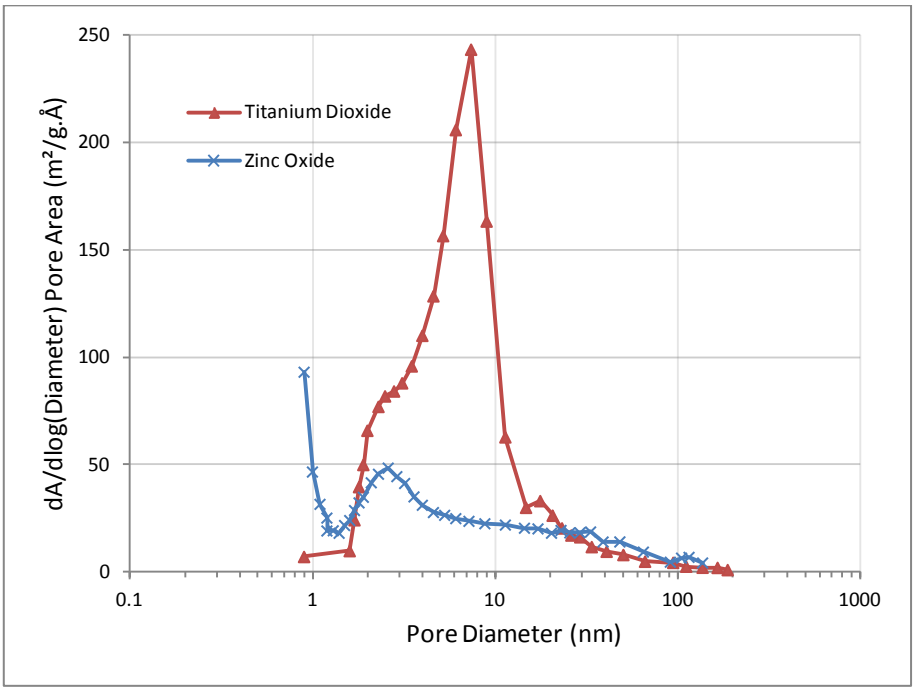

Figure 56: Zinc oxide and titanium dioxide BJH adsorption

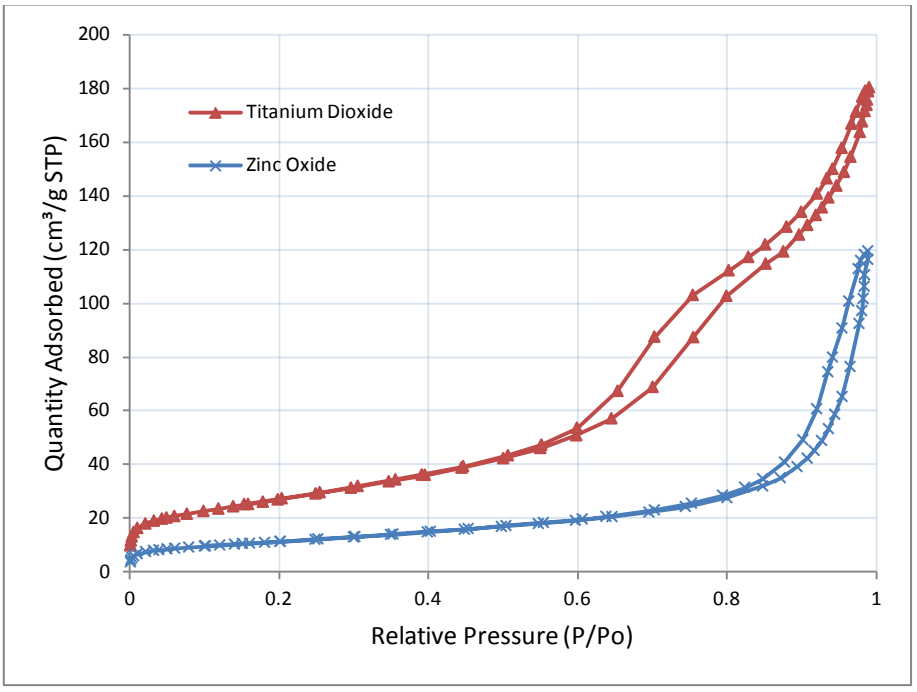

Figure 57: Nitrogen zinc oxide and titanium dioxide absorption/desorption isotherms

5.2.4 Rheological Properties

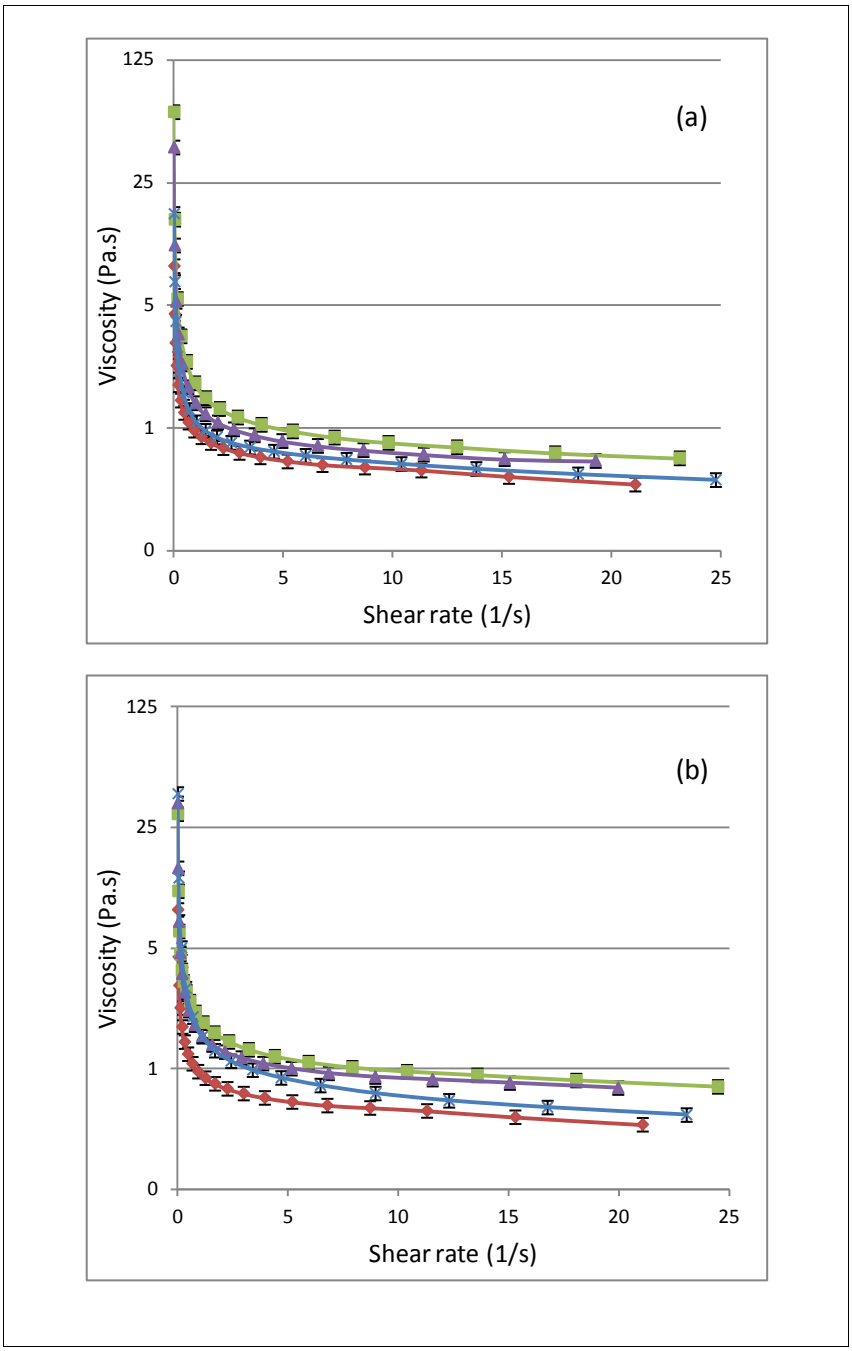

Figure 58: Continuous viscosity of *(a)* titanium dioxide and *(b)* zinc oxide emulsions; 0.1wt% (■), 0.3wt% (▲), 0.5wt% (×), against control (♦)

Emulsion rheology is of paramount interest as flow characteristics can help determine the mechanisms stabilising the emulsion. From rheological scrutiny of an emulsion it may also be determined how suitable the emulsion may be for its purpose. Figure 58 shows that the viscosity generally increased over a range of shear rates, as the viscosity of all nanoparticle emulsions was higher than that of the control sample. The

reduction in viscosity was inversely proportional to increasing nanoparticulate dispersion concentration, as the highest viscosities were measured at the lowest nanoparticle concentration (0.1wt%). Additionally, a slight increase in viscosity was observed for zinc oxide emulsions. Increase in viscosity presumably comes as consequence of reduced bonding effectiveness; the dispersion medium alters the continuous phase slip behaviour more extensively. For the zinc oxide emulsions, pronounced aggregation/larger size and irregular shape of zinc oxide result in less effective micelle adsorption; which increases the shear stress resistance. As the concentration of nanoparticles increases, the durability of the micelle interface is enhanced as it becomes a pseudo-stable entity, while the viscosity is very similar to that of the control. This is due to greater film thickness between micelles being achieved, as more colloidal dispersant is incorporated; thus the micelle slipping potential is increasing.

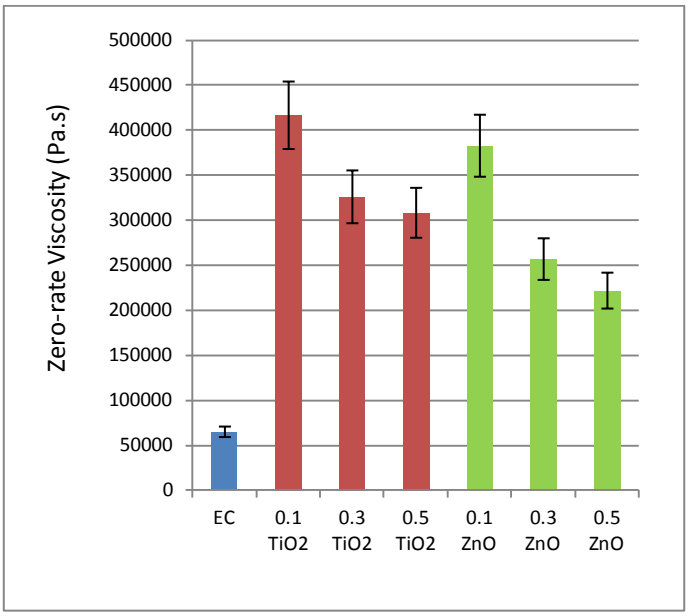

Figure 59: Zero-rate viscosity of nanoparticulate emulsions

Further rheological characteristics of the emulsions were evaluated with zero-rate viscosity estimates presented in Figure 59 and based on samples tested in triplicate. Nanoparticulate emulsions had distinctly higher viscosities than the control. Results indicate titanium dioxide emulsions are more viscous when under no shear than zinc oxide emulsions at similar nanoparticle concentrations. Smaller titanium dioxide particles allowed for more uniform incorporation into the emulsion system, which improved the emulsion properties through larger networking potential and steric

interaction. Figure 59 shows a reduced viscosity with increase in nanoparticulate dispersions due to the increase in ITES present aiding film forming between micelles, however increased networking by nanoparticulates as discussed earlier still dominated stabilisation over this dilution effect. Irregular and larger zinc oxide particles are not as efficient at stabilising the interface due to their shape and size, especially at higher concentrations.

Table 19: Mean yield stress and ratio index results

Nano-particulate Concentration (wt%)	Mean Zinc Oxide Yield Stress (Pa)	Mean Zinc Ratio Index	Mean Titanium Dioxide Yield Stress (Pa)	Mean Titanium Dioxide Index
0.0	0.16	0.81	0.16	0.81
0.1	0.26	0.85	0.29	0.85
0.3	0.35	0.86	0.41	0.85
0.5	0.46	0.86	0.45	0.85

Calculated yield properties and ratio index numbers are given in Table 19. Yield stress increased with nanoparticulate concentration which is expected for a more networked emulsion. A slight increase was noted for titanium emulsions at lower concentrations. Nevertheless, the estimated values were found to be very similar for both zinc and titanium emulsion. It is expected that the reason for the increase in yield stress was the increase in bonding occurring and was not attributed to the viscosity of the emulsion. In essence the bonding occurring was dominating the yield stress more prominently than viscosity. Further study below shows this effect occurring and that it is only prominent at rest, under even low levels of shear, yield stress is drastically reduced as these networks providing the yield stress characteristics are broken. Ratio index numbers showed that all emulsions were shear thinning, which is beneficial for high oil content water repellent emulsions. Results confirm networking as an underlying stabilising mechanism even with the film forming achieved through excess dispersion medium altering flow characteristics.

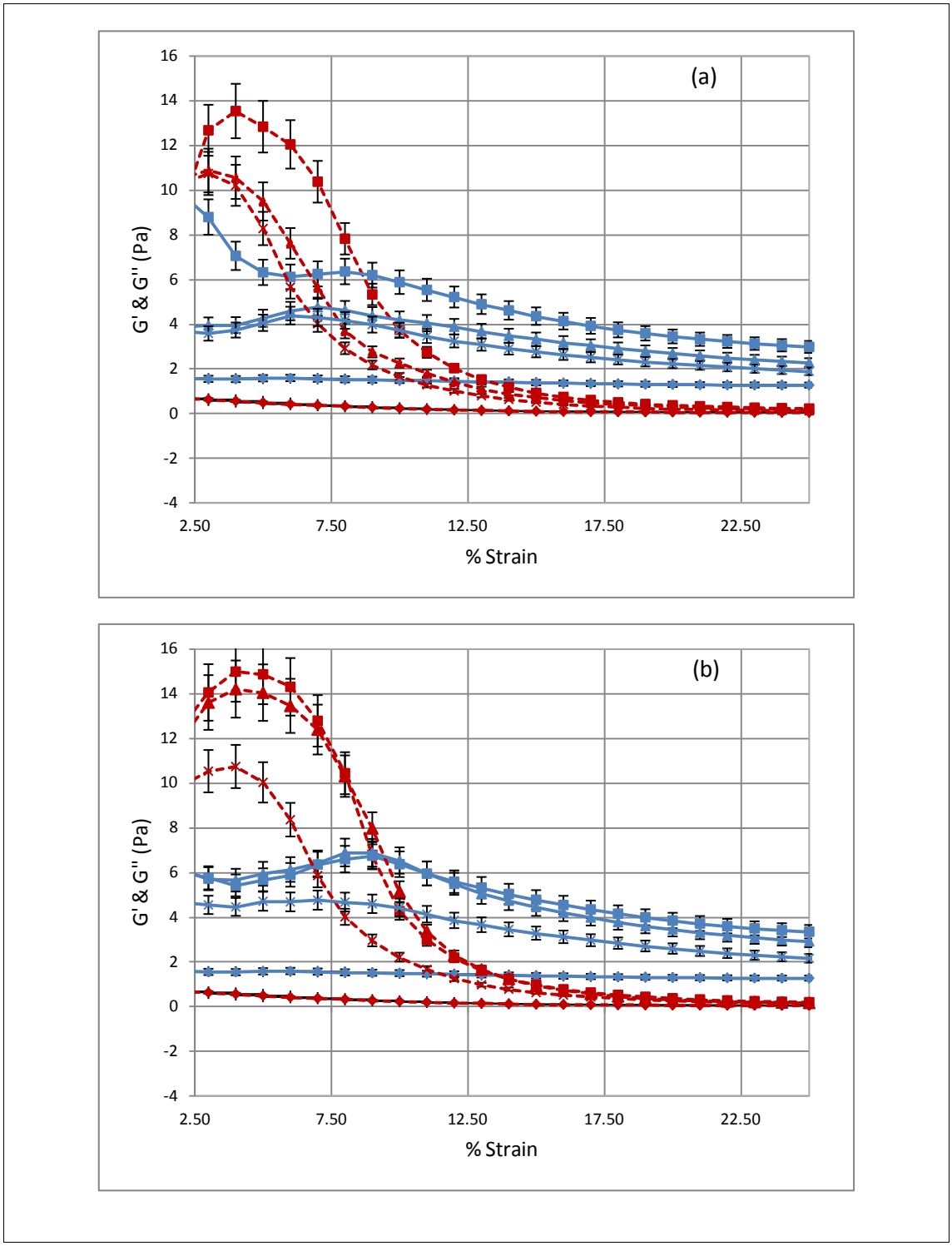

Figure 60: Storage *G'* (dashed line) and loss *G''* (solid line) moduli of *(a)* titanium dioxide; and *(b)* zinc oxide emulsions. Symbols used: 0.0wt% (♦), 0.1wt% (■), 0.3wt% (▲), and 0.5wt% (×) concentrations

Figure 60 shows storage (*G'*) and loss moduli (*G''*) of the nano-particulate emulsions. All emulsions had considerably greater *G'* than *G''* at low strain amplitude, with both seemingly independent of one another. Both graphs show a sharp and continuous

decrease of *G'* with increasing strain, while *G''* increases at intermediate strains and decreases at higher strain rates. Specific behaviour characteristic for flocculated gelled structures is revealed at low strains ($tan\ \delta < 1$) as elastic modulus dominates, while larger deformation leads to a partial collapse of the multiphase structure as viscous behaviour ($tan\ \delta > 1$) is detected at >10% strain regions. Enhanced elasticity of all systems was alleviated by inter-dispersion interaction [**125**]. Larger *G'* was found at lower strains for lower nanoparticulate concentrations, showing better elastic characteristics, but also higher loss moduli. Better networking and less flocculation produced more bonds that required breaking before slip could occur, and caused the decrease of both moduli. This is also valid for zinc oxide emulsions, which exhibited higher moduli than titanium dioxide, corroborating lower stabilisation influence of zinc nanoparticles due to their specific aggregate shape and larger size over simpler and less aggregation-prone titanium nano-oxides. Previous studies [**135**] [**143**] confirm similar emulsified systems work due to better flocculation (ca. 1% - 5% solids) around a micelle. However, in this study effective networking is achieved with small quantities of the surfactant and nanoparticulates which allows the latter to exhibit advanced interfacial activity.

5.3 Summary

TEM results showed that size of nanoparticulates did not seem to be affected by ultrasonic mixing over a range of processing times. However, nanoparticulate aggregates did breakdown from ca. 1hr of ultrasonic mixing. Further mixing may be potentially possible to break aggregates down further however a redesign of the ultrasonicating apparatus would be required to relieve overheating issues.

The role of metallic nanoparticles as emulsion additives was investigated. Nano-sized titanium and zinc oxides were added to silane/siloxane o/w emulsions in low concentrations, <0.5wt%. It was found that the addition of nanoparticulates increased mechanical and thermodynamic stability of the emulsions. Enhanced emulsion properties were found to be dependent on the concentration and the nature of the colloidal nanoparticles: the aggregate size, shape and agglomeration characteristics in particular. Particle morphology dictated the networking and flocculation mechanisms. Larger zinc oxide nanoparticles had lower networking potential than titanium ones. Experimental results confirmed zinc oxide emulsions were less physically and

thermodynamically stable than titanium dioxide counterparts. Additionally, the shape of nanoparticle aggregate was identified as a crucial parameter for successful incorporation of nanostructures into the emulsions. Loosely packed fractional aggregates of zinc oxide experienced hindered micelle absorption and bridging due to their specific geometry, while pseudo-spherical and visually more compact titanium dioxide absorbed on the micelle interface to a greater extent while providing extensive bond sites. Finally, the nanoparticulate addition altered rheological properties, increasing emulsion viscosity, yield stress and dynamic moduli of nanoparticulate incorporated emulsions.

Chapter 6: Pore and Interface Modification

6.1 Overview

This chapter deals with how pore and interface modification by each treatment was achieved and to what extent. This is of importance with regard to all three key treatment influences; water repellence, thermal insulation, and antifouling.

6.2 Mercury Intrusion Porosimetry (MIP) of Terracotta Tiles

To assess the effect the treatments had on pore modification, mercury intrusion porosimetry was conducted. The following results show a comparison against the control emulsion. Horizontal shifts in capillary size between the emulsion control and nanoparticulate treatments show the capillary restrictions attributed to the treatments used to modify the internal capillaries. Since variation is expected at larger and smaller capillary sizes due to material variation and sintering inconsistencies, mid-range capillary diameters are used to make a comparison. For this study tiles were used due to their relatively homogenous structure to help reduce variables.

Washburn's equation states that the pressure required to force a non-wetting liquid into a capillary of circular cross-section is inversely proportional to the diameter of the capillary and directly proportional to the surface tension of the liquid and the solid surface contact angle [**155**]. Increased internal pressure had to be applied to cause the mercury to penetrate into the decreasing pore size of the samples; from this pore diameter could be calculated.

Figure 61 shows the emulsion control (EC) against untreated terracotta tile (TC). The emulsion does seem to reduce the pore diameter by approximately 2-3 microns. Figure 62 shows the titanium dioxide treatment reducing the pore size even further than the emulsion control. Figure 63 shows the zinc oxide treatment producing a similar profile to the titanium dioxide treatment.

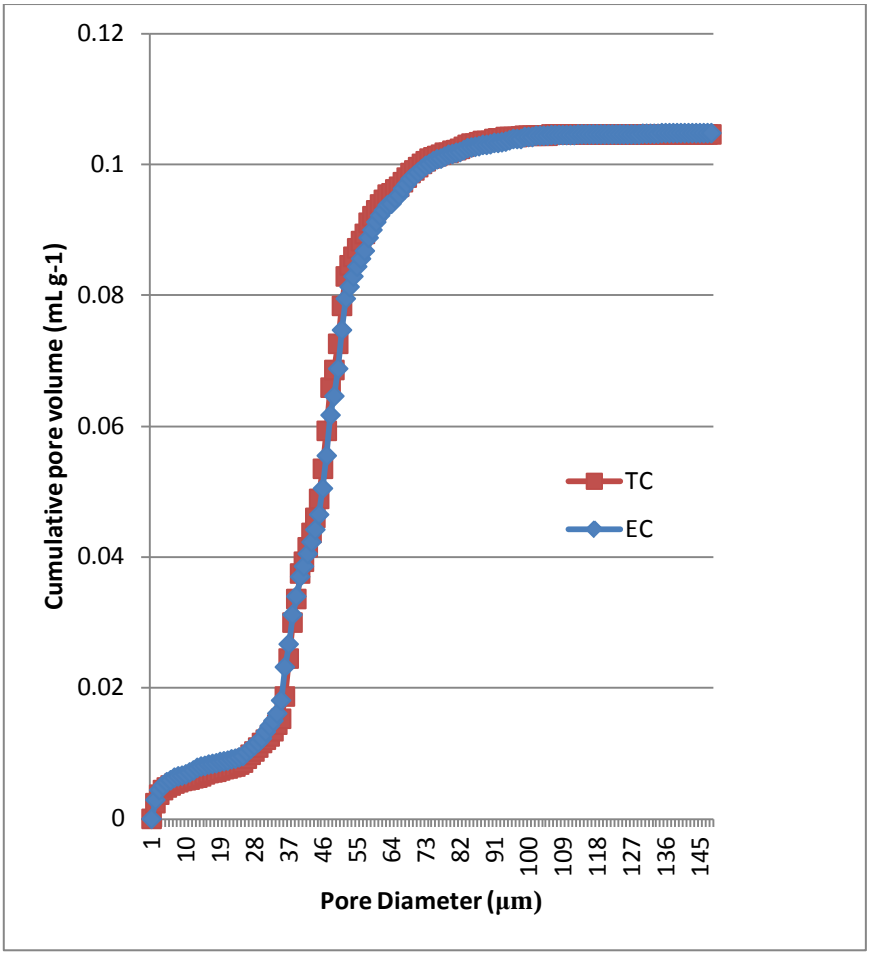

Figure 61: cumulative pore volume of the terracotta control (TC) compared to the emulsion control (EC) treated sample

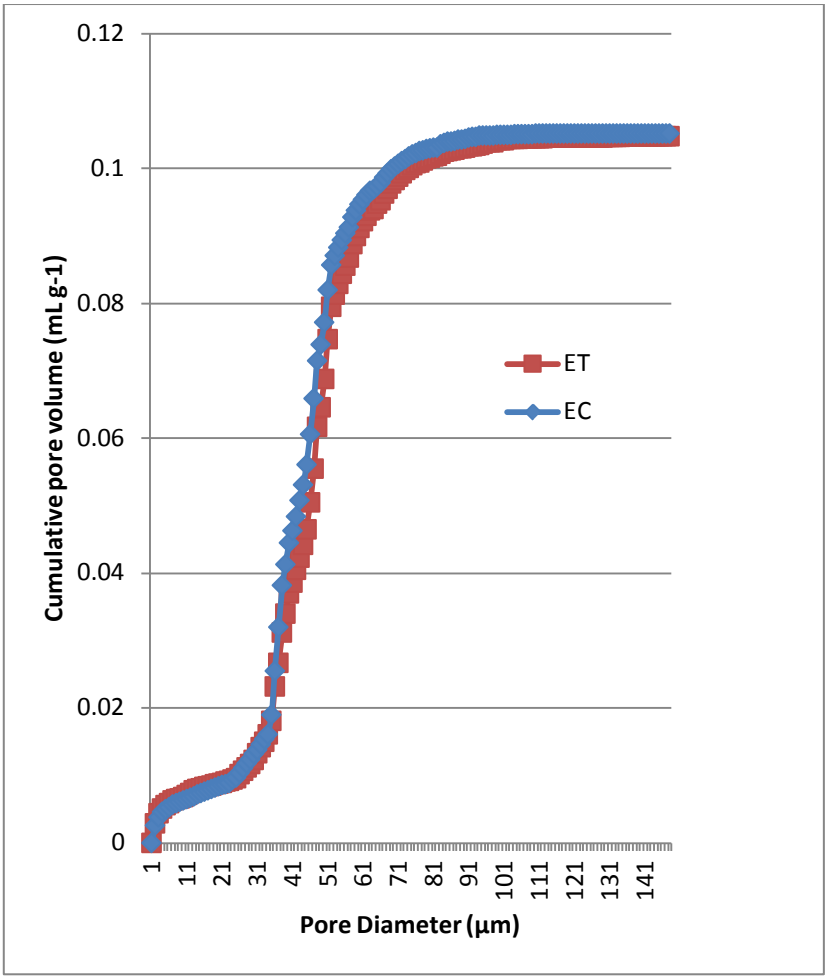

Figure 62: cumulative pore volume of the emulsion control (EC) compared to the titanium dioxide treated sample (ET)

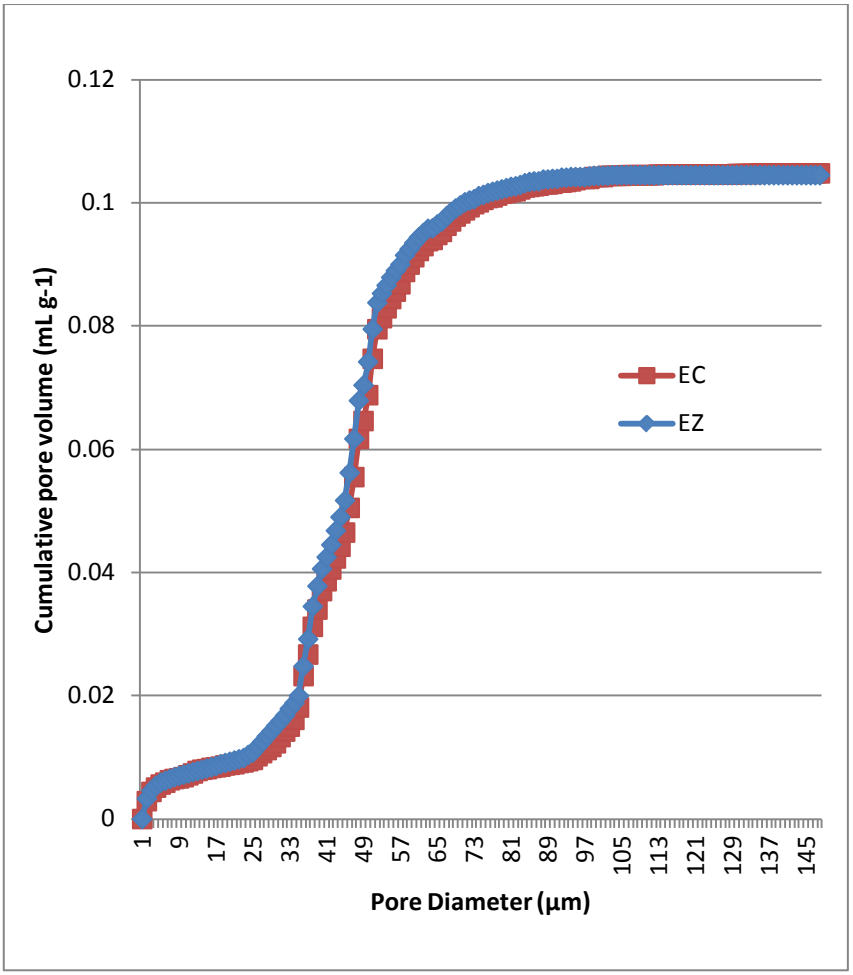

Figure 63: cumulative pore volume of the emulsion control (EC) compared to the zinc oxide treated sample (ET)

Table 20 shows the results from testing. It should be noted as a by-product of a slower test the bulk density and apparent density was also calculated for (BC) and (TC).

Bulk density is the mass of the bulk quantity divided by bulk volume. *Apparent density* is the mass divided by the skeletal volume remaining after the volume of all open pores larger than 0.005µm have been subtracted [**151**].

It should be noted that the bulk volume includes pores open and closed pores and anything within the form fitting envelope used to calculate the volume. However the apparent (skeletal) volume is the solid volume only. Helium pycnometry may be used to assess micropores (diameter <0.002µm) below the threshold for mercury intrusion to help evaluate this [**151**].

Table 20: Mercury intrusion results for terracotta tile samples

Parameters	Brick Control (BC)	Tile Control (TC)	Emulsion Control (EC)	Titanium dioxide Emulsion (ET)	Zinc Oxide Emulsion (EZ)
Total intrusion volume (mL/g)	0.1930	0.1046	0.1048	0.1052	0.1045
Total Pore Area (m2/g)	1.672	1.894	2.288	1.690	1.750
Median Pore Diameter – volume (µm)	0.7935	0.5390	0.4666	0.8327	0.6283
Median Pore Diameter – Area (µm)	0.2432	0.0765	0.0611	0.0753	0.0799
Average Pore Diameter (4V/A)	0.4618	0.2210	0.1833	0.2490	0.2390
Bulk Density at 0.32 psia (g/mL)	1.7061	2.0333			
Apparent (skeletal) Density (g/mL)	2.5437	2.5828			
Porosity (%)	32.9256	21.2740			

Table 20 does not show a true picture of the effect each treatment has on the terracotta substrate. To get a better understanding, by plotting the log differential intrusion and pore size a better understanding may be achieved.

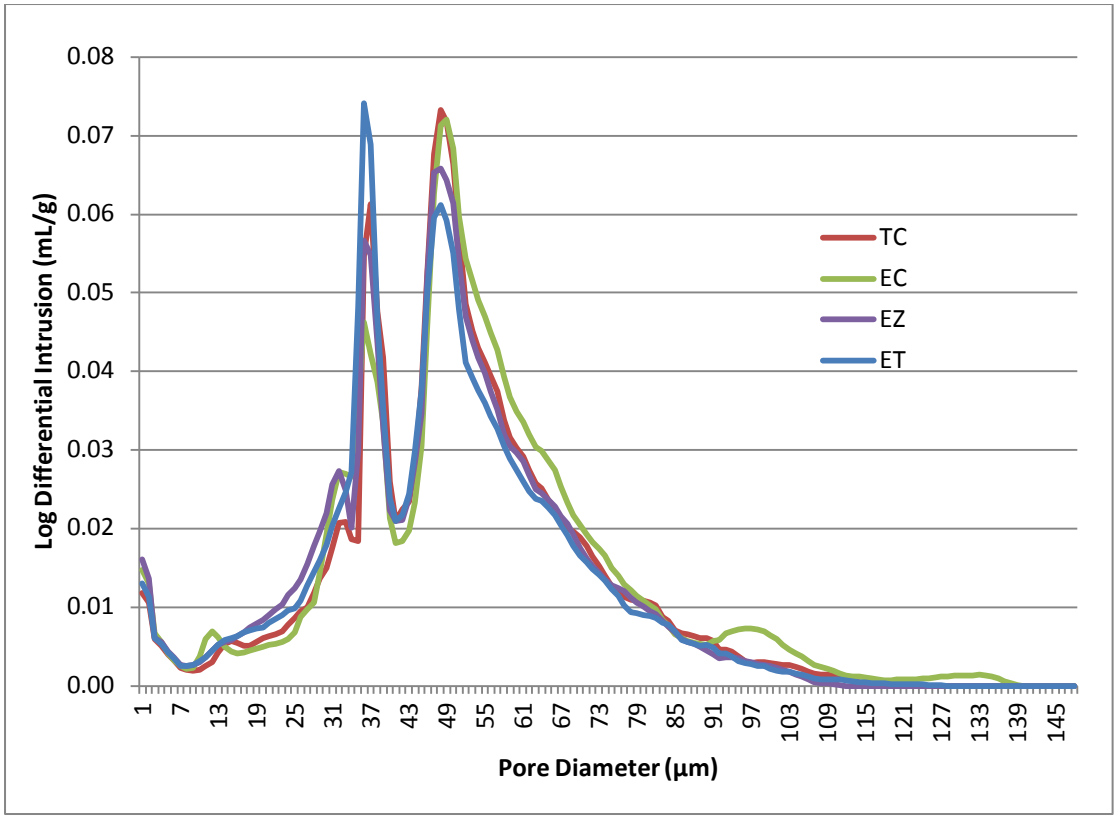

Figure 64: Log differential vs. pore size diameter comparison

Figure 64 shows some changes to the pore size at approximately 50µm and 35µm. The emulsion control reduces mercury intrusion at 50µm and 35µm compared to the control. This shows that there are fewer pores of these diameters present after

treatment. However, for the nanoparticulate emulsions the spike at 50μm reduces in a proportional manner as the 35μm spike increases. This would seem to imply that these emulsions were converting the 50μm pores to 35μm. It should be pointed out that the morphology of the samples still remains strongly bimodal in nature, and thus the results in Table 20 should be evaluated with discretion. In addition, the titanium dioxide emulsion had seemingly a stronger influence on pore modification than the zinc oxide equivalent. This may be due to less aggregation, leading to better distribution of treatment and uniform curing of such. Emulsions seem to show alteration to the substrate morphology down to around 7μm which gives some indication of the extent these emulsions can penetrate into a porous substrate. However the increase exhibited of 35μm would seem to suggest that the 50μm pores are being converted to this diameter on average by the nanoparticulate treatments. If this is compared with the emulsion control, it would seem that the emulsion control is slightly more uniform at modifying pores than the nanoparticulate treatments, suggesting a thicker pore modification.

6.3 Comparison of Brick and Tile by Mercury Intrusion Porosimetry

Although terracotta tiles were used for MIP, most applications for the treatments under scrutiny would be for brickwork applications. This section gives a general comparison between the untreated brick and tiles used in this study.

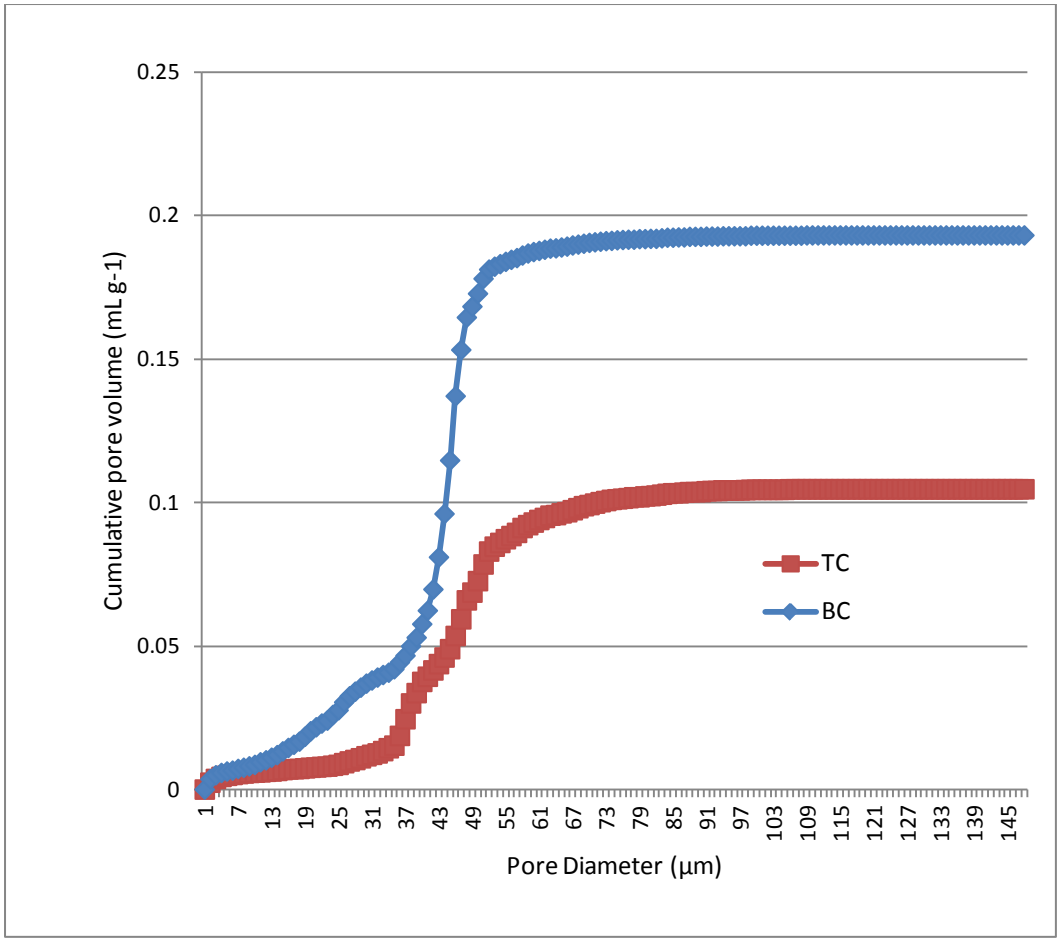

Figure 65: Cumulative pore volume of brick and tile substrates

Figure 65 shows the cumulative pore volumes of each sample. The results show that the tile has a lower porosity and in general less pores across the range of pressures tested. Table 21 shows a comparison of calculated data from the test and would seem to agree with the cumulative pore volume data.

Table 21: Brick and tile results comparison

Parameters	Brick Sample	Tile Sample
Total intrusion volume (mL/g)	0.1930	0.1046
Total Pore Area (m^2/g)	1.672	1.894
Median Pore Diameter – volume (µm)	0.7935	0.5390
Median Pore Diameter – Area (µm)	0.2432	0.0765
Average Pore Diameter (4V/A)	0.4618	0.2210
Bulk Density at 0.32 psia (g/mL)	1.7061	2.0333
Apparent (skeletal) Density (g/mL)	2.5437	2.5828
Porosity (%)	32.9256	21.2740

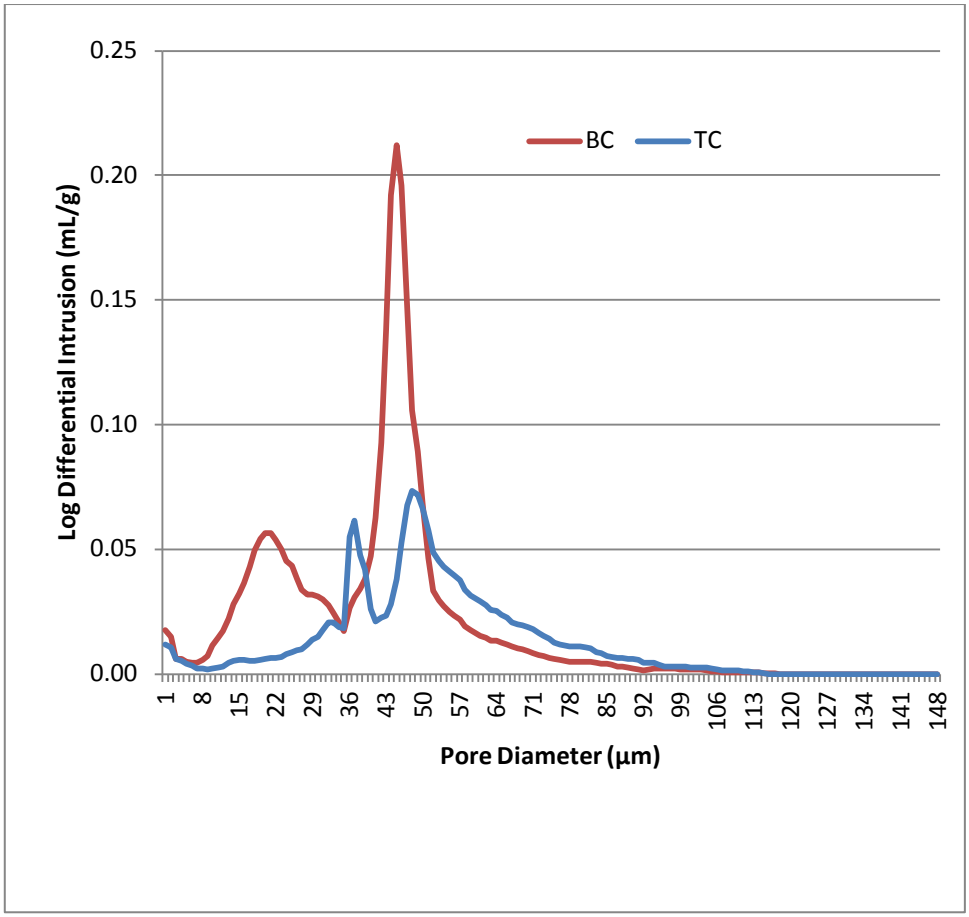

Figure 66: Brick and mortar pore size comparison

Figure 66 shows a pore size comparison between the two materials. The terracotta tile sample seems to be more bimodal in nature than the brick sample. If what was considered in the last section applied to the brick perhaps similar changes would be occurring around 20µm and 45µm. Since the brick sample has smaller pores in the lower range emulsion treatments may have greater beneficial impact on rising damp, capillary action, or water ingress than on terracotta tile substrates.

6.4 Water Beading of Brickwork

In order to assess the initial water repellence of a treated structure, goniometry measurement was conducted to assess the effectiveness of each treatment to bead water on the exposed rough side of a conventional brick.

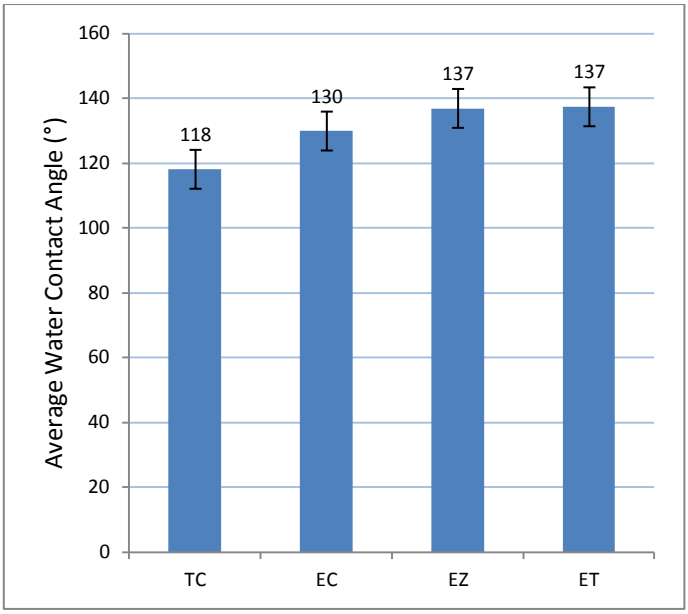

Figure 67: Brick average water contact angles

Figure 67 shows that the WCA is improved on average by approximately 10° when the control emulsion is used; 5 readings were taken for each sample type. In addition, approximately 5% improvement can be achieved on top of the base emulsion performance with the addition of either nano-particulate to the emulsion for only <0.1wt% incorporation. It is considered that the nano-particles improve the WCA by providing nucleation points for silane/siloxane bonding, increasing the interfacial roughness. This reduces the overall interfacial tension by reducing net charge density and hence making the treated surface more water repellent. Essentially a greater distance between the substrate and the water bead can be produced by the alteration of the surface morphology, which reduces the probability of respective charge or steric interaction. This increased distance could be compared to the MIP results discussed earlier. Perhaps the interface is rougher due to the nanoparticulate treatments and this may be reflected on the internal pore modification morphology.

6.5 Water Vapour Permeability

A build-up of humidity in a structure is undesirable, especially in a cavity wall where it could become trapped and cause damp related problems. In order to assess the ability of treated substrates to allow water vapour to permeate when a structure is trying to equalise internal humidity, a water vapour permeability test was conducted.

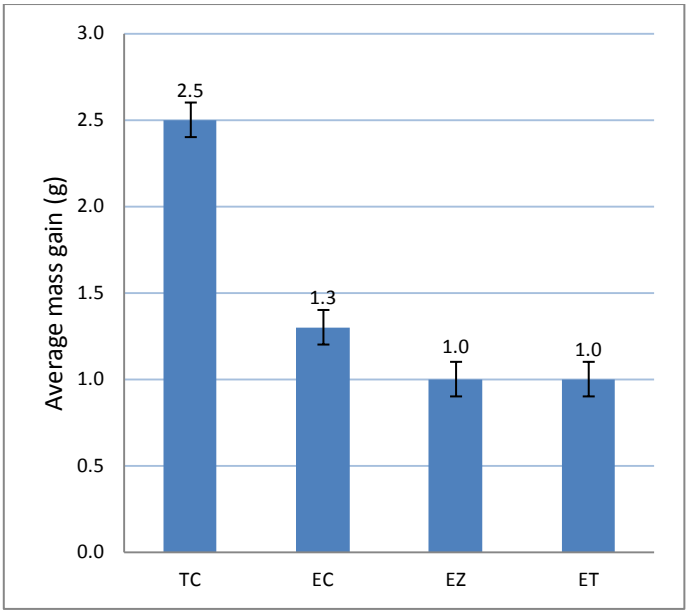

Figure 68: Brick water vapour permeation

Although Figure 68 shows that water vapour is reduced using the presented treatments, it does confirm that they do allow water vapour to be transmitted through the substrate. The nano-treatments show a larger reduction in water vapour permeation compared with the control emulsion, which is considered to be due to the increase in treatment interfacial roughness causing pore constriction. Five samples were used for each type and the average temperature and humidity during testing was 20.3℃ and 71.6%RH, respectively. Pore constriction by the treatments also supports the MIP results.

6.6 Thermal Conductivity

Thermal conductivity is of interest as a better insulated structure should require less energy to heat it and maintain the warmth inside. Therefore this test was carried out over wet and dry scenarios to help assess the effectiveness of the respective treatments to insulate during these conditions.

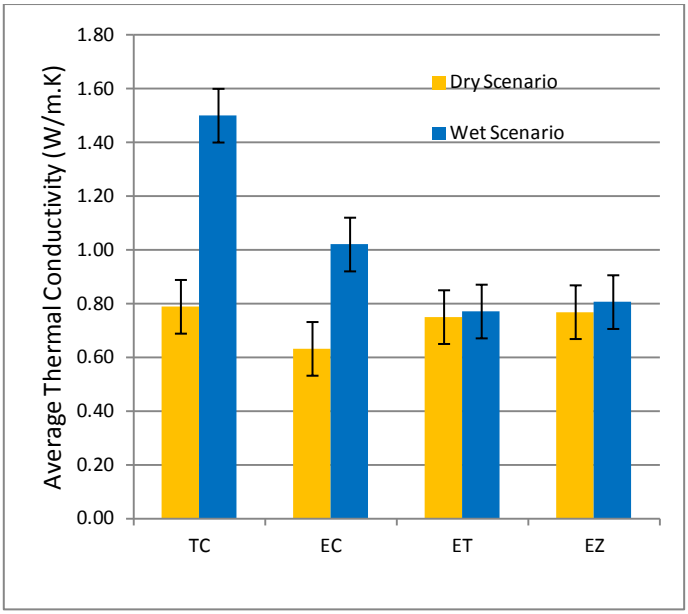

Figure 69: Brick thermal conductivity

Figure 69 shows the thermal conductivity of the treated samples is slightly reduced compared with the terracotta control in dry conditions and is attributed to the treatments providing better thermal insulation. The nanoparticulate emulsions in dry conditions even with an altered morphology still comprised of conductive metal oxide components, which increased the thermal conductivity of the nanoparticulate samples. In the wet scenario results show that water increases the conductivity of the brick substrate significantly. Since each treatment reduced the ingress of the water over the 24hr exposure time it can be clearly seen that a significant reduction in thermal conductivity can be achieved by all treatments. Again, due to the alteration of the interfacial morphology by the respective nanoparticulates it is the reduction of surface energy interaction potential that reduces retained water. Nanoparticulate samples after wet conditioning had a lower thermal conductivity on average than that of the control emulsion. This would indicate that polar interaction between the treatment and water due to the nanoparticulates at the interface is less significant than the effect they have on surface roughness.

6.7 SEM and EDX Analysis of Nanoparticulates and Treatment Depth

Treatment depth is an important factor when dealing with rising damp and service life durability. If a chip is made in a coating, it reduces the efficacy of the coating to protect and repel water. Conversely, treatments penetrate deep into the substrate; thus, compromises in protection should be significantly lower. In addition, treatment depth is also an important factor when assessing rising damp remedial treatments.

EC, EZ, and ET produced average treatment depth results of 13mm, 13mm, and 14mm respectively. These results show that the treatments can penetrate deep into the substrate.

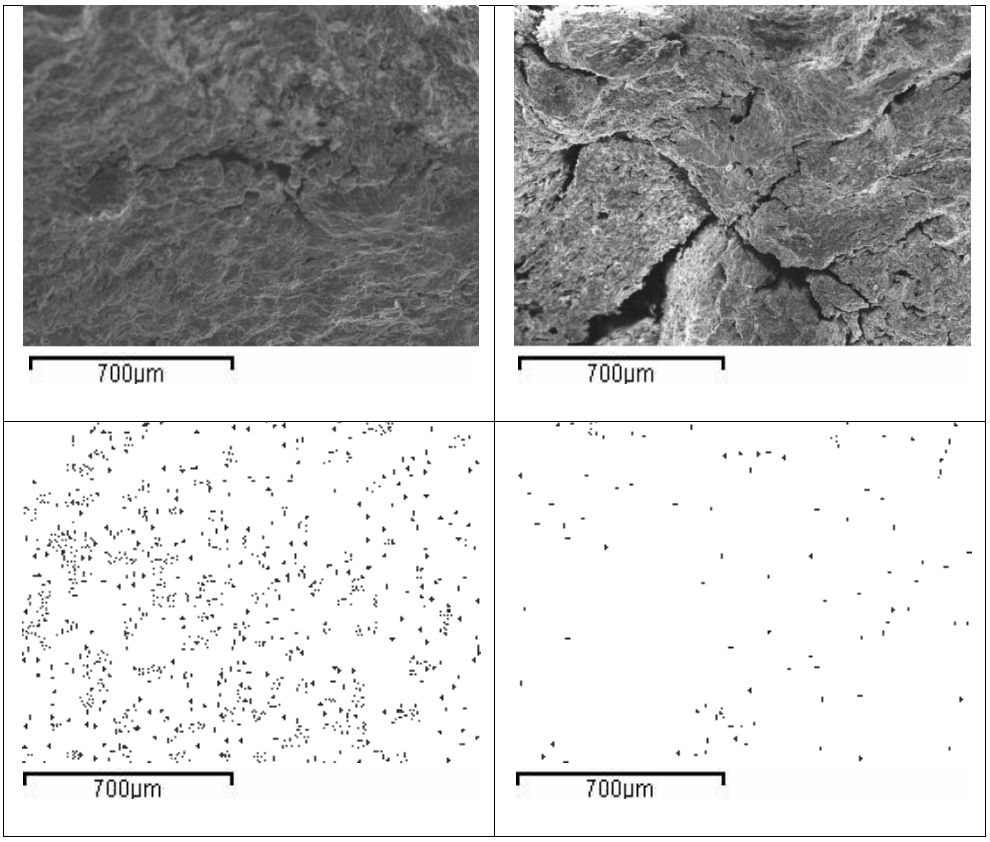

Figure 70: EDAX titanium readings (bottom); brick exterior (bottom left) from brick cross-section approximately 5mm from surface (bottom right), (top) SEM images used for lower EDAX results respectively

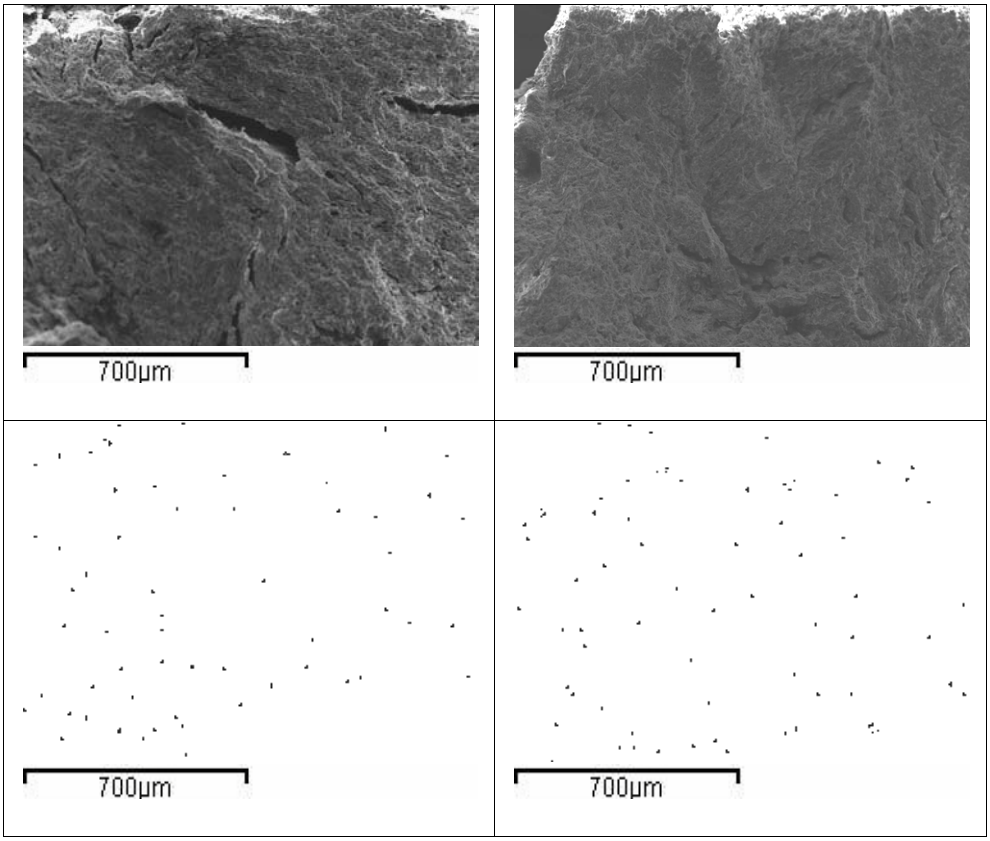

Figure 71: EDAX zinc readings (bottom); brick exterior (bottom left) from brick cross-section approximately 5mm from surface (bottom right), (top) SEM images used for lower EDAX results respectively

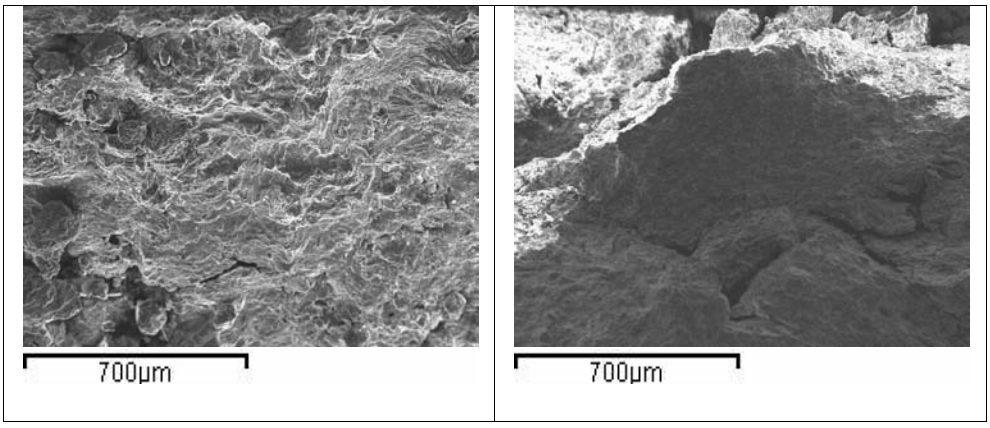

Figure 72: SEM of emulsion control (left); brick exterior, (right) brick cross-section approximately 5mm from surface

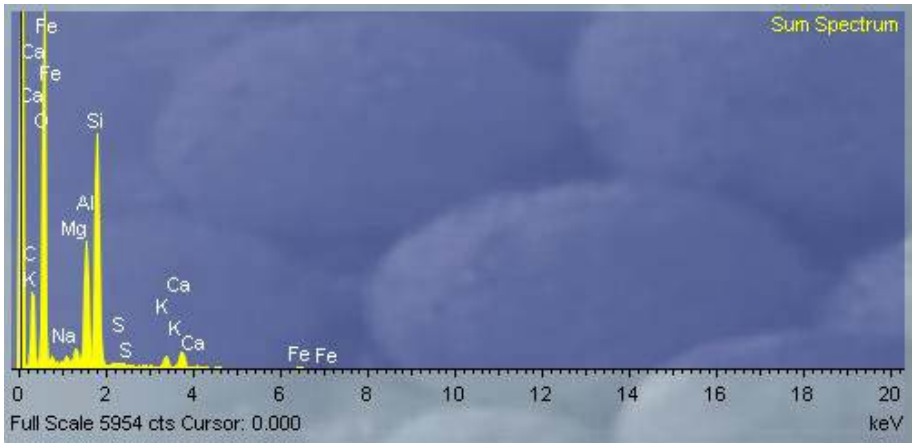

Figure 73: EDAX spectrum of emulsion control; brick exterior

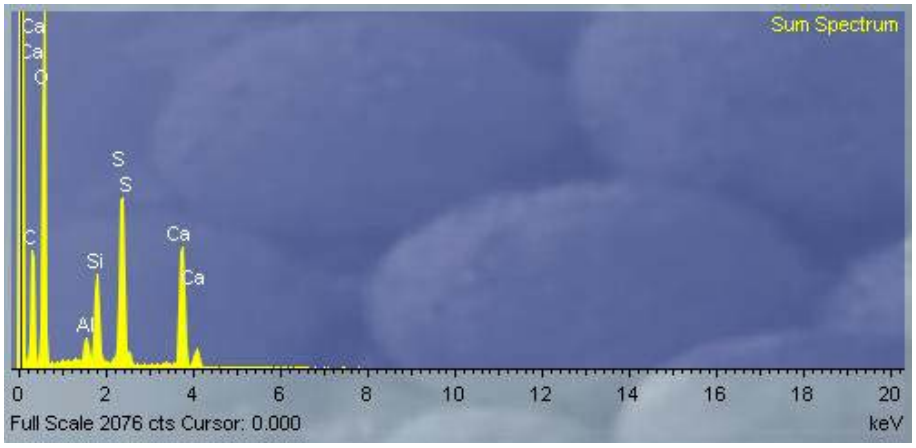

Figure 74: EDAX spectrum of emulsion control; brick interior approximately 5mm from surface

Figure 70 shows that some proportion of the nanoparticulates used in the treatment also get absorbed into the substrate interior when the emulsion has been applied. This implies that the interfacial morphology would be altered throughout the treatment depth similar to that of the surface. Since a nanoparticulate treatment in two dimensions would not be nearly as effective as that of one in three dimensions, this helps verify the validity of the water vapour permeability and MIP results. The hydrophobic nature of treated samples would therefore be dependent on two things; the surface energy characteristics of the silane used, and the contour profile of the interface. Similar results were observed with the zinc oxide samples, shown in Figure 71. The difference in Ti and Zn sites seems to follow the results of aggregation observed by TEM analysis. Since Zn aggregates more due to its morphological characteristics discussed in the nitrogen isothermal analysis, it is dispersed less effectively than Ti. This would mean that ZnO emulsions may be less effective as an interface modifier at low concentrations. As a comparison Figure 72 shows the SEM

images of the emulsion control treated brick sample. Due to the sample EDAX not containing Ti or Zn no EDAX positions for these elements are given, however to confirm that these elements are not picked up by EDAX analysis Figure 73 and Figure 74 give the EDAX spectral results of external and internal surfaces respectively.

6.8 Water Absorption

One of the key water repellent tests is based on the ability for a sample to repel water over a prolonged period of exposure. If a facade is exposed to a short period of rain, it may repel it quickly without substrate absorption due to the surface energy profile exhibited at the interface. However, capillary action becomes a determining influence over longer periods of exposure. Therefore, evaluating a facades sorptivity is an effective means of assessing such long term exposure.

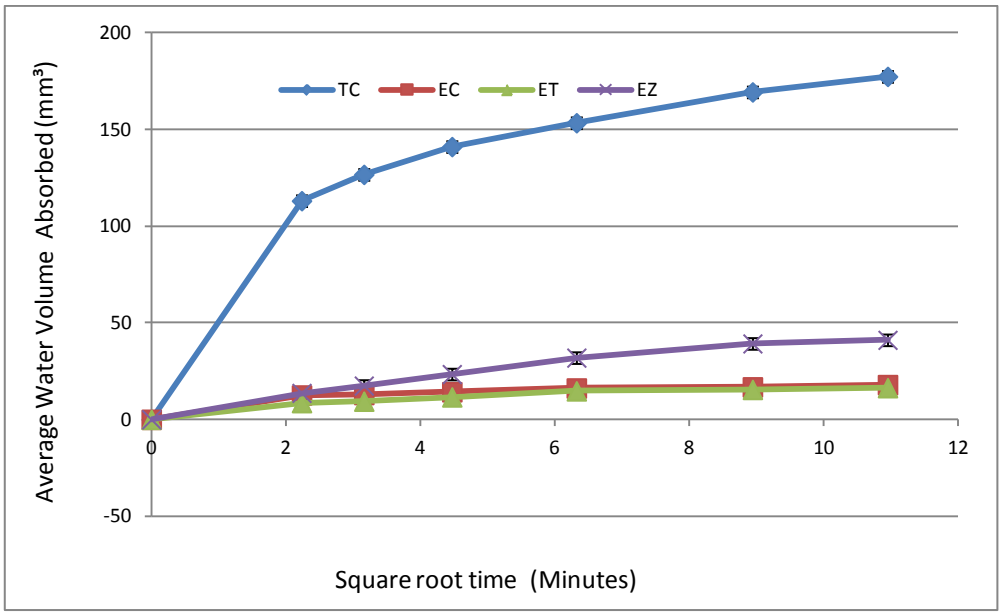

Figure 75: Brick water absorption

Figure 75 shows clearly that all treatments tested significantly reduce water absorption against the untreated terracotta samples (TC) samples. The titanium dioxide emulsion shows a significant improvement on reducing the rate of water absorption compared with other treatments. As stated previously, this is considered to be due to the interfacial modification providing less interfacial charge interaction. Since titanium dioxide has a higher potential for providing hydroxyl active sites for bonding, it may be this which differentiates its performance characteristics with that of the zinc oxide treatment. This may mean that in order to produce a comparable

performing zinc oxide emulsion, either a more exposed particulate surface area would be required or a greater particulate percentage by weight.

Table 22: Average brick sorptivity results

Sample	TC	EC	EZ	ET
Average Sorptivity ($mm^3\ min^{-1/2}$)	50.57	5.62	6.12	3.87

Table 22 shows the sorptivity results are significantly reduced compared with that of the brick control samples. The titanium dioxide treatment showed approximately 45% lower water ingress rate compared to the emulsion control. Since water absorption is considered generally a key characteristic in determining water repellent efficacy, it can be clearly seen that more work in this area could be of interest for facade remediation in future.

6.9 Summary

Results in this chapter show that the developed emulsions modify pores but do not essentially block them. Water vapour may permeate through a structure allowing it to dry out. Water repellence was shown to be improved by nanoparticulate incorporation during testing. Thermal conductivity was slightly increased for nanoparticulate treatments in dry conditions compared to the emulsion control, but were considerably reduced under wet scenarios. All treatments could penetrate deep into the substrate, with nanoparticulate treatments allowing particulates to become distributed uniformly within the substrate and at the interface. It was considered that aggregation of nanoparticulates in the prepared emulsions before application controlled distribution and thus may have a considerable affect on the cured treatment due to available particulate surfaces for interaction.

Chapter 7: Thermal Envelope Efficiency

7.1 Model House Study

7.1.1 Overview

In order to assess if such nanoparticulate treatments actually made a structure more energy efficient, two model houses were produced. One model was treated with a zinc oxide emulsion and the other used as a control. These models were tested across various temperature scenarios as well as in simulated wet conditions. The zinc oxide emulsion was also applied to respective brick and mortar samples to assess their influence on thermal envelope performance, as well as component mechanisms. Tests on these samples included; porosity, treatment depth, surface energy, water contact angle, thermal conductivity and visual aesthetics.

A heating and monitoring regime was developed for the models to quantitatively evaluate heating energy consumption in different conditions. It was found that the treatment imparted significant water repellence and enhanced thermal insulation to treated samples. The results from contact angle and surface energy measurements showed that the substrates became highly hydrophobic, and internal humidity was reduced across various temperature scenarios.

7.1.2 Treatment Depth and Porosity

Porosity of the brick was calculated as being 22%, base mortar was 9%, and main mortar 13%. Treatment depth for the brick was 13mm, base mortar was 4mm and the main mortar was 11mm. The higher porosity of the bricks led to deeper penetration depths. The base mortar was used to bond the masonry to the foam base and included a relatively large quantity of latex powder. This powder helped reduce the open cell potential of the mortar by providing obstacles for crack propagation during curing.

Figure 76 shows examples of the darker hydrophilic regions where the treatment did not penetrate. These sites allowed water absorption to occur during dipping and hence the reason for the discoloration. It should be noted that the latex in the base mortar did not play a role in imparting hydrophobic properties. If this was the case, there would be no water absorption occurring in the centre of the sample. Instead the 2.2wt% polyvinyl alcohol latex (Vinnapas 8034; Wacker, particle size 0.3-9.0μm) reduced porosity and therefore decreased the treatment depth compared with the other mortar.

Although samples had slightly different sand/cement ratios, this cannot account for such significant differences observed.

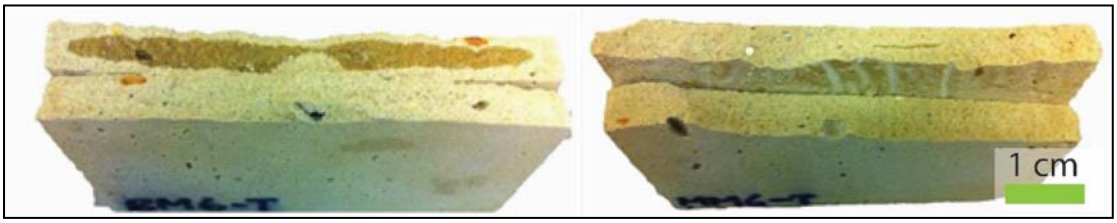

Figure 76: Examples of treated base mortar *(left)* and treated main mortar *(right)* after dipping with control cross-sections respectively

7.1.3 Thermal Conductivity

Figure 77 shows the thermal conductivity results of both treated and untreated bricks and mortar. In dry conditions treated samples had approximately the same thermal conductivity as the untreated samples. This is due to the treatments relatively small thickness which does not effectively alter the interface. The emulsions in this study were initially designed for deep penetration and so the siloxane content was minimised. In wet conditions, treated samples showed significantly reduced thermal conductivity compared to the untreated samples. It has been widely recognised that water has significantly higher thermal conductivity and greater heat capacity than air, leading to greater heat loss in wet weather. The dry scenario presented may be drier than that expected for an exterior facade in service. All substrates were stored indoors to reduce variables such as morning dew and 24 hour humidity variation over the course of a day. It would be reasonable to assume that the treated samples therefore would have lower water content in real world 'dry' scenarios than the untreated counterparts. In addition, it should be possible to save energy in humid conditions when air-conditioning is needed to cool the residence to a comfortable level. Better insulated bricks and mortar would retard the heat transfer, generating less demand for conditioning, which may be further complemented by the additional benefits of keeping all the problems associated with moisture ingress at bay [**157**].

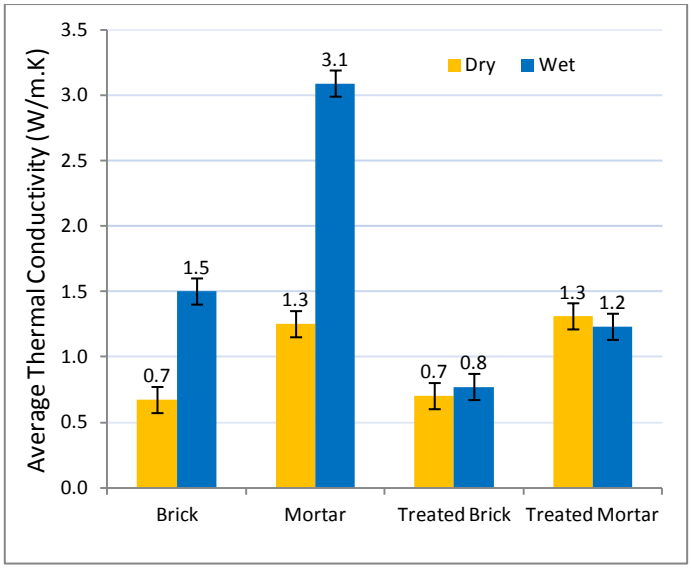

Figure 77: Average thermal conductivity

7.1.4 Water Contact Angle & Surface Energy

Figure 78 & Figure 79 show the water contact angles and surface energy of the substrates, respectively. The pronounced increase in hydrophobicity of the treated samples leads to greater beading potential and lower surface energy compared to the untreated samples. Treatment decreases the surface energy of the substrate, and water contact angle increases due to the diminished tendency for water to interact with the interface. If water has a tendency to bead on a low surface energy facade, it runs off more easily. Resting water has a potential to be drawn into a porous substrate through capillary action. This unfavourable interaction between the water and the surface is reduced with the use of the treatment; helping the wall to become drier and better insulated.

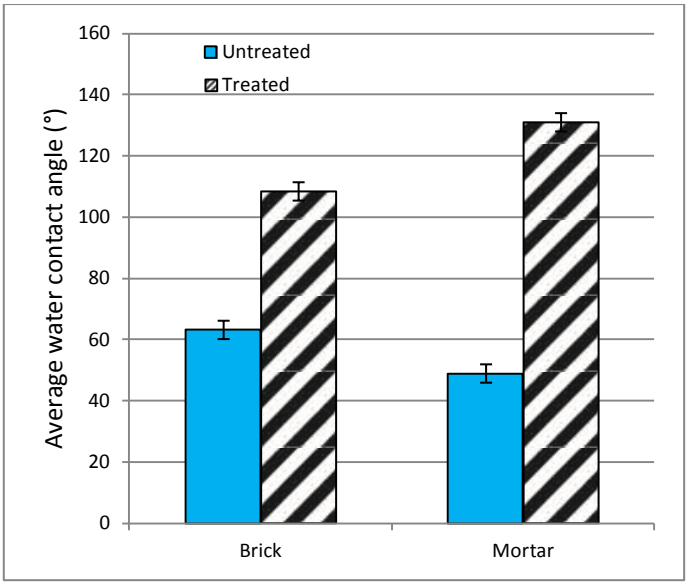

Figure 78: Average water contact angles of treated and untreated brick and mortar

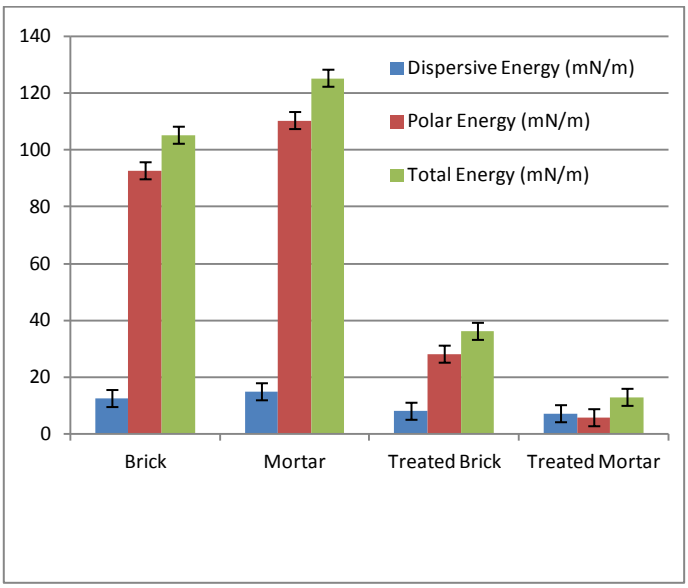

Figure 79: Surface energy characteristics of treated and untreated brick and mortar

7.1.5 Spectrophotometry

Aesthetical alteration of a substrate is detrimental to large scale remediation, heritage and retrofit projects. To assess the zinc oxide treatments impact on visual aesthetics in a quantitative manner the CIElab D65/10° test standard was used.

Table 23: Average CIE65/10° results

	L*	a*	b*	Gloss (Ill/Obs)	ΔE*	ΔC*	ΔH*
Untreated Brick	58.78	18.23	20.08	1.1	64.74	0.16	0.10
Treated Brick	59.35	15.35	21.16	1.1	64.99		

Table 23 shows a very small hue variation (ca. 0.10) caused by the treatment. The average gloss value for the untreated control was 1.1Ill/Obs with all treated samples averaging the same. This indicates that the colour and gloss of the treatments when cured is similar to that of the natural aesthetics of the substrate before treatment. This is a major advantage for the remediation of heritage buildings and retrofit projects.

7.1.6 Model House Thermal Insulation Efficiency

There are numerous variables to be considered when estimating the possible energy savings through the facade modification by such treatments. This study investigated the effect of major heat loss factors by testing miniature representations of a building. For each model house, the duration of the internal heating was gathered from the PCB data records and the bulb power was ascertained by the mains power meter. The results were taken for a fixed two hour period during the end of each test when the temperature was recorded as constant in order to ensure that equilibrium had been reached.

Table 24: Energy saving of treated model house in dry conditions

Internal Temperature (°C)	External Temperature (°C)	Model	Relay On (s)	Energy (J)	Energy Reduction (%)
25	22	Treated	524	20960	5.3
		Control	552	22080	
30	24	Treated	1042	41680	6.9
		Control	1114	44560	
35	23	Treated	2220	88800	4.1
		Control	2310	92400	

Table 24 shows the energy saving of the treated model house in comparison with the control house in dry testing scenarios. Results deviated depending upon the internal/external temperatures ranges. At elevated internal temperatures it took longer for the energy to be transferred to the external environment; this reduced heating time and a lower energy reduction is observed. In addition, trapped moisture was reduced in both structures making both drier, reducing differences and making it harder to distinguish one structure from the other. Therefore it would seem prudent to assess treatments by their average service environment.

Table 25: Energy saving of treated model house in wet conditions

Internal Temperature (°C)	External Temperature (°C)	Model	Relay On (s)	Energy (J)	Energy Reduction (%)
25	22	Treated	590	23600	19.3
		Control	704	28160	
30	23	Treated	1274	50960	12.1
		Control	1428	57120	
35	23	Treated	2246	89840	8.7
		Control	2442	97680	

Table 25 shows that the energy saving achieved in wet conditions is substantially greater than that of the dry conditions. The greater heat capacity and higher thermal conductivity of water compared to air is considered to be the driving force behind this [**157**]. Specific heat characteristics of the facade may be a more dominant factor than the thermal conductivity alone. Treated samples in dry conditions were found to have similar thermal conductivity characteristics to the control substrates. However, even a slight ingress of water into the facade may alter the specific heat of the facade and seriously affect the actual efficiency of the substrate to insulate. However, when the emulsion was applied, heat loss was diminished and substantial energy savings were achieved.

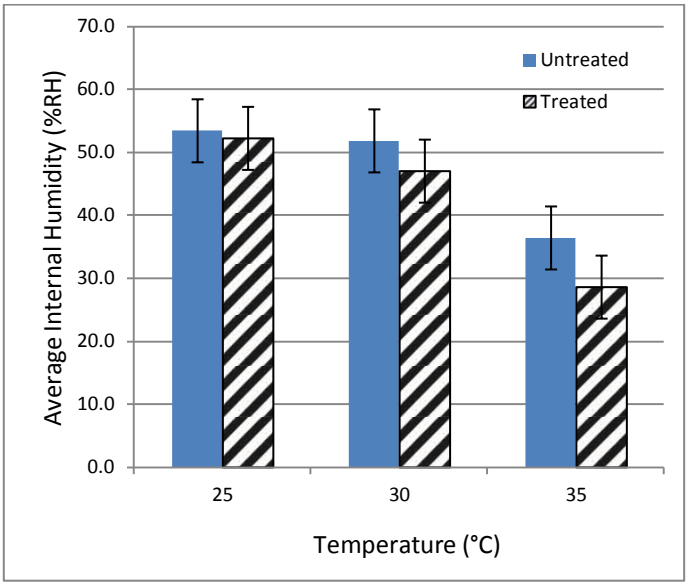

Figure 80: Average internal humidity for dry scenario

Figure 80 shows how the internal humidity in dry conditions is affected by the treatment. There is a reduction in internal humidity for both model houses. The humidity is reduced due to the treatment, allowing moisture to permeate through the

masonry upon heating while reducing its ingress at the same time. As the internal temperature increases, a drier environment is produced and hence the reason for greater humidity improvements. In wet conditions humidity of each structure was approximately the same, even though energy was saved. This may have been due to any water penetrating from application taking longer to permeate through the treated brickwork and outside. The force of brushing may have overcome the surface energy of the treatment allowing impregnation to occur. It is reasonable to assume that a bigger difference in humidity and energy saving may be made in wet scenarios if the water was applied passively.

A lower internal humidity can improve both the physical and mental health of occupants of a structure [**178**] [**179**]. Treatments may alleviate and circumvent persistent elevated internal humidity induced problems in buildings. These include mould and fungal growth inside wall cavities as well as internal decorative degradation. It should be noted that neither wet nor dry conditions should be used individually to predict possible energy consumption. In addition, the treatment may also behave differently depending on its constituents. Work showed a high siloxane content emulsion should be used to alter the interfaces thermal conductivity and water beading characteristics. Conversely, problems involving rising damp may be better remedied by a high silane content treatment, which would also help mitigate prolonged water contact situations [**92**]. The best practice for determining the energy efficiency would involve taking into account both scenarios with various degrees of each used, depending upon the geographical location, meteorological data for that area and the type of treatment.

These nanoparticulate enhanced treatments have many advantages compared with other traditional solvent based counterparts. The water repellent emulsions are cost effective in terms of labour and materials. Simple application means specialist skills or prior knowledge are not required. The treatment may be applied by brush or roller and can penetrate deep into a substrate. Colour and texture of the facade is retained, allowing these emulsions to be applied to heritage buildings or buildings requiring retrofit.

7.2 Modelling of Energy Dissipation Rates

To assess the energy and financial saving potential of each respective emulsion, the following theoretical testing scenarios based on a single wall model were produced.

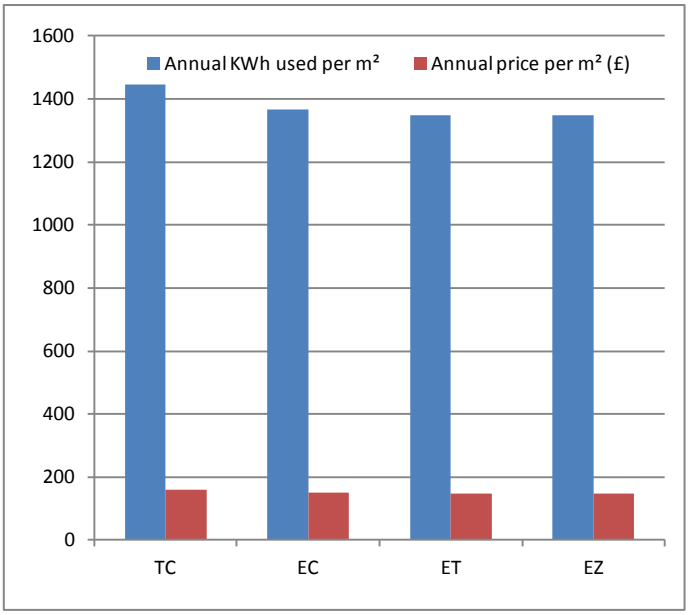

Figure 81: Temperature difference 10°C-25°C results from dry modelling scenario

Figure 81 shows the time required to heat the walls up and dissipate the energy back to achieve an ambient temperature in a dry scenario. It may be seen that there was little difference in the dry wall heat retention times when treated. This is considered due to the treatment not blocking pores in a significant manner.

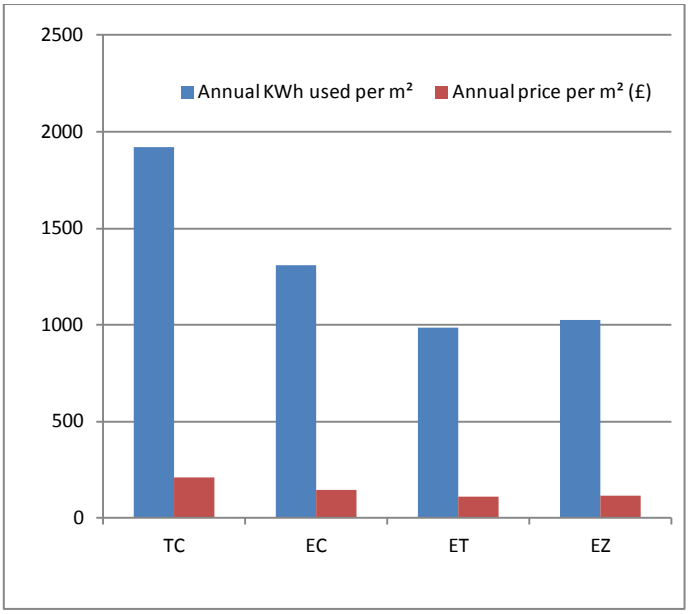

Figure 82: Temperature difference 10°C-25°C results from wet modelling scenario

Figure 82 shows during the wet scenario that the emulsions all retained heat considerably better than the terracotta control. This is attributed to the emulsions reducing water absorption. In this scenario, the nanoparticulate interface modification may have allowed water to have less contact with the substrate and provide less time for water to be absorbed into the substrate, thus reducing energy used.

Table 26: Annual UK energy and economic consumption per meter squared

	TC	EC	ET	EZ
Annual KWh used per m²	1468	1364	1330	1332
Annual price per m² (£)	161.51	150.09	146.29	146.53

Table 26 shows the possible energy and financial costs for the 10-25°C model. It assumes a 5% annual heavy rain precipitation similar to that received by the UK in 2011 [**180**]. The cost of electricity was taken as 11p per unit.

Table 27: Theoretical annual UK energy and economic saving per square meter

	Annual KWh saving per m²	Annual saving per m² (£)	Saving Improvement against EC (%)
EC	104	11.43	N/A
ET	138	15.23	33
EZ	136	14.98	31

Table 27 shows the possible savings produced by the model. The energy savings may not look much, however the results are for one square meter of wall. In context of a conventional residential building this means a great deal of money could be saved each year with all respective treatments. In addition, CO_2 emissions would be reduced significantly. A high degree of electrical energy is wasted before it reaches a home, with only around 2% used from the raw material [**181**]. So a small saving at the residential level would mean a much larger CO_2 reduction overall in an electrically heated scenario. It is important to note that the model did not take into account the effects of evaporation and was of simple design to show possible savings. Results would most likely be more conservative since the structures are not heated in a continuous manner unlike the presented model. However the results do confirm that a saving can be made and nano-particulate emulsions would be more suited to achieve this. From this it seems reasonable to deduce that the real world testing produced sensible results and that savings were made through creating a drier environment. Finally it should be noted that if a treatment altered the interface to a greater extent through higher siloxane content for example, this may help mitigate the possible thermal conductivity issues associated with the metal oxide incorporation at the interface, however more work into this is required.

7.3 Summary

Based upon the water repellent and thermal insulation properties of constituent materials with and without treatment and their implications on heating energy saving, the following conclusions may be made;

- Treatments could penetrate deep into both brick and mortar showing around 13mm and 11mm penetration for brick and mortar respectively. Brick and mortar had a porosity of approximately 22% and 13%, indicating that porosity of the substrate influences the treatment depth.
- Water contact angle and surface energy results showed that a hydrophobic surface can be produced by using the nano-particulate treatment on brick and mortar. Treated bricks were improved by approximately one third of the untreated samples, and more than one half improvements were exhibited by the 5:1 sand and cement mortar used.

- Thermal conductivity of untreated brick and mortar in wet conditions was approximately twice that of the dry untreated samples. The thermal conductivity of the treated samples however showed little difference between wet and dry conditions, indicating improved thermal insulation by the treatment which was attributed to the significant reduction in water absorption occurring.
- Energy can be saved using the nanoparticulate enhanced treatment on walls in both wet and dry conditions based upon the model house testing. Approximately 5% energy was saved in dry conditions compared to 20% in wet conditions with only approximately 3°C difference in internal and external temperatures. This saving may be more significant as external conditions in reality may be wetter and colder than that tested.
- The internal humidity in the model house after treatment was reduced in dry conditions; showing typical problems associated with damp may be alleviated. Further work is required to assess accurately the wet humidity which may require a passive water application method.
- Theoretical modelling showed energy and financial savings may be made through use of such emulsions which seem to comply with the real world test results; although it is considered that actual savings compared to the calculated savings would be more conservative.

Chapter 8: Antifouling Characterisation

8.1 Photocatalytic Potential

To determine the effectiveness of each photo-catalytic metal oxide treatment with regard to breaking down soiling matter, oleic acid was put on treated terracotta samples and placed under a UV light source. The water contact angle was periodically tested during the UV exposure as shown in Figure 83.

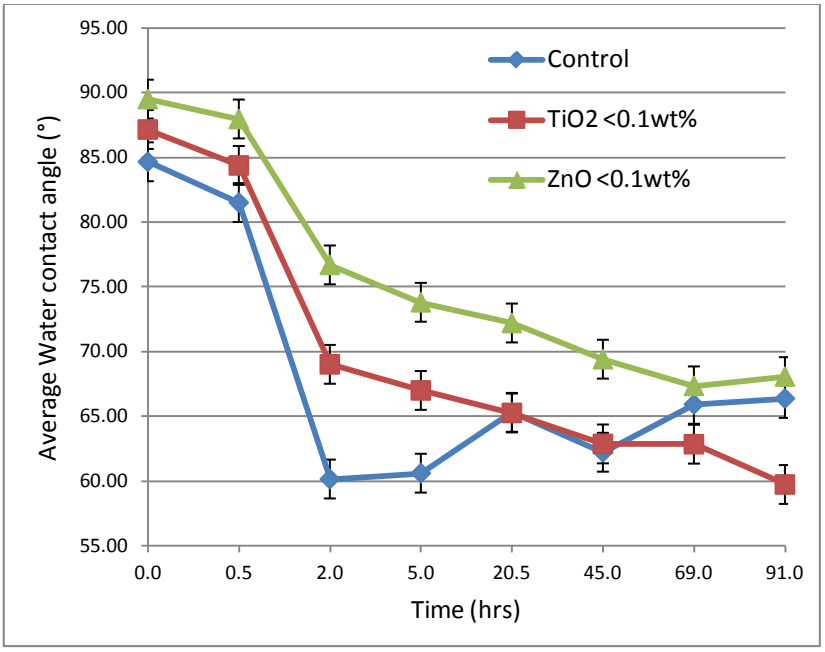

Figure 83: Photo-induced oxidisation characteristics of oleic acid on terracotta tiles with regard to water contact angle

Figure 83 shows that, after coating of samples by oleic acid, they were more hydrophobic in nature than after prolonged exposure to UV light. Since all samples were treated in the same manner, it is clear that the titanium dioxide treatment was more hydrophilic at the start of testing. This difference is expressed over the course of the study compared to the zinc oxide samples. This implies that the titanium dioxide is more effective at breaking up the contaminant than the zinc oxide counterpart. It seems that treatments with <0.1wt% nanoparticulate content can therefore be used for the breakdown of fouling matter; thus the surface is self-sanitising.

The nature of the nanoparticulates to aggregate may attribute to the differences in performance observed; larger available surface areas for photo-induced sanitisation increases efficacy. The chemical nature of each type of particulate would suggest that

titanium dioxide would be more effective due to its better suited band gap for photo-induced activity.

For longer time periods results show that oleic acid aligns the hydrophobic functionalities away from the hydrophilic polar groups of the control emulsion treated substrate; indicating possible hydrogen bonding with free hydroxyl sites. The metal oxides in the treatments however are increasing hydrophilic tendency due to the photo-induced sanitisation reaction.

It should be noted that the temperature and humidity of the sample environment may be the cause of the variation over time. Testing was carried out in a cellar with only small periods of artificial light exposure. Average temperature was recorded as 22°C and average humidity as 55%RH according to remote datalogger results. Since UV, air and water from the environment are variables for photocatalytic reactions, it must be noted that external environments will differ considerably allowing such test to be relative for treatment comparison only.

8.2 Antifouling in Practice

8.2.1 Overview

Although the self-cleaning rate shows interesting photocatalytic performance by nanoparticulate treatments, it does not show performance encountered in real world conditions, such as against microbiological fouling. Thus, the following section evaluates the mechanisms that are considered to control fouling on facade substrates and how the formulated treatments perform against biofouling caused by locally sourced algae. In order to control variables, treatments were applied to specifically formulated mortar designed to reflect similar mortar used in modern building construction.

8.2.2 General Treatment Characteristics

To assess the extent of influence the treatments had on the substrate and thus its ability to resist colonisation, treatment depth was evaluated. All treated samples showed total penetration and since the thickness of mortar samples was 20±1mm, possible treatment depth would be greater or equal to 10mm for each emulsion. It should be noted that since emulsions were brushed by hand onto the mortar substrates,

penetration may vary depending on application. This test however shows that a deep penetration may be achieved by all treatments with no substantial compromise shown by the nanoparticulate incorporation. Untreated samples showed ~3mm carbonation zone arond the edge of the cross-section of samples (Figure 84). This is a continual process where calcium hydroxide with carbon dioxide from the air reacts with water and forms insoluble calcium carbonate, altering the water repellent attributes of the affected surfaces. Since this process relies on carbon dioxide exposure this would explain the difference in hydrophilic tendency near the interface of the mortar [**169**]. Figure 85 shows that water beads are formed on treated samples after submersion throughout the cross-section and hence total penetration was achieved. This shows that these treatments should be effective even if the mortar cracks or chips. From this it is clear that hydrophobic pore modification may influence bioreceptivity considerably as well as carbonation due to diminished moisture/contaminant ingress.

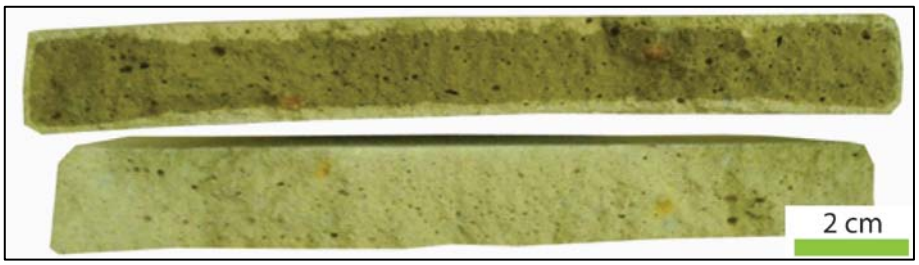

Figure 84: Water absorbed by TC *(above)* viewed against the control cross-section *(below)*

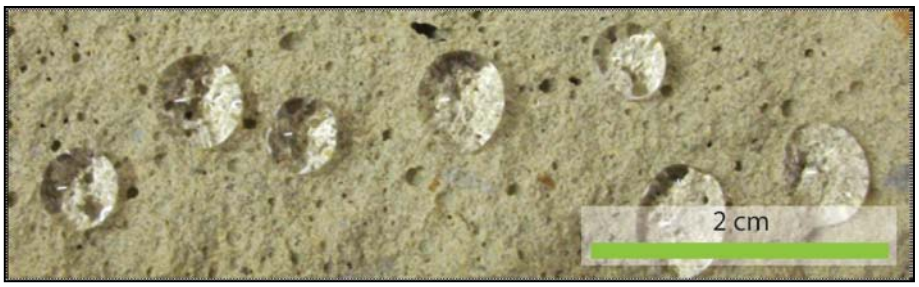

Figure 85: Standard treatment depth cross-section result for treated samples after dipping

In addition to treatment depth, the extent of visual alteration is also of vital interest in assessing the usefulness of such treatments. Aesthetical alteration of a substrate is detrimental to large scale remediation, heritage and retrofit projects. To assess each treatments impact on visual aesthetics in a quantitative manner, photospectrometry was conducted using the CIElab D65/10° test standard.

Table 28: Average Photospectrometry results

	L*	a*	b*	Gloss	ΔE*	ΔC*	ΔH*	ΔH* (%)
TC	62.60	2.17	16.95	0.9	64.89	1.35	15.69	0.24
EC	57.15	2.17	15.60	0.7	59.28			
EZ	57.59	2.34	15.90	0.8	59.79	1.04	16.04	0.16
ET	58.38	2.22	15.75	0.7	60.51	1.19	15.86	0.20

Table 28 shows a very small hue variation of approximately < 0.3% and a small gloss variation caused by the treatments. Figure 86 shows that the average photospectra is very similar over the visible light range for each sample. Thus, treatments when cured are similar to that of the natural aesthetics of the substrate before treatment. These results in addition to the treatment depth attributes also show favourable characteristics useful for the remediation of heritage buildings and retrofit projects.

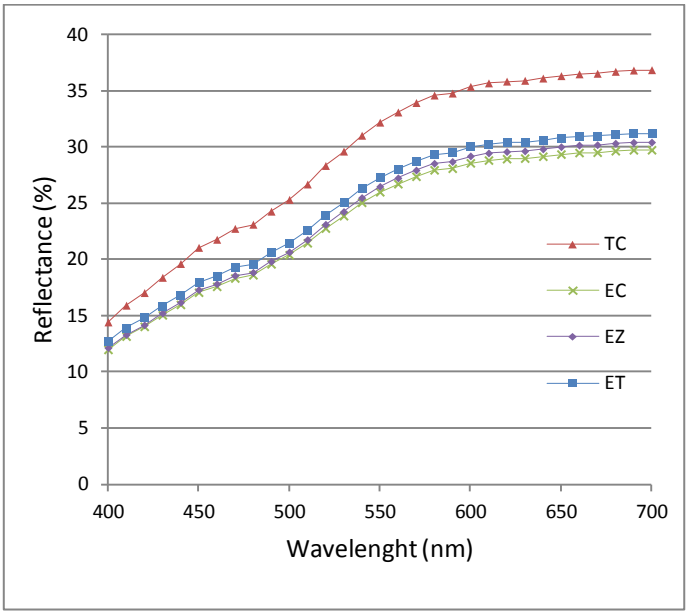

Figure 86: Average D65/10 photospectra results

8.2.3 Biofouling Specific Treatment Characteristics

Bioreceptivity, a concept developed by Guillitte (1995) [**182**] has become the principal method used to characterise colonisation. According to Guillitte and Dreesen (1995) [**166**] and comments by Gaylarde and Gaylarde (2005) [**183**], mechanisms that govern colonisation are; surface roughness, initial porosity, mineralogical nature of the substrate, and other environmental factors. These mechanisms have also been successfully supported by various studies [**184**]. Thus, to

evaluate bioreceptivity effectively in this study assessment of these mechanisms was conducted independently to help establish the predominant factors.

To assess the general characteristics and pore morphology of the mortar samples, MIP was conducted. Table 29 shows similar porosity and density values calculated from the obtained data. Figure 87 shows apparent bimodal distribution in all samples with average pore diameters around 42µm and 52µm. The total pore area measurements (Figure 88) show pore sizes being reduced by the treatments. Despite the pores being constricted, they are not blocked. Porosity results also help verify that the pores are not being blocked due to similarity in values for each sample type.

Table 29: Porosity, density, surface roughness and sorptivity of mortar samples

Sample	Porosity (%)	Bulk Density at 0.32 psia (Kg/m^3)	Apparent (Skeletal) Density (Kg/m^3)	Surface Roughness Ra (µm)	Sorptivity (mm $min^{-1/2}$)
TC	26.1	1832.5	2480.5	9.7	29.4
EC	24.5	1880.1	2489.1	9.0	2.6
EZ	27.5	1752.8	2416.1	8.9	2.4
ET	23.6	1906.7	2495.7	8.1	2.3

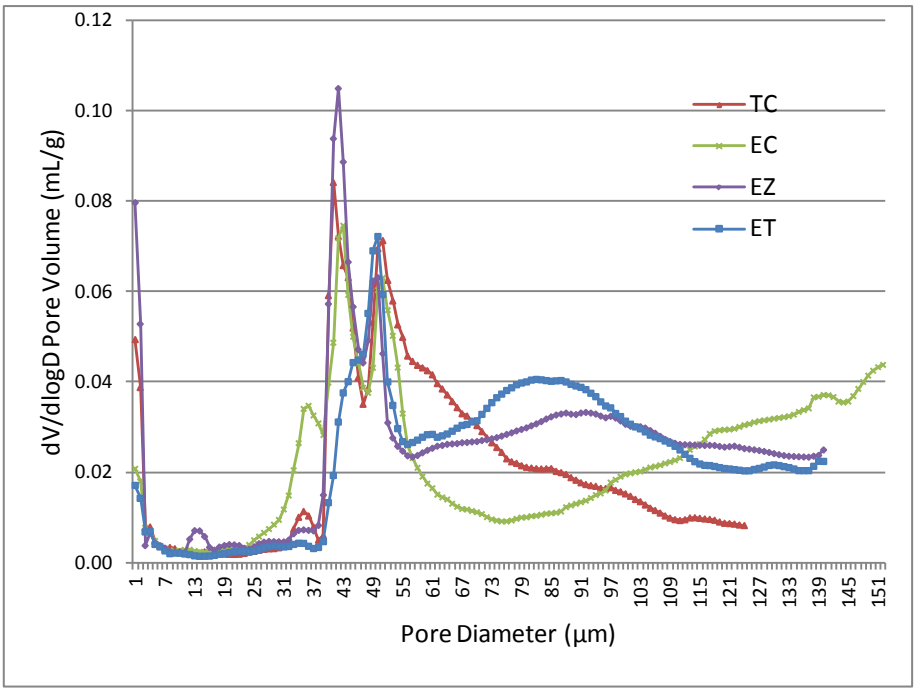

Figure 87: MIP pore diameters of treated and untreated mortar samples

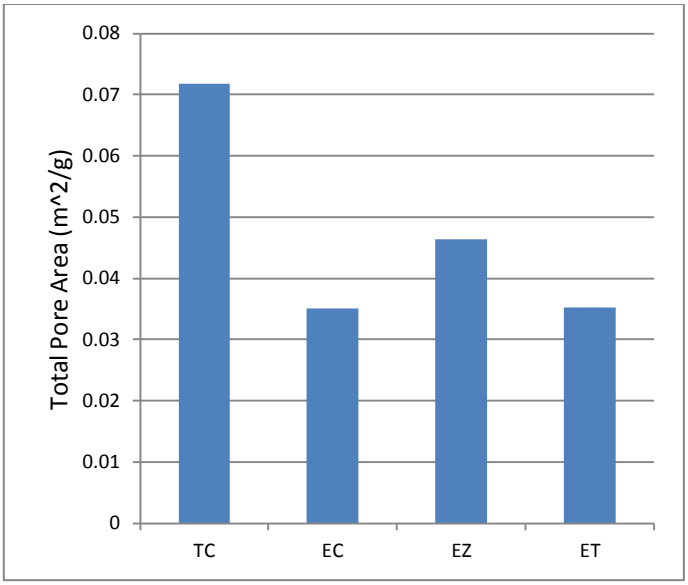

Figure 88: Total pore area of treated and untreated mortar samples

The ability for a facade to repel water before it is absorbed into a porous substrate is a critical requirement for any exterior building material. Figure 89 shows the average water contact angle results for each sample type. Due to the untreated substrates being too hydrophilic, total wetting occurred and the contact angle was estimated ca 3°. All treated samples exhibited higher water contact angles than the untreated samples. Zinc oxide and titanium dioxide treatments reached slightly higher water contact angles than the control emulsion. It is due to the fact that the metal oxides have a high concentration of polar groups that act as bonding sites for the silane and siloxane components. This allows a more structured and uniform interfacial morphology to be produced; hydrophilic domains are attracted to the interior of the system, with hydrophobic parts of the treatment governing the interfacial characteristics. Additionally, it was found from earlier EDX work not only this process is occurring, but also that metal oxides are present at the surface of the treatments. It was also discovered that zinc oxide tended to aggregate more than the titanium dioxide, reducing distribution potential during application; thus the reason for the difference in performance observed. Due to goniometry occurring in 'UV limited' conditions, the treated surface becomes highly hydrophobic with contact angles ca. 150°. This allows for any suspended soiling matter to be removed more effectively in these conditions as it has less interaction potential with the substrate. Contaminant removal in this way would be due to runoff and evaporation [**168**]. Although this means that interface hydrophobicity varies, treated pore surfaces that are not exposed to UV light should

retain high water contact angles. This treatment characteristic therefore is perfect for rising damp remediation and biofouling inhibition; essentially imparting duel functionality to the treatment.

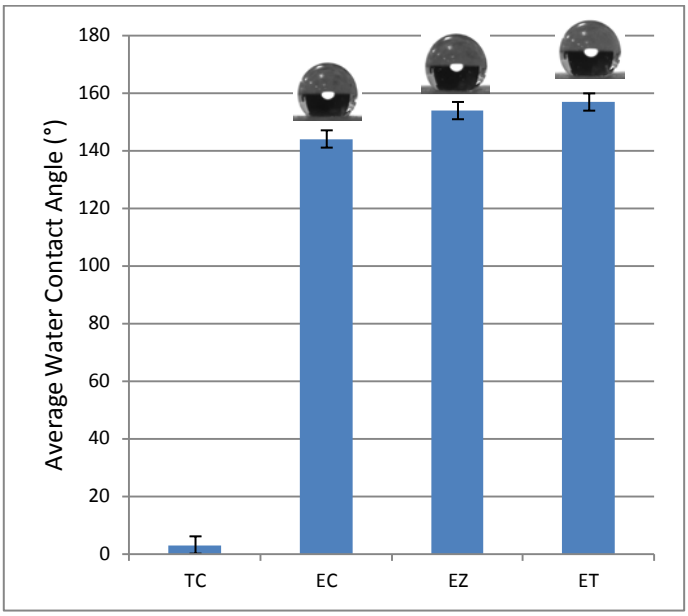

Figure 89: Average water contact angles of treated and untreated mortar samples

In addition to water beading exhibited at short time scales, absorption characteristics through mechanisms such as capillary action must be considered for longer durations of water contact at the substrate interface. Calculated sorptivity values for the treated samples (Table 29) shows that the sorptivity of treated samples is significantly reduced compared with the untreated mortar. Significantly more water could be absorbed by the untreated mortar than the treated samples over a longer period. Reduced sorptivity by the nanoparticulate treatments is considered due to the reduced surface energy achieved by the structuring of the treatment and metal oxide characteristics as discussed prior. From these results it is clear that the fouling rates are significantly diminished for treated mortars as reduced sorptivity would constrain transportation water and nutrients for growth.

Earlier studies suggested that surface roughness may have dominant influence on biofouling colonisation through producing sites for retention and propagation [**169**]. Table 29 shows that the average surface roughness of the samples seemed to be reduced by the treatments used. Better networking achieved by nanoparticle addition made treatments 'smoother' by decreasing the number and extent of surface

irregularities. However since surface roughness was on average reduced to such a small degree, this factor could be considered negligible for bioreceptivity assessment.

8.2.4 Culture Streaming Study

To assess the effectiveness of the nanoparticulate treatments to resist biofouling a culture streaming test was conducted. Figure 90 shows that carbonation in addition to biofouling was abundant on untreated samples. Table 30 shows the extent of biofouling as well as the impact of carbonation on aesthetical alteration of the various substrates over the testing duration. Nanoparticulate treatments effectively reduced carbonation, most likely due to better bonding and structuring allowing less potential for the substrates to be subjected to pore moisture or carbon dioxide interaction. It should be noted that although pH was not monitored in this study it has a marked influence on bioreceptivity; reduced carbonation would allow more biofouling to occur [**185**] [**186**]. Thus, treatments are expected to be more effective than shown in this study.

Figure 90: Untreated mortar before *(Left) and* after *(right)* 8 weeks of streaming test

Table 30: Example of culture streaming sample modification over time

	Weeks								
	0	1	2	3	4	5	6	7	8
TC	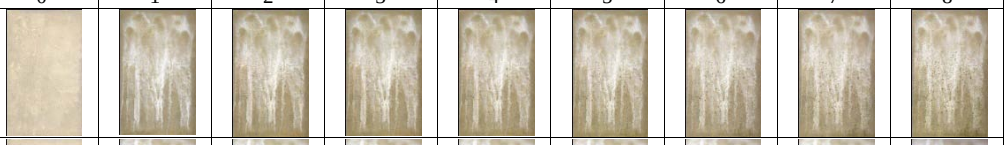								
EC									
ET									
EZ									

Figure 91 shows the change in mean intensity compared to the original value; all samples were darkened with soiling matter. The results show that titanium dioxide and zinc oxide treatments resisted biofouling to a greater extent than the control emulsion, while untreated samples showed extensive colonisation. The average biofouling surface coverage is shown in Figure 92. All treatments showed significantly reduced surface coverage over the test duration compared to the untreated samples. Nanoparticulate treatments again performed better than the control emulsion. Since biofouling did not follow a visibly consistent deposition with streaming paths, this may be the reason for the low surface coverage rate shown in later weeks [**171**].

From the results it can be seen that intensity varies for the treated samples by ~4% between the emulsion control and the nanoparticulate emulsions. However, when assessing the treated samples biofouling coverage area there was only ca. <1% difference achieved. Thus, the coverage area is relatively consistent for all three treated samples, but much lighter in colour for the titanium dioxide and zinc oxide treatments. This may be considered due to photo-induced breakdown occurring of the soiling matter lightening the interface. Carbonation cannot account for this difference as the control treatment was observed to have been more susceptible to its influence. Additionally, it cannot be attributed to water retention, differences in surface roughness, or porosity, since the preliminary tests showed that all samples and treatments used were comparable in nature. If improved water repellence was the

main reason for the reduced intensity difference, it would not explain the similar coverage area observed for the treatment control and nanoparticulate samples, which were almost identical. This means that photo-induced sanitisation had to be the reason for the lighter colour.

Table 31 shows the data logger results for the 8 weeks of testing. It can be seen that UV irradiation and humidity varied over the 24hr cycles; thus, photocatalytic performance at the surface must have varied. Since surface conditions change due to variable environmental conditions, water beading will vary as will the efficacy of the nanoparticulate treatments. In order to assess the results effectively in terms of bioreceptivity three elements are of interest; the substrate, the surface in 'optimised photocatalytic' conditions, and the surface in 'constrained photocatalytic' conditions.

The difference observed for the nanoparticulate treatments is related to the following. Titanium dioxide has band gap energy levels more suited to natural light applications than zinc oxide, which could explain the reduced fouling intensity produced by the titanium dioxide treatments [**187**] [**188**]. Conversely, it has been found that zinc oxide does not alter its structure during the photocatalytic process unlike the titanium dioxide [**188**]. This could explain the seemingly improved reduction in biofouling surface coverage over the duration of testing since it is not constrained by the silane/siloxane alteration of the particulate. Although zinc oxide would be less efficient at breaking down contaminants with a poorer distribution per unit area due to aggregation found by prior investigation [**147**], it should be more stable and effective over the duration of the treatments service life.

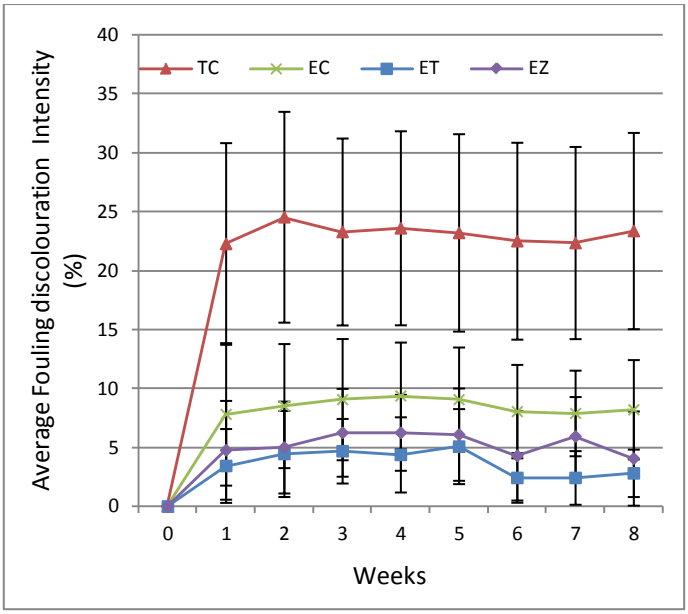

Figure 91: Average intensity of streaming test samples.

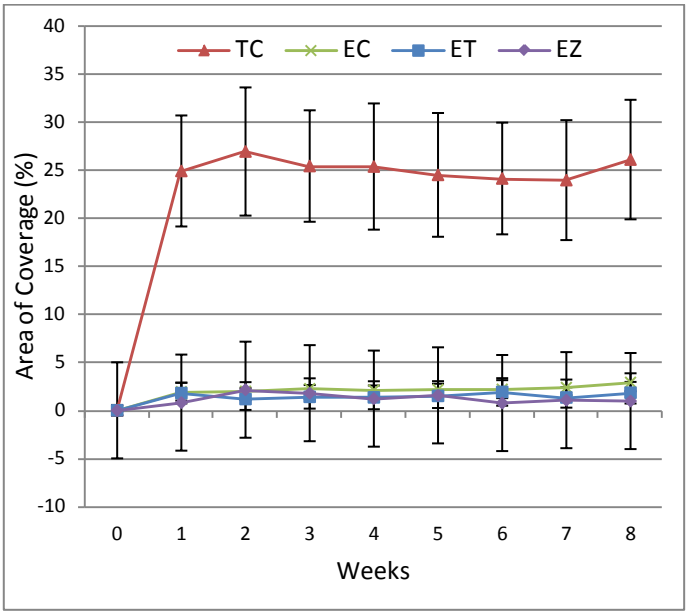

Figure 92: Evaluation of average biofouling surface coverage over test duration

Table 31: Remote Probe Results for streaming test

	Average 'Day' Value	Average 'Night' Value	Test Duration Average Value
Temperature (°C)	30.8	23.6	27.1
Humidity (%RH)	53	83	67
Illumination (Lx)	1743	0.0	1024.1
UV Irradiance (mW/cm^2)	0.0770	0.0000	0.0407

8.2.5 Bioreceptivity

All tested samples showed relatively similar values for the surface roughness and initial porosity, and therefore were not considered dominant bioreceptivity factors in this study. It is clear that the photocatalytic attributes of these treatments studied reduce bioreceptivity but are dependent on conditions. Interface soiling intensity in 'optimised photocatalytic conditions' may be different from 'constrained photocatalytic conditions' due to varied chemical breakdown and runoff characteristics. Conversely, water beading may remain consistently high inside pores due to the lack of UV exposure. Thus, subsurface biofouling may grow at different rates to surface counterparts. This makes any bioreceptivity prediction for such treatments difficult due to the variation in conditions that these treatments may be exposed to.

8.3 Summary

Photo-induced sanitisation seems to have been observed through goniometric assessment which implies that <0.1wt% nanoparticulate metal oxide can achieve this effect. The reaction rate/film forming rate of the treatments were similar. External environmental conditions may differ greatly with those of the experiment, allowing only a treatment comparison to be made. Titanium dioxide was more effective than zinc oxide at photo-sanitization and considered due to the available surface area available at the treatments interface. In addition it was observed that the metal oxide samples also produced the largest WCA beading effect before UV exposure potentially reducing possible fouling in UV absent conditions.

The biofouling study assessed bioreceptivity of nanoparticulate treatments through a controlled culture streaming study and independently characterised morphological, visual and water repellent alteration of the substrate to determine governing factors and treatment impact. From the field of study presented the following conclusions were drawn;

- A significant treatment depth could be obtained and was not compromised by the incorporation of nanoparticulates.

- Surface roughness, pore morphology and visual aesthetics were not effectively altered by the treatments.
- For the nanoparticulate treatments water contact angle varied at the facade surface, but remained high inside pores due to the absence of UV light.

Biofouling intensity and surface coverage was significantly reduced through the use of nanoparticulate additives when compared to the control treatment, and was attributed to the photo-induced breakdown of contaminants.

Chapter 9: Conclusions and Recommendations

9.1 Conclusions

Throughout the presented project, investigation and development of fundamental knowledge and understanding of this virgin field has been achieved. Development and optimisation of a base emulsion through the assessment of the stability mechanisms via morphological, stress and rheological testing has occurred. Nanoparticulate dispersion and optimisation was achieved through morphological characterisation of particulate interfacial characteristics and morphological properties. Incorporation and dispersion of these colloidal mediums in the base emulsion were then assessed through thermodynamic stressing, gravitational stressing, turbidity, and droplet morphology. From these studies, a practical and novel nanoparticulate enhanced facade emulsion was developed. To this end, the project was highly successful as the final treatments did not effectively alter the aesthetics of tested masonry materials, making them universally viable for retrofit applications while expanding the field of facade remediation. From the presented project, the following conclusions were made;

1. Formulation of silane/siloxane macroemulsions was successfully achieved through investigation of surfactant and volume ratios, siloxane type and mixing procedure, to achieve an optimised emulsion. From various systematic tests, a 'base emulsion' was successfully produced. In addition, further testing helped also to identify that hydroxyl terminated siloxane could be integrated into such systems to improve the 'green credentials' of the emulsions; water and not ethanol or methanol was the by-product of the condensation reaction. No information has been found on the use of such siloxanes in this manner and thus may be a new development in the field.

2. Titanium dioxide and zinc oxide nanoparticulates were incorporated into the formulated silane/siloxane emulsions and assessed before application. Successful dispersion of nanoparticulates was achieved through ultrasonic mixing. These nanoparticulate colloids were then added to the developed emulsions and stress tests showed that the nanoparticulate emulsions were substantially more stable than the emulsion control. Performance was considered to have been governed by nanoparticulate distribution within the emulsions; increasing available bonding and steric barrier potential between phases. The titanium dioxide and zinc oxide particulates were found through TEM and nitrogen isothermal analysis to

aggregate to a different extent, and this was considered the governing influence controlling emulsion stabilisation and rheological characteristics. Rheological study showed that a gelled network structure was produced by the incorporation of the nanoparticulate colloidal dispersion. Nanoparticulate dispersions through networking increased the zero-rate viscosity of the emulsion and thus helped to improve stability. The nanoparticulates also helped produce a steric barrier between the polar phases, helping to reduce interaction and retain micelle formation.

3. SEM and EDX analysis showed that nanoparticulates could be applied in a uniform and distributed manner through the system developed, to both the surface and pore interior of masonry substrates when dispersed in the continuous phase. The novel nature of this, is that the particulates helped stabilise the emulsion system, and then after treatment also provides beneficial facade protection. Conventionally, nanoparticulates are functionalised and integrated into the dispersed phase of a colloid, however here it can be shown that this is not necessary and that particulate capping is not required. This allows nanoparticulate emulsions to be prepared quickly and easily, making them highly suited for commercial applications.

4. Developed treatments did not effectively block pores but modify them altering the water repellent characteristics of the substrate. Water repellent attributes were found to be governed predominantly by the chemical nature of the treatment and to a lesser extent the surface roughness. Small quantities of nanoparticulates influenced water repellence considerably. It was also found that due to zinc oxide aggregating more than titanium dioxide, due to morphological characteristics, dispersion controlled performance extensively.

5. Thermal envelope efficiency improved through the reduction of retained water in various forms. To assess this, both physical and modelled analysis was conducted using model houses. It was found that humidity became trapped, particularly in wet conditioning of the exterior of the structures, reducing thermal envelope efficiency. Results implied that a treatment unlike a coating would be more useful for removing unwanted humidity passively, and thus reduce possible

microbiological decay of the interior, and health related problems posed to the occupants.

6. A biofouling study was conducted within a rig that was designed to help reduce variables associated with other similar studies. The rig included UV lights as well as standard florescent lamps and can be claimed to be the first of its kind for bioreceptivity testing of photo-catalytic materials. Biofouling results showed that treatments with <0.1wt% of the aforementioned nanoparticulates could reduce bioreceptivity through what is considered photo-induced sanitisation. Due to photo-induced sanitisation only being achievable in UV conditions, bioreceptivity at the surface is considered to be different from that of the subsurface of the substrate. This implies that internal pores would remain highly hydrophobic regardless of surface conditions; a novel attribute for simultaneous photo-induced sanitisation and rising damp remediation. The significance of this work is that a treatment that does not affect the aesthetics of the substrate can be achieved and provide photo-induced sanitisation, a breakthrough in facade protection.

9.2 Recommendations

Based upon the work carried out during this study the following are recommended points for future work;

- Development and further characterisation of the emulsions presented would need to be conducted to assess compliance to UK building regulations (Bulding Act 1984 and Building (Scotland) Act 2003). Specifically sections pertaining to; fire (part A), toxic substances (part D), ventilation (part F), conservation of fuel and power (part L), and regulation 16 relating to Standard Assessment Procedure (SAP) rating and labelling. New amendments to building regulations in 2006 now also state that alteration of energy efficiency needs to be assessed and stated according to regulation 16, which would compliance after treatment application to relevant structures [**193**].
- UV degradation may also be of interest for such treatments to assess their suitability during service.

- Leaching of nanoparticulates and other constituents would need analysis and consideration, both to assess the service life of treatments, and the toxicological impact they have on humans and the environment.
- Further research should lead to a life cycle assessment being conducted to assess the environmental impact of such treatments.
- Cryogenic TEM, X-ray photoelectron spectroscopy (XPS), secondary ion mass spectrometry (SIMS), and atomic force microscopy (AFM) may help elucidate upon the nanoparticulate dispersion mechanisms occurring within the emulsions and on what happens during and after curing. Due to the nature of these test methodologies, they are considered suited for such nano-scale investigations.
- Further testing is required to ascertain the full extent water effects thermal envelope efficiency and how the various treatments reduce water content in relation to this. Research may lead to regression analysis and give an insight into specific mechanisms governing thermal insulation for such treatments.
- Further testing and assessment of biofouling using different conditions and microbiological species may be of interest for other common forms of biofouling. In addition, work on a more suitable theoretical model of bioreceptivity with respect to the treatments tested could be developed.
- Incorporation and testing of novel visible light band-gap sensitive photo-catalytic molecules, impurity doped nanoparticulates, and oxide semiconductor photocatalysts may be of interest as they may allow more photo-induced sanitisation to be achieved [**194**] [**195**] [**196**].

References

[1] I. Lorenzoni, S. Nicholson-Cole, and L. Whitmarsh, "Barriers perceived to engaging with climate change among the UK public and their policy implications," *Global Environmental Change*, vol. 17, pp. 445-459, 2007.

[2] M. Odenberger and F. Johnsson, "Achieving 60% CO2 reductions within the UK energy system-Implications for the electricity generation sector," *Energy Policy*, vol. 35, pp. 433-2452, 2007.

[3] D. Williams, L. Elghali, R. Wheeler, and C. France, "Climate change influence on building lifecycle greenhouse gas emissions: case study of a UK mixed-use development," *Energy and Buildings*, vol. 48, pp. 112-126, 2012.

[4] M. Osmani and A. O'Reilly, "Feasibility of zero carbon homes in England by 2016: A house builder's perspective," *Building and Environment*, vol. 44, pp. 1917-1924, 2009.

[5] H. Meier and K. Rehdanz, "Determination of residential space heating expenditures in Great Britain," *Energy Economics*, 2009.

[6] Z. Yu, F. Haghighat, B.C.M. Fung, and H. Yoshino, "A decision tree method for building energy demand modelling," *Energy and Buildings*, vol. 42, pp. 1637-1646, 2010.

[7] A.T. Booth, R. choudhary, and D.J. Spiegelhalter, "Handling uncertainty in housing stock models," *Building and Environment*, vol. 48, pp. 35-47, 2012.

[8] M. Alam, H. Singh, and M.C. Limbachiya, "Vacuum Insulation Panels (VIPs) for building construction industry - A review of the contemporary developments and future directs," *Applied Energy*, vol. 88, pp. 3595-3602, 2011.

[9] C.A. Balaras et al., "European residential buildings and empirical assessment of the Hellenic building stock, energy consumption, emissions and potentual energy savings," *Building and Environment*, pp. 1298-1314, 2007.

[10] M. Abuku, H. Janssen, and S. Roels, "Impact of wind-driven rain on historic brick wall buildings in a moderately cold and humid climate: Numerical analyses of mould growth risk, indoor climate and energy consumption," *Energy and buildings*, vol. 41, pp. 101-110, 2009.

[11] H.S. Shang, Y.P. Song, and L.K. Qin, "Experimental study on strength and deformation of plain concrete under triaxial compression after freeze-thaw cycles," *Building and Environment*, vol. 43, pp. 1197-1204, 2008.

[12] A. Hyvonen, P. Piltonen, and J. Niinimaki, "Biodegradation substances in wood protection," in *Sustainable use of Renewable Natural Resources - from Principles to Practices*.: University of Helsinki Department of Forest Ecology Publications, 2005, vol. 34.

[13] P. Verma, J. Dyckmans, and H. Militz, "Determination of fungal activity in modified wood by means of micro-calorimetry and determination of total esterase," *Applied Microbiology and Biotechnology*, vol. 80, pp. 125-133, 2008.

[14] Z.Y. Zhang et al., "Investigation into nanoclay enhanced coatings for brick moisture reduction and salt formation prevention," in *Protection of Historic Buildings - PROHITECH Conference*, Rome, 2009.

[15] E. Rirsch and Z.Y. Zhang, "Rising damp in masonry walls and the importance of mortar properties," *Construction and Building Materials*, vol. 24, pp. 1815-1820, 2010.

[16] Minglin Ma and Randal M. Hill, "Superhydrophobic surfaces," *Current Opinion in Colloid & Interface Science*, pp. 193-202, 2006.

[17] Louis Theodore, *Nanotechnology Basic Calculations for Engineers and Scientists*. New Jersey: John Wiley & Sons Inc., 2006.

[18] Franck Casse and Geoffrey W. Swain, "The development of microfouling on four commercial antifouling coatings under static and dynamic immersion," *International Biodeterioration & Biodegradation* , pp. 179-185, 2006.

[19] Ana Andres, Carmen Diaz, Alberto Coz, Jose Abellan, and Javier Viguri, "Physico-chemical characterisation of bricks all through the manufacture process in relation to efflorescence salts," *Journal of the European Ceramic Sociaty*, pp. 1869-1877, 2009.

[20] Paul Berdahl, Hashem Akbari, Ronnen Levinson, and William A. Miller, "Weathering of roofing materials - An overview," *Construction and Building Materials*, pp. 423-433, 2008.

[21] J. Ranogajec, S. Radosavljevic, R. Marinkovic-Neducin, and B. Zivanovic, "Chemical Corrosion Phenomena of Roofing Tiles," *Ceramics International*, pp. 99-103, 1997.

[22] Kiyohiko Ikeda, Hyung-Sun Kim, Koichi Kaizu, and Atsushi Higashi, "Influence of firing temperature on frost resistance of roofing tiles," *Journal of the European Ceramic Society*, pp. 3671-3677, 2004.

[23] K.M. Green, M.A. Carter, W.D. Hoff, and M.A. Wilson, "The effects of lime and admixtures on the water-retaining properties of cement mortars," *Cement and Concrete Research*, vol. 29, pp. 1743-1747, 1999.

[24] W. P.S. Dias, G. A.P.S.N. Seneviratne, and S. M.A. Nanayakkara, "Offshore sand for reinforced concrete," *Construction and Building Materials*, pp. 1377-1384, 2008.

[25] Guoxue Zhang, Jianxia Song, Jianxia Yang, and Xiyuan Liu, "Performance of mortar and concrete made with a fine aggregate of desert sand," *Building and Environment*, pp. 1478-1481, 2006.

[26] Jeffrey S. Schweitzer et al., "Nanoscale studies of cement chemistry with 15N resonance reaction analysis," *Nuclear Instruments and Methods in Physics Research*, pp. 441-445, 2005.

[27] Pierre-Claude Aitcin, "Cements of yesterday and today Concrete of tomorrow," *Cement and Concrete Research*, pp. 1349-1359, 2000.

[28] S. C. Kou and C. S. Poon, "Properties of self-compacting concrete prepared with recycled glass aggregate," *Cement & Concrete Composites*, pp. 107-113, 2009.

[29] Rafat Siddique, "Effect of fine aggregate replacement with Class F fly ash on the mechanical properties of concrete," *Cement and Concrete Research*, pp. 539-547, 2003.

[30] C. S. Poon, L. Lam, and Y. L. Wong, "A study on high strength concrete prepared with large volumes of low calcium fly ash," *Cement and Concrete Research*, pp. 447-455, 2000.

[31] Rafat Siddique, "Performance characteristics of high-volume Class F fly ash concrete," *Cement and Concrete Research*, pp. 487-493, 2004.

[32] Luc Schueremans, Dionys Van Gemert, and Sabine Giessler, "Chloride penetration in RC-structures in marine environment - Long term assessment of a preventive hydrophobic treatment," *Construction and Building Materials*, pp. 1238-1249, 2007.

[33] Dai Jian-Guo, Y. Akira, F. H. Wittmann, H. Yokota, and Peng Zhang, "Water repellent surface impregnation for extension of service life of reinforced concrete structures in marine environments: The role of cracks," *Cement & Concrete Composites* , pp. 101-109, 2010.

[34] J de Vries and R B Polder, "Hydrophobic Treatment of Concrete,"

Construction and Building Materials, pp. 259-265, 1997.

[35] M. I. Khan and C. J. Lynsdale, "Strength, permeability, and carbonation of high-performance concrete," *Cement and Concrete Research*, pp. 123-131, 2002.

[36] Ha-Won Song, Seung-Jun Kwon, Keun-Joo Byun, and Chan-Kyu Park, "Predicting carbonation in early-aged cracked concrete," *Cement and Concrete Research*, pp. 979-989, 2006.

[37] Aidan Walker, Lucinda Leech, Bill lincoln, and Jane Marshall, *The Encyclopedia of wood*. London: Quarto Publishing PLC, 2005.

[38] A. Walker, *The Encyclopaedia of Wood*. London: Quarto Publishing plc, 2005.

[39] Oliver Weigenand, miha Humar, Geoffrey Daniel, Holger Militz, and Carsten Mai, "Decay resistance of wood treated with amino - silicone compounds," *Holzforschung*, pp. 112-118, 2008.

[40] F. Cardias Williams and M. D. Hale, "The resistance of wood chemically modified with isocyanates: the role of moisture content in decay suppression," *International Biodeterioration & Biodegradation*, pp. 215-221, 2003.

[41] Jun Zhang, D. Pascal Kamden, and Ali Temiz, "Weathering of copper-amine treated wood," *Applied Surface Science*, pp. 842-846, 2009.

[42] Gil Goncalves, Paula A.A.P. Marques, Ricardo J.B. Pinto, Tito Trindade, and Carlos Pascoal Neto, "Surface modification of cellulosic fibres for multi-purpose TiO2 based nanocomposites," *composites Science and technology*, pp. 1051-1056, 2009.

[43] Francois de Buyl, "Silicone Sealants and Structural Adheasives," *International Journal of Adhesion & Adhesives*, pp. 411-422, 2001.

[44] P, et al. Somasundaran, "Silicone Emulsions," *Advances in Colloid and Interface Science*, pp. 103-109, 2006.

[45] R.R. leVier, M.C. Harrison, R.R. Cook, and T.H. Lane, "What is Silicone," *Journal of Clinical Epidemiology*, vol. 48, pp. 513-517, 1995.

[46] Mandla A. Tshabalala, Peter Kingshott, Mark R. VanLandingham, and David Plackett, "Surface Chemistry and Moisture Sorption Properties of Wood Coated with Multifunctional Alkoxysilanes by Sol-Gel Process," *Journal of Applied Polymer Science*, pp. 2828-2841, 2003.

[47] R.M. Hill, *Silicone Surfactants*, 10th ed. New York, USA: Marcel Dekker, 1999, vol. 86.

[48] D.F. Sweeney, *Silicone Hydrogels Continuous-Wear Contact Lenses*, 2nd ed. London, UK: Butterworth Heinemann, 2000.

[49] S.J. Clarson, J.J. Fitzgerald, M.J. Owen, S.S. Smith, and M.E. Van Dyke, *Science and Technology of Silicones and Silicone-Modified Materials*. Washington DC: American Chemistry Society, 2007.

[50] Gerald L. Witucki, "A Silane Primer: Chemistry and Applications of Alkoxy Silanes," *Journal of Coatings Technology*, pp. 57-60, 1993.

[51] C.A. Garcia-Gonzalez, J. Fraile, A. Lopez-Periago, and C. Domingo, "Preparation of silane-coated TiO2 nanoparticles in supercritical CO2," *Journal of Colloid and Interface Science*, vol. 338, pp. 491-499, 2009.

[52] Yon Ju-Nam and Jamie R. Lead, "Manufactured nanoparticles: An overview of their chemistry, interactions and potential environmental implications," *Science of the Total Environment*, pp. 396-414, 2008.

[53] C.E. Bygott, *Preparation and characterisation of nanoparticulate titanium dioxide for optimum UV shielding to enhanced the stability of polymers*. Manchester: The Manchester Metropolitan University, 2006.

[54] H. Schmidt, M. Naumann, T. S. Muller, and M. Akarsu, "Application of spray techniques for new photocatalytic gradient coatings on plastics," *Thin Solid Films*, pp. 132-137, 2006.

[55] Shu Song, Liqiang Jing, Shudan Li, Honggang Fu, and Yunbo Luan, "Superhydrophilic anatase TiO2 film with the micro- and nanometer-scale hieratchical surface structure," *Materials Letters*, pp. 3503-3505, 2008.

[56] J. Han, Y. Liu, N. Singhal, L. Wang, and W. Gao, "Comparative photocatalytic degradation of estrone in water by ZnO and TiO2 under artificial UVA and solar irradiation," *Chemical Engineering Journal*, vol. 213, pp. 150-162, 2012.

[57] C.P. Jacovides et al., "Solar global UV-B (280-315 nm) and UVA (315-380 nm) radiant fluxes and their relationships with broadband global radient flux at an eastern Mediterranean site," *Agricultural and Forest Meterology*, vol. 149, pp. 1188-1200, 2009.

[58] D.J. Turnbull, A.V. Parisi, and M.G. Kimlin, "Vitamin D effective ultraviolet wavelengths due to scattering in shade," *Journal of Steroid Biochemistry &*

Molecular Biology, vol. 96, pp. 431-436, 2005.

[59] R.H. Grant, G.M. Heisler, and W. Gao, "Photosynthetically-active radiation: sky radience distributions under clear and overcast conditions," *Agrecultural and Forest Meteorology*, vol. 82, pp. 267-292, 1996.

[60] M. Rashvand, Z. Ranjbar, and S. Rastegar, "Nano zinc oxide as a UV-stabilizer for aromatic polyurethane coatings," *Progress in Organic Coatings*, vol. 71, pp. 362-368, 2011.

[61] O. Carp, C.L. Huisman, and A. Reller, "Photoinduced reactivity of titanium dioxide," *Progress in Solid State Chemistry*, vol. 32, pp. 33-177, 2004.

[62] Charles Hegedus, Frank Pepe, Denise Lindenmuth, and Detlef Burgard, "Zinc Oxide Nanoparticle Dispersions as Unique Additives for Coatings," *Coatings Tech*, pp. 42-52, April 2008.

[63] H.K. Jeon, S. Nath Sarma, Y.J. Kim, and J.C. Ryu, "Toxicokinetics and metabolisms of benzophenone-type UV filters in rats," *Toxicology*, vol. 248, pp. 89-95, 2008.

[64] V. Bojinov and I. Grabchev, "Synthesis and properties of new adducts of 2,2,6,6-tetramethylpiperidine and 2-hydroxyphenylbenzotriazole as polymer photostabilizers," *Journal of Photochemistry and Photobiology*, vol. 150, pp. 223-231, 2002.

[65] S. Grelier, A. Castellan, and L. Podgorski, "Use of low molecular weight modified polystyrene to prevent photodegradation of clear softwoods for outdoor use," *Polymer Degradation and Stability*, vol. 92, pp. 1520-1527, 2007.

[66] C. Elif Cansoy, H. Yildirim Erbil, O. Akar, and T. Akin, "Effect of pattern size and geometry on the use of Cassie-Baxter equation for superhydrophobic surfaces," *Colloids and Surfaces A: Physicochemical and Engineering Aspects*, vol. 386, pp. 116-124, 2011.

[67] T. Watanabe et al., "Photocatalytic activity and photoinduced hydrophilicity of titanium dioxide coated glass," *Thin Solid Films*, vol. 351, pp. 260-263, 1999.

[68] A. Nakajima, S. Koizumi, T. Watanabe, and K. Hashimoto, "Effect of repeated photo-illumination on the wettability conversion of titanium dioxide," *Journal of Photochemistry and Photobiology A: Chemistry*, vol. 146, pp. 129-132, 2001.

[69] S. Madaeni, N. Ghaemi, A. Alizadeh, and M. Joshaghani, "Influence of Photo-induced superhydrophilicity of titanium dioxide nanoparticles on the anti-fouling performance of ultrafiltration membranes," *Applied Surface Science*, vol. 257, pp. 6175-6180, 2011.

[70] E. Bormashenko, "General equation describing wetting of rough surfaces," *Journal of Colloid and Interface Science*, vol. 360, pp. 317-319, 2011.

[71] Doyoung Byun et al., "Wetting Characteristics of Insect Wing Surfaces," *Journal of Bionic Engineering*, pp. 63-70, 2009.

[72] K. Kurogi, H. Yan, and K. Tsujii, "Importance of pinning effect of wetting in super water-repellent surfaces," *Colloids and Surfaces A: Physicochemical Engineering Aspects*, vol. 317, pp. 592-597, 2008.

[73] Ken Yamamoto and Satoshi Ogata, "3-D thermodynamic analysis of superhydrophobic surfaces," *Journal of Colloid and Interface Science*, pp. 471-477, 2008.

[74] Nan Gao and Yuying Yan, "Modeling Superhydrophobic Contact Angles and Wetting Transition," *Journal of Bionic Engineering*, pp. 335-340, 2009.

[75] Zhiqing Yuan et al., "Facile method to prepare stable superhydrophobic Co3O4 surface," *Applied Surface Science*, pp. 9493-9497, 2009.

[76] D. K. Sarkar and N. Saleema, "One-step fabrication process of superhydrophobic green coatings," *Surface & Coatings Technology*, p. Article in Press, 2010.

[77] Xingfu Zhou, Xuefeng Guo, Weiping Ding, and Yi Chen, "Superhydrophobic or superhydrophilic surfaces regulated by micro-nano structured ZnO powders," *Applied Surface Science*, pp. 3371-3374, 2008.

[78] On-Uma Nimittrakoolchai and Sitthisuntorn Supothina, "Deposition of organic-based superhydrophobic films for anti-adhesion and self-cleaning applications," *Journal of the European Ceramic Sociaty*, pp. 947-952, 2008.

[79] Zeshan Hu, Xiaoyan Zen, Jian Gong, and Yulin Deng, "Water resistance improvement of paper by superhydrophobic modification with microsized CaCO3 and fatty acid," *Colloids and Surfaces A: Physicochemical and Engineering Aspects*, pp. 65-70, 2009.

[80] Bi Xu, Zaisheng Cai, Weiming Wang, and Fengyan Ge, "Preparation of superhydrophobic cotton fabrics based on SiO2 nanoparticles and ZnO nanorod arrays with subsequent hydrophobic modification," *Surface &*

Coatings Technology, pp. 1556-1561, 2010.

[81] Z. J. Wei, W. L. Lui, D. Tain, C. L. Xiao, and X. Q. Wang, "Preparation of lotus-like superhydrophobic fluoropolymer films," *Applied Surface Science*, p. Artical in press, 2010.

[82] R. V. Lakshmi and Bharathibai J. Basu, "Fabrication of superhydrophobic sol-gel composite films using hydrophobically modified colloidal zinc hydroxide," *Journal of Colloid and Interface Science*, pp. 454-460, 2009.

[83] E. Rirsch and Z. Zhang, "Rising damp in masonry walls and the importance of mortar properties," *Construction and Building Materials*, vol. 24, pp. 1815-1820, 2010.

[84] C. Hall and W.D. Hoff, "Rising damp: capillary rise dynamics in walls," *Proceedings of the Royal Society A*, vol. 463, pp. 1871-1884, 2007.

[85] M.A. Shirakawa, I.B. Beech, R. Tapper, M.A. Cincotto, and W. Gambale, "The development of a method to evaluate bioreceptivity of indoor mortar plastering to fungal growth," *International Biodeterioration & Biodegradation*, vol. 51, pp. 83-92, 2003.

[86] P.S. Burge, "Sick Building Syndrome," *Occupational and environmental medicine*, vol. 61, pp. 185-190, 2004.

[87] J.L. Leyten and S.R. Kurvers, "Robustness of buildings and HVAC systems as a hypothetical construct explaining differences in building related health and comfort symptoms and complaint rates," *Energy and Buildings*, vol. 38, pp. 701-707, 2006.

[88] B. Crook and N.C. Burton, "Indoor moulds, Sick Building Syndrome and building related illness," *Fungal Biology Reviews*, vol. 24, pp. 106-113, 2010.

[89] B. Painter, N. Brown, and M.J. Cook, "Practical application of a sensor overlay system for building monitoring and commissioning," *Energy and Buildings*, vol. 48, pp. 29-39, 2012.

[90] A. Webster and E. May, "Bioremediation of weathered-building stone surfaces," *TRENDS in Biotechnology*, vol. 24, pp. 255-260, 2006.

[91] F. Frossel, *Masonry drying and cellar rehabilitation*. Munich, Verlag Fraunhofer: IRB, 2007.

[92] M. Tretiach, S. Bertuzzi, and O. Salvadori, "Chlorophyll a fluorescence as a practical tool for checking the effects of biocide treatments on endolithic

lichens," *International Biodeterioration & Biodegradation*, vol. 64, pp. 452-460, 2010.

[93] M. Grube and G. Berg, "Microbial consortia of bacteria and fungi with focus on the lichen symbiosis," *Fungal Biology Reviews*, vol. 23, pp. 72-85, 2009.

[94] G. Escadeillas, A. Bertron, E. Ringot, P.J. Blanc, and A. Dubosc, "Accelerated testing of biological stain growth on external concrete walls. Part 2: Quantification of growths," *Materials and Structures*, vol. 42, pp. 937-945, 2009.

[95] P.H. Raven, R.F. Evert, and S.E. Eichhorn, *Biology of Plants*, 7th ed. New York: W.H. Freeman and Company, 2005.

[96] R.W.S. Weber, "Vacuoles and the fungal lifestyle," *Mycologist*, vol. 16, pp. 10-20, 2002.

[97] S.K. Walker, K. Chitcholtan, Y. Yu, G.M. Christenhusz, and A. Garrill, "Invasive hyphal growth: An F-actin depleted zone is associated with invasive hyphae of the oomycetes Achlya bisexualis and Phytophthora cinnamomi," *Fungal Genetics and Biology*, vol. 43, pp. 357-365, 2006.

[98] P. Baldrian, "Interactions of heavy metals with white-rot fungi," *Enzyme and Microbial Technology*, vol. 32, pp. 78-91, 2003.

[99] J. Karys and J. Wazny, "Wood dry-rot fungi as biodegradation factors of porous building materials," *Folia Forestalia Polonica*, vol. 38, pp. 33-40, 2007.

[100] M. Jorday, *The Encyclopaedia of Fungi of Britain and Europe*. London: Frances Lincoln Ltd, 2004.

[101] H.L. Brown, A. Bruce, and H.J. Staines, "Assessment of the biocontrol potentual of a Trichoderma viride isolate Part II: Protection against soft rot and basidiomycete decay," *International Biodeterioration & Biodegradation*, vol. 44, pp. 225-231, 1999.

[102] I. Mohammed-Ziegler, I. Tanczos, Z. Horvolgyi, and B. Agoston, "Water-repellent acylated and silylated wood samples and their surface analytical characterisation," *Colloids and Surfaces A: Physicochemical Engineering*, vol. 319, pp. 204-212, 2008.

[103] D. Panov and N. Terziev, "Study on some alkoxysilanes used for hydrophobation and protection of wood against decay," *International Biodeterioration & Biodegradation*, vol. 63, pp. 456-461, 2009.

[104] C. Hsieh, B. Chang, and J. Lin, "Improvement of water and oil repellency on wood substrates by using fluorinated silica nanocoating," *Applied Surface Science*, vol. 257, pp. 7997-8002, 2011.

[105] H. Barberousse, B. Ruot, C. Yepremian, and G. Boulon, "An assessment of facade coatings against colonisation by arial algae and cyanobacteria," *Building and Environment*, vol. 42, pp. 2555-2561, 2007.

[106] J. Marijnissen and L. Gradon, *Nanoparticles in Medicine and Environment; Inhalation and Health Effects*. London: Springer, 2010.

[107] M. Lippmann, *Environmental Toxicants; human exposures and their health effects*. New Jersey: John Wiley & Sons Inc., 2009.

[108] European Council, Directive 98/8/EC; concerning the placing of biocidal proudcts on the market, Feb. 16, 1998.

[109] N. Serpone, D. Dondi, and A. Albini, "Inorganic and organic UV filters: Their role and efficacy in sunscreens and suncare products," *Inorganica Chemica Acta*, pp. 794-802, 2007.

[110] Urs A. Boelsterli, *Mechanistic Toxicology*. New York: Taylor & Francis, 2003.

[111] Steven D. Garber, *Biology*. New Jersey: John Wiley & Sons Inc., 2002.

[112] Andre Goffeau, "The fight against fungi," *Nature*, pp. 541-542, 2008.

[113] Robert A. Goyer, Curtis D. Klaassen, and Michael P. Waalkes, *Metal Toxicology*. San Diego: Academic Press Inc., 1995.

[114] M.D. Newman, M. Stotland, and J.I. Ellis, "The safety of nanosized particles in titanium dioxide - and zinc oxide-based sunscreen," *Journal of the American Academy of Dermatology*, vol. 61, pp. 685-92, 2009.

[115] A. Fairbrother and J.R. Fairbrother, "Are environmental regulations keeping up with innovation? A case study of the nanotechnology industry," *Ecotoxicology and Environmental Safety*, vol. 72, pp. 1327-1330, 2009.

[116] European Union, "Regulation (EC) No 1907/2006 of the European Parliament and of the Council concerning the Registration, Evaluation, Authorisation and Restriction of Chemicals (REACH)," Obligatory, European Directive (EC) 1907/2006, 2006.

[117] A. Fairbrother and J.R. Fairbrother, "Are environmental regulations keeping up with innovation? A case study of the nanotechnology industry,"

Ecotoxicology and Environmental Safety, vol. 72, pp. 1327-1330, 2009.

[118] University of Portsmouth. (2010, January) University of Portsmouth. [Online]. http://www.port.ac.uk/aboutus/newsandevents/frontpagenews/title,106658,en.html

[119] L. Perez-Lombard, J. Ortiz, J.F. Coronel, and I.R. Maestre, "A review of HVAC systems requirements in building energy regulations," *Energy and Buildings*, vol. 43, pp. 255-268, 2011.

[120] P. Becher, *Emulsions: theory and Practice*. New York: Reinhold, 1959.

[121] G. S. Banker, *Modern Pharmaceutics*. New York: Informa Healthcare, 2007.

[122] T. Tadros, *Surfactants*. London: Academic Press, 1984.

[123] C. Solans, P. Izquierdo, J. Nolla, N. Azemar, and M.J. Garcia-Celma, "Nano-emulsions," *Current Opinion in Colloid & Interface Science*, vol. 10, pp. 102-110, 2005.

[124] W. Ramsden, "Separation of solids in the surface-layers of solutions and suspensions (observations on surface-membranes, bubbles, emulsions, and mechanical coagulation) - Primary account," *Proceedings of the Royal Society of London*, vol. 72, pp. 156-164, 1903.

[125] S.U. Pickering, "Emulsions," *Journal of the Chemical Society*, vol. 91, pp. 2001-2021, 1907.

[126] T.N. Hunter, R.J. Pugh, G.V. Franks, and G.J. Jameson, "The role of particles in stabilising foams and emulsions," *Advances in Colloid and Interface Science*, vol. 137, pp. 57-81, 2008.

[127] H. Huang, B. You, S. Zhou, and L. Wu, "Rheological behaviour of aquous organosilicone resin emulsion stabilised by colloidal nanosilica particles," *Journal of Colloid and Interface Science*, vol. 310, pp. 121-127, 2007.

[128] N.G. Eskandar, S. Simovic, and C.A. Prestide, "Interactions of hydrophilic silica nanoparticles and classical surfactants at non-polar oil-water interface," *Journal of Colloid and Interface Science*, vol. 358, pp. 217-225, 2011.

[129] S. Simovic and C.A. Prestidge, "Hydrophilic silica nanoparticles at the PDMS droplet-water interface," *Langmuir*, vol. 19, pp. 3785-3792, 2003.

[130] I. Hussain, H. Zhang, M. Brust, J. Barauskas, and A.I. Cooper, "Emulsions-directed assembly of gold nanoparticles to molecularly-linked and size-controlled spherical aggregates," *Journal of Interface Science*, vol. 350, pp.

368-372, 2010.

[131] A. Kawazoe and M. Kawaguchi, "Characterisation of silicone oil emulsions stabilised by TiO2 suspensions," *Colloids and Surfaces A*, vol. 392, pp. 283-287, 2011.

[132] C. Morishita and M. Kawaguchi, "Rheological and interfacial properties of Pickering emulsions prepared by fumed silica suspensions pre-adsorbed poly-(N-isopropylacrylamide)," *Colloids and Surfaces A*, vol. 335, pp. 138-143, 2009.

[133] G.M. Eccleston, "Functions of mixed emulsifiers and emulsifying waxes in dermatological lotions and creams," *Colloids and Surfaces A: Physicochemical and Engineering Aspects*, vol. 123-124, pp. 169-182, 1997.

[134] D.R. Karsa, *Surfactants in Polymer, Coatings, Inks and Adheasives*. Oxford: Blackwell Publishing, 2003.

[135] R. H. Ottewill, "Introduction," in *Surfactants*. London: Academic Press Inc. Ltd, 1984, pp. 1-18.

[136] J. T.G. Overbeek, "Microemulsions," in *Surfactants*. London: Academic Press Inc., 1984, pp. 111-132.

[137] Kathleen, et al., Barnes, 10/559525, 2004.

[138] B. Midmore, "Synergy between silica and polyoxyethylene surfactants in the formation of O/W emulsions," *Colloids and Surfaces A: Physicochemical and Engineering Aspects*, vol. 145, pp. 133-143, 1998.

[139] W. Im-Emsap and J. Siepmann, "Disperse Systems," in *Modern Pharmaceutics*. New York: Informa Healthcare, 2007, pp. 237-285.

[140] A. Wade, *Pharmaceutical Handbook*. London: The Pharmaceutical Press, 1980.

[141] G. M. Eccleston, "Emulsions and Microemulsions," in *Encyclopedia of Pharmaceutical Technology*. New York: Marcel Dekker Inc., 2002, pp. 1066-1085.

[142] N.H. Tkachenko, Z.M. Yaremko, C. Bellmann, and M.M. Soltys, "The influence of ionic and nonionic surfactants on aggregative stability and electrical surface properties of aqueous suspensions of titanium dioxide," *Journal of Colloid and Interface Science* , vol. 299, pp. 686-695, 2006.

[143] S. Kubowicz et al., "Mixed-Monolayer-Protected Gold Nanoparticles for Emulsion Stabilisation," *Langmuir*, vol. 26, pp. 1642-1648, 2010.

[144] N.H. Tkachenko, Z.M. Yaremko, and C. Bellmann, "Effect of 1-1-charged ions on aggregative stability and electrical surface properties of aqueous suspensions of titanium dioxide," *Colloids and Surfaces A: Physicochemical Engineering Aspects*, vol. 279, pp. 10-19, 2006.

[145] N.H. Tkachenko, Z.M. Yaremko, C. Bellmann, and M.M. Soltys, "Influence of poly(methacrylic acid) on aggregative stability and electrical surface properties of aqueous suspensions of titanium dioxide," *Colloids and Surfaces A: Physicochemical Engineering Aspects*, vol. 279, pp. 149-158, 2006.

[146] V. Duecoffre, W. Diener, C. Flosbach, and W. Schubert, "Emulsifiers with high chemical resistance: a key to high performance waterborne coatings," *Progress in Organic Coatings*, vol. 34, pp. 133-143, 1998.

[147] F. Leal-Calderon and V. Schmitt, "Soild-stabilised emulsions," *Current Opinion in Colloid & Interface Science*, vol. 13, pp. 217-227, 2008.

[148] J. Zhou, L. Wang, X. Qiao, B. Binks, and K. Sun, "Pickering emulsions stabilised by surface-modified Fe3O4 nanoparticles," *Journal of Colloid and Interface Science*, vol. 367, pp. 213-224, 2012.

[149] D.J. Adams, S. Adams, J. Melrose, and A.C. Weaver, "Influence of particle surface roughness on the behaviour of Janus particles at interfaces," *Colloids and surfaces A: Physicochem. Eng. Aspects*, vol. 317, pp. 360-365, 2008.

[150] C. Vashisth, C.P. Whitby, D. Fornasiero, and J. Ralston, "Interfacial displacement of nanoparticles by surfactant molecules in emulsions," *Journal of Colloid and Interface Science*, vol. 349, pp. 537-543, 2010.

[151] J. MacMullen et al., "Titanium dioxide and zinc oxide nano-particulate enhanced oil-in-water (O/W) facade emulsions for improved masonry thermal insulation and protection," *Energy and Buildings*, vol. 52, pp. 86-92, 2012.

[152] British Standards International, BS EN 771-1, Specification for Masonry Units - Part 1: Clay Masonry Units, 2003.

[153] Y. Jin, H. Zhang, Y. Yin, and K. Nishinari, "Comparison of curdlan and its carboxymethylated derivative by means of rheology, DSC, and AFM," *Carbohydrate Research*, vol. 341, pp. 90-99, 2006.

[154] L. Krishnamurthy, E. Weigert, N. Wagner, and D. Boris, "The shear viscosity of polyampholyte (gelatin) stabilized colloidal dispersions," *Journal of*

Colloid and Interface Science, vol. 280, pp. 264-275.

[155] P.A. Webb. (2001, January) An introduction to the physical characterisation of materials by mercury intrusion porosimetry with emphasis on reduction and presentation of experimental data.

[156] D.D. Do, D.H. Do, and D.A. Nicholson, "A computer study of BET theory, BET surface area and the calculation of surface excess for gas adsorption on a graphite surface," *Chemical Engineering Science*, vol. 65, pp. 3331-3340, 2010.

[157] I. Ioannou, W.D. Hoff, and C. Hall, "On the role of organic adlayers in the anomalous water sorptivity of Lepine limestone," *Journal of Colloid and Interface Science*, vol. 279, pp. 228-234, 2004.

[158] British Standards International, BS EN 828: 1998; Adheasives - Wettability - Determination by measurement of contact angle and critical surface tension of solid surface, 1998.

[159] F. Awaja, M. Gilbert, G. Kelly, B. Fox, and P. J. Pigram, "Adheasion of polymers," *Progress in Polymer Science*, vol. 34, pp. 948-968.

[160] E. Hernandez-Baltazar and J. Garcia-Fadrique, "Elliptic solution to the Young-Laplace differential equation," *Journal of Colloid and Interface Science*, vol. 287, pp. 213-216, 2005.

[161] L. Ferri, P. P. Lottici, A. Lorenzi, A. Montenero, and E. Salvioli-Mariani, "Study of silica nanoparticles - polysiloxane hydrophobic treatments for stone-based monument protection," *Journal of Cultural Heritage*, vol. 12, pp. 356-363, 2011.

[162] E.A. Adam and P.J. Jones, "thermophysical Properies of Stabilised Soil Building Blocks," *Building and Environment*, vol. 30, pp. 245-253, 1995.

[163] P.G. Down, *Heating and Cooling Load Calculation*. Oxford: Pergamon Press, 1969.

[164] M.G. Davies, *Building Heat Transfer*. Chichester: John Wiley & Sons Ltd, 2004.

[165] P.E. Vaughn Bradshaw, *the Building Environment: Active and Passive Control Systems*, 3rd ed. New Jersey: John Wiley & Sons Inc.

[166] M. Zukowski and G. Haese, "Experimental and numerical investigation of a hollow brick filled with perlite insulation," *Energy and Buildings*, vol. 42, pp.

1402-1408, 2010.

[167] British Standards International, BS ISO 27448 Fine ceramics, advanced technical ceramics) - Test method for self-cleaning performance of semiconducting photocatalytic materials - Measurement of water contact angle, 2009.

[168] D.J. Giannantonio, J.C. Kurth, K.E. Kurtis, and P.A. Sobecky, "Effects on concrete properties and nutrients on fungal colonisation and fouling," *International Biodeterioration & Biodegradation*, vol. 63, pp. 252-259, 2009.

[169] O. Guillitte and R. Dreesen, "Laboratory chamber studies and petrographical analysis as bioreceptivity assessment tools of building materials," *The Science of the Total Environment*, vol. 167, pp. 365-374, 1995.

[170] A. Dubosc, G. Escadeillas, and P.J. Blanc, "Characterisation of biological stains on external concrete walls and influence of concrete as underlying material," *Cement and Concrete Research*, vol. 31, pp. 1613-1617, 2001.

[171] W.D. Muynck, A.M. Ramirez, N.D. Belie, and W. Verstraete, "Evaluation of strategies to prevent algal fouling on white architectural and cellular concrete," *International Biodeterioration & Biodegradation*, vol. 63, pp. 679-689, 2009.

[172] T.H. Tran et al., "Influence of the intrinsic characteristics of mortars on biofouling by Klebsormidium Flaccidum," *International Biodeterioration & Biodegradation*, vol. 70, pp. 31-39, 2012.

[173] H. Belcher and E. Swale, *A Beginner's Guide to Freshwater Algae*. London: HMSO.

[174] J.S. Nambam and J. Philip, "Competitive adsorption of polymer and surfactant at a liquid droplet interface and its effect on flocculation of emulsion," *Journal of Colloid and Interface Science*, vol. 366, pp. 88-95, 2012.

[175] G. Petzold, M. Mende, and N. Kochurova, "Polymer-surfactant complexes as flocculants," *Colloids and Surfaces A: Physicochemical Engineering Aspects*, vol. 298, pp. 139-144, 2007.

[176] Y. Xie, C. Hill, Z. Xaio, H. Militz, and C. Mai, "Silane coupling agents used for natural fiber/polymer composites: A review," *Composites: Part A*, vol. 41, pp. 806-819, 2010.

[177] R. Pal, "Shear viscosity behaviour of emulsions of two immiscible liquids," *Journal of Colloid and Interface Science*, vol. 225, pp. 359-366, 2000.

[178] K.L. Mittal and P. Kumar, *Emulsions, foams, and thin films*. New York: Marcel Dekker Inc., 2000.

[179] Y. Saiki, C. Prestidge, R. Horn, and C.A. Prestidge, "Effects of droplet deformability on emulsion rheology," *Colliods and Surfaces A: Physiochem. Eng. Aspects*, vol. 299, pp. 65-72, 2007.

[180] Z. Zhao, W. Liu, Liu Z., P. Ding, and H. Li, "Phase inversion of TiO2 nanoparticle stabilised emulsions of alkenyl succinic anhydride," *Chemical Engineering Science*, vol. 87, pp. 246-257, 2013.

[181] Z. Darvishi and A. Morsali, "Synthesis and characterisation of nano-bentonite by sonochemical method," *Ultrasonic Sonochemistry*, vol. 18, pp. 238-242, 2011.

[182] C. Housecroft and E. Constable, *Chemistry*, 3rd ed. Harlow, UK: Pearson Education Limited, 2006.

[183] B. Gilbert, R.K. Ono, K.A. Ching, and C.S. Kim, "The effects of nanoparticle aggregation processes on aggregate structure and metal uptake," *Journal of Colloid and Interface Science*, vol. 339, pp. 285-295, 2009.

[184] U. Diebold, "The surface science of titanium dioxide," *Surface Science Reports*, vol. 48, pp. 53-229, 2003.

[185] N. Shortt and J. Rugkasa, ""The walls were so damp and cold" fuel poverty and ill health in Northern Ireland: Results from a housing intervention," *Health & Practice*, vol. 13, pp. 99-110, 2007.

[186] N. Djongyang, R. Tchinda, and D. Njomo, "A study of coupled heat and mass transfer across a porous building component in intertropical conditions," *Energy and Buildings*, vol. 41, pp. 461-469, 2009.

[187] Met Office. (2011) Met Office. [Online]. http://www.metoffice.gov.uk/climate/uk/2011/annual.html

[188] The National Academies. The National Academies. [Online]. http://www.nap/reports/energy/sources.html

[189] O. Guillitte, "Bioreceptivity: a new concept for building ecology studies," *The Science of the Total Environment*, vol. 167, pp. 215-220, 1995.

[190] C.C. Gaylarde and P.M. Gaylarde, "A comparative study of the major microbial biomass of biofilms on exteriors of buildings in Europe and Latin America," *International Biodeterioration & Biodegradation*, vol. 55, pp. 131-

139, 2005.

[191] A.Z. Miller et al., "Bioreceptivity of building stones: A review," *Science of Total Environment*, 2012.

[192] M.A. Shirakawa, I.B. Beech, R. Tapper, M.A. Cincotto, and W. Gambale, "The development of a method to evaluate bioreceptivity of indoor mortar plastering to fungal growth," *International Biodeterioration & Biodegradation*, vol. 51, pp. 83-92, 2003.

[193] V. Wiktor et al., "Accelerated laboratory test to study fungal biodeterioration," *International Biodeterioration & Biodegradation*, vol. 63, pp. 1061-1065, 2009.

[194] U. Diebold, "The surface science of titanium dioxide," *Surface Science Reports*, vol. 48, pp. 53-229, 2003.

[195] S. Baruah and J. Dutta, "Hydrothermal growth of ZnO nanostructures," *Science and Technology of Advanced Materials*, vol. 10, pp. 1-18, 2009.

[196] UK Government. (2013, Feburary) Planning Portal. [Online]. http://www.planningportal.gov.uk

[197] D. Wu and M. Long, "Enhanced visible-light activity of the self-cleaning TiO2-coated coated cotton fabrics by loading Agl particles," *Surface & Coatings Technology*, vol. 206, pp. 1175-1179, 2011.

[198] K. Qi, B. Fei, and J.H. Xin, "Visible light-active iron-doped anatase nanocrystallites and their self-cleaning property," *Thin Solid Films*, vol. 519, pp. 2438-2444, 2011.

[199] Q. Xu et al., "Transparent visible light activated C-N-F-codoped TiO2 films for self-cleaning applications," *Journal of Photochemistry and Photobiology A: Chemistry*, vol. 210, pp. 181-187, 2010.

[200] O. Schalm, K. Janssens, and J. Caen, "Characterisation of the main causes of deterioration of grisaille paint layers in 19th century stained-glass windows by J.-B. Capronnier," *Spectrochimica Acta Part B*, pp. 589-607, 2003.

[201] A. Stuke, H. Behrens, B.C. Schmidt, and R. Dupree, "H2O speciation in float glass and soda lime silica glass," *Chemical Geography*, pp. 64-77, 2006.

[202] Cheng-Kuang Chen and I-Ming Chu, "Effect of hydrogen bonding on the glass transition behavior of poly(acrylic acid)/silica hybrid materials prepared by sol-gel process," *Polymer*, pp. 6089-6093, 2001.

[203] S. C. See, Z. Y. Zhang, and M. O.W. Richardson, "A study of water absorption characteristics of a novel nano-gelcoat for marine application," *Progress in Organic Coatings*, pp. 169-174, 2009.

[204] European Council Directive, "Council Directive (EC) 98/8EC of 16th Febuary 1998 Concerning the Placing of Biocidal Products on the Market," 1998.

[205] T. J. Pinnavaia and G. W. Beall,.: John Wiley & Sons Ltd, 2000, p. 224.

[206] Mark Clarey, 6,050,509, 2000.

[207] Z. Wang, J. Massam, and T. J. Pinnavaia, "Epoxy-Clay Nanocomposites," in *Polymer-Clay Nanocomposites*.: John Wiley & Sons Ltd, 2000, pp. 129-131.

[208] Danqing Zhu and Wim J. Ooij, "Corrosion protection of metals by water-based silane mixtures of bis-[trimethoxysilylpropyl]amine and vinyltriacetoxysilane," *Progress in Organic Coatings*, pp. 42-53, 2004.

[209] Rafat Siddique and Albert Noumowe, "Utilization of spent foundry sand in controlled low-strength materials and concrete," *Resources Conservation and Recycling*, pp. 27-35, 2008.

[210] A. N. Khramov, V. N. Balbyshev, L. S. Kasten, and R. A. Mantz, "Sol-gel coatings with phosphonate functionalities for surface modification of magnesium alloys," *Thin Solid Films*, pp. 174-181, 2006.

[211] S. Gunasekaran and G. Anbalagan, "Spectroscopic characterisation of natural calcite minerals," *Spectrochimica Acta Part A*, pp. 656-664, 2007.

[212] David E. Searle and David J. Mitchell, "The effect of coal and diesel particulates on the weathering loss of Portland Limestone in an urban environment," *Science of the Total Environment*, pp. 207-223, 2006.

[213] Z. Agioutantis and S. Maurigiannakis, "Evaluation of silicon-based strengthening agents of porous limestones," *Progress in Organic Coatings* , pp. 140-148, 2006.

[214] P. Maravelaki-Kalaitzaki, N. Kallithrakas-Kontos, Z. Agioutantis, S. Maurigiannakis, and D. Korakaki, "A comparative study of porous limestones treated with silicon-based strenghtening agents," *Progress in Organic Coatings*, pp. 49-60, 2008.

[215] Antonia Moropoulou, Asterios Bakolas, and Eleni Aggelakopoulou, "The effects of limestone characteristics and calcination temperature to reactivity of the quicklime," *Cement and Concrete Research*, pp. 633-639, 2001.

[216] B. Doherty et al., "Efficiency and resistance of the artificial oxalate protection treatment on marble against chemical weathering," *Applied Surface Science*, pp. 4477-4484, 2007.

[217] K. Malaga-Starzec, U. Akesson, J. E. Lindqvist, and B. Schouenborg, "Microscopic and macroscopic characterization of the porosity of marble as a function of temperature and impregnation," *Construction and Building Materials*, pp. 939-947, 2006.

[218] Liesbeth De Vetter, Marc Stevens, and Joris Van Acker, "fungal decay resistance and durability of organosilicon - treated wood," *International Biodeterioration & Biodegradation*, pp. 130-134, 2009.

[219] Hongta Yang and Yulin Deng, "Preparation and physical properties of superhydrophobic papers," *Journal of Colloid and Interface Science*, pp. 588-593, 2008.

[220] Walter D'Alessandro, Salvatore Giammanco, Sergio Bellomo, and Francesco Parello, "Geochemistry and mineralogy of travertine deposites of the SW flank of Mt. Etna (Italy): relationships with past volcanic and degassing activity," *Journal of Volcanology and Geothermal Research*, pp. 64-70, 2007.

[221] S. L. Shvartsev, O. E. Lepokurova, and Yu. G. Kopylova, "Geochemical mechanisms of travertine formation from fresh waters in southern Siberia," *Russian Geography and Geophysics*, pp. 659-667, 2007.

[222] Allan Pentecost, "Geochemistry of carbon dioxide in six travertine - depositing waters of Italy," *Journal of Hydrology*, pp. 263-278, 1995.

[223] G. L. Witucki, "A Silane Primer: Chemistry and Applications of Alkoxy Silane," *Journal of Coatings Technology*, pp. 57-60, 1993.

[224] Shyamal C. Ghosh, Holger Militz, and Carsten Mai, "Decay resistance of treated wood with functionalised commercial silicones," *BioResources*, pp. 1303-1314, 2008.

[225] S. N. Kartal, F. Green III, and C. A. Clausen, "Do the unique properties of nanomaterials affect leachability or efficacy against fungi and termites," *International Biodererioration & Biodegradation*, pp. 490-495, 2009.

[226] Yaohui Lv et al., "Silver nanoparticle-decorated porous ceramic composite for water treatment," *Journal of Membrane Science*, pp. 50-56, 2009.

[227] Elisabete Almeida, Teresa C. Diamantino, and Orlando de Sousa, "Marine paints: The particular case of antifouling paints," *Progress in Organic*

Coatings, pp. 2-20, 2007.

[228] Fabienne Fay, Isabelle Linossier, Jean Jacques Peron, Valerie Langlois, and Karine Vallee-Rehel, "Antifouling activity of marine paints: Study of erosion," *Progress in Organic Coatings*, pp. 194-206, 2007.

[229] Wei Bai, Kongshuang Zhao, and Koji Asami, "Effects of copper on dielectric properties of E.coli cells," *Colloids and Surfaces B: Biointerfaces*, pp. 105-115, 2007.

[230] Ki-Young Yoon, Jeong Hoon Byeon, Jae-Hong park, and Jungho Hwang, "Susceptibility constants of Escherichia coli and Bacillus subtilis to silver and copper nanoparticles," *Science of the Total environment*, pp. 572-575, 2007.

[231] Russell E. Lewis. Doctor Fungus. [Online]. http://www.doctorfungus.org/thedrugs/antif_pharm.htm

[232] Acu-Cell Nutrition. [Online]. http://www.acu-cell.com/crcu.html

[233] World Health Organisation. World Health Organisation. [Online]. http://www.who.int/water_sanitation_health/dwq/chemicals/copper.pdf

[234] L. Theodore, *Nanotechnology basic calculations for engineers and scientists*. New Jersey: John Wiley & Sons Inc., 2006.

[235] K.A.D. Guzman, M.P. Finnegan, and J.F. Banfield, "Influence of surface potentual on aggregation and transport of titania nanoparticles," *Environmental Science & Technology*, vol. 40, pp. 7688-7693, 2006.

[236] N.S. Allen et al., "Factors affecting the interfacial adsorption of stabilsers on to titanium dioxide particles (flow microcalorimetry, modelling, oxidation and FTIR studies): Nano versus pigmentary grades," *Dyes and Pigments*, vol. 70, pp. 192-203, 2006.

[237] E. Bormashenko, "Why does the Cassie-Baxter equation apply?," *Colloids and Surfaces A: Physicochemical and Engineering Aspects*, vol. 324, pp. 47-50, 2008.

[238] F. Aloui et al., "Inorganic UV absorbers for the photostabilisation of wood-clearcoating systems: Comparison with organic UV absorbers," *Applied Surface Science*, vol. 253, pp. 3737-3745, 2007.

Appendices

Appendix A: Pilot Study - Volume Fraction Testing

Table 32: Initial volume fraction test overview *(to be used in conjunction with Table 33)*

Test Name	Oil Percentage (wt%)	Surf A + B Ratio
A1	n-octyltriethoxysilane 9	A70/30B
A2	n-octyltriethoxysilane 19	A70/30B
A3	n-octyltriethoxysilane 29	A70/30B
A4	n-octyltriethoxysilane 39	A70/30B
A5	n-octyltriethoxysilane 49	A70/30B
A6	n-octyltriethoxysilane 59	A70/30B
A7	n-octyltriethoxysilane 69	A70/30B
A8	n-octyltriethoxysilane 79	A70/30B
A9	n-octyltriethoxysilane 89	A70/30B
A10	Isooctyltriethoxysilane 9	A70/30B
A11	Isooctyltriethoxysilane 19	A70/30B
A12	Isooctyltriethoxysilane 29	A70/30B
A13	Isooctyltriethoxysilane 39	A70/30B
A14	Isooctyltriethoxysilane 49	A70/30B
A15	Isooctyltriethoxysilane 59	A70/30B
A16	Isooctyltriethoxysilane 69	A70/30B
A17	Isooctyltriethoxysilane 79	A70/30B
A18	Isooctyltriethoxysilane 89	A70/30B

Table 33: Emulsion composition for initial volume fraction test

A1	Phase	Mass for 100g (g)	Volume For 100g (ml)
A10	Oil	9	9.0
	Water	89	89.0
	Surf A	1.4	1.4
	Surf B	0.6	0.7
	Total	100	100.1
A2	**Phase**	**Mass for 100g (g)**	**Volume For 100g (ml)**
A11	Oil	19	19.0
	Water	79	79.0
	Surf A	1.4	1.4
	Surf B	0.6	0.7
	Total	100	100.1
A3	**Phase**	**Mass for 100g (g)**	**Volume For 100g (ml)**
A12	Oil	29	29.0
	Water	69	69.0
	Surf A	1.4	1.4
	Surf B	0.6	0.7
	Total	100	100.1

A4	**Phase**	**Mass for 100g (g)**	**Volume For 100g (ml)**
A13	Oil	39	39.0
	Water	59	59.0
	Surf A	1.4	1.4
	Surf B	0.6	0.7
	Total	100	100.1
A5	**Phase**	**Mass for 100g (g)**	**Volume For 100g (ml)**
A14	Oil	49	49.0
	Water	49	49.0
	Surf A	1.4	1.4
	Surf B	0.6	0.7
	Total	100	100.1
A6	**Phase**	**Mass for 100g (g)**	**Volume For 100g (ml)**
A15	Oil	59	59.0
	Water	39	39.0
	Surf A	1.4	1.4
	Surf B	0.6	0.7
	Total	100	100.1
A7	**Phase**	**Mass for 100g (g)**	**Volume For 100g (ml)**
A16	Oil	69	69.0
	Water	29	29.0
	Surf A	1.4	1.4
	Surf B	0.6	0.7
	Total	100	100.1
A8	**Phase**	**Mass for 100g (g)**	**Volume For 100g (ml)**
A17	Oil	79	79.0
	Water	19	19.0
	Surf A	1.4	1.4
	Surf B	0.6	0.7
	Total	100	100.1
A9	**Phase**	**Mass for 100g (g)**	**Volume For 100g (ml)**
A18	Oil	89	89.0
	Water	9	9.0
	Surf A	1.4	1.4
	Surf B	0.6	0.7
	Total	100	100.1

Table 34: Phase separation results of initial volume fraction testing

Test No.	Total Emulsion Volume (ml)	Separated Phase volume Total (ml)	Percentage Separation (%)
A1	14.0	2.0	14.3
A2	14.0	3.5	25.0
A3	14.0	5.5	39.3
A4	14.0	7.5	53.6
A5	14.0	9.0	64.3
A6	14.0	11.5	82.1
A7	13.0	11.5	88.5
A8	13.0	12.5	96.2
A9	14.0	1.5	10.7
A10	14.0	2.0	14.3
A11	14.0	3.5	25.0
A12	14.0	5.5	39.3
A13	14.0	7.5	53.6
A14	14.0	9.0	64.3
A15	14.0	11.2	80.0
A16	12.5	11.4	91.2
A17	12.0	11.6	96.7
A18	14.0	1.0	7.1

Table 35: Test overview of second volume fraction testing *(to be used in conjunction with Table 36)*

Sample No.	Oil Weight Percentage (wt%)	Surfactant Ratio B + C	Surfactant Concentration
A1	Isotriethoxysilane 69	B90/10C	2%
A2	Isotriethoxysilane 74	B90/10C	2%
A3	Isotriethoxysilane 79	B90/10C	2%
A4	Isotriethoxysilane 84	B90/10C	2%
A5	Isotriethoxysilane 89	B90/10C	2%
B1	3500 cSt PDMS 69	B90/10C	2%
B2	3500 cSt PDMS 74	B90/10C	2%
B3	3500 cSt PDMS 79	B90/10C	2%
B4	3500 cSt PDMS 84	B90/10C	2%
B5	3500 cSt PDMS 89	B90/10C	2%
C1	Isotriethoxysilane 68	B90/10C	4%
C2	Isotriethoxysilane 73	B90/10C	4%
C3	Isotriethoxysilane 78	B90/10C	4%
C4	Isotriethoxysilane 83	B90/10C	4%
C5	Isotriethoxysilane 88	B90/10C	4%
D1	3500 cSt PDMS 68	B90/10C	4%
D2	3500 cSt PDMS 73	B90/10C	4%
D3	3500 cSt PDMS 78	B90/10C	4%
D4	3500 cSt PDMS 83	B90/10C	4%
D5	3500 cSt PDMS 88	B90/10C	4%

Table 36: Formula compositions tested for second volume fraction testing

A1	Phase	Mass for 100g (g)	Density (g/cc)	Volume For 100g (ml)
	Oil	69	0.9	76.7
	Water	29	1	29.0
	Surf B	1.8	1	1.8
	Surf C	0.2	0.92	0.2
A2	**Phase**	**Mass for 100g (g)**	**Density (g/cc)**	**Volume For 100g (ml)**
	Oil	74	0.9	82.2
	Water	24	1	24.0
	Surf B	1.8	1	1.8
	Surf C	0.2	0.92	0.2
A3	**Phase**	**Mass for 100g (g)**	**Density (g/cc)**	**Volume For 100g (ml)**
	Oil	79	0.9	87.8
	Water	19	1	19.0
	Surf B	1.8	1	1.8
	Surf C	0.2	0.92	0.2

A4	**Phase**	**Mass for 100g (g)**	**Density (g/cc)**	**Volume For 100g (ml)**
	Oil	84	0.9	93.3
	Water	14	1	14.0
	Surf B	1.8	1	1.8
	Surf C	0.2	0.92	0.2
A5	**Phase**	**Mass for 100g (g)**	**Density (g/cc)**	**Volume For 100g (ml)**
	Oil	89	0.9	98.9
	Water	9	1	9.0
	Surf B	1.8	1	1.8
	Surf C	0.2	0.92	0.2
B1	**Phase**	**Mass for 100g (g)**	**Density (g/cc)**	**Volume For 100g (ml)**
	Oil	69	0.9	76.7
	Water	29	1	29.0
	Surf B	1.8	1	1.8
	Surf C	0.2	0.92	0.2
B2	**Phase**	**Mass for 100g (g)**	**Density (g/cc)**	**Volume For 100g (ml)**
	Oil	74	0.9	82.2
	Water	24	1	24.0
	Surf B	1.8	1	1.8
	Surf C	0.2	0.92	0.2
B3	**Phase**	**Mass for 100g (g)**	**Density (g/cc)**	**Volume For 100g (ml)**
	Oil	79	0.9	87.8
	Water	19	1	19.0
	Surf B	1.8	1	1.8
	Surf C	0.2	0.92	0.2
B4	**Phase**	**Mass for 100g (g)**	**Density (g/cc)**	**Volume For 100g (ml)**
	Oil	84	0.9	93.3
	Water	14	1	14.0
	Surf B	1.8	1	1.8
	Surf C	0.2	0.92	0.2
B5	**Phase**	**Mass for 100g (g)**	**Density (g/cc)**	**Volume For 100g (ml)**
	Oil	89	0.9	98.9
	Water	9	1	9.0
	Surf B	1.8	1	1.8
	Surf C	0.2	0.92	0.2
C1	**Phase**	**Mass for 100g (g)**	**Density (g/cc)**	**Volume For 100g (ml)**

	Oil	68	0.9	75.6
	Water	28	1	28.0
	Surf B	3.6	1	3.6
	Surf C	0.4	0.92	0.4
C2	**Phase**	**Mass for 100g (g)**	**Density (g/cc)**	**Volume For 100g (ml)**
	Oil	73	0.9	81.1
	Water	23	1	23.0
	Surf B	3.6	1	3.6
	Surf C	0.4	0.92	0.4
C3	**Phase**	**Mass for 100g (g)**	**Density (g/cc)**	**Volume For 100g (ml)**
	Oil	78	0.9	86.7
	Water	18	1	18.0
	Surf B	3.6	1	3.6
	Surf C	0.4	0.92	0.4
C4	**Phase**	**Mass for 100g (g)**	**Density (g/cc)**	**Volume For 100g (ml)**
	Oil	83	0.9	92.2
	Water	13	1	13.0
	Surf B	3.6	1	3.6
	Surf C	0.4	0.92	0.4
C5	**Phase**	**Mass for 100g (g)**	**Density (g/cc)**	**Volume For 100g (ml)**
	Oil	88	0.9	97.8
	Water	8	1	8.0
	Surf B	3.6	1	3.6
	Surf C	0.4	0.92	0.4
D1	**Phase**	**Mass for 100g (g)**	**Density (g/cc)**	**Volume For 100g (ml)**
	Oil	68	0.9	75.6
	Water	28	1	28.0
	Surf B	3.6	1	3.6
	Surf C	0.4	0.92	0.4
D2	**Phase**	**Mass for 100g (g)**	**Density (g/cc)**	**Volume For 100g (ml)**
	Oil	73	0.9	81.1
	Water	23	1	23.0
	Surf B	3.6	1	3.6
	Surf C	0.4	0.92	0.4
D3	**Phase**	**Mass for 100g (g)**	**Density (g/cc)**	**Volume For 100g (ml)**
	Oil	78	0.9	86.7
	Water	18	1	18.0

	Surf B	3.6	1	3.6
	Surf C	0.4	0.92	0.4
D4	**Phase**	**Mass for 100g (g)**	**Density (g/cc)**	**Volume For 100g (ml)**
	Oil	83	0.9	92.2
	Water	13	1	13.0
	Surf B	3.6	1	3.6
	Surf C	0.4	0.92	0.4
D5	**Phase**	**Mass for 100g (g)**	**Density (g/cc)**	**Volume For 100g (ml)**
	Oil	88	0.9	97.8
	Water	8	1	8.0
	Surf B	3.6	1	3.6
	Surf C	0.4	0.92	0.4

Table 37: Phase separation results of second volume fraction testing

Test No.	Total Emulsion Volume (ml)	Separated Phase volume Total (ml)	Percentage Separation after 3 days (%)
A1	12.2	1.8	14.8
A2	13.2	1.5	11.4
A3	12.0	0.7	5.8
A4	13.5	0.4	3.0
A5	13.6	0.2	1.5
B1	12.0	0.9	7.5
B2	12.0	0.5	4.2
B3	12.5	0.2	1.6
B4	13.5	13.2	97.8
B5	14.0	13.8	98.6
C1	12.0	0.9	7.5
C2	13.0	0.7	5.4
C3	13.5	0.5	3.7
C4	13.0	0.3	2.3
C5	13.4	12.4	92.5
D1	13.4	0.0	0.0
D2	12.8	0.0	0.0
D3	13.3	0.0	0.0
D4	14.0	9.5	67.9
D5	14.2	11.5	81.0

Appendix B: Pendent Drop Testing

The following tables in this section give phase definitions used for the pendent drop experiment.

Table 38: Distilled water phase definition

Characteristic	Value
Density (g/cm^3)	0.9986
γ (mN/m)	72.80
γd (mN/m)	21.80
γ+ (mN/m)	25.50
γ- (mN/m)	25.50

Table 39: Air phase definition

Characteristic	Value
Density (g/cm^3)	0.0013

Table 40: Ethanol phase definition

Characteristic	Value
Density (g/cm^3)	0.7937
γ (mN/m)	22.40
γd (mN/m)	18.80
γ+ (mN/m)	0.02
γ- (mN/m)	68.00
MW	46.1

Table 41: n-isooctyltriethoxysilane phase definition

Characteristic	Value
Density (g/cm^3)	0.88

Appendix C: Rheology of POE (60) in Base Emulsion

Table 42 shows sample descriptions used during testing of surfactant concentration requirement without particulate incorporation.

Table 42: Surfactant concentration test sample descriptions

		7.5% APDMS
409A-E1	Constituent mass (g)	Density (g/cc^3)
POE (60)	0.2	1.00
ITES	72.0	0.88
APDMS	7.5	0.98
Distilled Water	20.1	1.00
		7.5% APDMS
409A-E2	Constituent mass (g)	Density (g/cc^3)
POE (60)	0.3	1.00
ITES	72.0	0.88
APDMS	7.5	0.98
Distilled Water	20.0	1.00
		7.5% APDMS
409A-E3	Constituent mass (g)	Density (g/cc^3)
POE (60)	0.4	1.00
ITES	72.0	0.88
APDMS	7.5	0.98
Distilled Water	19.9	1.00
		7.5% APDMS
409A-E4	Constituent mass (g)	Density (g/cc^3)
POE (60)	0.5	1.00
ITES	72.0	0.88
APDMS	7.5	0.98
Distilled Water	19.8	1.00

Appendix D: Emulsification Optimisation

Section A: Colloidal Emulsification Optimisation

Aim: to evaluate the mixing time required to incorporate 10wt% titanium dioxide and 10wt% colloidal dispersions into the base emulsion (excluding PDMS).

Apparatus

n-isooctyltriethoxysilane 95% (ITES)
non-ionic polyoxyethylene(15) and (60) stearylamine (POE)
Distilled water (0 PPM)
Titanium dioxide 15nm (anatase 99%)
Zinc oxide 20nm (99.5%)
Ultrasonic mixer
Homogeniser
Mixer 175W with blade head

Method

1. ITES and surfactant were put into a container with distilled water placed into another container. Both were heated at 90°C in a water bath until the surfactant dissolved.
2. All of the water was added quickly to the oil mixture.
3. The oil container was removed from the water bath and homogenised through making localised concentration of emulsion at the phase interface and then increasing this by moving the homogeniser up. This process took approximately 30s.
4. 10wt% nanoparticulate colloidal dispersions produced through ultrasonication was produced and incorporated at the relevant concentrations.
5. The homogeniser was replaced with a blade headed mixer and each respective emulsion was mixed for different times at this stage and then assessed through centrifugation and turbidity.
6. Finally 50v/v% solutions were produced by diluting each respective emulsion with distilled water. These emulsions were then fixed using a water based fixative to microscope slides and pictures of each emulsion taken through

microscopy. These images were then transformed into 256 bit greyscale images and a threshold of 130-256 was used to produce droplet size data.

7. All results were evaluated.

Results and Discussion

Table 43: Average droplet diameters against mixing time

Control Emulsion		
Mixing Time (Mins)	**Mean Diameter (µm)**	**Standard Deviation**
0.0	17.4	14.7
0.5	12.5	8.7
1.0	9.7	7.5
2.0	10.6	6.6
3.0	12.2	10.1
4.0	9.9	6.5
5.0	12.9	10.0
TiO2 Emulsion		
Mixing Time (Mins)	**Mean Diameter (µm)**	**Standard Deviation**
0.0	14.1	12.9
0.5	12.2	8.4
1.0	14.4	9.0
2.0	11.3	9.9
3.0	13.0	10.4
4.0	10.6	8.9
5.0	16.0	13.4
ZnO Emulsion		
Mixing Time (Mins)	**Mean Diameter (µm)**	**Standard Deviation**
0.0	12.9	10.0
0.5	11.6	9.3
1.0	7.7	4.3
2.0	10.3	7.8
3.0	11.4	9.4
4.0	11.0	9.0
5.0	13.1	10.7

Table 43 shows that a highly polydispersed emulsion was produced from mixing with little difference between the control and the nanoparticulate emulsions. Thus at the concentration tested, colloidal incorporation through the method discussed does not effectively alter the morphology of the emulsion. Results seem to suggest that since mixing adds energy (and heat) to the emulsion, micelles formed earlier in the mixing process are broken down, most probably through coalescence. Micelles may be

pushed together after overcoming the physical barriers presented by the solid and surfactant system.

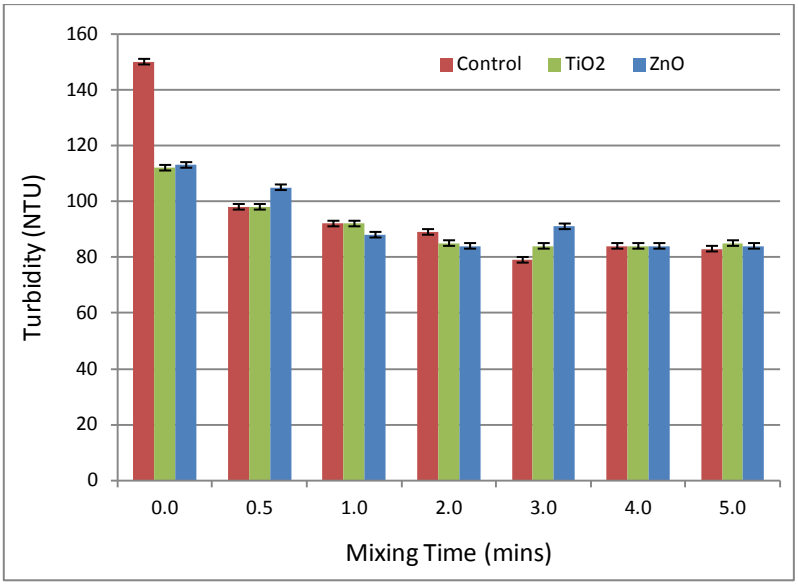

Figure 93: Average turbidity against mixing time

Figure 93 shows the average turbidity of samples against mixing time. The results show that the haze of an emulsion regardless of nanoparticulate incorporation seems to stabilise. This combined with the results in Table 43 may help show that after 2 minutes of mixing the droplets will not get any smaller. It may be that after 2 minutes of mixing a larger proportion of droplets coalesce and thus increase the droplet size average, however the continuous water phase may still be more distributed in the emulsion and thus the reason for the levelling off shown after two minutes.

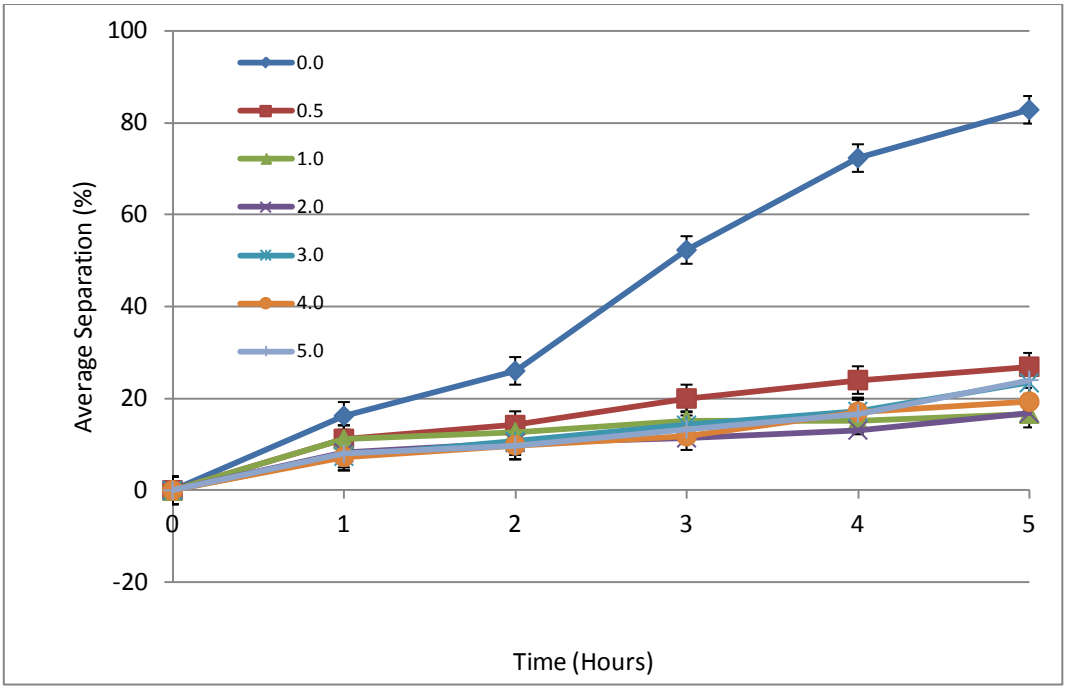

Figure 94: Average separation of control emulsion against various mixing times

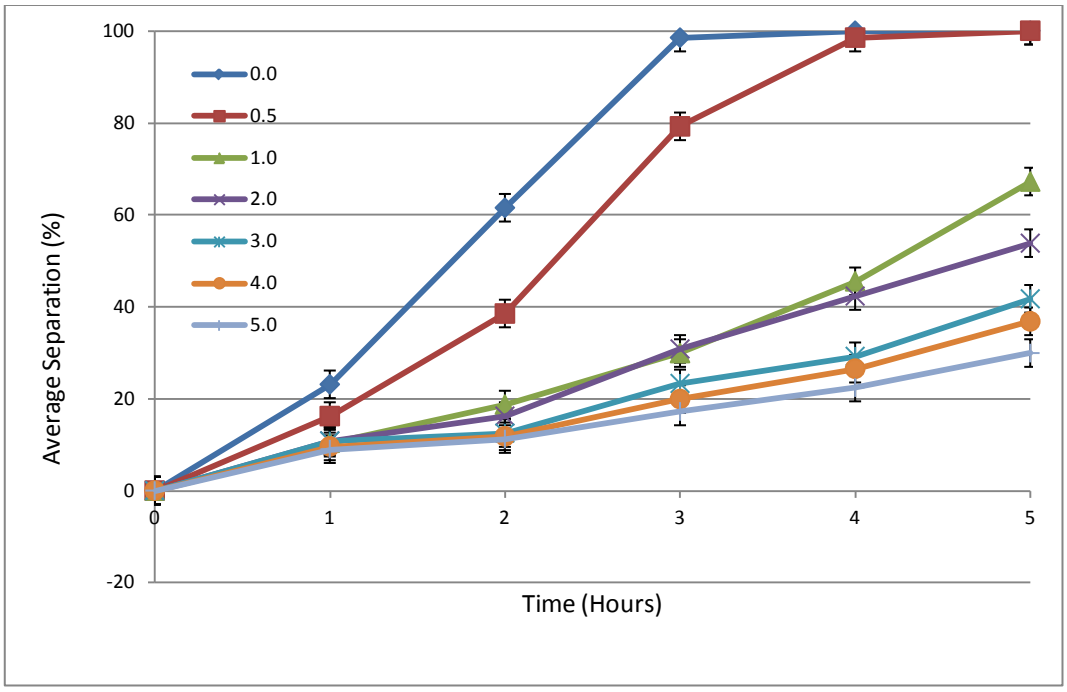

Figure 95: Average separation of titanium dioxide emulsion against various mixing times

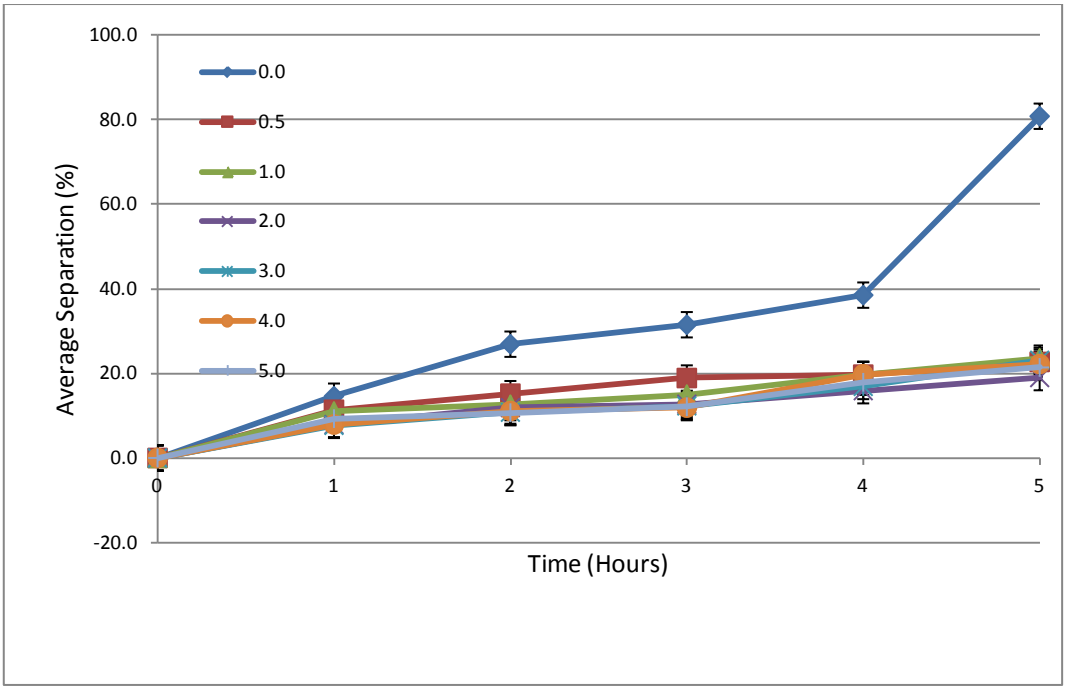

Figure 96: Average separation of zinc oxide emulsion against various mixing times

The results shown in Figure 95 show a greater separation than the results in Figure 94 and Figure 96. Centrifugation for results in Figure 95 was conducted in a relatively hot environment and thus the results may be considered anomalous. It however would be reasonable to assume that results would be similar to the zinc oxide results as they seem sensible when comparing to the control.

Conclusions

Results show that optimised mixing time is between 1 and 3 minutes when mixing 100ml of emulsion using the method described.

Section B: Siloxane Emulsification Optimisation

Stage 4a Aim: to evaluate the mixing time required to incorporate 5wt% OH terminated PDMS 3500cSt at 2000rpm using a lab mixer.

Apparatus

n-isooctyltriethoxysilane 95% (ITES)

non-ionic polyoxyethylene(15) and (60) stearylamine (POE)

3500cSt 0.08% OH terminated polydimethylsiloxane (OH-PDMS)

Distilled water (0 PPM)

Titanium dioxide 15nm (anatase 99%)

Zinc oxide 20nm (99.5%)
Ultrasonic mixer
Homogeniser
Mixer 175W with blade head
Lab mixer with impeller head

Method

1. ITES and surfactant were put into a container with distilled water placed into another container. Both containers were heated at 90°C in a water bath until the surfactant dissolved.
2. All of the water was added quickly to the oil mixture.
3. The oil container was removed from the water bath and homogenised through making localised concentration of emulsion at the phase interface and then increasing this by moving the homogeniser up. This process took approximately 30s.
4. The emulsion was mixed using a mixer with a blade head for 2 minutes.
5. 5wt% siloxane was then added to the base emulsion (at the expense of the oil fraction wt%) and mixed at various times using a lab mixer at 2000rpm for various times.
6. Turbidy and physical stability was assessed.

Results & Discussion

Figure 97 shows the turbidity results for 5wt% 3500cSt PDMS mixed at 2000rpm for various durations. The results show that mixing time is optimised at ca. 1 minute. Figure 98 shows the physical stress results after centrifugation. Emulsions mixed for ca 1 minute showed the best results with less mixing achieving a better stability. This may be due to silane and siloxane dispersed phases not being completely soluble in such a system. This therefore shows why dispersing the two phases would actually reduce stability at longer mixing times. Alternatively, mixing speed for incorporation may be too high and lead to micelle rupturing and emulsion separation.

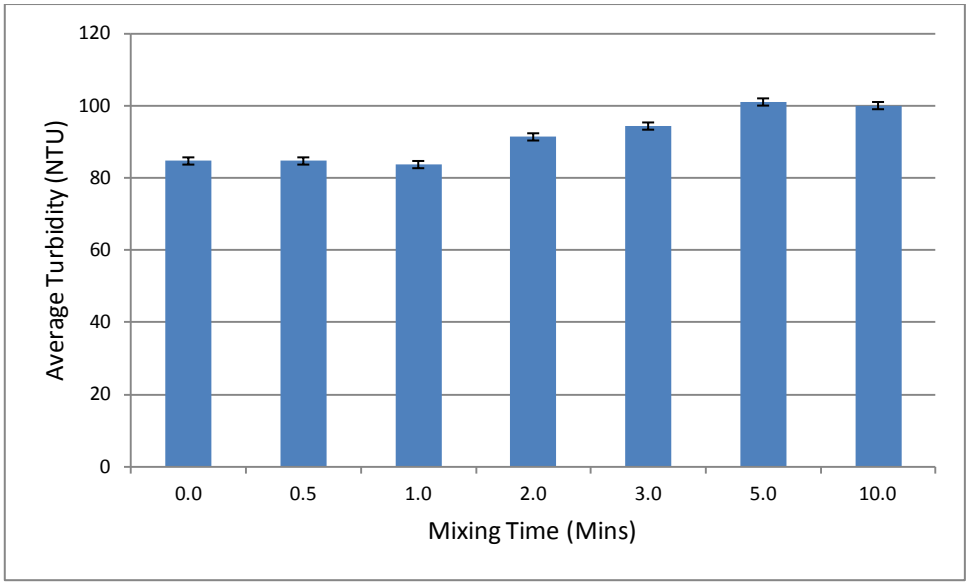

Figure 97: Average turbidity results for emulsions containing 5wt% 3500cSt OH-PDMS, mixed at 2000rpm over different periods of time

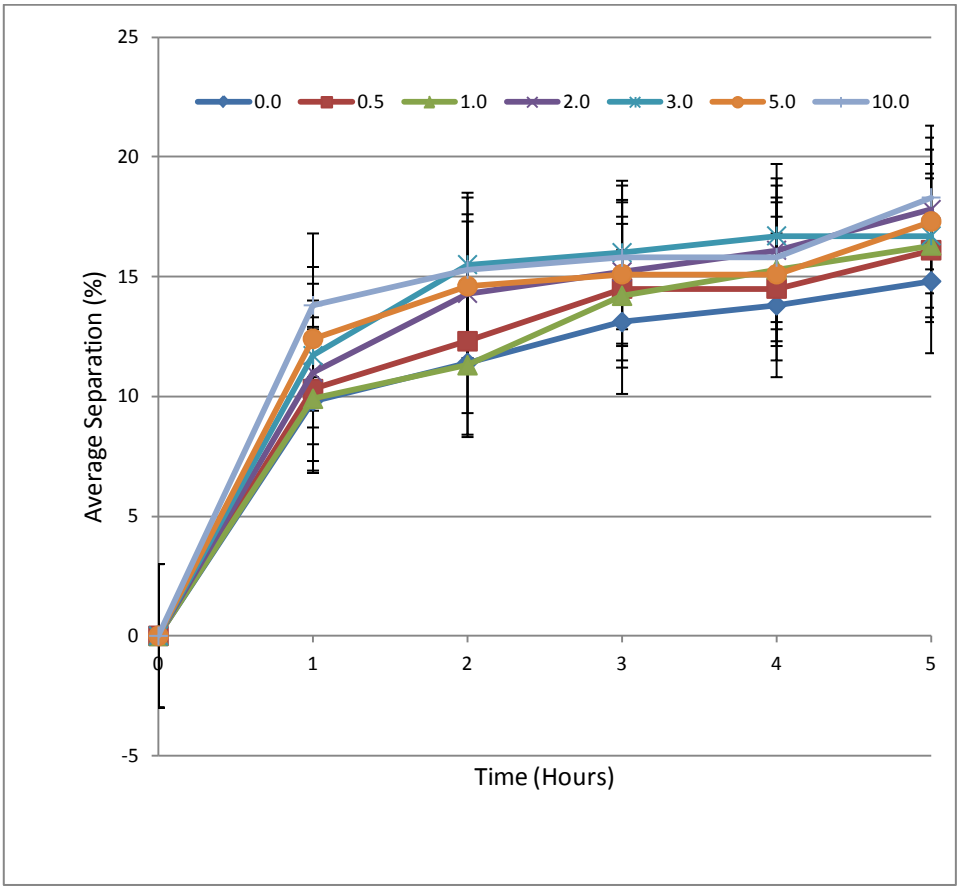

Figure 98: Average separation of base emulsion containing 5wt% 3500cSt OH-PDMS against various mixing times at 2000rpm

Conclusions

Results seem to indicate that mixing siloxane into the emulsion is optimised ca 1 minute at 2000rpm using the method described.

Section C: Siloxane Incorporation and Optimisation in Base Emulsion

Table 44 shows sample descriptions used to assess hydroxyl terminated siloxane viscosity and concentration in the base emulsion. N.B. a small quantity of polyvinyl alcohol (PVA 18-88; Sigma Aldrich) was added initially in the water phase as a 1:4wt% distilled water solution to help reduce film forming during testing.

Table 44: Sample descriptions for siloxane viscosity and concentration test

			0% PDMS
1	**B1-7**	**Constituent mass (g)**	**Density (g/cc^3)**
	POE (15)	0.6	1.00
	PVA 18-88 25wt% Conc.	0.9	(Dry 0.4-0.6) taken as 1 in solution
	Iso Silane	79.6	0.88
	PDMS 3500	0.0	0.98
	Distilled Water	18.9	1.00
			7.5% PDMS 3500
2	**B8-14**	**Constituent mass (g)**	**Density (g/cc^3)**
	POE (15)	0.6	1.00
	PVA 18-88 25wt% Conc.	0.9	(Dry 0.4-0.6) taken as 1 in solution
	Iso Silane	72.1	0.88
	PDMS 3500	7.5	0.98
	Distilled Water	18.9	1.00
			15% PDMS 3500
3	**B15-21**	**Constituent mass (g)**	**Density (g/cc^3)**
	POE (15)	0.6	1.00
	PVA 18-88 25wt% Conc.	0.9	(Dry 0.4-0.6) taken as 1 in solution
	Iso Silane	64.6	0.88
	PDMS 3500	15.0	0.98
	Distilled Water	18.9	1.00
			30% PDMS 3500
4	**B22-28**	**Constituent mass (g)**	**Density (g/cc^3)**
	POE (15)	0.6	1.00
	PVA 18-88 25wt% Conc.	0.9	(Dry 0.4-0.6) taken as 1 in solution
	Iso Silane	49.6	0.88
	PDMS 3500	30.0	0.98
	Distilled Water	18.9	1.00
			45% PDMS 3500

5	**B29-35**	**Constituent mass (g)**	**Density (g/cc^3)**
	POE (15)	0.6	1.00
	PVA 18-88 25wt% Conc.	0.9	(Dry 0.4-0.6) taken as 1 in solution
	Iso Silane	34.6	0.88
	PDMS 3500	45.0	0.98
	Distilled Water	18.9	1.00
			7.5% PDMS 50,000
6	**B36-42**	**Constituent mass (g)**	**Density (g/cc^3)**
	POE (15)	0.6	1.00
	PVA 18-88 25wt% Conc.	0.9	(Dry 0.4-0.6) taken as 1 in solution
	Iso Silane	72.1	0.88
	PDMS 3500	7.5	0.98
	Distilled Water	18.9	1.00
			15% PDMS 50,000
7	**B43-49**	**Constituent mass (g)**	**Density (g/cc^3)**
	POE (15)	0.6	1.00
	PVA 18-88 25wt% Conc.	0.9	(Dry 0.4-0.6) taken as 1 in solution
	Iso Silane	64.6	0.88
	PDMS 3500	15.0	0.98
	Distilled Water	18.9	1.00
			30% PDMS 50,000
8	**B50-56**	**Constituent mass (g)**	**Density (g/cc^3)**
	POE (15)	0.6	1.00
	PVA 18-88 25wt% Conc.	0.9	(Dry 0.4-0.6) taken as 1 in solution
	Iso Silane	49.6	0.88
	PDMS 3500	30	0.98
	Distilled Water	18.9	1.00
			45% PDMS 50,000
9	**B57-63**	**Constituent mass (g)**	**Density (g/cc^3)**
	POE (15)	0.6	1.00
	PVA 18-88 25wt% Conc.	0.9	(Dry 0.4-0.6) taken as 1 in solution
	Iso Silane	34.6	0.88
	PDMS 3500	45.0	0.98
	Distilled Water	18.9	1.00
			7.5% PDMS 90-120,000
10	**B64-70**	**Constituent mass (g)**	**Density (g/cc^3)**
	POE (15)	0.6	1.00
	PVA 18-88 25wt% Conc.	0.9	(Dry 0.4-0.6) taken as 1 in solution
	Iso Silane	72.1	0.88
	PDMS 3500	7.5	0.98
	Distilled Water	18.9	1.00
			15% PDMS 90-120,000
11	**B71-77**	**Constituent mass (g)**	**Density (g/cc^3)**
	POE (15)	0.6	1.00

	PVA 18-88 25wt% Conc.	0.9	(Dry 0.4-0.6) taken as 1 in solution
	Iso Silane	64.6	0.88
	PDMS 3500	15.0	0.98
	Distilled Water	18.9	1.00
			30% PDMS 90-120,000
12	**B78-84**	**Constituent mass (g)**	**Density (g/cc^3)**
	POE (15)	0.6	1.00
	PVA 18-88 25wt% Conc.	0.9	(Dry 0.4-0.6) taken as 1 in solution
	Iso Silane	49.6	0.88
	PDMS 3500	30.0	0.98
	Distilled Water	18.9	1.00
			45% PDMS 90-120,000
13	**B85-91**	**Constituent mass (g)**	**Density (g/cc^3)**
	POE (15)	0.6	1.00
	PVA 18-88 25wt% Conc.	0.9	(Dry 0.4-0.6) taken as 1 in solution
	Iso Silane	34.6	0.88
	PDMS 3500	45.0	0.98
	Distilled Water	18.9	1.00

Appendix E: Emulsion Morphology

Table 45 shows the emulsion descriptions of samples used during optical microscopy assessment.

Table 45: Emulsion optical microscopy descriptions

			0 min /2,000rpm
STG3A-1	**Material**	**Constituent mass (g)**	**Density (g/cc^3)**
	POE (15/60) 20:80	0.3	1.00
	Iso Silane	79.8	0.88
	10% TiO2 Solution	0.6	
	Distilled Water	19.3	1.00
			1 min /2,000rpm
STG3A-2	**Material**	**Constituent mass (g)**	**Density (g/cc^3)**
	POE (15/60) 20:80	0.3	1.00
	Iso Silane	79.8	0.88
	10% TiO2 Solution	0.6	
	Distilled Water	19.3	1.00
			3 min /2,000rpm
STG3A-3	**Material**	**Constituent mass (g)**	**Density (g/cc^3)**
	POE (15/60) 20:80	0.3	1.00
	Iso Silane	79.8	0.88
	10% TiO2 Solution	0.6	
	Distilled Water	19.3	1.00
			5 min /2,000rpm
STG3A-4	**Material**	**Constituent mass (g)**	**Density (g/cc^3)**
	POE (15/60) 20:80	0.3	1.00
	Iso Silane	79.8	0.88
	10% TiO2 Solution	0.0	
	Distilled Water	19.9	1.00
			10 min /2,000rpm
STG3A-5	**Material**	**Constituent mass (g)**	**Density (g/cc^3)**
	POE (15/60) 20:80	0.3	1.00
	Iso Silane	79.8	0.88
	10% TiO2 Solution	0.0	
	Distilled Water	19.9	1.00
			20 min /2,000rpm
STG3A-6	**Material**	**Constituent mass (g)**	**Density (g/cc^3)**
	POE (15/60) 20:80	0.3	1.00

	Iso Silane	79.8	0.88
	10% TiO2 Solution	0.0	
	Distilled Water	19.9	1.00
			30 min /2,000rpm
STG3A-7	**Material**	**Constituent mass (g)**	**Density (g/cc^3)**
	POE (15/60) 20:80	0.3	1.00
	Iso Silane	79.8	0.88
	10% TiO2 Solution	0.0	
	Distilled Water	19.9	1.00
			0 min /2,000rpm
STG3A-8	**Material**	**Constituent mass (g)**	**Density (g/cc^3)**
	POE (15/60) 20:80	0.3	1.00
	Iso Silane	79.8	0.88
	10% TiO2 Solution	0.6	
	Distilled Water	19.3	1.00
			1 min /2,000rpm
STG3A-9	**Material**	**Constituent mass (g)**	**Density (g/cc^3)**
	POE (15/60) 20:80	0.3	1.00
	Iso Silane	79.8	0.88
	10% TiO2 Solution	0.6	
	Distilled Water	19.3	1.00
			3 min /2,000rpm
STG3A-10	**Material**	**Constituent mass (g)**	**Density (g/cc^3)**
	POE (15/60) 20:80	0.3	1.00
	Iso Silane	79.8	0.88
	10% TiO2 Solution	0.6	
	Distilled Water	19.3	1.00
			5 min /2,000rpm
STG3A-11	**Material**	**Constituent mass (g)**	**Density (g/cc^3)**
	POE (15/60) 20:80	0.3	1.00
	Iso Silane	79.8	0.88
	10% TiO2 Solution	0.6	
	Distilled Water	19.3	1.00
			10 min /2,000rpm
STG3A-12	**Material**	**Constituent mass (g)**	**Density (g/cc^3)**
	POE (15/60) 20:80	0.3	1.00
	Iso Silane	79.8	0.88
	10% TiO2 Solution	0.6	

	Distilled Water	19.3	1.00
			20 min /2,000rpm
STG3A-13	**Material**	**Constituent mass (g)**	**Density (g/cc^3)**
	POE (15/60) 20:80	0.3	1.00
	Iso Silane	79.8	0.88
	10% TiO2 Solution	0.6	
	Distilled Water	19.3	1.00
			30 min /2,000rpm
STG3A-14	**Material**	**Constituent mass (g)**	**Density (g/cc^3)**
	POE (15/60) 20:80	0.3	1.00
	Iso Silane	79.8	0.88
	10% TiO2 Solution	0.6	
	Distilled Water	19.3	1.00
			0 min /2,000rpm
STG3A-15	**Material**	**Constituent mass (g)**	**Density (g/cc^3)**
	POE (15/60) 20:80	0.3	1.00
	Iso Silane	79.8	0.88
	10% ZnO Solution	0.6	
	Distilled Water	19.3	1.00
			1 min /2,000rpm
STG3A-16	**Material**	**Constituent mass (g)**	**Density (g/cc^3)**
	POE (15/60) 20:80	0.3	1.00
	Iso Silane	79.8	0.88
	10% ZnO Solution	0.6	
	Distilled Water	19.3	1.00
			3 min /2,000rpm
STG3A-17	**Material**	**Constituent mass (g)**	**Density (g/cc^3)**
	POE (15/60) 20:80	0.3	1.00
	Iso Silane	79.8	0.88
	10% ZnO Solution	0.6	
	Distilled Water	19.3	1.00
			5 min /2,000rpm
STG3A-18	**Material**	**Constituent mass (g)**	**Density (g/cc^3)**
	POE (15/60) 20:80	0.3	1.00
	Iso Silane	79.8	0.88
	10% ZnO Solution	0.6	
	Distilled Water	19.3	1.00

			10 min /2,000rpm
STG3A-19	**Material**	**Constituent mass (g)**	**Density (g/cc^3)**
	POE (15/60) 20:80	0.3	1.00
	Iso Silane	79.8	0.88
	10% ZnO Solution	0.6	
	Distilled Water	19.3	1.00
			20 min /2,000rpm
STG3A-20	**Material**	**Constituent mass (g)**	**Density (g/cc^3)**
	POE (15/60) 20:80	0.3	1.00
	Iso Silane	79.8	0.88
	10% ZnO Solution	0.6	
	Distilled Water	19.3	1.00
			30 min /2,000rpm
STG3A-21	**Material**	**Constituent mass (g)**	**Density (g/cc^3)**
	POE (15/60) 20:80	0.3	1.00
	Iso Silane	79.8	0.88
	10% ZnO Solution	0.6	
	Distilled Water	19.3	1.00

Table 46 shows the emulsion descriptions used during the phase dilution test.

Table 46: Phase dilution sample descriptions

STG4-70	**Material**	**Constituent mass (g)**	**Density (g/cc^3)**
	POE (15/60) 20:80	0.3	1.00
	Iso Silane	74.8	0.88
	10% TiO2 Solution	0.0	
	PDMS 3500cSt	5.0	
	Distilled Water	19.9	1.00
STG4-71	**Material**	**Constituent mass (g)**	**Density (g/cc^3)**
	POE (15/60) 20:80	0.3	1.00
	Iso Silane	74.8	0.88
	10% TiO2 Solution	0.6	
	PDMS 3500cSt	5.0	
	Distilled Water	19.3	1.00
STG4-72	**Material**	**Constituent mass (g)**	**Density (g/cc^3)**
	POE (15/60) 20:80	0.3	1.00
	Iso Silane	74.8	0.88
	10% ZnO Solution	0.6	
	PDMS 3500cSt	5.0	
	Distilled Water	19.3	1.00

Appendix F: Nanoparticulate Optimisation

Table 47: Nanoparticulate emulsion descriptions used in assessing emulsions stability mechanisms

		Emulsion Control
1	**A-M1**	Constituent mass (g)
	POE (15/60) 20:80	0.3
	Iso Silane	73.0
	Nanoparticulate	0.0
	PDMS 3500cSt	7.5
	Distilled Water	19.2
		Emulsion Titanium Dioxide
2	**A-M2**	Constituent mass (g)
	POE (15/60) 20:80	0.3
	Iso Silane	73.0
	Titanium Dioxide (10wt%)	0.1
	PDMS 3500cSt	7.5
	Distilled Water	19.1
		Emulsion Titanium Dioxide
3	**A-M3**	Constituent mass (g)
	POE (15/60) 20:80	0.3
	Iso Silane	73.0
	Titanium Dioxide (10wt%)	0.3
	PDMS 3500cSt	7.5
	Distilled Water	18.9
		Emulsion Titanium Dioxide
4	**A-M4**	Constituent mass (g)
	POE (15/60) 20:80	0.3
	Iso Silane	73.0
	Titanium Dioxide (10wt%)	0.5
	PDMS 3500cSt	7.5
	Distilled Water	18.7
		Emulsion Zinc Oxide
5	**A-M5**	Constituent mass (g)
	POE (15/60) 20:80	0.3
	Iso Silane	73.0
	Zinc Oxide (10wt%)	0.1
	PDMS 3500cSt	7.5
	Distilled Water	19.1
		Emulsion Zinc Oxide
6	**A-M6**	Constituent mass (g)
	POE (15/60) 20:80	0.3
	Iso Silane	73.0
	Zinc Oxide (10wt%)	0.3
	PDMS 3500cSt	7.5

	Distilled Water	18.9
		Emulsion Zinc Oxide
7	**A-M7**	Constituent mass (g)
	POE (15/60) 20:80	0.3
	Iso Silane	73.0
	Zinc Oxide (10wt%)	0.5
	PDMS 3500cSt	7.5
	Distilled Water	18.7